Modelling Ecosystem Dynamics In The Turbulent Surface Layers of the Ocean

Rosa María Barciela Fernández

Doctor of Philosophy

December 2002

University of Southampton

Modelling Ecosystem Dynamics In The Turbulent Surface Layers of the Ocean

Rosa María Barciela Fernández

A thesis submitted in candidature for the degree of
Doctor of Philosophy
School of Ocean and Earth Science

December 2002

UNIVERSITY OF SOUTHAMPTON

ABSTRACT

FACULTY OF SCIENCE
OCEAN AND EARTH SCIENCE

Doctor of Philosophy

MODELLING ECOSYSTEM DYNAMICS IN THE TURBULENT SURFACE LAYERS OF THE OCEAN

by Rosa Maria Barciela Fernandez

A size-dependent ecological model based on the original developed by Fasham *et al.* (1990) was used to investigate the ecosystem dynamics in the North Atlantic at 47°N 20°W, as this location has been the site of intensive oceanographic and biological studies so an important background of data are available. The model has eight different compartments: diatom and non-diatom phytoplankton, micro and mesozooplankton, nitrate, ammonium, silicate and detritus. It was calibrated using data provided by the North Atlantic Bloom Experiment for 1989 (NABE89). An optimisation technique based on Powell's method (Press *et al.*, 1992) was applied to estimate unknown parameters by fitting the model output to NABE observations. The uncertainty and correlation in the optimal model parameters were estimated by analysing the cost function. Finally, tests on the choice of the "initial guess" for parameters as well as on the time-stepping technique used were carried out.

A series of twin experiments using "synthetic" data of the same type and frequency (weekly data throughout the year and daily data during the spring bloom only) were performed to investigate the role of sparse observations on parameter recovery and on reproducing the North Atlantic annual cycle. The same experiments were also used to estimate model parameters when either noise-free or noisy data were assimilated as model observations. The sensitivity to the model structure was also tested.

The ecosystem model was embedded into a 1-D physical model, the Miami Isopycnic Co-ordinate Ocean Model (MICOM) so as to study the effect of realistic physical forcing on the development of the spring bloom and the seasonal plankton cycle. The coupled model was forced with physical fields provided by the NCEP group from 1988 to 1996, which permitted the study of the intra and interannual variability of the ecosystem. The inclusion of an extra compartment (detrital biogenic silica) and the parameterisation of nitrification processes were needed in order to accurately reproduce the vertical gradient of nutrients in the ocean. The coupled model was tuned to the NABE area (using the NABE89 data set) and validated with data from the German JGOFS phase for 47°N and 20°W during 1996. Model tuning and validation highlighted the inadequacy of several parameters (detrital remineralisation, detrital sinking and phytoplankton nutrient uptake rates as well as light efficiency). The 1-D model differed from the 0-D one in terms of the seasonal development of the mixed layer as well as the seasonal cycles of the state variables. However, a good agreement to field and literature data was obtained. The initiation of the spring bloom strongly depended on the rate of shoaling of the mixed layer. Summer mixing events encouraged mesozooplankton growth, which better prepared them for over wintering.

The coupled model also predicted the annual occurrence of a deep chlorophyll maximum (DCM), at the depth of the ammonium maximum, which developed as a consequence of nutrient limitation in the mixed layer. A diatom DCM was observed every year and ended due to mesozooplankton grazing. A non-diatom DCM was only observed in the years where the shallowest summer mixed layer depths were modelled and ended by a combination of microzooplankton grazing and light limitation. Primary production (PP) at the DCM accounted for up to 40% of the PP predicted in the mixed layer, being mainly regenerated production (65-79%). The sensitivity analysis showed that the presence/absence of the non-diatom DCM is affected by the nitrogen and silicate remineralisation rates, which determine the vertical distribution of nutrients and control the degree of oligotrophy in the mixed layer.

CONTENTS

page

LIST OF FIGURES

LIST OF TABLES

ACKNOWLEDGMENTS

I have been very fortunate to find wonderful people at the Southampton Oceanography Centre who gave me so much that this acknowledgment section is not merely a formality but a very sincere expression of gratitude to all of them.

I would first of all like to thank my supervisors: Mike Fasham, Meric Srokosz and Kelvin Richards for their constant support, encouragement, guidance and scientific stimulation. My special thanks go to Peter Killworth who chaired regular advisory panel meetings that greatly contributed towards the completion of this thesis.

I have had countless enlightening discussions with numerous remarkable people at SOC. Adrian Martin, John Hemmings, Andrew Yool and Joanna Waniek particularly contributed to various areas of this research and provided insightful comments and constructive suggestions. Thanks also to Andrew Shaw, whose help with MATLAB proved to be invaluable, and to all JRD and GDD staff for being such a great bunch of people to work with. I want to express my thanks to Ian Rouse, who kindly let me used his printer to produce the final version of this thesis when all the other printers failed.

I would also like to thank the JGOFS community for collecting and making available the NABE data. Special thanks go to Thomas Mitzka and Joachim Hemann, who provided data from the German JGOFS phase for the NABE site during 1996, and to Roy Lowry at BODC for being so efficient dealing with all my queries.

Thanks also to my examiners, Arnold Taylor and Peter Challenor, who contributed with valuable comments to make this thesis better.

Finally, I want to thank most of all my family (in Vigo and Newcastle) who shared all my joys and sorrows throughout the course of this roller-coaster ride. I want to express my great love for my mum, dad, my sister, Pat, Andy, Sarah, and my husband Simon. My deepest love goes to Simon for being my inspiration and making me smile everyday!.

Far better an approximate answer to the "right" question,
which is often vague,
than an exact answer to the "wrong" question,
which can always be made precise.

John W. Tukey, 1962.

Chapter 1:

Introduction

Chapter 1: Introduction

1.1 The carbon cycle in the ocean

Simulation models of ecosystem dynamics existed as early as 1939 (Fleming, 1939). Since 1939, diverse modelling approaches have developed in order to gain understanding of the dynamics of planktonic marine ecosystems, because of their importance to the global biogeochemical cycle. Special attention has been paid to the carbon cycle in the ocean as there exists great concern about the role of CO_2 as a greenhouse gas, as anthropogenic activities have led to a secular increase in atmospheric CO_2 (rising above 365 ppm). Whether or not this increase will have significant climatological effect is the centre of great international discussion.

Atmospheric CO_2 is rapidly exchanged with ocean and terrestrial ecosystems. Its rate of absorption by those reservoirs and the rate of CO_2 emissions determine the overall rate of CO_2 change. Both ocean and terrestrial ecosystems act as CO_2 sinks and reduce the excess of CO_2. However, the oceans play a major buffering role in the global carbon cycle. They are of great importance in climate regulation because: they have a huge capacity to store heat, water and greenhouse gases such as carbon dioxide or dimethyl sulfide; global-scale ocean currents transport these properties over large distances and the oceans exchange these and other properties with the atmosphere.

The oceans contain large reservoirs of dissolved inorganic carbon (DIC) in gaseous state ($CO_{2(g)}$) and also bicarbonate (HCO_3^-) and carbonate (CO_3^{2-}) ions. The concentration of DIC is 50 times higher in the ocean than in the atmosphere (Falkowski *et al.*, 2000) and for this reason, the ocean ultimately determines the atmosphere's CO_2 content but not vice versa (Siegenthaler and Sarmiento, 1993). Moreover, the carbon in living terrestrial

biomass and soil is approximately 3 times higher than the CO_2 in the atmosphere but the turnover time of terrestrial carbon is of order of decades. The rate of global change of CO_2 depends not only on anthropogenic activities but also on biogeochemical and climatological processes and their interactions with the carbon cycle. The long term geological record holds evidence that global scale changes in the transfer of carbon to the ocean interior by biological processes have played a role in past changes in atmospheric CO_2 concentrations and climate.

In the upper ocean, the carbon cycle relies on ecosystem dynamics which determine the efficiency of nutrient uptake, carbon export (in the form of sinking carbon particles) and production of recycled and exported particulate carbon. The export of organic carbon from surface to deep waters is about 11-16 Gt of carbon per year, a process that keeps the concentration of atmospheric CO_2 about 150-200 ppmv (parts per million of volume) lower than in an abiotic ocean (Falkowski *et al.*, 2000). Furthermore, ocean biota cycle almost the same amount of carbon per year as terrestrial ecosystems even though algae biomass in the ocean account for less than 0.05% of that on land (Field *et al.*, 1998).

1.2 Why size matters

Phytoplankton fixation of inorganic carbon in surface waters is not limited by carbon but by the availability of dissolved macronutrients such as nitrate (utilised by all phytoplankton groups) and silicate (mainly used by diatoms) and the micronutrient iron, which constrain the export of carbon to the deep sea by marine phytoplankton. Biological activity in the surface layers of the ocean also plays a crucial role in large-scale geochemistry by producing particles that sink into deeper waters, creating a vertical gradient of certain elements such as carbon and nitrogen, amongst others, which will finally end up as part of the sediments where they will be trapped and excluded from the global cycle for

hundreds to thousands of years (biological pump). Biological pumping of carbon to the deep waters is generally thought to be mostly in the form of large fast-sinking organic particles and proportional to the amount of nitrate mixed upwards across the base of the euphotic zone (Eppley and Peterson, 1979), which maintains lower concentrations of carbon and nutrients in the surface ocean than within the thermocline waters below. Lampitt *et al.* (1993) established the importance of seasonal sinking particles as a major biogeochemical effect of moving elements to deep water. As larger particles sink faster, they have the greatest potential to contribute to vertical fluxes, therefore systems dominated by larger plankton groups (net phytoplankton, mesozooplankton) will produce quickly sinking fecal material, relative to the slow sinking velocity microbial loop (microphytoplankton, microzooplankton) fecal material. In fact, approximately 25% of the carbon fixed in the upper ocean sinks to the ocean interior (Falkowski *et al.*, 2000; Laws *et al.*, 2000).

The same reasoning applies to nutrient recycling, with lower efficiency in systems dominated by larger grazers (producing quickly sinking fecal material), relative to the slow sinking velocity of microbial grazer fecal material. Ultimately, the potential of fish production is also limited by the size characteristics of organisms at the bottom of the food chain (Ryther, 1969), which show that size really matters in plankton modelling.

Changes in the biological pump could also be responsible for large changes in atmospheric CO_2 due to changes in nutrient utilization efficiency in the high latitude oceans (Sarmiento and Toggweiler, 1984; Knox and McElroy, 1984; Siegenthaler and Wenk, 1984) or changes also in the balance between ecosystems dominated by calcitic or siliceous organisms (Archer and Maier-Reimer, 1994). Calcium carbonate ($CaCO_3$) shells sink into the ocean interior where some fraction dissolves, leading to a decrease in the surface concentration of dissolved inorganic carbon (DIC) relative to the deep ocean

(the "carbonate pump"). Precipitation of carbonates lead to an increase of partial pressure of CO_2 in the surface ocean. Hence, on time scales of centuries while the carbonate pump lowers DIC concentrations, it simultaneously leads to the release of CO_2 from the ocean to the atmosphere, suggesting size distribution of phytoplankton as a major controller of recycling efficiency and carbon export from the surface ocean, a fundamental variable in climate change.

Yakushev (1998) pointed out the importance of the different "biological pumps" in the carbon cycle during the phytoplankton bloom as CO_2 uptake causes an imbalance in the equilibrium of the carbonate system, which can trigger the activity of "other pumps" like, for instance, "carbonate pump" and the "solubility pump" (a term that refers to the removal of CO_2 to ocean interior by physical processes). The dynamics of the carbon cycle are ruled by complex processes such as the ones described in the following table (adapted from Yakushev, 1998) which clearly shows the difficulties in the study of the carbon cycle.

Process	**Rate Estimates**
Ocean–atmosphere gas exchange	Tens of seconds
Hydrolysis and carbonate system changes	Tens of seconds
Synoptic eddies and turbulence	days-year
Chemical-biological processes	days-year
Advection and turbulence (surface waters)	several years
Anthropogenic CO_2	30-40 years
Advection and turbulence (deep waters)	100-1000 years
Overturning and thermohaline circulation	100-1000 years
Sedimentation	>10000 years

Modelling diatoms as part of the plankton groups involved in sinking particles is of particular interest. First, they are large organisms that seem to dominate the spring blooms in temperate areas such as in the North Atlantic. When diatoms are grazed by

zooplankton, they are packaged into fecal pellets which will be excreted into the ocean and will also sink fast into deeper waters. Second, transparent exopolymer particles (TEP) play an important role in the aggregation of "marine snow" and act as promoters of particle flux. Such TEP-promoted export has been described mainly for diatom blooms (Jackson, 1995). Third, the relative production rates of calcite and organic carbon can affect significantly the pH of the ocean and the pCO_2 of the atmosphere (Archer and Maier-Reimer, 1994). The balance between organic carbon and calcite could easily be perturbed by shifting globally from calcitic (coccolithophorid) production towards siliceous (diatom) based ecosystems. This shift seems to be controlled by temperature and dissolved silicate (Lisitzin, 1967) as well as by dissolved iron as suggested by recent field experiments (SOIREE – Southern Ocean Iron Release Experiment; see Hannon *et al.*, 2001; Boyd and Law, 2001). The partitioning between calcitic and siliceous based ecosystems could be a key component to predicting the long-term ocean carbon cycle. However, the details of this are not clear and prediction of the calcite/silicate ecosystem response of the upper ocean to changes in climate and ocean circulation are issues that need to be investigated.

Finally, in addition to their alleged long-term effect on atmospheric CO_2, the functional characteristics of phytoplankton production can also be significant to trace gases such as dimethyl sulfide (DMS), produced in high concentrations by dinoflagelates and prymnesiophytes and also by diatoms in smaller quantities (Keller *et al.*, 1989; Martin *et al.*, 2001).

1.3 Biogeochemical modelling

Until recently, most ecosystem modellers have not introduced more biological and chemical diversity than found in classic models like those of Riley *et al.* (1949) or Steele

(1974) which were based on a simple three-stage foodchain: limiting nutrient (N) – phytoplankton (P) – zooplankton (Z). Simple NPZ models (such as Wrobleski, 1989; Denman and Gargett, 1995) have shown the ability to reproduce patterns of seasonal plankton variability in the ocean as well as their importance as a tool for exploring physical structure, parameter estimation, etc. However, synecological studies have demonstrated that the number of functional compartments must be larger, to include dissolved and particulate organic matter and the biological compartments which are responsible for its mineralisation in water (heterotrophic bacteria or microzooplankton). The size structure of the community (Vézina & Platt, 1987), the complexity of food web links (Frost, 1984; Goldman and Caron, 1985) and the activity of sea microbes (Ducklow *et al.*, 1986; Pomeroy and Deibel, 1986) are especially important contributors to particulate losses from the trophogenic zone.

Biogeochemical models have continued to develop rapidly over the past decade, expanding phytoplankton, zooplankton and nutrients themselves in a series of more relevant units (Fasham *et al.*, 1990; Moloney and Field, 1991; Taylor *et al.*, 1993), providing a better understanding of the ecological dynamics and laying the foundations for understanding the ocean's role in climate change. A significant number of model studies have been carried out in the North Atlantic, being specially relevant those of Taylor *et al.* (1993), Taylor *et al.* (1997), Marra and Ho (1993), Sarmiento *et al.* (1993), McGuillicuddy *et al.* (1995) and Fasham and Evans (1995).

Taylor *et al.* (1993) developed a complex mixed-layer plankton model to investigate spatial and temporal phytoplankton seasonal succession driven by differences in the physical forcing (mixed layer depth, solar irradiance and temperature). Their model included four classes of phytoplankton, three classes of heterotrophs (mesozooplankton grazing was modelled as an external forcing function), three nutrients (nitrate,

ammonium, silicate), dissolved organic matter (DOC) and detritus. It is one-dimensional as it includes a "thermocline" layer below the mixed layer. The model spatial variability was given by variation in the amplitudes of the model functions, different physical parameters and sub-thermocline nutrient concentrations and successfully reproduced the general features described by NABE observations.

Taylor *et al.* (1997) studied the seasonal and latitudinal dependencies of phytoplankton carbon to chlorophyll ratio using a one-dimensional model. The biological model has only two compartments (phytoplankton and nitrogen). The 1-D model has a prescribed mixed layer which is rescaled at different latitudes based on known values of summer and winter mixed layer depths at each latitude. Numerical simulations were performed at 0°, 25°, 35°, 47° and 60° N. They found that chlorophyll concentration predicted by the model was similar to observations at 35°, 47° and 60° N but unrealistically low at at 0°, 25° N. A possible explanation for the model's failure in those tropical and subtropical surface waters was the neglection of several potentially important sources of nitrogen input to the euphotic zone in those areas.

Marra and Ho (1993) applied a mixed layer model and a simple NPZ model to investigate the spring phytoplankton bloom. The physical model used was a one-dimensional bulk mixed layer model (as it assumes that the mixed layer acts as a uniform "slab") as described by Price *et al.* (1986) in which the criteria for vertical mixing is based on density profiles and bulk and gradient Richardson numbers. This model also obtained a good agreement with NABE observations and was able to reproduce the subsurface chlorophyll maximum, observed in field data, by assuming photoinhibition on phytoplankton growth above a certain irradiance value.

The work of McGuillicuddy *et al.* (1995) introduced an eddy resolving coupled physical-

biological model, with a fully coupled surface boundary layer. The biological model consisted of four compartments (nitrate, ammonium, phytoplankton and heterotrophs). Model results were compared with two time series of observations taken from different water masses. This model overpredicted phytoplankton biomass, underpredicted primary production (PP) and was not able to match the chlorophyll vertical structure seen in the NABE data. The authors suggested several reasons for this behaviour such as photoadaption by cells in the real ocean, changes in species composition and/or a change in the C:N and C:Chl Redfield ratios amongst others.

Fasham and Evans (1995) addressed the issue of non-linear optimisation techniques in ecological modelling (see next section). They chose a seven compartment model (nitrate, ammonium, DON, phytoplankton, zooplankton, bacteria and detritus) to fit a time series observations derived from all the available data from the NABE site, considering spatial variability as noise superimposed on the seasonal cycle. The mixed layer depth was prescribed based on climatic values from Levitus (1982) and NABE observations. A total of 28 parameters were needed. Overall, this approach was incapable of fitting the whole observation set simultaneously. The authors pointed at the use of more complex models or models involving other nutrients (such as silicate) as a means to investigate the improvement of their results.

The first 3-D modelling approach embedding an ecological model (Fasham *et al.*, 1990) into a general circulation model (GCM) was taken by Sarmiento *et al.* (1993). The model predicted chlorophyll was compared with observations from the Coastal Zone Color Scanner (CZCS), showing that the model was able to realistically respond to different physically forced environments. The ecosystem model was resolved down to 123 m and calibrated with observations from Bermuda Station S. High pigment concentrations were found where supply of nitrate was high (subpolar and northern subtropical gyres) and low

pigment concentrations where nitrate was low (southern subtropical gyre) as observed in the CZCS data. Major disagreement between CZCS and model were found in the Gulf of Guinea and the interior of the equatorial region.

1.4 Coupled bio-physical models

It is well known that physical processes play an important role in marine ecosystem dynamics (Mann and Lazier, 1991) and can modify or limit biological production through the nutrient supply and the irradiance field (McClain *et al.*, 1990; Mitchell *et al.*, 1991). The seasonal variation in the mixed layer depth (Evans and Parslow, 1985) and the turbulent fluxes through the seasonal thermocline turn out to be among the most significant physical phenomena for understanding the patterns and timing of biological productivity. Therefore, the physics of mixing and light transmission are the main drivers of the ecosystem dynamics in the upper ocean. The depth of surface momentum and buoyancy flux driven mixing are predictable using physical models, if meteorological conditions at the sea surface are known. Primary production is mainly controlled by the depths of turbulent mixing as well as to the depth of sunlight penetration (the "euphotic zone"). The mixing time of waters within the mixed layer is fast compared to plankton motility which means that, when the mixed layer depth is greater than some critical depth (the "Sverdrup depth"), the rate of photosynthesis is light limited. Sverdrup (1953) showed that if thermal stratification drives the shoaling of the mixed layer to shallower depths than the critical depth (which usually happens in spring), the phytoplankton bloom is triggered. Being able to reproduce a mixed layer depth that is right is a key issue not only in terms of light availability but also in terms of nutrient supply. Nutrients are brought into the euphotic zone by the exchange between nutrient-depleted surface water and nutrient-rich deep water. Current understanding of this matter is not yet clear as rates of mixing

required to balance nutrient uptake estimates appear to be higher than values predicted by turbulent studies (Archer, 1995). There is some evidence suggesting that episodic mixing events, driven by frontal and mesoscale motions, might be able to explain a significant fraction of vertical nutrient transport (Archer, 1995). Thus, fluctuations in the mixed layer depth drive phytoplankton variability which motivates the coupling of ecosystem dynamic models with models of physical mixing.

In the previous section, several 1-D models were described but only 2 of them (McGuillicuddy *et al.*, 1995 and Marra and Ho, 1993) were vertically-resolved physical models. Other 1-D approaches include work from Varela *et al.* (1992), Kawamiya *et al.* (1995), Prunet *et al.* (1996), Kühn and Radach (1997) and Waniek (2002).

Varela *et al.* (1992) aimed to model the deep chlorophyll maximum (DCM) in two oligotrophic regions (Sargasso Sea and Mediterranean) using a biological model that considers two types of primary producers, heterotrophs and atmospheric as well as internal nitrate inputs. Model results were able to reproduce the DCM structure (depth and magnitude), which was mainly determined by the vertical eddy diffusion and light extinction. The grazing parameters affected the intensity of the DCM. This suggested that DCM is primarily the result of a balance between upward nutrient flux and light field characteristics, regenerated production playing a secondary role.

The work of Kawamiya *et al.* (1995) described a seven compartment biological model (phytoplankton, zooplankton, nitrate, ammonium, particulate organic nitrogen, dissolved organic nitrogen and dissolved oxygen) coupled to a mixed layer model applied to Station Papa. The coupled model had 28 layers. The first 20 layers were 5 m thick and the remaining 8 layers had varying thickness (from 10 m to 60 m). Model depth was 240 m. The mixed layer scheme was of the type Mellor and Yamada level 2 closure scheme

(Mellor and Yamada, 1982). Overall, the model showed reasonable agreement with the observations, although it failed to reproduce a phytoplankton bloom in autumn/winter and overestimated surface nitrate.

Prunet *et al.* (1996) also applied their coupled model to Station Papa. The physics of the mixed layer were modelled following Gaspar *et al.* (1990) and the ecosystem model was a NPZD plus total dissolved inorganic carbon and alkalinity. After assimilating surface chlorophyll, nitrate and sea surface temperature, model results gave a good fit to the seasonal cycle of surface chlorophyll (tested using independent chlorophyll and nitrate data). They also found that adjusting the C:N ratios was necessary to reproduce the observed surface pCO_2 concentrations.

The work of Kühn and Radach (1997) was applied to the North Sea. The physical model uses a second-order turbulence closure model developed by Mellor and Yamada (1982) while the biological model is a depth-resolved version of the Fasham *et al.* (1990). As the parameter set employed by Fasham *et al.* (1990) did not yield satisfying results, a new parameter set adapted to the North Sea was employed. This way, the model was able to hindcast the onset, duration, magnitude and daily variability of the primary production, the magnitude of the particulate organic nitrogen export flux to the bottom of the ocean as well as bacterial production and nitrogen regeneration in the mixed layer.

Waniek (2002) employed a NPZD model with a fast and a slow detritus compartment to study the interannual variability in the onset of the phytoplankton bloom in the North Atlantic, from 1989 to 1997. The physical model used the Kraus and Turner (1967) mixed layer scheme. Her model focused in the mixed layer, where model results agreed well with chlorophyll and nitrate observations.

In all these cases, simple ecosystem models were tested as sophisticated models require

large amount of computer time and can be almost as difficult to understand as the real system. Consequently, simplified models also play a very important role in studies of plankton dynamics. Indeed, most of our understanding of how the marine ecosystem works has come from studies with simplified models. However, as stated in previous sections simple models present serious limitations in order to understand differential particle sinking, primary and export production amongst other processes.

1.5 Optimisation and data assimilation

For the reasons explained in earlier sections, much scientific effort has been spent in developing robust ecosystem models for the ocean. However, there are two major problems when modelling the ocean ecosystem. The first one is the lack of a universal set of equations (as opposed to the Navier-Stokes equations of fluid dynamics) describing the ocean ecosystem. The second problem, is the need of a large number of parameters (great uncertainty is associated to most of them) to describe the ecosystem components accurately, which strongly constrains the model applicability. Although some of these parameters can be experimentally estimated, there is a general lack of many others due to the difficulty involved in their measurement such as, for instance, natural mortality rates. Until recently, most modellers used empirical parameters when available and then, adjusted the remaining set until a satisfactory result was achieved. There are obvious problems with such approximations but one of the most important is the uncertainty as to whether a model's failings are due to inadequacies in its structure or to an inaccurate set of parameters. In order to deal with this problem, data assimilation and optimisation methods, borrowed from physical sciences (Parker, 1977; Wunsch, 1978), have started to be applied in ecological modelling in the last decade so as to fit model results to data, to better determine model parameters (Matear, 1995; Hurt and Armstrong,

1996 among others) as well as to merge information from empirical data with theoretical models. Both techniques rely on the availability of biological measurements, which are in itself a source of model limitation. Most measurements come from data taken on board oceanographic vessels, which are limited temporally and spatially. There are time series available from several sites such as Ocean Station Papa (Tabata and Weichselbaumer, 1992) and the Hawaii Ocean Time-series (HOTS; Karl and Lucas, 1996) in the Pacific, or the Bermuda Atlantic Time Series (BATS; Michaels *et al.*, 1994) in the Atlantic. There are also experiments which focus on a particular feature of the biogeochemical system, such the North Atlantic phytoplankton bloom, theme of the North Atlantic Bloom Experiment (NABE; see Ducklow and Harris, 1993). Another problem is the variables that need to be measured. Although variables such as chlorophyll, nitrate or ammonium and fluxes such as primary production have been sampled on a regular basis, other important ones such as zooplankton and bacterial biomass are more often than not missed. Very rarely size-dependent variable sampling is carried out. The recent development of remote sensing techniques for ocean color (SeaWiFS- Sea-viewing Wide Field-of-view Sensor; see Hooker and Esaias, 1993) provide measures that allow to derive surface chlorophyll on a global rather than regional scale, which can be assimilated into ecological models.

Data assimilation as well as optimisation techniques in biological models are starting to develop, as yet no consensus on what the best technique has been reached yet. The formalism can process eclectic data on food web structure and dynamics (standing stocks, flux rate measurements, physiological constrains, etc.) and generate estimates of the flows of several elements (for instance, carbon and nitrogen) simultaneously. The solution ensures internal consistency and allows for uncertainties and redundancies in the data (Vézina & Platt, 1988).

In this introduction we will give an overview of the most relevant work carried out up to

date. Basically, the work of Fasham and Evans (1995), Lawson *et al.* (1995, 1996), Matear (1995), Prunet *et al.* (1996), Spitz *et al.* (1998), Fennel *et al.* (2001), Schartau *et al.* (2001) and Vallino (2000).

Fasham and Evans (1995) used a nonlinear optimisation technique (Powell's conjugate direction method) to fit a wide range of NABE data (see previous section). The model had seven compartments and 28 parameters. Their penalty function measured the misfit between model results and observations as well as determined the best parameter set leading to such fit. Different observations were given different weights in order to improve the fit but nevertheless, it was not possible to get a good fit to all data.

Prunet *et al.* (1996) used a variational assimilation technique in a 1-D coupled physical-biogeochemical model (described in section 1.4), in which surface chlorophyll, nitrate and sea surface temperature were used simultaneously. They found that assimilation of chlorophyll alone only partially constrained the model parameters. However, surface temperature was able to constrain vertical diffusion below the mixed layer while nitrate represented a strong constraint on the balance between vertical diffusion and particle sinking rate.

The work of Lawson *et al.* (1995, 1996), Spitz *et al.* (1998), Fennel *et al.* (2001) and Schartau *et al.* (2001) applied an adjoint technique to the assimilation of data into an ecological model. Lawson *et al.* (1995) based their experiments on a simple predator-prey model whereas a 5 compartment model (phytoplankton, zooplankton, nitrate, ammonium and detritus) was tried by Lawson *et al.* (1996). In both cases, twin experiments were used to test the efficiency of the model to recover parameters and model initial conditions.

Twin experiments consist of model-generated observations that will be considered as the

'real world'. That is, they can be sampled sparsely, following the frequency of data collection usually taken in scientific cruises in order to get a known set of observations from this scenario to feed into the ecological model. This way, one has the certainty of using a data set consistent with the model, free of random and/or measurement errors and expressed in the same units as the model results.

Lawson *et al.* (1996) found that the efficiency of their model was dependent on the frequency and type of data assimilated. Bi-weekly data gave better recoveries than monthly ones, whereas weekly data provided no significant improvement. When zooplankton information was available, in addition to phytoplankton data, the parameter recovery rate was improved, even when data were more widely spaced in time. The model ability to recover episodic events was dependent on the timing of the sampling relative to the event, rather than to the sampling frequency.

The experiments of Spitz *et al.* (1998) focused on the fit of the Fasham *et al.* (1990) model to observations collected at the BATS site. They performed twin experiments, using simulated data matching type and frequency of BATS observations, to show the capability of the observations to estimate model parameters as well as the ecosystem annual cycle. They concluded that the model was not appropriate for the annual cycle of the BATS ecosystem as they assumed a constant nitrate concentration below the mixed layer when vertical profiles of nitrate observations at BATS show a linear variation with depth below 100m.

The modelling studies carried out by Fennel *et al.* (2001) were based on a NPZD model. They calculated and analysed a posteriori errors for the estimated parameters by calculating the Hessian matrix. An optimisation technique was applied to nitrate and chlorophyll data collected at BATS and due to its poor performance concluded that the

features of the BATS ecosystem were unresolved in their model.

Schartau *et al.* (2001) applied a NPZ model, as proposed by Evans and Parslow (1985), to the BATS site. Once again, twin experiments (with and without added noise) were performed. Model results showed that the model was not adequate for this site, either.

A simulated annealing (SAN) technique was employed by Matear (1995) to fit three different ecosystem models (NPZ, NP plus micro and mesozooplankton and the 7 compartment model of Fasham *et al.*, 1990) to data from Station P. The major advantages of this technique, *versus* any of the techniques discussed earlier, are its independence of the initial guess (which is randomly performed) and that they provide a globally optimised parameter set, whereas the previous techniques might be easily trapped in a local optimal solution (of which there could be more than one, depending on the initial guess chosen). He also calculated the Hessian matrix. Matear concluded that the simplest model successfully reproduced the observations and that additional data (such as ammonium and bacteria biomass) were required to justify the use of a more complicated model.

A thorough study on data assimilation techniques applied to ecosystem models can be found in Vallino (2000). He used data assimilation to find the optimum set of parameter values that minimised differences between model output and observations. The model had 10 compartments: autotrophs, heterotrophs, dissolved inorganic nitrogen, dissolved labile organic carbon and nitrogen, dissolved refractory organic carbon and nitrogen, detrital carbon and nitrogen and bacteria. Data collected from marine mesocosms experiments were used as observations. A total of 12 different algorithms were tested, 4 of them attempted to locate the global minimum (SAN, genetic algorithms (GA), quasi-Newton methods and stochastic differential equations) and 8 algorithms only able to

determine local minima (Truncated Newton, several quasi-Newton, Levenberg-Marquardt and Powell's conjugate gradient). SAN located the minimum with the smallest penalty function but was computationally very expensive, while the remaining global techniques did rather poorly. Local optimisation routines such as Powell's, Levenberg-Marquardt and the adaptative Newton scheme did almost as well as SAN, but were computationally cheaper to run.

1.6 About this work

For the reasons explained in previous sections, the work presented in this thesis focuses on a size-dependent, 0-D and 1-D, biogeochemical model employed to study the pelagic ecosystem in the North Atlantic at 47°N 20°W. The ecological model consists of eight compartments (diatoms, non-diatoms, micro and mesozooplankton, nitrate, ammonium, silicate and detritus) and is thoroughly described in chapter 2. The application of an optimisation technique, based on Powell's algorithm (Press *et al.*, 1992), is used to explore the model parameter space and to test the model ability to fit observational data, as is also presented in chapter 2. The observations set was obtained from measurements taken as part of the North Atlantic Bloom Experiment (NABE) at 47°N 20°W. They comprised total chlorophyll, diatoms biomass, meso and microzooplankton biomass, nitrate, ammonium, silicate as well as total primary production and were taken in 1989. Model calibration and fit to observations are also included in chapter 2.

In chapter 3, a series of twin experiments are outlined. Such experiments were performed so as to explore the feasibility of using sparse observations to estimate model parameters and to reproduce the ecosystem annual cycle in the North Atlantic. A brief synopsis of all the experiments carried out is given, as well as the results obtained.

The uncertainty associated to the model parameter space is explored in chapter 4, looking at the analysis of the Hessian matrix as well as the sensitivity of the model to the time stepping technique used.

After testing the ecological model and estimating its correspondent parameters, the model was embedded into a 1-D physical model (a simplified version of the Miami Isopycnic Co-ordinate Ocean Model), which is described in chapter 5.

Chapter 6 looks at the different aspects inherent to the coupling process. It describes 0-D model adaptations necessary to obtain an accurate representation of the biogeochemical processes of interest. It also describes the one-dimensional coupled-model tuning and validation. The coupled model was tuned to the 1989 NABE observation set while model validation was carried out using an independent data set (only comprising total chlorophyll, nitrate, ammonium, silicate and particulate organic matter) obtained during autumn in 1996 at 47°N 20°W, as part of the German Joint Global Ocean Flux Study (JGOFS) phase.

Chapter 7 investigates the biogeochemical intra and interannual variability of the one-dimensional model, as a response to changing environmental conditions, over a nine-year period (from 1988 until 1996) and describes methodological problems encountered.

As the tuning of the one-dimensional model highlighted the inadequacy of some biological parameters, a sensitivity analysis, described in chapter 8, was performed.

Finally, a summary of the main conclusions obtained in this study and suggested future work is given in chapter 9.

Chapter 2:

The 0-D Ecosystem Model

Chapter 2: The 0-D Ecosystem Model

2.1 Introduction

The ecosystem model used in this thesis is based on the model originally developed by Fasham, Ducklow and McKelvie (Fasham *et al.*, 1990), hereafter referred to as FDM, initially built to model the annual plankton cycle within the upper ocean mixed layer at Station "S" near Bermuda. FDM model has been widely used in previous studies not only in Bermuda (Lawson *et al.*, 1996; Spall, 1997; Spitz et al., 1998) but also in the North Atlantic (Fasham and Evans, 1995; Spall, 1997; Fasham and Evans, 2000), in the Pacific at station P (Matear, 1995) and is one example of an ecological model incorporated into an ocean general circulation model (Fasham *et al.*, 1993).

2.2 The Model Description

The model described here is more complex that FDM. It is a 0-D mixed-layer model, based on nitrogen and which includes size-dependence to describe the seasonal variation of the phytoplankton and zooplankton biomass, nutrient concentration as well as primary production in the open ocean.

Eight compartments were defined in order to model the nitrogen cycling within the mixed layer: diatom (P_d) and non-diatom (P_{nd}) phytoplankton, mesozooplankton (Z_m), microzooplankton (Z_{mi}), nitrate (N_n), ammonium (N_r), silicate (S) and detritus (D) (see figure 2.1). Phytoplankton growth rate depends on photosynthetically available radiation (PAR) and nutrients. Microzooplankton grazes on non-diatom phytoplankton while mesozooplankton is assumed to graze on diatoms and microzooplankton . The distinction between ammonium and nitrate allows primary production to be partitioned into new

production (fuelled by nitrate) and regenerated production (fuelled by ammonium) (Dudgale and Goering, 1967).The model recycles nitrogen in the form of ammonium via zooplankton in addition to the recycling of phytoplankton losses.

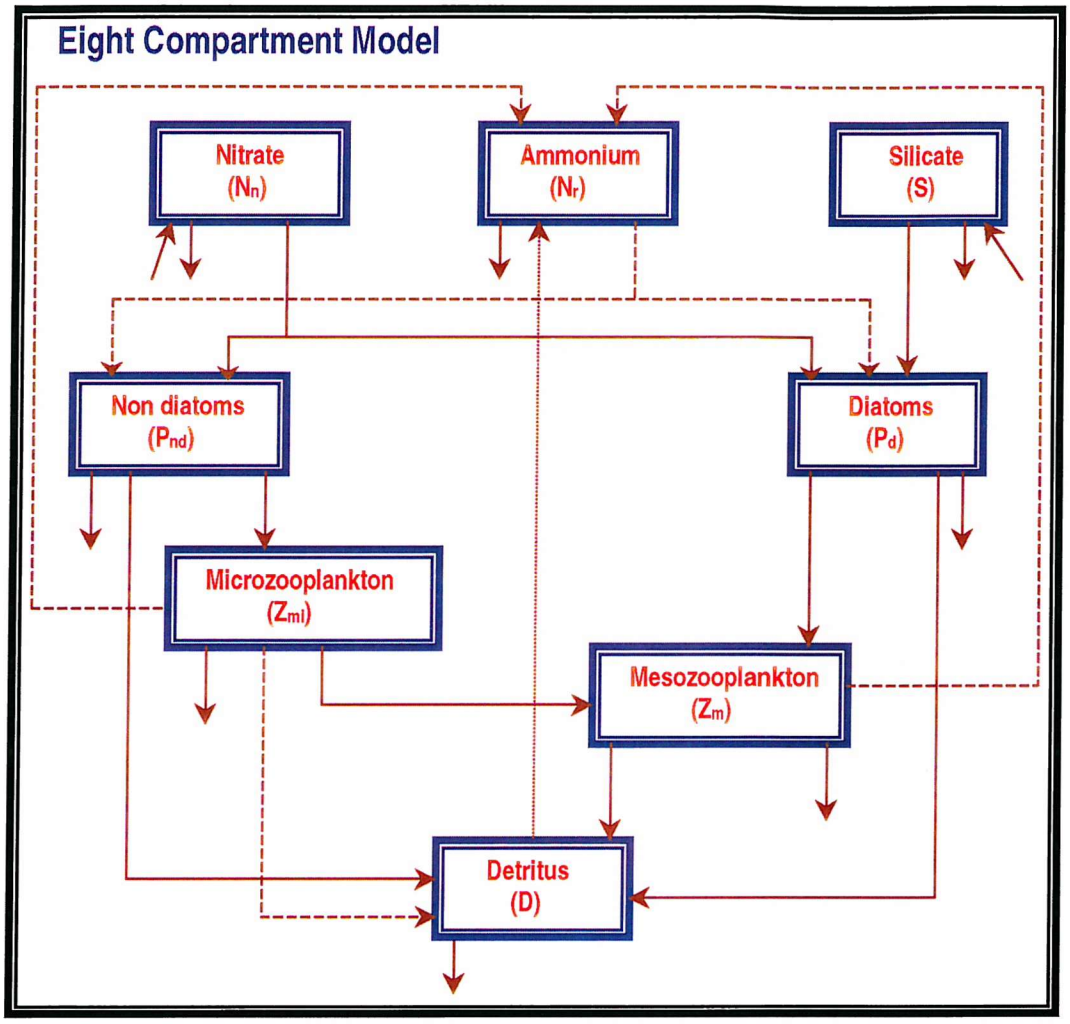

Figure 2.1: Schematic diagram of the ecological model

Although heterotrophic bacteria can play an important role in nutrient remineralisation within the mixed layer as part of the microbial loop (Azam *et al.*, 1983; Taylor and Joint, 1990), they have not been explicitly modelled. Bacteria's role in terms of nutrient remineralisation has been indirectly modelled by a slow detrital sinking rate and a high detrital dissolution rate.

Horizontal advection and diffusion were ignored and the pelagic ecosystem consisted of an homogeneous mixed layer, where phytoplankton and zooplankton were assumed to be confined and homogeneously distributed, overlying a deeper abiotic layer (Steele, 1974). The seasonal varying mixed-layer depth (MLD) is specified in advance based on data provided by the North Atlantic Bloom Experiment (NABE) for spring and summer as well as climatic mixed layer depths (Levitus 1982) for the rest of the year, to define its seasonal change as a function of time, and to force the model with an observed annual cycle. Depths were interpolated between given values, in order to obtain a datum corresponding to the varying time step of the model, using polynomial interpolation (Press *et al.*, 1992). Therefore, ecosystem seasonality is driven by changes in mixed layer depth as well as changes in the incident photosynthetically available radiation.

Following Evans and Parslow (1985) the effect of mixed layer changes on state variables was modelled by:

$$\frac{dM}{dt} = h(t) \qquad [2.1]$$

where M represents the mixed layer depth and $h(t)$ is the temporal change of the mixed layer depth. They suggested that the effect of mixed layer changes is different on state variables describing motile and non-motile organisms. In the case of motile organisms like zooplankton, it is assumed that they are able to swim and maintain their position within the mixed layer depth so its volumetric concentration will decrease or increase with increasing or decreasing mixed layer depths. In the case of non-motile organisms, like phytoplankton, nutrients and detritus, their volumetric concentrations will decrease when a deepening in the mixed layer depth occurs while they will not change when the mixed layer depth shallows.

Evans and Parslow dealt with this asymmetry using $h^+(t)$ instead of $h(t)$ in equations representing non-motile organisms, which is defined as:

$$h^+(t) = [0, h(t)] \quad [2.2]$$

All the state variables in the model are expressed in mmol N m^{-3}. In order to convert units between silicate (Si) and nitrogen (N) a constant N:Si Redfield ratio (Re) was used (see table 2.1 for symbols and units and table 2.2 for parameter values).

2.3 The Model Equations

2.3.1 Non-diatoms

The dynamics followed by non-diatoms are described by the following equation:

$$\frac{dP_{nd}}{dt} = \sigma_1(t,M,N_n,N_r)P_{nd} - G_1 - \mu_1 P_{nd}^{\ 2} - \frac{[m + h^+(t)]P_{nd}}{M} \quad [2.3]$$

where $\sigma_1(t,M,N_n,N_r)$ is the average daily phytoplankton specific growth rate, G_1 represents microzooplankton grazing, μ_1 is the specific natural mortality rate, m is mixing velocity (0.1 m d^{-1}) and parameterizes processes that affect mixing of organisms across the pycnocline such as breaking internal waves, diurnal convective mixing, intermittent storm events and upwelling due to Ekman suction and $h^+(t)$ has been defined above (see table 2.2).

Non-diatoms mortality rate has been modelled by a quadratic function which enhances phytoplankton losses with a rapid increase in biomass. It represents aggregation processes as modelled by Doney *et al.* (1996).

Phytoplankton growth rate depends on photosynthetically available radiation (PAR), the relationship photosynthesis-irradiance as well as on the nature of nutrient limitation. Light and nutrient limitation are independent and their effect on non-diatoms cells growth is given by:

$$\sigma_1(t,M,N_n,N_r) = J(t,M)Q(N_n,N_r) \quad [2.4]$$

where $J(t,M)$ is the light limited growth rate at time t and depth M and $Q(N_n, N_r)$ is the nutrient limitation factor.

$J(t,M)$ is calculated based on the method described by Evans and Parslow (1985) who assumed that the time spent by a particular cell at a given depth is long compared to the photosynthesis reaction time, but short compared to the cell division time. This assumption allows to calculate the total daily growth rate by integrating the PAR over the length of the day and the depth of the mixed layer depth:

$$J(t,M) = \frac{2}{M}\int^{\tau}\int^{M} F[I_o(t)e^{-K_d}]dzdt \qquad [2.5]$$

where 2τ is the day length, F is a function describing the photosynthesis-irradiance curve depending on the maximum photosynthetic or growth rate (P_{max}) and the initial slope of the P-I curve (α), I_o is the PAR at the surface and K_d is the light attenuation coefficient which varies with depth according to:

$$K_d = [K_w + (P_d + P_{nd})K_p]M \qquad [2.6]$$

in which K_w represents the light attenuation coefficient due to water (0.04 m^{-1}), K_p is the light attenuation coefficient due to phytoplankton and P_d and P_{nd} are diatom and non-diatom phytoplankton, respectively.

Although in this work we have opted for Beer's law (equation 2.5) to model the attenuation of light with depth, there are other model approaches that could have been adopted. Taylor *et al.* (1991) used a double exponential to differentiate between red and blue wavelenghts, as the former are rapidly absorbed in the upper 10 m of the ocean whereas the latter are absorbed more slowly. A more complex approach was that of Anderson (1993) who developed a complex spectral model divided into a large number of wavebands. However, this work uses the approach taken by Fasham *et al.* (1990) as it has provided good results in numerous ecosystem models.

I_o is calculated as follows:

$$I_o = I_s(1-0.7C)T\ q \qquad [2.7]$$

where C represents the cloudiness as a constant fraction (0.75), T is transmittance (0.75) at the surface, q is the fraction of PAR respect to the total irradiance (0.5) and I_s is the irradiance coming onto the surface of the ocean (Brock, 1981; Peixoto & Ooit, 1992):

$$I_S = \int_0^{\pi} S[\cos\delta\ \cos\Phi\ \cos(sunset) + \sin\delta\ \sin\Phi] = S[\cos\delta\ \cos\Phi\ \sin(sunset) + \sin\delta\ \sin\Phi sunset] \qquad [2.8]$$

where S (884 ly) is the solar constant, δ is the declination, which in the northern hemisphere is given by:

$$\delta = -0.409\cos\psi \qquad [2.9]$$

where ψ is the date expressed as an angle in radians (2π *day /365) and *sunset* is the total amount of daylight calculated as:

$$sunset = 2\tau = \frac{1}{2\pi} arccos[-\tan(\delta)\tan(\Phi)] \qquad [2.10]$$

where Φ is latitude in radians (degrees of latitude * $2\pi/360$).

The nutrient limitation is described by using $Q(N_n, N_r)$, a dimensionless factor that was modelled following a Michaelis-Menten approximation. The inhibiting effect of ammonium on nitrate uptake must be considered as pointed out by Dortch (1990). Phytoplankton will preferentially take up ammonium instead of nitrate, when the first is present in significant concentrations and it has been parameterized as suggested by Wroblewski (1977).

$$Q(N_n, N_r) = Q_1(N_n, N_r) + Q_2(N_n, N_r) = \frac{N_n e^{-\psi_1 N_r}}{K_1 + N_n} + \frac{N_r}{K_2 + N_r} \qquad [2.11]$$

where ψ_1 is a constant representing the inhibition of nitrate uptake by ammonium and K_1 and K_2 are the half-saturation constants for nitrate and ammonium uptake, respectively. The inhibiting effect of ammonium is strongly dependent on ψ_1 and this parameter should never be zero. However, it is worth noting that the optimisation technique used in section 2.5 constrains parameters between a lower and an upper limit. In this case, ψ_1 lower limit was set to zero but its optimised and initial values are never less than 3.35 $(\text{mmol m}^{-3})^{-1}$ as shown in tables 2.2 and 2.3. The same reasoning applies to ψ_2 in equation 2.14.

2.3.2. Diatoms

Diatoms are subjected to the same dynamics followed by non-diatom phytoplankton. The differences between them is found in terms of parameters, sinking rate and nutrient limitation as the importance of silicate, as a new nutrient to be modelled, has to be considered:

$$\frac{dP_d}{dt} = \sigma_2(t, M, N_n, N_r, S)P_d - G_2 - \mu_2 {P_d}^2 - \frac{[m + Sink + h^+(t)]P_d}{M} \quad [2.12]$$

For this reason, one more term must be added to the equation describing nutrient limitation, which will read as follows:

$$\sigma_2(t, M, N_n, N_r, S) = J(t, M)Q_s(N_n, N_r, S) \quad [2.13]$$

$$Q_s(N_n, N_r, S) = [Q_{1d}(N_n, N_r) + Q_{2d}(N_n, N_r)]Q_3(S) = \left(\frac{N_n e^{-\psi_2 N_r}}{K_3 + N_n} + \frac{N_r}{K_4 + N_r}\right)\frac{S}{K_5 + S} \quad [2.14]$$

where K_5 is the half saturation constant for silicate uptake.

An alternative, and possibly better, nutrient limitation on diatoms could also have been modelled according to Liebig's law of the minimum which states that the total yield of

biomass of any organism will be determined by the nutrient present in the lowest (minimum) concentration. However, we decided to follow the approach taken by Droop (1973) and model nutrient limitation in terms of the multiplicative law (equation 2.14).

The effects of seasonal changes in the mixed layer depth were modelled as usual plus an extra sinking term for diatoms, according to the following equation (Pondaven, pers. com.):

$$Sink = S_{\max} \frac{K_5}{S + K_5} \quad [2.15]$$

where S_{max} is the maximum sinking rate, so the rate of phytoplankton sinking accelerates as nutrients are depleted.

2.3.3 Microzooplankton

Microzooplankton dynamics vary according to the following equation:

$$\frac{dZ_{mi}}{dt} = \beta_1 G_1 - \nu_1 Z_{mi} - \xi_1 Z_{mi}^2 - G_3 - h(t)\frac{Z_{mi}}{M} \quad [2.16]$$

where β_1 represents the assimilation efficiency on non-diatoms, G_1 is the specific ingestion rate of microzooplankton grazing on non-diatoms, ν_1 is the fraction of microzooplankton excretion that contributes to ammonium, ζ_1 is mortality and G_3 is mesozooplankton grazing on microzooplankton.

G_1 was parameterized as a Michaelis-Menten equation:

$$G_1 = g_1 Z_{mi} \frac{P_{nd}}{K_6 + P_{nd}} \quad [2.17]$$

where g_1 represents the microzooplankton maximum grazing rate and K_6 is the half-saturation constant for grazing.

The first term of equation 2.16 represents the assimilation efficiency of microzooplankton and its contribution to detritus. The second term is the contribution to the ammonium pool. The third term is derived from a quadratic function and represents microzooplankton mortality. The fourth term is microzooplankton grazing by mesozooplankton and the last term reflects the effects of seasonal changes in the mixed layer depth.

2.3.4 Mesozooplankton

The dynamic variation in mesozooplankton abundance is described in the same way than microzooplankton. The differences between them both are due to the multiple sources of food that mesozooplankton can take:

$$\frac{dZ_m}{dt} = \beta_2 (G_2 + G_3) - \nu_2 Z_m - \xi_2 Z_m^2 - h(t)\frac{Z_m}{M} \qquad [2.18]$$

The mesozooplankton growth rate (G_i) depends not only on diatoms but also on microzooplankton and it was modelled by using a non-linear switching function (Fasham *et al.*, 1990) according to the equation:

$$G_i = g_2 p_i Z_m \frac{I^2}{K_7 F + F_1} \qquad [2.19]$$

where $I = P_d, Z_{mi}$ corresponds to indexes $i = 2,3$ respectively; g_2 represents the maximum grazing rate, K_7 is the grazing half-saturation constant, F and F_1 are a measure of total food and p_i is the preference either for diatoms or microzooplankton.

$$F = p_2 P_d + p_3 Z_{mi} \qquad [2.20]$$

$$p_3 = 1 - p_2 \qquad [2.21]$$

$$F_1 = p_2 P_d^2 + p_3 Z_{mi}^2 \qquad [2.22]$$

The terms representing excretion, contribution to the ammonium pool, mortality and sinking are similar to the ones described in section 2.3.3 for microzooplankton.

2.3.5 Nitrate

The nitrate equation is:

$$\frac{dN_n}{dt} = -J(t,M)[Q_1(N_n,N_r)P_{nd} + Q_{1d}(N_n,N_r)Q_3(S)P_d] + (N_o - N_n)\frac{[m + h^+(t)]}{M} \qquad [2.23]$$

where the first term on the right hand side of the equation represents the uptake by phytoplankton and the second term represents the diffusive mixing of nitrate across the thermocline, N_o being the nitrate concentration below the mixed layer which was linearly modelled (Steele and Henderson, 1993) as:

$$N_0 = N_{nsurf} + N_{ngrad} M \qquad [2.24]$$

where $N_{n\ surf}$ represents the sub-surface nitrate concentration and $N_{n\ grad}$ is the vertical nitrate gradient (units are mmol N m^{-4}; see table 2.1).

2.3.6 Ammonium

The ammonium concentration in the model evolves according to:

$$\frac{dN_r}{dt} = -J(t,M)[Q_2(N_n,N_r)P_{nd} + Q_{2d}(N_n,N_r)Q_3(S)P_d] + (\upsilon_1 + \varepsilon\xi_1 Z_{mi})Z_{mi} + (\upsilon_2 + \varepsilon\xi_2 Z_m)Z_m + \\ + \delta D - N_r\frac{[m + h^+(t)]}{M} \qquad [2.25]$$

where the first term refers to uptake by phytoplankton. The second and third terms are due zooplankton excretion and mortality where the term ε gives the fraction of zooplankton mortality that is recycled to ammonium within the mixed layer. The remainder is exported directly from the mixed layer. The fourth term represents detritus contribution being δ its breakdown rate.

2.3.7 Silicate

The silicate concentration is similar to the nitrate equation:

$$\frac{dS}{dt} = -\frac{J(t,M)Q_3(S)[Q_{1d}(N_n,N_r) + Q_{2d}(N_n,N_r)]P_d}{Re} + (S_o - S)\frac{[m + h^+(t)]}{M} \qquad [2.26]$$

where *Re* represents the Redfield ratio (N:Si) and S_o is the silicate concentration below the thermocline which varies according to equation 2.24 but depending on S_{surf} and S_{grad}, the sub-surface silicate concentration and the vertical silicate gradient (units are mmol S m^{-4}; see table 2.1), respectively.

2.3.8 Detritus

The detritus equation is given by:

$$\frac{dD}{dt} = \mu_1 P_{nd}^2 + \mu_2 P_d^2 + (1-\beta_1)G_1 + (1-\beta_2)(G_2 + G_3) - \delta_1 D - D\frac{[m + h^+(t) + V]}{M}$$

[2.27]

where the first two terms represent the contribution of dead phytoplankton to the detritus pool, the third and fourth terms represent the egestion of fecal pellets due to micro and mesozooplankton grazing, δ_1 is the breakdown of detritus *(remineralisation)* and V is the detritus sinking rate.

2.4 The Observations

In 1989, the Joint Global Ocean Flux Study (JGOFS) conducted several cruises to study the phytoplankton bloom above 47°N in the North Atlantic, which constituted the so called North Atlantic Bloom Experiment (NABE) (Ducklow and Harris, 1993). The ecosystem model considered in this study was fit to NABE data due to the fact that this location (47°N 20°W) has been the site of intensive oceanographic and biological studies so an important background of data is available for this area. Different field measurements collected over 1989 on British cruises DI182, DI183, DI184, American cruises Atlantis II 119/4 and 119/5, German cruise Meteor 10/2 and Dutch Cruise Tyro were assimilated as observations into the model. The dates in which these cruises occurred as well as the data used in the model can be seen below and the data they provided are also shown in figure 2.2. In order to get modelled chlorophyll values to be compared with the observations, a constant 1.05 chlorophyll/nitrogen ratio was used.

Dates of cruises whose data have been used in this study collected at 47°N 20°W during 1989.

Cruise	Starting date	Finishing date
Atlantis II 119/4	24/04/89	09/05/89
Atlantis II 119/5	18/05/89	31/05/89
Discovery 182	08/05/89	08/06/89
Discovery 183	10/06/89	12/07/89
Discovery 184	14/07/89	14/08/89
Meteor 10/2	02/05/89	13/06/89
Tyro	22/08/89	25/08/89

Most measurements were taken on American cruises Atlantis I/II and German Meteor covering the spring bloom period. Other measurements were taken on British cruises Discovery 182/183 and 184 and also on Dutch Tyro later in the year (from July until August). Some variables were covered better than others. There are many observations available for diatoms, nitrate, silicate, chlorophyll and primary production. Microzooplankton observations were few and collected over four different cruises. Mesozooplankton data were only provided by German cruise Meteor but there is high variability within the data set. Ammonium observations were also scarce and data obtained from cruise Tyro are highly variable and inconsistent with Atlantis data.

To provide data comparison with the model, all values obtained for a given day were averaged within the mixed layer. Data have been converted to units of mmol N m^{-3} (or mmol N m^{-3} d^{-1} for primary production) using standard conversion constants (Fasham and Evans, 1995).

During the spring bloom nitrate and silicate concentrations declined rapidly due to phytoplankton uptake. Nitrate declines from 7 mmol N m^{-3} to less than 0.2 mmol N m^{-3}. On the other hand, silicate declines from over 2 mmol m^{-3} to less than 0.1 mmol m^{-3} (before nitrate does) parallel to an increase in diatoms from ca. 0.5 mmol N m^{-3} to a maximum value just over 2 mmol N m^{-3} (figure 2.2a). The increase in diatom biomass is also noticeable in the chlorophyll observations, reaching 2.5 mg chl m^{-3} (figure 2.2h). Diatoms start to decline as silicate is depleted.

Nitrate decline starts at the same time than silicate but it is not consumed as quickly (figures 2.2b and 2.2c). Nitrate is being removed from the water column after the diatom bloom has finished (presumably due to the development of non-diatom phytoplankton), being nearly depleted by Julian day 150. Chlorophyll data show the occurrence of a

second bloom (presumably a non-diatom bloom), after the diatom one, reaching chlorophyll values of ca. 3 mg chl m^{-3}. Microzooplankton data show an increase in their biomass from Julian day 130, reaching a maximum (over 0.8 mmol N m^{-3}) on Julian day 150, shortly after the second chlorophyll peak occurred (figure 2.2e). Unfortunately, nothing can be said regarding mesozooplankton biomass and diatoms as mesozooplankton observations are highly variable (figure 2.2f).

Sieracki *et al.* (1993) studied the nutrient availability and physical conditions during the onset of the spring bloom and they concluded that the rapidly silicate depletion that occurred before nitrate depletion coincided with a shift in dominant phytoplankton from diatoms to small flagellates.

In terms of primary production, intercalibration exercises were carried out among Atlantis II, Meteor and Discovery 182. Possible Zinc contamination was detected on measurements coming from British and German cruises and, for this reason, only Atlantis data were used for the April-May period. Primary production observations show the same pattern than chlorophyll data (figures 2.2g and 2.2h) and Lochte *et al.* (1993) suggested that the first bloom was dominated by diatoms while other phytoplankton groups were more important primary producers when silicate was depleted. According to Lochte *et al.* (1993), the decline in chlorophyll is partly due to seasonal development but also might have been influenced by the existence of cyclonic eddies in the area at the time that this study took place (Robinson *et al.*, 1993).

For the rest of the sampling period (July and August), nitrate and silicate concentrations remained below 0.5 mmol m^{-3}. Chlorophyll data for this period shown concentrations up to 1 mg m^{-3} whereas primary production was less than 0.4 mmol m^{-3} d^{-1}.

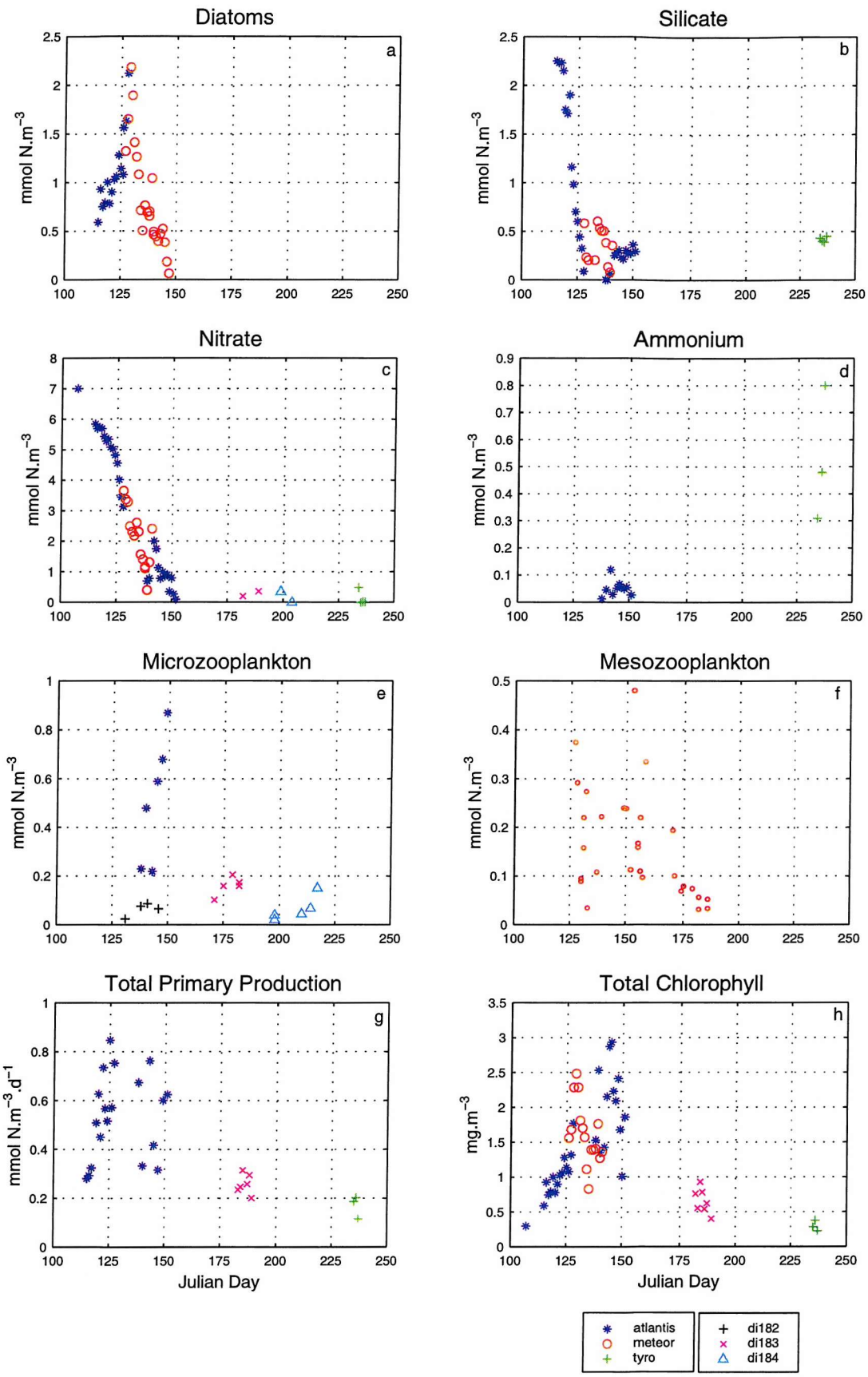

Figure 2.2: Observations available from NABE cruises during 1989.

2.5 The Optimisation Module

The traditional approach to parameterising an ecosystem model is to take parameter values from relevant studies from the literature, when available, and then adjust the rest of the parameters until a good agreement between the model and the observations set is achieved. Although it can seem rather simple, there are, at least, three major drawbacks to this approach. First, it is often difficult to find a good fit when a large set of parameters is involved and many parameters like, for instance, natural mortality rates are almost impossible to measure accurately. Second, when a model does not fit the data it is rarely clear whether it is the model's structure or the parameter values that are at fault. The third is that literature studies rarely yield unambiguous values for model parameters (Hurtt and Armstrong, 1996). Those problems have been approached here by using an optimisation technique to determine model parameters from the data. The optimisation provides a set of objective ecosystem model parameters that is most consistent with the available information.

The use of non-linear optimisation techniques have proven to be successful in fitting ecosystem models to observations at different locations like station P (Matear, 1995), the North Atlantic (Fasham and Evans, 1995) and Bermuda (Hurtt and Armstrong, 1996) when modelling the seasonal cycle of plankton dynamics.

Following Fasham and Evans (1995), hereafter referred to as FE95, we have used a conjugate direction-set algorithm based on Powell's method (Press *et al.*, 1992) to deduce unknown parameters from a set of observations (NABE) and the ecosystem model described above (sections 2.3 and 2.4).

The present work differs from FE95 in the model complexity. FE95 used a model with no size-dependency but especifically modelled the microbial loop by including bacteria and dissolved organic nitrogen. This study does not explicitly model the microbial loop, but focuses on the role played by different phytoplankton and zooplankton groups. Our model also involves a larger number of parameters and increases the difficulties in finding a good estimate of the best model solution in terms of good fit to the real observations and also realistic parameter estimation.

Although the method has been extensively described in Evans (1999), I will explain its basic features.

The basic idea of the method is to choose a set of conjugate set of directions or 'non-interfering' directions such that a minimisation conducted along one search direction, $\mathbf{u}_1$, does not corrupt a minimisation conducted along a previous search direction, $\mathbf{u}_2$. The method takes vectors u_1, u_2,..., u_n as a set of directions and moves along the first direction to its minimum, then from this point, it moves along the second direction to its minimum and so on until the cost function stops decreasing (Press *et al.*, 1992). One of the advantages of this method is that the choice of directions does not require the explicit computation of the cost function's gradient and so it is a computationally cheap technique. On the other hand, an important shortcoming of this method is that the previous procedure will minimise a quadratic cost function but it might not find the global minimum, but a local one, for cost functions that are not of non-quadratic form.

The total misfit measure or cost function (*ssq*) is defined as the misfit due to observations (ssq_o) and parameters (ssq_p):

$$ssq = ssq_o + ssq_p \qquad [2.28]$$

The observations misfit is defined as:

$$ssq_o = \sum_{i=1}^{t}\sum_{j=1}^{n}(\sqrt{x_{obs}} - \sqrt{x_{pred}})^2 W_j \qquad [2.29]$$

where W_j has units x^{-1} and represents the relative data quality or the weight that each observation carries, X_{obs} and X_{pred} are the observed and model predicted values, respectively over all the observation times t and all observed variables n. Equation 2.29 assumes that variance increases as the square root of the actual value and represents a compromise between constant absolute and constant relative error (see Fasham and Evans, 1995).

Each observation type (X_{obs}) corresponds to a modelled state variable and the optimisation will perform better when a greater number of observations are available. It is important to notice that not every state variable of the model can be directly compared with observational data and, in some cases, a conversion between units is needed, like for instance, when comparing phytoplankton nitrogen based biomass to chlorophyll.

The parameters misfit depends on our knowledge of the parameter set (p) as it is constrained by an upper (U) and lower (L) parameter bound limit, a suggested or target value (T) and by the parameter estimated variance (v) according to:

$$ssq_p = \sum_{i=1}^{t}\sum_{k=1}^{p}\begin{Bmatrix}\left[\frac{T-p}{(L-p)}\right]^2 W_k \text{ if } L<p\leq T \\ \left[\frac{p-T}{(U-p)}\right]^2 W_k \text{ if } T<p\leq U\end{Bmatrix} \qquad [2.30]$$

where W_k is dimensionless and represents: $W_k = \frac{1}{v^2}$

Equation (2.30) represents the *a priori* knowledge of the system (parameter space) and ensures that the model output will be achieved under realistic and credible ecological

conditions, for example, by not allowing parameters, such as mortality rates, being negative. A target value (T) would be chosen when there is no good constraint by data but it would be ignored if the data strongly suggest a different value.

We have chosen a value of $W_k = 0.1$ (v = 10) for most parameters or $W_k = 0.03$ (v = 30) for those parameters for which little *a priori* information was available.

The contribution to the total misfit varies depending on the parameter weight W_k so that if it is small (v is large), ssq_p will also be small and the majority of the misfit would come from data rather than from parameters.

In order to ensure a repeatable cycle, the model runs for two years and prints out the simulation for the third year. The optimisation technique returns the values of the optimized parameters that minimize the difference between real and model data only for the third year.

It is important to mention that the optimized solution is not expected to be perfect due to both errors in the data and inadequacies of the model. The residuals can be used to assess a particular solution or to compare different solutions for the same data set. On the other hand, the contribution of the observations to the solution varies according to the weight each observation carries. These weights can vary from almost zero to any upper limit we choose, in this particular case, from five to 600. The solution will be less sensitive to observations with low or mid-range weights than to those with weights closer to the upper value and different solutions would arise from imposing different weights on the data. This method generates a possible solution which is not necessarily the "true" one. The non-uniqueness of the solution is a consequence of the lack of information on ecosystem dynamics in the ocean and these methods are a valuable tool to explore a number of different solutions compatible with the data.

2.6 Calibrating the model

2.6.1 Initial Parameters

The ecosystem model was first run (without being optimised) using an initial set of parameters (*P1*) and also NABE observations. *P1* (see table 2.2) was obtained through a preliminary optimisation of the model to a reduced (no mesozooplankton) data set of observations provided by M. J. R. Fasham (pers. com.). The NABE observations, which provided data for diatoms, silicate, nitrate, ammonium, micro and mesozooplankton, total chlorophyll and total primary production, were given different weights comprising a range of values from one to ten (see table 2.4). Fasham *et al.* (1999) showed that model solutions for variables with good data coverage (such as nutrients) were little affected by the choice of weight values, whereas the solutions for data poor variables (zooplankton biomass) were more variable. The choice of weights reflects our assessment that biomass observations were more reliable than flux observations (therefore the former were given higher weights than the latter) and that it was more important to obtain a good fit to the former.

This scenario gave a solution that was unstable over the years. In order to get a better parameter set, the model was run and optimised to the NABE observations, using *P1* as initial constraint, and a new parameter set, called *P2*, was obtained.

When the ecosystem model was rerun (without optimising), using *P2* as the new initial set of parameters, the model provided a repeatable seasonal cycle after running for two years (see figure 2.3 for schematic diagram).

The main parameter changes are observed in both phytoplankton groups when *P1* and *P2* are compared. Non-diatoms are five times less efficient taking ammonium, the initial

slope of the P-I curve is reduced by 40% and so is their mortality rate (23%). Diatoms increase their efficiency taking nitrate and silicate by reducing both half-saturation constants by 50%. Their maximum sinking rate increases dramatically (more than 200%) and, by contrast, there is a reduction in their mortality rate by 79%.

Regarding micro and mesozooplankton, a reduction in 44% and 70% in their excretion rates was observed. Microzooplankton also graze more efficiently when using *P2* as initial parameters, which is shown by a 20% reduction in the ingestion half-saturation constant, K_6. Mesozooplankton is less efficient assimilating food and show less preference for diatoms when *P2* is used as the initial parameter set.

So, hereafter when the text refers to the model initial parameters, it should be understood that such set is *P2*.

2.6.2 Observations

In order to obtain the best fit to the NABE data, several runs, in which optimisation was also performed, were carried out. In all cases, the model was run for two years, with *P2* as initial parameters, and the third year data set was studied.

Different runs were performed in which, by trial and error, different weights were given to the NABE observations. Fasham and Evans (1995) observed that the choice of some target values can affect the optimisation and the solutions obtained. Fort this reason, several target values were also tested.

It was observed that the fit to primary production data improved when several target values regarding phytoplankton and mesozooplankton were changed: phytoplankton maximum growth rates ($Pmax_1$ and $Pmax_2$) were set to 3, diatoms half-saturation constant for silicate uptake (K_5) was set to 0.13 and mesozooplankton grazing half saturation constant (g_2) to 0.05.

The best performance was obtained when using the target values mentioned above as well as a range of weights (for the different variables available as observations) varying from five (assigned to ammonium and silicate) to 250 (assigned to primary production) for all the different variables except for total chlorophyll, which was given a weight of 50 for most part of the year and weights of 500 (between Julian days 128 to 130) and 600 (for Julian days 144 and 145) (see table 2.4). The variable weights provide a better fit to chlorophyll as well as to primary production. When chlorophyll weights were all set up to 50, the model performance was very similar but with varying weights (50, 500 and 600) a higher chlorophyll concentration (as well as a better fit to the double peak) and diatom biomass during the spring bloom are obtained.

2.7 The *standard* run

The *standard run* represents the best model fit to the real observations and it was obtained within the following scenario: the model is fed with an initial set of parameters, *P2*, and NABE data as observations. The weights given to the observations are between five and 250, with the exception of chlorophyll which uses a variable weighting scheme as described in section 2.6.2. Then, the model is run for two years and the third year data set provides the best model solution (solution 1) and the best estimated set of parameters (*P3*) that minimized the differences between model and real observations after optimising the initial parameters (see figure 2.3 and table 2.3 for parameter details).

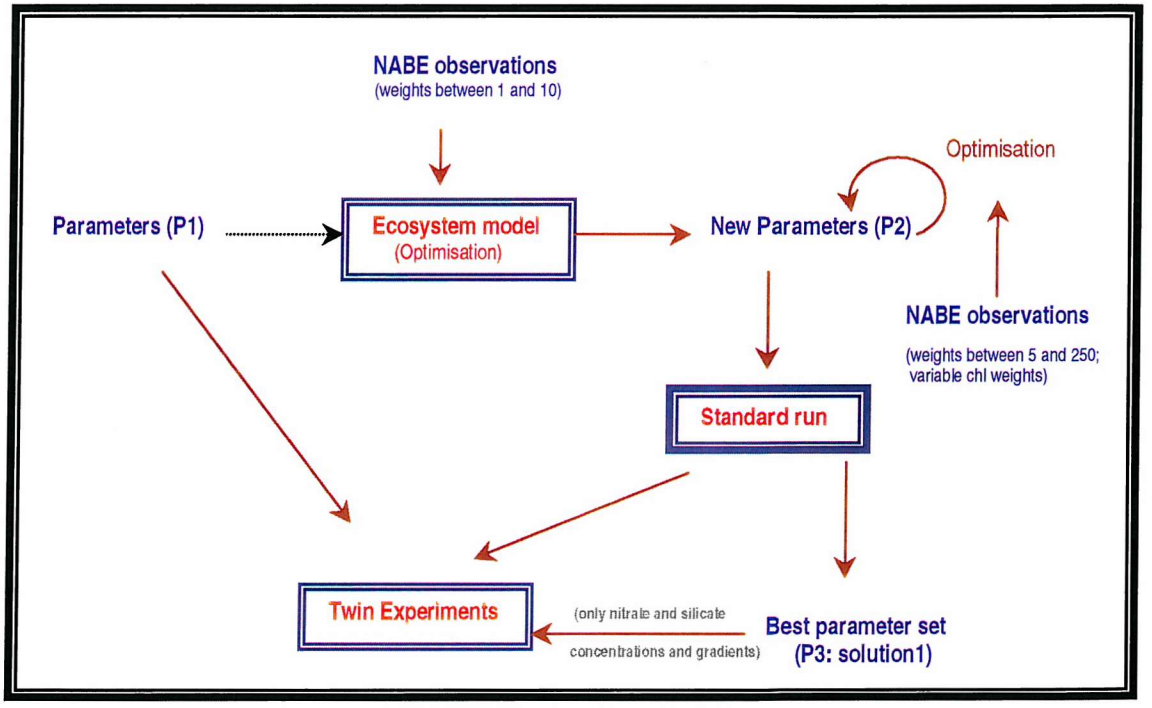

Figure 2.3: Schematic diagram of the *standard run*.

2.7.1 General Dynamics

The simulated results for all the state variables as well as total chlorophyll and primary production are shown in figure 2.4.

Reduced vertical mixing and increased irradiance allow diatoms to grow rather quickly as there is no nutrient limitation, diatoms are more efficient assimilating nitrate than non-diatoms (K_3 smaller than K_1), are also better suited to low light (α_2 greater than α_1) and have fastest intrinsic growth rates (P_{max2} greater than P_{max1}). As result of the favorable conditions, as observed in most temperate and warm seasonally-stratified environments, diatoms are the first phytoplankton community to bloom in the water column, sustained by winter concentrations of silicate, nitrate and also ammonium. The response of diatoms to higher silicate availability provides enough food for mesozooplankton to grow and reach their maximum biomass (0.68 mmol N m^{-3}) in Julian day 125 (figure 2.5c). A late diatom bloom occurs in autumn (0.63 mmol N m^{-3}) caused by the onset of vertical mixing which brings silicate into the mixed layer and which also drives to slightly higher mesozooplankton biomass. Diatom decline is due to mesozooplankton grazing pressure and lack of silicate. Furthermore, non-diatom phytoplankton develops as diatoms decline and its growth is sustained by nitrate and ammonium originating from zooplanktonic metabolic activities.

Regarding non–diatoms, apart from the spring bloom, there are also three very small blooms taking place. As explained above, the result of better light conditions and a shallower mixed layer generate a small bloom (0.65 mmol N m^{-3}) based on ammonium (as non-diatoms are more efficient assimilating ammonium than diatoms), around Julian day 100 (figure 2.5e). Immediately afterwards, when diatoms start to decay after silicate has been consumed, and due to the availability of nitrate and ammonium, the spring

bloom takes place (reaching 2.23 mmol N m^{-3}) until all nitrogen is depleted. Later in the year, around Julian day 215, ammonium is still available in low concentration and nitrate is brought into the mixed layer by physical mixing so a third small bloom occurs (0.76 mmol N m^{-3}) after which non-diatom biomass decreases and remains fairly low until they bloom again, around Julian day 313, reaching a value of only 0.50 mmol N m^{-3} as light conditions worsen and irradiance decreases. The increases of both phytoplankton groups are soon halted by the growth of herbivorous zooplankton. Microzooplankton responds to variability in non-diatom biomass blooming twice in a very short period of time (seven days) during spring, reaching a biomass of 0.44 and 0.42 mmol N m^{-3}, respectively and blooming again at the end of summer (figure 2.5e). The low microzooplankton biomass as response to the main non-diatom spring bloom is caused by high natural mortality and also grazing exerted by mesozooplankton which prevents microzooplankton reaching higher values. By contrast, mesozooplankton first peak in spring is due to microzooplankton abundance while the second peak is due to a combination of both, diatom and microzooplankton abundances.

Detritus and ammonium are also affected by the zooplankton response to changes (figure 2.4). The main two peaks in terms of detritus are explained by the higher zooplankton biomass in spring. The first peak (Julian day 125) is mainly due to microzooplankton and to a lesser extent to mesozooplankton and also diatoms. The second peak (Julian day 150) is mainly due to microzooplankton with little contribution from non-diatoms. The increase in detritus concentration later in the year could be mainly explained in terms of microzooplankton. Regarding ammonium, high values are observed before the spring bloom due to regeneration processes involving mesozooplankton excretion and detritus breakdown processes, the latter being the most important one at this stage. Once the spring bloom takes place, excretion from mesozooplankton becomes the most relevant

contribution to this pool although there is also contribution from microzooplankton. Ammonium concentration decays from Julian day 125 until the end of the spring bloom as it is consumed by phytoplankton. Its replenishment after Julian day 150 is due to detritus breakdown processes.

The seasonal variation in total primary production (TPP) shows two maxima in spring, the fist one mainly due to diatoms (around Julian day 125) and the second one due to non-diatoms (around Julian day 150) which reach a value of ca. 0.60 mmol N m^{-3} (figure 2.5f). The model estimates an annual TPP of 0.71 mol N m^{-2} y^{-1} of which 0.41 mol N m^2 y^{-1} are due to regenerated production (RP) and 0.30 mol N m^2 y^{-1} to new production (NP). In terms of phytoplankton group, non-diatoms account for 54% of the total NP and 71% of the total RP while diatoms are responsible of 46% and 29%, respectively.

The estimated annual *f* ratio (defined as the ratio of new to total primary production) was 0.42 (figure 2.5d). It declined from a winter value over 0.6 to a minimum of ca. 0.1 around Julian day 150, after which it increases again due to a deepening mixed layer depth bringing nitrate upwards as a result of mixing. The annual *f* ratios for diatoms and non-diatoms given by the model were 0.54 and 0.35, respectively.

Total chlorophyll, which reflects changes in phytoplankton biomass, starts to increase gradually from late winter until the first bloom occurs around Julian day 125 (reaching over 2 mg chl m^{-3}) due to diatom development (figure 2.4). Afterwards, chlorophyll concentration starts to decline for a short period but due to the presence of non-diatoms, a second bloom occurs around Julian day 150, reaching over 2.50 mg chl m^{-3}. From that time onwards, chlorophyll steadily declines until Julian day 200 when small blooms succeed until the onset of winter where chlorophyll concentration remains below 0.50 mg chl m^{-3}.

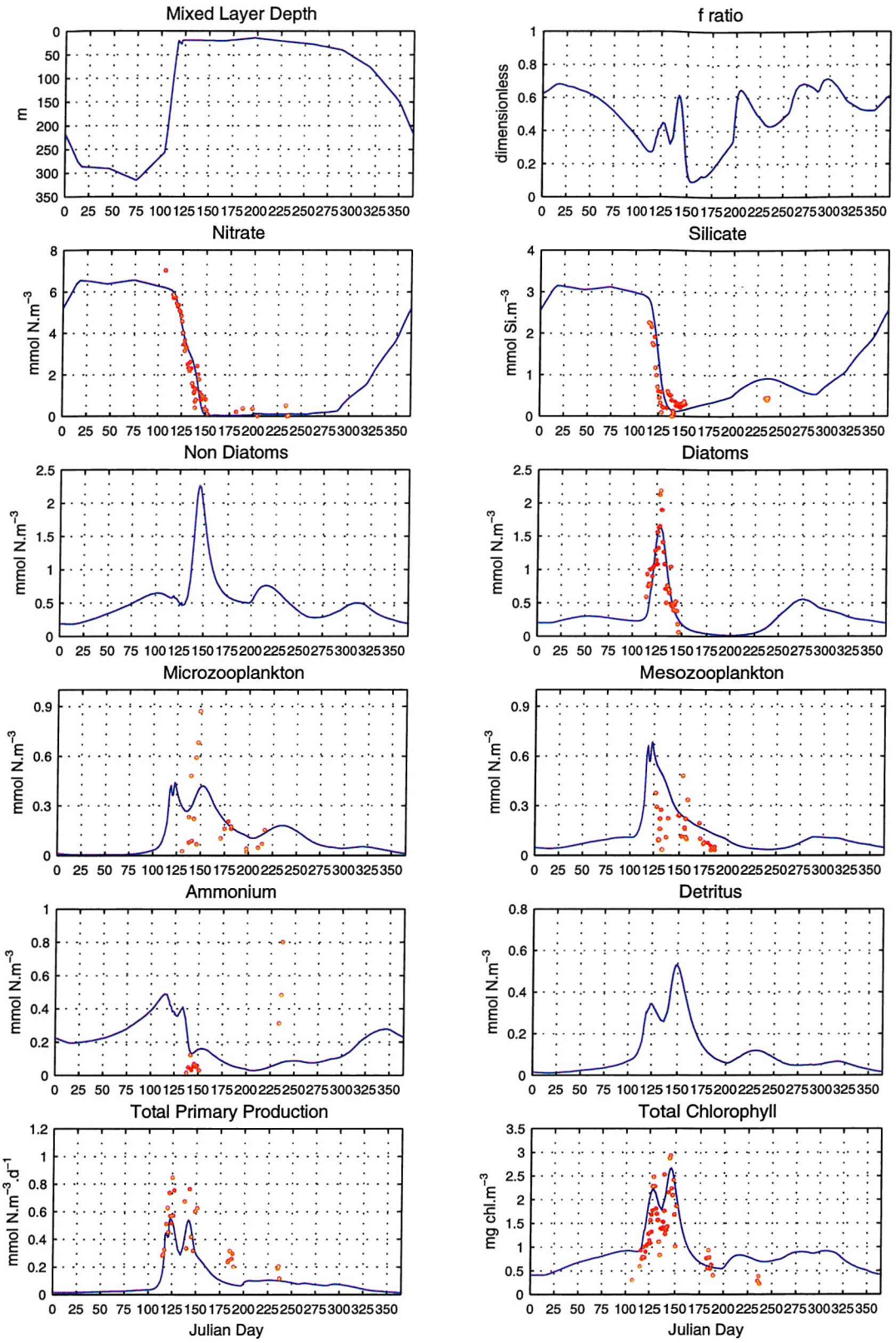

Figure 2.4: Seasonal variability of all the state variables corresponding to the *standard run* (blue) predictions based on real NABE observations (red dots).

2.7.2 Fitting the observations

The comparison between simulated state variables and observations is shown in figure 2.6 as well as the corresponding correlation coefficients (r) and the number of observations considered (n). Nitrate and silicate are the best fitted observations ($r_{nitrate}$ = 0.96, $n_{nitrate}$ = 47; $r_{silicate}$ = 0.92, $n_{siiicate}$ = 39). This is likely due to the large number of observations available which define the decline in nutrients very well. By contrast, ammonium is poorly estimated by the model ($r_{ammonium}$ = -0.66, $n_{ammonium}$ = 13) which can be explained by several reasons. First, ammonium real data come from two different cruises which estimated very different concentrations, nevertheless, no attempt was made to weight them by relative data quality. Second, ammonium observations carry smaller weights than nitrate and silicate so there will be little ammonium contribution to the misfit. Although several trials were initially performed, in which ammonium observations were weighted higher, and the model achieved a slightly better fit to this nutrient, the fit to nitrate was poorer. Bearing this fact in mind, and also the high variability within the ammonium data set (as data provided by cruise Tyro are up to four times higher than data collected on board Atlantis), it was decided to give low weights to ammonium observations in order to get a better fit to other nutrients (nitrate and silicate) better constraint by the observations.

The initial spring increase in diatoms is also modelled very well ($r_{diatoms}$ = 0.84, $n_{diatoms}$ = 37) although their maximum biomass is underestimated. The model also predicts only half observed value of the microzooplankton biomass peak when compared to NABE observations ($r_{microzoo}$ = 0.65, $n_{microzoo}$ = 17). By contrast, mesozooplankton biomass is overestimated in spring ($r_{mesozoo}$ = 0.32, $n_{mesozoo}$ = 29), reaching its maximum biomass at the same time as diatoms and showing no time-lag response due to their ability to prey on microzooplankton, which is already present when diatoms start to develop.

Fasham and Evans (1995) could not reproduce the double phytoplankton peak observed in the NABE data. They pointed out that it could be due to the simplicity of their model as FDM had only one class of phytoplankton. Recently, Evans (1999) presented an improved FDM model which still included only one phytoplankton compartment. Evan's model also failed to reproduce the double phytoplankton peak and he suggested that "NABE observations could have been taken in a different water mass" to explain this. However, Fasham and Evans (2000) reproduced the double phytoplankton peak, when using a model with diatoms but only one zooplankton group, although their model underestimated peak values. Our model accurately predicts the double chlorophyll peak ($r_{\text{total chlorophyll}} = 0.86$, $n_{\text{total chlorophyll}} = 49$), not only in terms of time of the year but also in magnitude, showing that their suspicion about the need of a more complex model with zooplankton also split into two different classes was right.

The annual total and new primary production estimated by the model (0.71 and 0.30 mol N m^{-2} y^{-1}, respectively) are in good agreement with primary production estimates from Berger (1989) of 0.44-0.75 mol N m^{-2} y^{-1} (being $r_{TPP} = 0.80$, $n_{TPP} = 28$). Martin *et al.* (1993) estimated an average PP value for the top 35 meters of the water column of 0.37 mmol N m^{-3} d^{-1} between Julian days 114 and 152, the corresponding model estimates for this period being 0.41 mmol N m^{-3} d^{-1}.

Model values for total annual PP, NP and *f* ratio are also lower than model estimates from Fasham and Evans (1995) who obtained values of 1.54, 0.82 mol N m^{-2} y^{-1} and 0.53, respectively.

In terms of phytoplankton growth rates, Verity *et al.* (1993) empirically calculated an average value of 0.69±0.20 d^{-1}, using the dilution method, between Julian days 138 and 149, and a growth rate, calculated by dividing PP by phytoplankton biomass, of

0.26±0.10 d^{-1}. Fasham and Evans (1995, 2000) obtained an averaged modelled rate over this period of 0.26±0.10 d^{-1} and 0.38±0.01 d^{-1}, respectively, whereas our model gives a value of 0.20±0.04 d^{-1}. The growth rate for diatoms and non-diatoms was 0.04±0.01 d^{-1} and 0.24±0.07 d^{-1}, respectively (figure 2.5b).

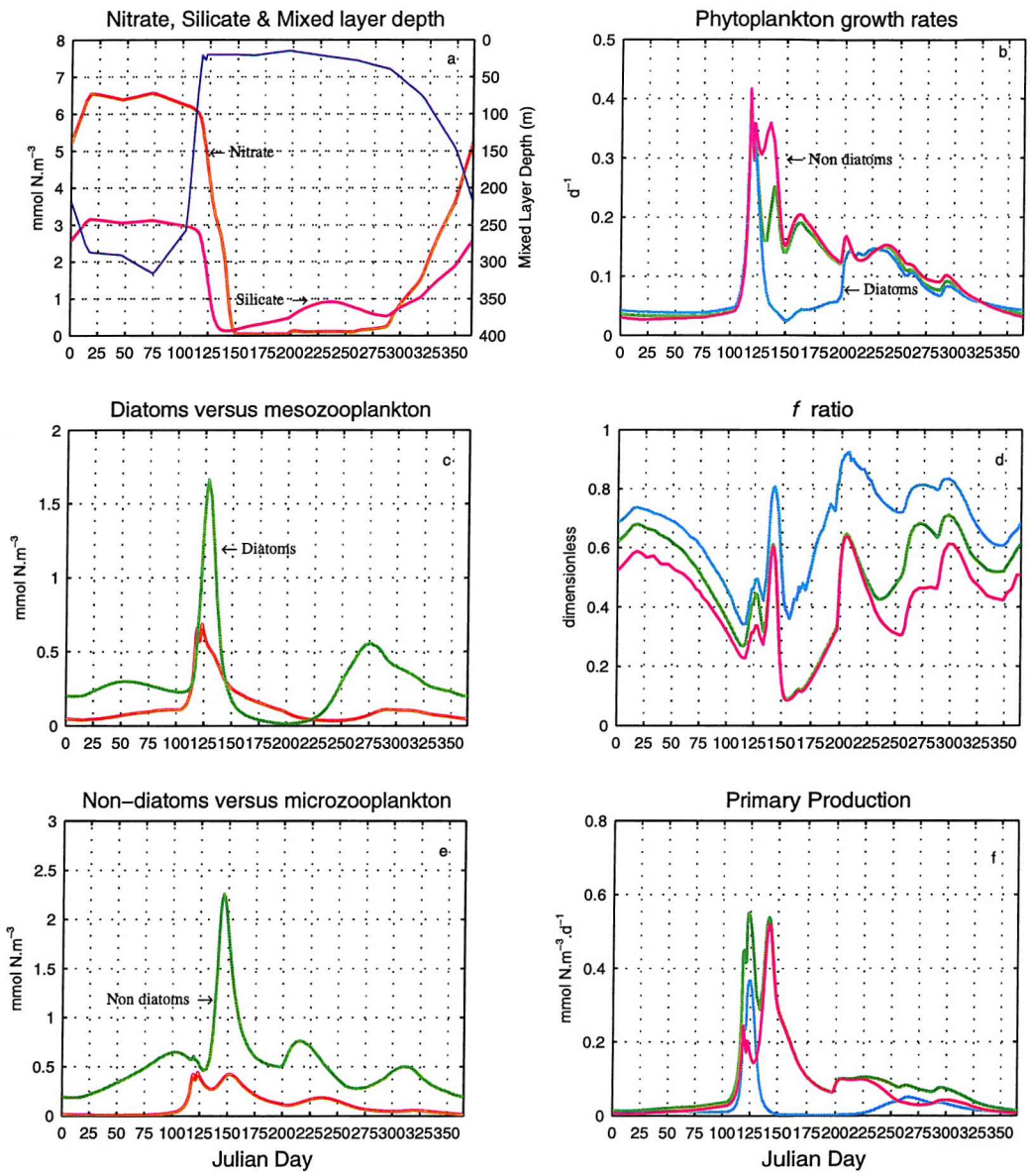

Figure 2.5: Seasonal variability of nutrients and mixed layer depth (a), phytoplankton and zooplankton (c, e), total and size-fractionated phytoplankton growth rates (b), *f* ratio (d) and primary production (f). Plots b, d and f show total phytoplankton in green color, diatoms in light blue and non diatoms in magenta.

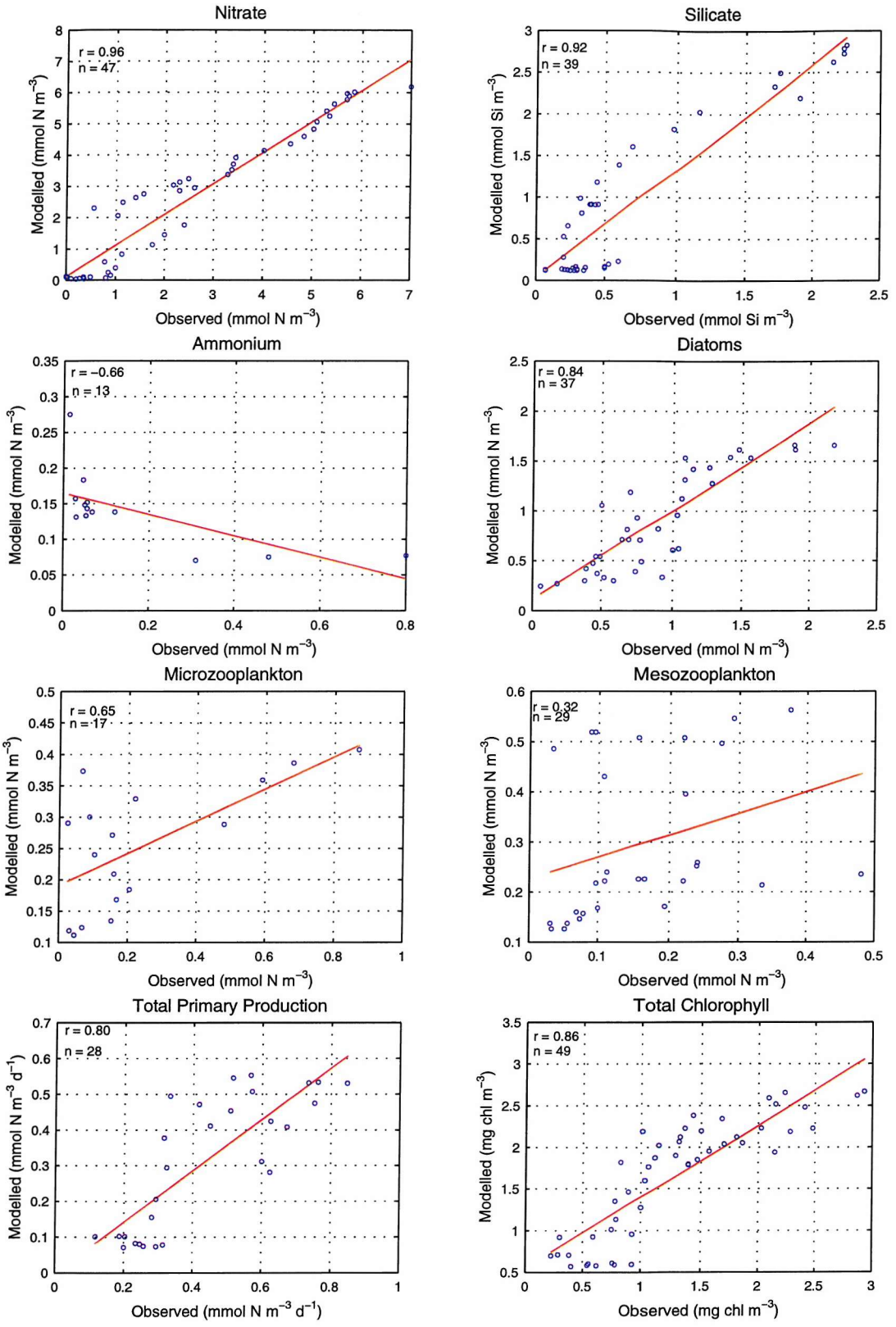

Figure 2.6: Predicted model results against observed (NABE) data. All variables have units of mmol N m^{-3} except silicate (mmol Si m^{-3}), total primary production (mmol N m^{-3} d^{-1}) and total chlorophyll (mg chl m^{-3}). Linear fit (red), correlation coefficients (r) and number of data points (n) are shown in each plot.

2.8 Summary of key points

- Parameter optimisation of an ecosystem model provides a direct technique for determining model parameters in a way that produces results that are consistent with the observed data.

- The 0-D, size-dependent ecosystem model is able to provide a good fit to observations for the North Atlantic at 47°N 20°W and reproduce the ecological seasonal cycle of phytoplankton, zooplankton, nutrients as well as primary production.

  The model also reproduced the double chlorophyll peak present in the observations data set as a result of explicitly modelling diatom and non-diatom phytoplankton, which have different efficiencies in terms of light and nutrient assimilation as well as different nutrient requirements.

- The best fitted state variables were those for which a larger number of observations were available (nitrate, silicate, chlorophyll and diatoms).

Table 2.1: Model parameters, symbols, ecosystem group and units. Units always refer to nitrogen unless stated otherwise.

Parameter	Symbol	Group	Units
Mortality rate	μ_1	P_{nd}	d^{-1}
Half saturation constant for nitrate uptake	K_1	P_{nd}	mmol m^{-3}
Half saturation constant for ammonium uptake	K_2	P_{nd}	mmol m^{-3}
Nitrate uptake ammonium inhibition parameter	ψ_1	P_{nd}	(mmol m^{-3})$^{-1}$
Initial slope of P-I curve	α_1	P_{nd}	(ly d^{-1})$^{-1}$ d^{-1}
Phytoplankton self-shading coefficient	K_p	P_{nd}, P_d	m^2 (mmol)$^{-1}$
Maximum growth rate	P_{max1}	P_{nd}	d^{-1}
Assimilation efficiency on non-diatoms	β_1	Z_{mi}	Dimensionless
Fraction of zooplankton mortality recycled to ammonium	ε	Z_{mi}, Z_m	d^{-1}
Excretion rate	ν_1	Z_{mi}	d^{-1}
Mortality parameter	ζ_1	Z_{mi}	(mmol m^{-3} d)$^{-1}$
Maximum ingestion rate	g_1	Z_{mi}	d^{-1}
Ingestion half-saturation constant	K_6	Z_{mi}	mmol m^{-3}
Detrital breakdown rate	δ_1	D	d^{-1}
Detrital sinking rate	V	D	m d^{-1}
Maximum growth rate	P_{max2}	P_d	d^{-1}
Initial slope of P-I curve	α_2	P_d	(ly d^{-1})$^{-1}$ d^{-1}
Half saturation constant for silicate uptake	K_5	P_d	mmol Si m^{-3}
Mortality rate	μ_2	P_d	d^{-1}
Half saturation constant for nitrate uptake	K_3	P_d	mmol m^{-3}
Half saturation constant for ammonium uptake	K_4	P_d	mmol m^{-3}
Nitrate uptake ammonium inhibition parameter	ψ_2	P_d	(mmol m^{-3})$^{-1}$
Redfield ratio (N:Si)	Re	P_d	Dimensionless
Maximum sinking rate	S_{max}	P_d	m d^{-1}
Assimilation efficiency	β_2	Z_m	Dimensionless
Excretion rate	ν_2	Z_m	d^{-1}
Mortality parameter	ζ_2	Z_m	(mmol m^{-3} d)$^{-1}$
Maximum grazing rate	g_2	Z_m	d^{-1}
Ingestion half-saturation constant	K_7	Z_m	mmol m^{-3}
Preference for diatoms	p_2	Z_m	Dimensionless
Sub-surface nitrate concentration	$N_{n\,surf.}$	N_n	mmol m^{-3}
Nitrate gradient across the thermocline	$N_{n\,grad.}$	N_n	mmol m^{-4}
Sub-surface silicate concentration	$S_{surf.}$	S	mmol Si m^{-3}
Silicate gradient across the thermocline	$S_{grad.}$	S	mmol Si m^{-4}
Non-diatoms initial biomass	$P_{nd\,start}$	P_{nd}	mmol m^{-3}
Microzooplankton initial biomass	$Z_{mi\,start}$	Z_{mi}	mmol m^{-3}
Ammonium initial concentration	$N_{r\,start}$	N_r	mmol m^{-3}
Nitrate initial concentration	$N_{n\,start}$	N_n	mmol m^{-3}
Detritus initial concentration	D_{start}	D	mmol m^{-3}
Initial diatoms biomass	$P_{d\,start}$	P_d	mmol m^{-3}
Silicate initial concentration	S_{start}	S	mmol m^{-3}
Mesozooplankton initial biomass	$Z_{m\,start}$	Z_m	mmol m^{-3}

Table 2.2: List of parameter set *P1* used in the ecological model.
Target, Lower, Upper and Var correspond to T, L, U, v in equation 30 and define the target value, the lower and upper parameter limits and the parameter estimated variance, respectively. Opt. states wheter or not the corresponding parameter will be optimized.

Parameter	P1	Target	Lower	Upper	Var	Opt.
μ_1	0.137	0.04	0	0.3	10	1
K_1	0.832	0.5	0.05	1	10	1
K_2	0.100	0.5	0.01	1	10	1
ψ_1	3.352	1.5	0	4	10	1
α_1	0.032	0.05	0	0.2	10	1
K_p	0.047	0.05	0	0.1	10	1
P_{max1}	1.616	1.5	0	4	10	1
β_1	0.807	0.75	0	1	10	1
ε	0.319	0.33	0	1	10	1
v_1	0.129	0.1	0	0.5	10	1
ζ_1	0.228	0.2	0	0.5	10	0
g_1	1.109	1	0	3	10	1
K_6	0.993	1	0.05	3	10	1
δ_1	0.242	0.05	0	0.3	10	1
V	6	6	0.3	15	30	0
P_{max2}	1.535	1	0.7	4	10	1
α_2	0.140	0.05	0	0.2	10	1
K_5	4.248	0.3	0.05	10	10	1
μ_2	0.050	0.05	0	0.3	10	1
K_3	0.398	0.5	0.05	1	10	1
K_4	0.820	0.5	0.01	1	10	1
ψ_2	2.831	1.5	0	4	10	1
Re	1.113	1	0.2	2	10	1
S_{max}	0.528	10	0	50	10	1
β_2	0.652	0.5	0	0.7	10	1
v_2	0.095	0.1	0	0.3	10	1
ζ_2	0.266	0.2	0	0.3	10	1
g_2	0.361	0.2	0	0.5	10	1
K_7	0.628	1	0.5	3	10	1
p_2	0.464	0.9	0	1	10	1
$N_{n\,surf.}$	3.609	4	0	20	30	1
$N_{n\,grad.}$	0.029	0.02	-1.00E-06	0.2	30	1
$S_{surf.}$	1.702	20	0	30	30	1
$S_{grad.}$	0.016	0.02	-1.00E-06	0.5	30	1
$P_{nd\,start}$	0.200	0.02	0	2	1.00E+05	0
$Z_{mi\,start}$	0.020	0.002	0	2	1.00E+05	0
$N_{r\,start}$	0.100	1	0	0.2	1.00E+05	0
$N_{n\,start}$	5	1	0	20	1.00E+05	0
D_{start}	0.300	0.3	0	0.2	1.00E+05	0
$P_{d\,start}$	0.200	0.02	0	2	1.00E+04	0
S_{start}	2	4	1	6	1.00E+05	0
$Z_{m\,start}$	0.010	0.01	0.001	0.2	0	0

Table 2.3: List of parameter set *P2* used in the ecological model.

Target, Lower, Upper and Var correspond to T, L, U, v in equation 30 and define the target value, the lower and upper parameter limits and the parameter estimated variance, respectively. Opt. states wheter or not the corresponding parameter will be optimized. Solution1 (P3) refers to best parameter provided by the model.

	Parameter	P2	Target	Lower	Upper	Var	Opt.	Solution1 (P3)
Non Diatoms	μ_1	0.032	0.04	0	0.3	10	1	0.019
	K_1	0.679	0.5	0.05	1	10	1	0.772
	K_2	0.565	0.5	0.01	1	10	1	0.385
	ψ_1	3.475	1.5	0	4	10	1	3.455
	α_1	0.019	0.05	0	0.2	10	1	0.021
	K_p	0.086	0.05	0	0.1	10	1	0.079
	P_{max1}	1.834	**3**	0	4	10	1	1.819
Microzooplankton	β_1	0.400	0.75	0	1	10	1	0.361
	ε	0.125	0.33	0	1	10	1	0.095
	ν_1	0.073	0.1	0	0.5	10	1	0.112
	ζ_1	0.228	0.2	0	0.5	10	0	0.228
	g_1	1.131	1	0	3	10	1	1.130
	K_6	0.768	1	0.05	3	10	1	0.764
Det	δ_1	0.236	0.05	0	0.3	10	1	0.277
	V	6	6	0.3	15	30	0	6
Diatoms	P_{max2}	2.356	**3**	0.7	4	10	1	2.841
	α_2	0.080	0.05	0	0.2	10	1	0.088
	K_5	2.113	**0.13**	0.05	10	10	1	1.825
	μ_2	0.010	0.05	0	0.3	10	1	0.010
	K_3	0.208	0.5	0.05	1	10	1	0.208
	K_4	0.830	0.5	0.01	1	10	1	0.867
	ψ_2	3.351	1.5	0	4	10	1	3.368
	Re	1.619	1	0.2	2	10	1	1.707
	S_{max}	1.688	10	0	50	10	1	1.703
Mesozooplankton	β_2	0.505	0.5	0	0.7	10	1	0.631
	ν_2	0.028	0.1	0	0.3	10	1	0.038
	ζ_2	0.285	0.2	0	0.3	10	1	0.285
	g_2	0.387	**0.05**	0	0.5	10	1	0.372
	K_7	0.601	1	0.5	3	10	1	0.601
	p_2	0.217	0.9	0	1	10	1	0.489
Nutrients	$N_{n\ surf.}$	1.244	4	0	20	30	1	2.751
	$N_{n\ grad.}$	0.037	0.02	-1.00E-06	0.2	30	1	0.033
	$S_{surf.}$	1.368	20	0	30	30	1	1.350
	$S_{grad.}$	0.014	0.02	-1.00E-06	0.5	30	1	0.015
Starting values	$P_{nd\ start}$	0.200	0.02	0	2	1.00E+05	0	0.200
	$Z_{mi\ start}$	0.020	0.002	0	2	1.00E+05	0	0.020
	$N_{r\ start}$	0.100	1	0	0.2	1.00E+05	0	0.100
	$N_{n\ start}$	5	1	0	20	1.00E+05	0	5
	D_{start}	0.300	0.3	0	0.2	1.00E+05	0	0.300
	$P_{d\ start}$	0.200	0.02	0	2	1.00E+04	0	0.200
	S_{start}	2	4	1	6	1.00E+05	0	2
	$Z_{m\ start}$	0.010	0.01	0.001	0.2	1.00E+05	0	0.010

Table 2.4: Different weights given to the NABE observations when using either *P1* or *P2* as the initial parameter sets for the ecosystem model.

Observation	P1	P2
Ammonium concentration	1	5
Silicate concentration	1	5
Nitrate concentration	1	20
Mesozooplankton biomass	5	25
Microzooplankton biomass	10	50
Diatoms biomass	10	50
Total chlorophyll	10	50 (500,600)
Primary Production	1	250

Chapter 3:

The Twin Experiments

Chapter 3: The Twin Experiments

3.1 Introduction

The main objective of the twin experiments was to determine the feasibility of using sparse observations such as the ones collected on scientific cruises or by remote sensing to estimate model parameters and reproduce the ecosystem annual cycle in specific areas such as the North Atlantic.

When modelling ecosystem dynamics there are two major problems that one should be aware of as they introduce uncertainties into descriptions of ecosystem dynamics. The first one is that models used are never exact due to the approximations made to reduce the number of degrees of freedom (infinite in number, otherwise) sometimes by elimination of some of the physics involved and others by parameterizations using empirical coefficients of uncertain value.

The second problem is that the measured data available to determine model parameters are never wholly adequate. Apart from the common problem related with limited (poor) coverage of the area object of study, all data contain noise from instrumental or other errors, e. g. spatial patchiness.

In order to test the ability of ecosystem models to estimate individual parameters strongly responsible for the model behavior, twin experiments based on data mimicking the frequency of data collection available are starting to be used (Lawson *et al.*, 1996; Spitz *et al.*, 1998). Twin experiments using model-generated observations represent a reliable way to systematically test the ability of the assimilation data technique to recover parameters as the data set used is guaranteed to be consistent with the model, free of

random and/or measurement errors and expressed in the same units as the model results.

3.2 The Experiments

In order to perform the twin experiments, the model was run until it reached a steady annual cycle, which took 2 years. The third year data set (*solution1*: see section 2.7) constituted the model generated data to be used as the new input set of observations (subsequently referred to as *"synthetic observations"* to differentiate them from the real observations which comprised the NABE data). This set of data was subsampled at different intervals according to various sampling strategies. The subsampled variables only comprised mesozooplankton biomass, nitrate and silicate concentration and total chlorophyll. There are different reasons why those variables were chosen:

- We wanted to investigate the model performance in real conditions, when only a few variables are available as observations. They should be also feasible to be measured on scientific cruises.

- Determination of fractionated productivity is not yet as extended a practice as one would desire so the possibility of sampling diatom and/or non diatom phytoplankton was discarded. Instead, total chlorophyll is always a good choice as it is almost a "routine" variable sampled on biological cruises.

- Nitrate was chosen as all forms of phytoplankton have a nitrogen-based physiology and the silicate requirement of diatoms also justifies the need of silicate to be able to reproduce their seasonal cycle accurately.

- It was also thought that the model would provide a better fit to the simulated variables if, at least, data from one zooplankton group was used to constrain the model.

Although it is difficult to get zooplankton data from scientific cruises, it is more likely to obtain mesozooplankton data rather that microzooplankton as the latter is not a variable often surveyed.

The first sampling strategy consisted in weekly subsampling in order to generate the same density of data that would be available, for instance, from satellite data collection. The second strategy only subsampled during the bloom period (between days 100 and 150) on a daily basis according to the type of survey usually performed on scientific cruises.

As the equations governing the model are solved using a variable step-length algorithm, the subsampled data were polynomially interpolated (to obtain daily data) before being assimilated as *synthetic observations* back into the model. Then, the model was rerun, using *P1* as the new initial parameter set (first parameter guesses) but without optimizing nutrients (either nitrate or silicate) and using the already optimised nitrate and silicate parameters (concentrations and gradients across the thermocline) obtained with the *standard run* (*P3*) instead, as we only want to recover biological parameters.

This procedure provided us with a new output and a new optimal set of parameters (see figure 2.3). The output values were compared with the *synthetic observations*. The recovery of the parameters was calculated and expressed as a fractional change from the "*true*" value corresponding to the *standard run*, *P3*. Parameters were considered reasonably recovered when fractional changes were smaller than 0.30.

3.3 Data Assimilation

Different sampling methods can be found in the literature regarding data assimilation (Lawson *et al.*, 1996). We have chosen two different strategies: weekly and bloom-period sampling. In both cases, the sampled variables were the same in all the experiments performed (nitrate, silicate, mesozooplankton and total chlorophyll) and the collection of data was assumed to take place at the same time for all the variables involved.

3.3.1 Twin Experiment 1 (TE1): Weekly Data Assimilation

The weekly sampling provides a whole year of data starting the first day of the year (Julian day zero) and being carried out once a day, every seven days. Assimilation of this data set as *synthetic observations* resulted in an accurate (see table 3.1) model reproduction of the main patterns of seasonal variability in all the variables sampled (r between 0.95 and 1.00) although the model was not able to reproduce the double chlorophyll peak in spring (figure 3.1). In terms of non-assimilated variables, phytoplankton biomass was remarkably underestimated during the spring bloom (by half in the case of non-diatoms) while microzooplankton biomass was higher than mesozooplankton for the same period, due to a lesser mesozooplankton grazing pressure on microzooplankton and a high microzooplankton assimilation efficiency on non-diatoms, doubled compared to the *standard run*. Total primary production was also overestimated. Although the model predicted a high microzooplankton contribution to the detrital pool, there is a good agreement between model results for ammonium and detritus concentration and the *standard run*.

However, the model recovered a total of 17 out of 28 parameters. The worst performance was in terms of microzooplankton parameters as the model failed to recover all of them

except *g1*. The rest of the badly-recovered parameters were μ_1, K_2 (non-diatoms), K_5, S_{max} (diatoms), K_p (diatoms and non-diatoms), ν_2 and p_2 (mesozooplankton) (see figure 3.5 and table 3.3).

3.3.2 Twin Experiment 2 (TE2): Bloom Data Assimilation

The bloom-period strategy consisted of daily sampling of variables only when the spring phytoplankton bloom occurred (from Julian day 100 until day 150, as established by the s*tandard run*) and following the strategy usually performed on scientific cruises. This approach increased the availability of data for assimilation into the ecosystem model during the bloom while there is a lack of measurements throughout the rest of the year. As in the previous case, the data assimilation produced a good agreement (see table 3.1) between *synthetic observations* and model results (r between 0.96 and 1.00) for the state variables for which observations were available (figure 3.1). By contrast, a better performance in terms of chlorophyll was achieved this time as the model was able to generate the double peak observed in spring. Regarding the remaining variables, the model also overestimated microzooplankton biomass, ammonium concentration and total primary production and slightly underestimated detritus. In most cases, the model predictions were very similar to those obtained when a weekly sampling strategy was adopted.

The model was also able to recover 17 out of 28 parameters, failing to recover μ_1, K_1, K_2 (non-diatoms), β_1, ν_1, (microzooplankton), ε (micro and mesozooplankton), μ_2, K_3, K_5, S_{max} (diatoms), and ν_2 (mesozooplankton) (see figure 3.5 and table 3.3).

The cost function also decreased one order of magnitude but converged to a higher value of 40.07, compared to *TE1*, taking 17 iterations, with equal contribution to the misfit from observations and parameters (see table 3.2).

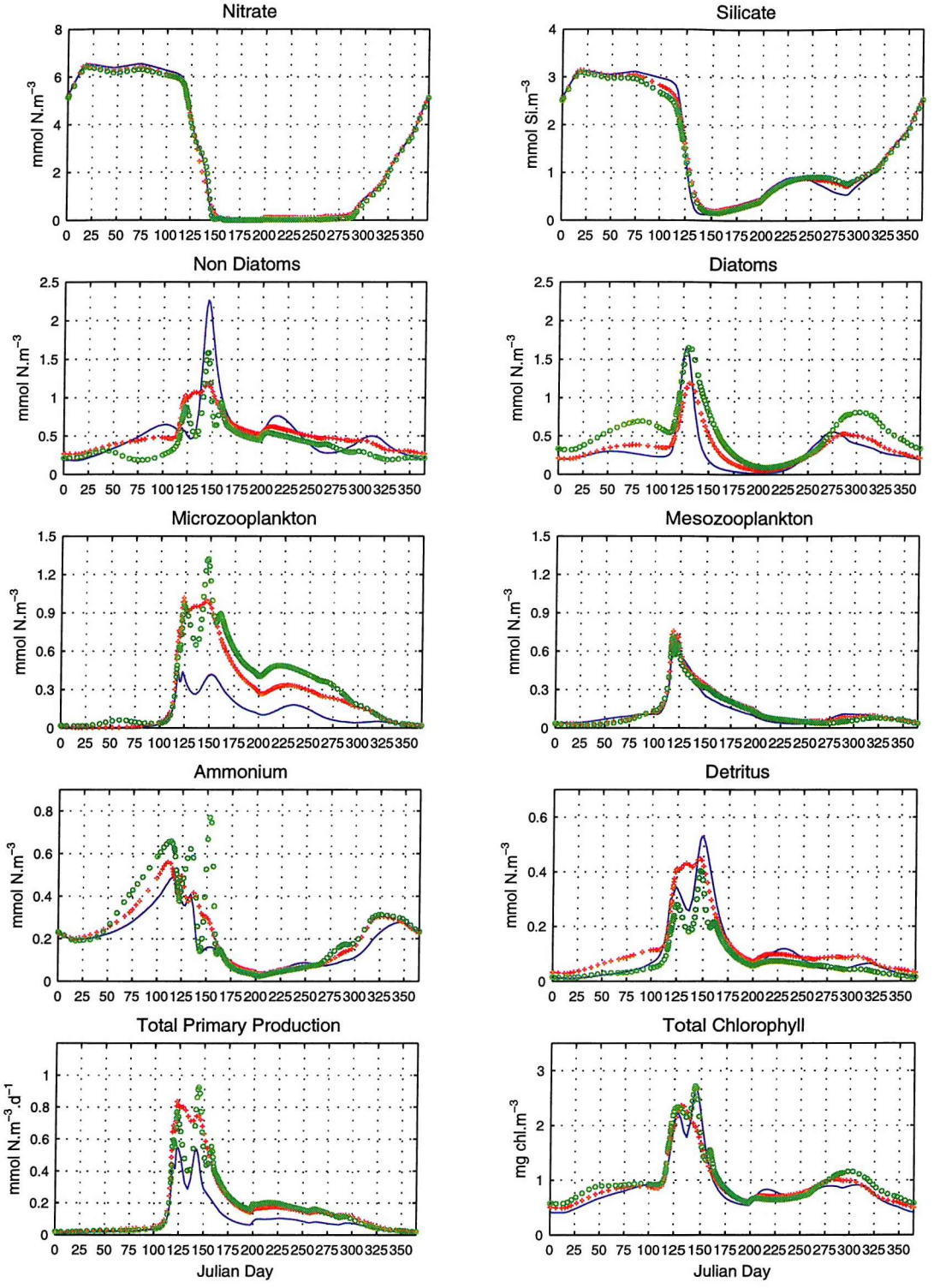

Figure 3.1: Seasonal variability of all the state variables corresponding to the *standard run* (solid blue) vs. the results from twin experiment 1 (*TE1*: red crosses) and twin experiment 2 (*TE2*: green circles) when nitrate, silicate, mesozooplankton and total chlorophyll were available as weekly and bloom *synthetic observations*, respectively.

3.4 Data Noise

The numerical experiments described in the previous section were carried out assuming that the measured data available for assimilation to determine model parameters were completely free of random and/or measurement errors. However, the acquisition of real biological data always carries a level of uncertainty inherent in the different sampling techniques which varies within each variable considered. This problem introduces uncertainties into the description of the marine ecosystem. Although according to previous studies (Lawson *et al.*, 1995; Spitz *et al.*, 1998), the addition of noisy data would not improve the rate of parameter recovery, it was thought that it will provide valuable information in order to investigate the ability of the model to describe the seasonal variability of the ecosystem using constant error information as data source. Previous work (Lawson *et al.*, 1995) found that the addition of noise had a very small effect (even for a high percentage of noise) on the results obtained from their simple predator-prey model.

To investigate the role that real measurements play, a new set of numerical twin experiments were performed in which normally (Gaussian) distributed random noise with varying amplitude, was added to the input data sets used as *synthetic observations*. The noise distribution has the following probability density function:

$$f(x) = \frac{1}{b\sqrt{2\pi}} exp\left(-\frac{(x-a)^2}{2b^2} \right)$$

where a and b are the mean (taken as zero) and the standard deviation of the distribution for each variable, respectively.

Three different experiments called *noise1*, *noise2* and *noise3* were performed in which nitrate and silicate standard deviations remained unchanged but total chlorophyll and

mesozooplankton varied (see table 3.4). The first experiment consisted in the addition of random noise on all the sampled variables (mesozooplankton, nitrate, silicate and chlorophyll) *synthetic* data. The second experiment was similar to the former but increasing the amount of noise added on chlorophyll while the third one was similar to the latter but more noise was added on mesozooplankton data instead (see table 3.4). Noise was calculated for each variable and added up to the third-year data generated in the *standard run*, to be assimilated as *synthetic observations* data back into the model. The sampling strategy carried out was as described above (section 3.2).

3.4.1 Twin Experiments 3, 4 and 5 (*TE3*, *TE4*, *TE5*):

Weekly Noisy Data Sampling

The assimilation of these three data sets of *synthetic observations* provided us with model outputs *TE3*, *TE4* and *TE5* corresponding to the addition of noise stated in *noise1*, *noise2* and *noise3*, respectively (figure 3.2).

All three twin experiments provided very similar results. In particular, variables for which *synthetic observations* were available (nitrate, silicate, mesozooplankton and total chlorophyll) performed better. There is almost no difference in the seasonal variability or magnitude of any of the state variables among the three runs. Nitrate and silicate were accurately predicted in all cases ($r_{nitrate}$ = 0.99; $r_{silicate}$ = 0.93; see table 3.1). The model overestimated zooplankton biomass during the spring bloom and microzooplankton reached higher biomass than mesozooplankton during the same period. Total chlorophyll dynamics were described reasonably well (r between 0.78 and 0.85) but the model failed to predict the double chlorophyll peak. Non-diatom estimates were very low due to high natural mortality and grazing pressure exerted by microzooplankton. It seems like the dynamics between non-diatoms and microzooplankton would be better described if there

were data available as observations to constrain either of them as it happens to be for the diatom-mesozooplankton dynamics. The lack of agreement, when compared to the *standard run*, is also reflected in the low number of parameters recovered corresponding to both groups. These results seem to point to the existence of "crucial" parameters responsible for this behaviour like, for instance, μ_1, which is very high and it has also never been recovered in either of the runs and β_1 (also high).

The model provides a good estimation of diatom biomass and also a good number of parameters were recovered. Mesozooplankton biomass is overestimated during the spring bloom and so is ammonium (during winter and onset of spring). Regarding detritus the model did not reproduce the double peak observed in the *standard run*, failing to match the second one (Julian day 150) due to an excessive efficiency of microzooplankton grazing on phytoplankton (β_1 increased dramatically).

In terms of parameter recovery, *TE3* provided slightly better results as it was able to recover 17 out of 28 parameters (the same number recovered in the non-noise cases) against *TE4* and *TE5* which only recovered 16 (see figure 3.5 and table 3.3).

In all cases, 14 parameters were always recovered, three (out of six) corresponding to non-diatoms, four (out of nine) to diatoms, one (out of four) to microzooplankton, five (out of six) to mesozooplankton and one (out of one) to detritus. Eight parameters were never recovered.

For all the experiments, the model only managed to recover the same phytoplankton parameters recovered before by *TE1*. *TE5* managed to recover all mesozooplankton parameters while *TE3* and *TE4* failed to recover p_2. *TE4* succeed to recover microzooplankton ingestion half-saturation constant (K_6) never recovered by the other twin experiments.

These results are consistent with the cost function values as the lowest parameter and observations misfits are achieved with *TE3,* whose cost function is almost three times smaller than the *standard run* value and took only six iterations to converge.

Those results seem to indicate that the model is not as sensitive to noise when variables are well constrained by data available as observations, if compared to *TE1* (same initial parameters, same *synthetic observations* but no noise added). All the constrained variables are reasonably predicted by the model, with the exception of mesozooplankton, whose biomass is overestimated during the spring bloom. Although the chlorophyll double peak is not reproduced, this is hardly surprising as it was not predicted by *TE1*, either.

The model seems to be equally sensitive to mesozooplankton as to chlorophyll noisy data as the model performances are almost the same. *TE4* added more noise on chlorophyll than on the other data regarding *synthetic observations*. The first noticeable effect is on non-diatoms which slightly increased their biomass and so did microzooplankton due to the availability of food. Mesozooplankton responded to those changes by increasing their biomass and the grazing pressure on diatoms. By contrast, *TE5* (which added more noise on mesozooplankton) caused mesozooplankton to reach higher biomass during the spring bloom as result of the increased grazing pressure mainly on microzooplankton.

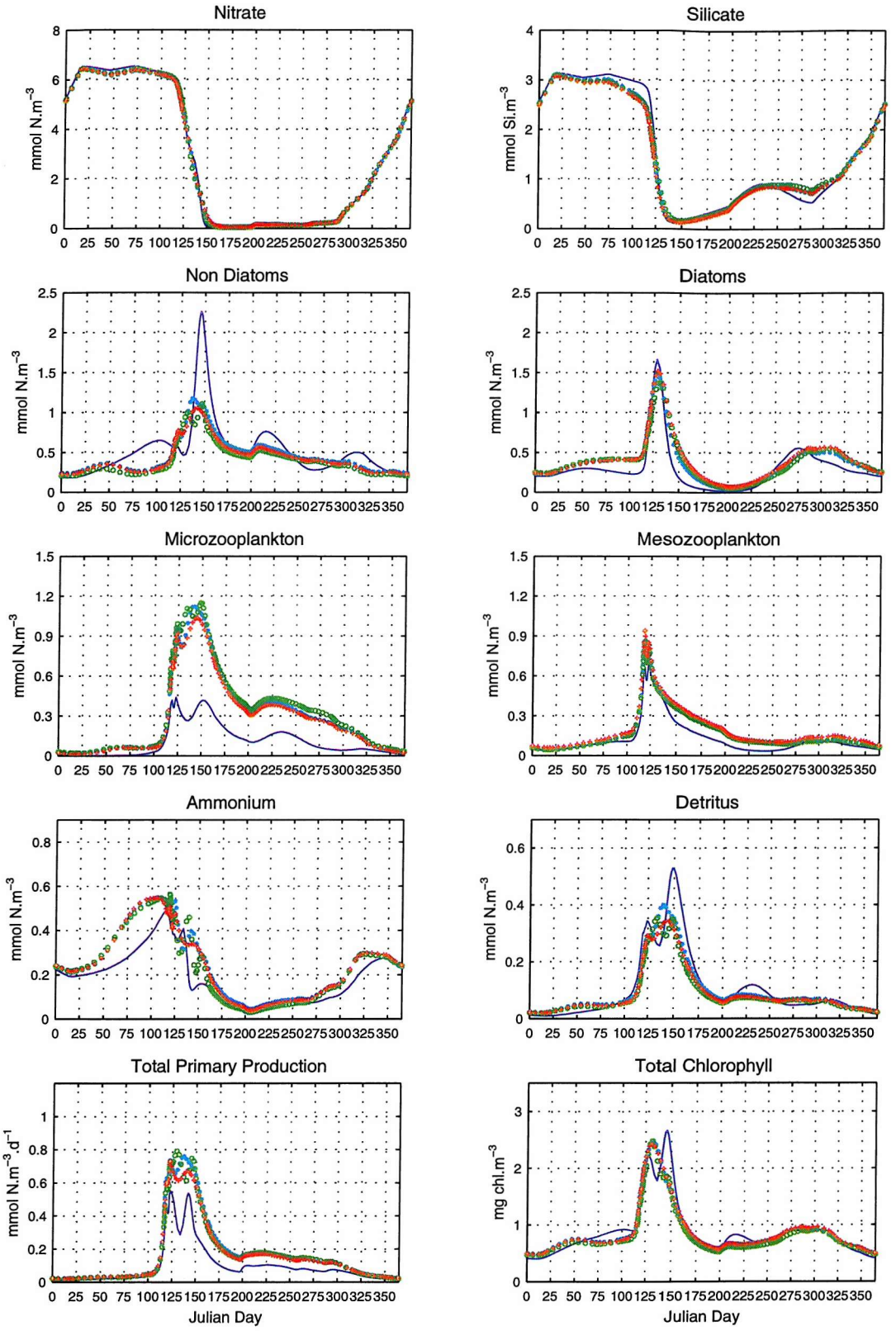

Figure 3.2: Seasonal variability of all the state variables corresponding to the *standard run* (blue line) vs. model predictions based on weekly noisy observations (nitrate, silicate, mesozooplankton and total chlorophyll). *TE3*: light blue dots, *TE4*: green circles and *TE5*: red crosses.

3.4.2 Twin Experiments 6,7 and 8 (*TE6, TE7, TE8*):

Bloom Noisy Data Sampling

In this case, the assimilation of bloom noisy data as *synthetic observations* provided us with model outputs *TE6, TE7* and *TE8* corresponding to the addition of noise stated in *noise1, noise2* and *noise3*, respectively (see table 3.4). The model results show greater variability among *TE6, TE7* and *TE8* than in the previous case, when weekly data were assimilated (figure 3.3).

As in section 3.4.1, all the runs performed similarly, specially, when variables were constrained by *synthetic observations* (nitrate, silicate, mesozooplankton and total chlorophyll). Silicate was underestimated in late winter and onset of spring due to the rapid development of diatoms as the mixed layer shallows and light becomes less limiting. *TE6* and *TE7* also predicted very high diatom biomass in autumn and winter. The model accurately estimated not only mesozooplankton biomass but also total chlorophyll, and successfully reproduced the double spring peak in all three experiments carried out.

Again, the results from these experiments resembled *TE2*. *TE8* performed slightly better than the other experiments in terms of diatoms biomass during winter, giving a more realistic approach. *TE6* and *TE7* provided unusually high diatom biomass in autumn and winter, preventing non-diatoms from developing until Julian day 125. Then, they bloomed twice: first supported mainly by nitrate (Julian day 125) and later, when nitrate was almost depleted (around Julian day 142) also supported by ammonium. Microzooplankton responded to non-diatoms growth by blooming twice, too. They reached very high biomass as a result of a high ingestion efficiency (β_1 was 0.80 in all these experiments and 0.36 in *P3*) from then on until winter. For the same reason, ammonium concentration

was also high, reflected by the non-recovery of ε in either case. All the noisy runs modelled detritus very well, specially *TE6*, which matched both peaks on Julian days 125 and 150 and all failed in terms of primary production by generating extremely high values.

In terms of parameter recovery, all the experiments performed similarly: *TE6* and *TE7* recovered 16 parameters and *TE8* recovered 15 out of 28.

In all cases, 12 parameters were always recovered, two (out of six) corresponding to non-diatoms, two (out of nine) to diatoms, one (out of one) corresponding to both types of phytoplankton, one (out of four) to microzooplankton, five (out of six) to mesozooplankton and one (out of one) to detritus. Eight parameters were never recovered (see figure 3.5 and table 3.3).

TE6 recovered v_1 and K_5, and *TE8* recovered K_1, parameters never recovered by *TE2*.

The cost function values ranged between the *standard run* and *TE2* values. The minimum error in terms of either observations and parameters is achieved with *TE6*, whose cost function is four and a half times smaller than the *standard run* value and took 16 iterations to converge. *TE8* provides the highest parameter error (more than four times) of the three.

As in the previous case, the model seemed to be equally sensitive to mesozooplankton and chlorophyll noisy data.

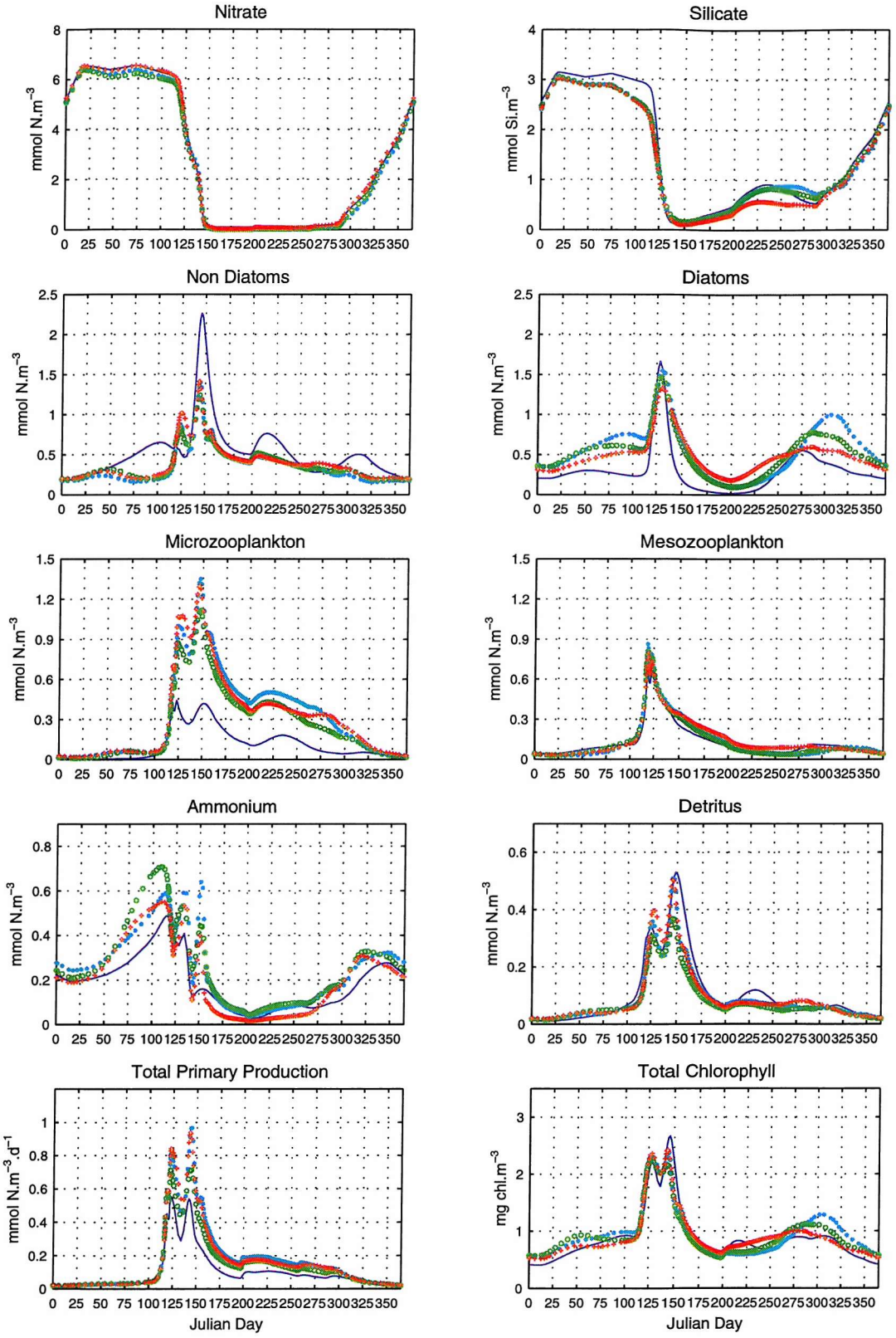

Figure 3.3: Seasonal variability of all the state variables corresponding to the *standard run* (blue line) vs. model predictions based on bloom noisy observations (nitrate, silicate, mesozooplankton and total chlorophyll). *TE6*: light blue dots, *TE7*: green circles and *TE8*: red crosses.

3.5 Sensitivity to a reduction in structural stability

Following Platt *et al.* (1981) and Matear (1995), two different ecosystem configurations were formulated in order to assess the model complexity required to reproduce observations. The twin experiment carried out was aimed to find out if a basic model could be used to reproduce the annual variability of a more complex ecosystem.

The approach taken in this experiment consisted in the assimilation of data provided by the *standard run* (as *synthetic observations*) into a simpler model with only seven compartments. The reason behind this experiment is the assumption that our model captures the ecosystem behaviour, being aware that it is a simpler representation of the complex model from which the observations came from, as it happens when modellers try to reproduce the dynamics observed in aquatic ecosystems by using computer simulations. The seven compartment model (referred to as 7CM, hereafter) has two classes of phytoplankton, in order to get the double chlorophyll peak discussed in various sections above, but only one class of zooplankton, mainly describing microzooplankton, which act as predators on both phytoplankton groups grazing preferentially on non-diatoms as in Fasham and Evans (2000).

The same strategy described before regarding data assimilation (section 3.2) was carried out to perform these set of experiments in terms of weekly and bloom-period observations.

3.5.1 Twin Experiment 9 (TE9): Weekly data assimilation

The degraded model results after the assimilation were reasonably good (see table 3.1) compared to the *standard run* (figure 3.4). The main difference between both runs lays on the lower phytoplankton biomass in spring but high diatoms biomass in winter as well as the lack of the double chlorophyll peak in spring predicted by the degraded model. The 7CM accurately reproduced nitrate and silicate although it slightly underestimated silicate late in winter just before the spring diatom bloom occurrence and it has also been slightly overestimated in autumn.

The degraded model did not reproduce the double microzooplankton peak, either. Due to their ability to graze on both groups of phytoplankton, microzooplankton declined very slowly after reaching their maximum biomass in Julian day 125. It is worth noting that microzooplankton did not show a response to the increasing diatom biomass in winter due to high respiration rates that there are not able to overcome by grazing until both types of phytoplankton are present in the column water in significant amounts.

When compared to the *standard run*, diatoms grew faster in winter until reaching their maximum biomass in spring. By contrast, non-diatoms biomass was fairly low for the same period due to very low efficiency regarding light (α_1 was not recovered) as well as higher grazing pressure by microzooplankton and natural mortality. They also bloomed earlier in spring and for longer time, as the end of the bloom occurred at the same time than in the *standard run*. The values obtained by the model are not realistic. Even when the model produced good seasonal fits for nitrate and silicate concentrations, it did not show a realistic behavior in terms of diatoms biomass, whose concentration reached a maximum in early winter almost similar in magnitude to the spring bloom.

Ammonium and detritus concentration predicted by the degraded model were very similar in magnitude to the *standard run.*

The degraded model performed a good recovery of parameters (12 out of 22), six corresponding to diatoms, two to non-diatoms, three to microzooplankton and one detrital parameter (see table 3.3).

TE9 gave a cost function value similar to *TE1* but with a greater misfit due to observations and taken 43 iterations.

3.5.2 Twin Experiment 10 (TE10): Bloom data assimilation

Basically, the degraded model estimated nitrate well but overestimated silicate concentration during autumn and winter when bloom period *synthetic observations* are assimilated (figure 3.4). As described for the weekly data, the model was not able to reproduce the double chlorophyll peak shown by the observations although it mimicked its dynamics very well and also matched its maximum concentration. Diatoms annual variability was better predicted than in the previous case and so was non-diatoms biomass although it is halved in spring. Microzooplankton double peak was successfully reproduced matching the tendency defined by the *synthetic observations.* The first one is related to the non-diatom bloom and the second one is due to the development of diatoms.

In terms of parameter recovery, *TE10* did not perform as well as *TE9* as only nine out of 22 parameters were successfully recovered: three corresponding to diatoms, three to non-diatoms, one to both phytoplankton groups (K_p) and two to microzooplankton (see table 3.3). As in the previous case, *TE10* gave a cost function value similar to *TE2* with similar contributions to the misfit by observations and parameters.

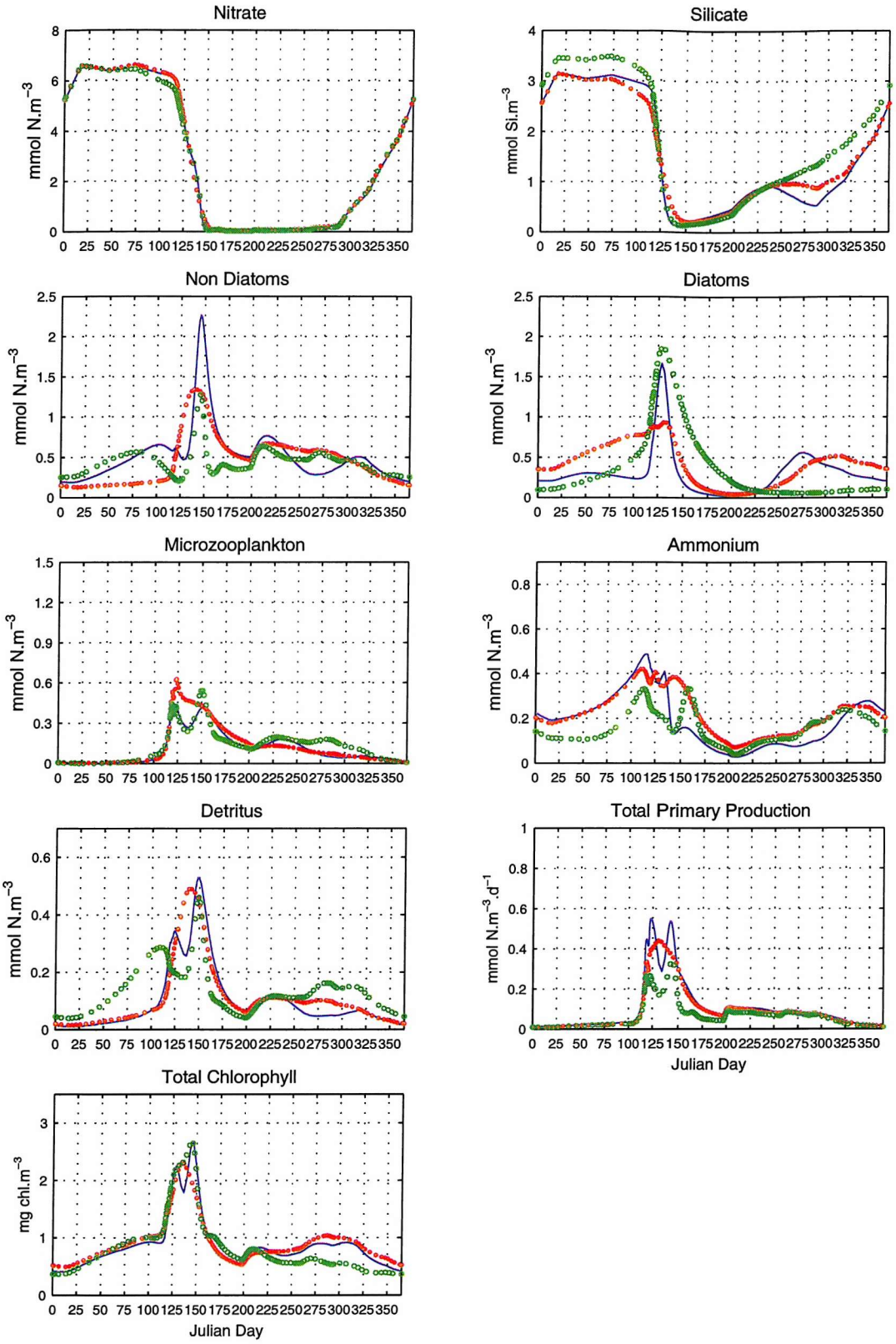

Figure 3.4: Seasonal variability of all the state variables and also total chlorophyll and primary production corresponding to the *standard run* (blue line) *vs.* the degraded model (7CM) predictions using weekly (red dots) and bloom (green circles) data (nitrate, silicate, zooplankton and total chlorophyll) as *synthetic observations.*

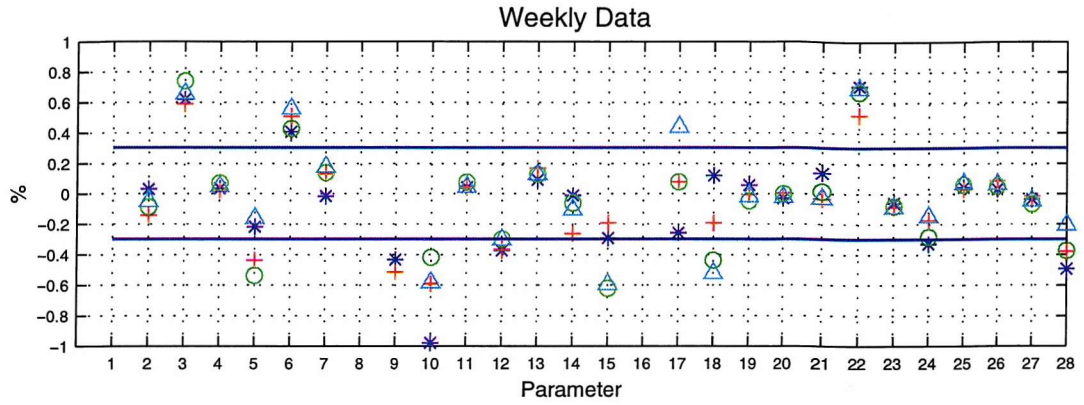

	1 $\mu1$	2 K1	3 K2	4 $\psi1$	5 $\alpha1$	6 Kp	7 Pmax1	8 $\beta1$	9 ε	10 $\nu1$	11 g1	12 K6	13 $\delta1$	14 Pmax2	15 $\alpha2$	16 K5	17 $\mu2$	18 K3	19 K4	20 $\psi2$	21 Re	22 Smax	23 $\beta2$	24 $\nu2$	25 $\zeta2$	26 g2	27 K7	28 p2
TE1		x		x	x		x				x		x	x	x		x	x	x	x	x		x		x	x	x	
TE3		x		x			x				x		x	x	x		x	x	x	x	x		x	x	x	x	x	
TE4		x		x			x				x	x	x	x			x		x	x	x		x	x	x	x	x	
TE5		x		x	x		x				x		x	x					x	x	x		x	x	x	x	x	x

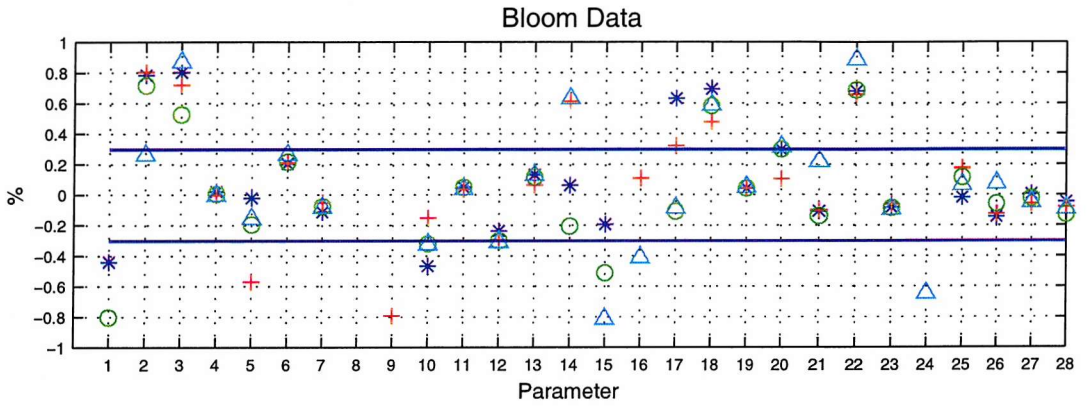

	1 $\mu1$	2 K1	3 K2	4 $\psi1$	5 $\alpha1$	6 Kp	7 Pmax1	8 $\beta1$	9 ε	10 $\nu1$	11 g1	12 K6	13 $\delta1$	14 Pmax2	15 $\alpha2$	16 K5	17 $\mu2$	18 K3	19 K4	20 $\psi2$	21 Re	22 Smax	23 $\beta2$	24 $\nu2$	25 $\zeta2$	26 g2	27 K7	28 p2
TE2				x	x	x	x				x	x	x	x	x			x	x	x		x		x	x	x	x	
TE6				x		x	x			x	x	x	x			x		x	x	x		x		x	x	x	x	
TE7				x	x	x	x				x	x	x	x			x		x		x	x		x	x	x	x	
TE8		x		x	x	x	x				x		x				x	x		x		x		x	x	x	x	

Figure 3.5: Parameters recovery corresponding to the noisy and non-noisy runs when weekly and bloom data where assimilated as *synthetic observations*. The blue band represents the limit of recovery arbitrary established (0.30). No_noise runs (*TE1*, *TE2*) are represented by blue stars, *noise1* (*TE3*, *TE6*) by red crosses, *noise2* (*TE4*, *TE7*) by green circles and *noise3* (*TE5*, *TE8*) by light blue triangles. The equivalence between the numbers on the x-axis and parameters is given in the table shown below each plot as well as if they were recovered (x) or not (blank).

3.6 Summary of key points

- Twin experiments have been shown to be a valuable tool to determine sensitivity of the model either to its structure as well as to data constraints needed when using ecosystem models.

- Data available as *synthetic observations* through regular sampling of the water column (as often as on a weekly regular basis for a year) provided as good approximation to the ecosystem dynamics as when sampling is only carried out for a shorter but well-defined period of time (spring bloom), in terms of model fit to observations. However, the model only reproduced the double chlorophyll peak observed in real data when systematically sampling over the bloom period took place but with a large penalty due to parameter estimation. Both sampling strategies recovered the same number of parameters although they were not always the same ones.

- The addition of noise, either weekly or in spring bloom time, showed a stronger effect on variables not constrained by observations. In general, both approximations yielded similar results: good representation of nutrient dynamics, mesozooplankton and diatoms; overestimation of the primary production. Mismatch between non-diatom-microzooplankton dynamics (when compared to the *standard run*) is due to the lack of observations available for either group. The main difference was found in terms of chlorophyll as weekly data never reproduced the double peak while bloom data did.

  Parameter recovery was also very similar: 14 and 12 parameters were always recovered by using the weekly and the bloom sampling strategy, respectively and

none of them recovered eight parameters (corresponding to phytopiankton and microzooplankton only) in either case.

- The model seemed to be equally sensitive to mesozooplankton and chlorophyll noisy data.

- Regarding model structure stability: twin experiments showed that the main ecosystem dynamics could be described using a simpler representation of the actual ecosystem when observations during spring are available although it is unable to predict the double chlorophyll peak. When using weekly observations some of the variables responded in a non-realistic way.

- In all the studied cases, the model recovered non-diatom parameters defining nitrate uptake inhibition due to ammonium (ψ_1) and non-diatom half saturation constant for ammonium (K_4). By contrast, diatom natural mortality (μ_1), half saturation constant for ammonium (K_2) and microzooplankton assimilation efficiency (β_1) were never recovered (see figure 3.5).

  With exception of the twin experiments carried out to test the model structure stability, the model always recovered ψ_1, $Pmax_1$ (non-diatoms), g_1 (microzooplankton), δ_1 (detritus), K_4 and Re (diatoms), β_2, ζ_2, g_2, K_7 (mesozooplankton). Never recovered were μ_1, K_2 (non-diatoms), β_1, (microzooplankton), ε (micro and mesozooplankton) and S_{max} (diatoms).

  Mesozooplankton parameters seem to be very robust to the model structure.

- As expected, variables for which observations were available were better predicted in all cases. There seems to be a need to constrain either non-diatoms or microzooplankton to improve the model fit.

Table 3.1: Parameter correlation (r) between model results and synthetic observations corresponding to the different twin experiments performed. n represents the number of data points.

Run	$r_{nitrate}$	$r_{silicate}$	$r_{mesozooplankton}$	$r_{total\ chlorophyll}$
TE1 (n = 53)	1.00	1.00	0.98	0.95
TE2 (n = 50)	1.00	1.00	0.97	0.96
TE3 (n = 53)	0.99	0.93	0.62	0.85
TE4 (n = 53)	0.99	0.93	0.62	0.78
TE5 (n = 53)	0.99	0.93	0.45	0.85
TE6 (n = 50)	0.98	0.95	0.73	0.84
TE7 (n = 50)	0.98	0.95	0.74	0.72
TE8 (n = 50)	0.98	0.95	0.57	0.85
	$r_{nitrate}$	$r_{silicate}$	$r_{microzooplankton}$	$r_{total\ chlorophyll}$
TE9 (n = 53)	1.00	0.98	0.93	0.94
TE10 (n = 50)	1.00	0.99	0.96	0.96

Table 3.2: Misfit components corresponding to the different twin experiments performed.
Misfit due to parameters (ssq_p), observations (ssq_o), total misfit (ssq) and number of iterations (it) taken for each run are shown.

Run	ssq_p	ssq_o	ssq	it
Standard	2.76	547.11	549.86	14
Test	3.88	518.34	522.22	16
TE1	4.83	14.88	19.71	12
TE2	19.41	20.66	40.07	17
TE3	4.72	178.16	182.88	6
TE4	5.03	307.13	312.16	7
TE5	7.82	200.83	208.66	8
TE6	5.95	114.13	120.09	16
TE7	8.64	204.84	213.48	15
TE8	34.20	137.38	171.58	12
TE9	1.37	19.46	20.84	43
TE10	24.38	24.20	48.58	15

Table 3.3: List of the optimal parameters for each twin experiment performed.
Bold figures show parameters which have been recovered according to the arbitrary criteria chosen.

Parameter	Standard (P3)	TE1	TE2	TE3	TE4	TE5	TE6	TE7	TE8	TE9	TE10
μ_1	0.0186	0.0981	0.0268	0.0591	0.0720	0.0573	0.0712	0.0335	0.0614	0.0946	0.0273
K_1	0.7718	**0.7505**	0.1638	**0.8850**	**0.8391**	**0.8101**	0.1488	0.2170	**0.5672**	0.4361	0.2400
K_2	0.3852	0.1469	0.0752	0.1599	0.0998	0.1321	0.1072	0.1811	0.0484	0.8662	0.8677
ψ_1	3.4546	**3.3433**	**3.3719**	**3.3993**	**3.2096**	**3.2843**	**3.4570**	**3.4243**	**3.4632**	**3.1439**	**3.3311**
α_1	0.0208	**0.0254**	**0.0212**	0.0300	0.0320	**0.0242**	0.0327	**0.0248**	**0.0240**	0.0145	**0.0268**
K_p	0.0795	0.0473	**0.0630**	0.0395	0.0456	0.0352	**0.0629**	**0.0621**	**0.0583**	**0.0763**	**0.0797**
P_{max1}	1.8188	**1.8542**	**2.0205**	**1.5898**	**1.5658**	**1.4984**	**1.9140**	**1.9557**	**1.9640**	2.8149	**1.6249**
β_1	0.3611	0.8513	0.8354	0.8425	0.8710	0.8376	0.8320	0.8030	0.8215	0.5484	0.5925
ε	0.0947	0.1361	0.2170	0.1439	0.2135	0.2202	0.1700	0.2807	0.2012	**0.0806**	0.7769
ν_1	0.1125	0.2230	0.1648	0.1793	0.1594	0.1780	**0.1296**	0.1482	0.1486	**0.1407**	0.1623
g_1	1.1299	**1.0861**	**1.0725**	**1.0824**	**1.0451**	**1.0826**	**1.0879**	**1.0701**	**1.0832**	0.7264	**0.9985**
K_6	0.7645	1.0519	**0.9443**	1.0463	**0.9934**	0.9959	**0.9893**	**0.9917**	**0.9988**	**0.7118**	**0.9074**
δ	**0.2769**	**0.2520**	**0.2402**	**0.2318**	**0.2421**	**0.2418**	**0.2593**	**0.2436**	**0.2398**	**0.2424**	**0.0251**
P_{max2}	2.8411	**2.8851**	**2.6556**	**3.6004**	**3.0170**	**3.1436**	1.0933	**3.4202**	1.0311	1.1607	1.2178
α_2	0.0877	**0.1135**	**0.1046**	**0.1049**	0.1422	0.1399	0.1781	0.1324	0.1588	**0.0735**	0.1620
K_5	1.8246	4.1059	4.3080	3.9686	4.0635	3.9847	**1.6275**	4.9984	2.5694	0.7375	4.2002
μ_2	0.0098	**0.0124**	0.0036	**0.0091**	**0.0090**	0.0055	0.0067	**0.0108**	**0.0106**	0.0184	**0.0070**
K_3	0.2076	**0.1834**	0.0631	**0.2485**	0.2984	0.3164	0.1084	0.0860	0.0846	**0.2276**	0.9242
K_4	0.8671	**0.8204**	**0.8292**	**0.8748**	**0.9079**	**0.8822**	**0.8285**	**0.8269**	**0.8204**	**0.8997**	**0.9576**
ψ_2	3.3677	**3.4739**	**2.3626**	**3.3758**	**3.3750**	**3.4456**	**3.0149**	2.3529	2.2976	**3.5138**	**2.9469**
Re	1.7066	**1.4793**	**1.8860**	**1.7754**	**1.6834**	**1.7608**	**1.8773**	**1.9370**	**1.3266**	**1.6988**	0.9898
S_{max}	1.7034	0.5016	0.5408	0.8329	0.5650	0.5283	0.5799	0.5264	0.1866	**1.4296**	0.5349
β_2	0.6307	**0.6691**	**0.6813**	**0.6876**	**0.6824**	**0.6892**	**0.6693**	**0.6827**	**0.6885**	N/A	N/A
ν_2	0.0379	0.0505	0.0997	**0.0447**	**0.0486**	**0.0437**	0.1012	0.0887	0.0623	N/A	N/A
ζ_2	0.2855	**0.2738**	**0.2902**	**0.2782**	**0.2688**	**0.2663**	**0.2352**	**0.2517**	**0.2657**	N/A	N/A
g_2	0.3720	**0.3610**	**0.4250**	**0.3421**	**0.3544**	**0.3494**	**0.4181**	**0.3929**	**0.3436**	N/A	N/A
K_7	0.6006	**0.6231**	**0.5955**	**0.6132**	**0.6418**	**0.6279**	**0.6348**	**0.6129**	**0.6276**	N/A	N/A
p_2	0.4890	0.7317	**0.5104**	0.6758	0.6720	**0.5896**	**0.5277**	**0.5500**	**0.5322**	N/A	N/A

Table 3.4: Actual noise added to the data to be used as observations.

Variable	Noise1	Noise2	Noise3
Total chlorophyll	±0.24	±0.40	±0.24
Mesozooplankton biomass	±0.14	±0.14	±0.21
Nitrate concentration	±0.44	±0.44	±0.44
Silicate concentration	±0.42	±0.42	±0.42

Chapter 4:

Parameter Uncertainty

Chapter 4: Parameter uncertainty

4.1 Introduction

The aim of this chapter is to asses the precision to which the model parameters are determined. Section 4.2 describes the second partial derivatives of the cost function, or Hessian matrix as well as the information provided by the Hessian and also by its inverse. Section 4.3 describes the model results and discusses the eigensystem of the Hessian matrix and, in particular, its indefiniteness. The relative uncertainty of the optimal parameters as well as parameter correlation are analysed in section 4.4. In section 4.5, the model sensitivity to the starting point in the parameter space is tested. Finally, the sensitivity of the 0-D model to the time-step chosen was tested.

A summary of the key points encountered is also included at the end of the chapter.

4.2 The Hessian matrix

The basic features of the optimisation module implemented as part of the ecological model were described in Chapter 2 (section 2.5). Recent studies (Fennel *et al.*, 2001; Matear, 1995) have shown the importance of investigating the uncertainty associated with the optimal model parameters by analysing the Hessian matrix of the cost function. The Hessian matrix is defined as the second partial derivatives matrix of a *p* variable function:

$$H(x) = \nabla^2 ssq(x) = \frac{\partial^2 ssq}{\partial x_i \partial x_j} \qquad \text{for } x = (x_1,\ldots,x_p) \qquad [4.1]$$

where *ssq* is the cost function and *i*, *j* =1,..., *p*, where *p* represents the number of parameters.

Because *ssq*(x) is smooth, it can be expanded in its Taylor series about the minimum x* yielding:

$$ssq(x^* + x) = ssq(x^*) + \frac{1}{2}(x^* + x)^T \nabla^2 ssq(x^* + x) \qquad [4.2]$$

where the third and higher order terms are neglected for practical computation. Thacker (1987) showed that if the neglected terms are sufficiently small, the uncertainties associated with the optimal model parameters follow a normal distribution with zero mean and with an error-covariance matrix given by the inverse of the Hessian. He also showed that the inverse of the Hessian matrix of the cost function is the error-covariance matrix of the best fit values of the independent variables, whose off-diagonal elements will indicate the degree of correlation (positive or negative) between two parameters.

The behaviour of equation 4.2 about the optimal solution x* is determined by the Hessian matrix. By definition:

$$H(x)\vec{u}_i = \lambda_i \vec{u}_i \qquad [4.3]$$

where $\vec{u}_i$ and λ_i represent the eigenvectors and eigenvalues of **H**(x), where i = 1, 2,..., p with $\lambda_1 \leq \lambda_2 \leq ... \leq \lambda_p$. When all the eigenvalues of **H**(x) are positive, **H**(x) will be positive definite and therefore, x* will be a strong local or possibly a global minimum of *ssq*. If **H**(x) is positive semi-definite (its eigenvalues are positive or equal to zero), x* is a weak local minimum. If **H**(x) is indefinite (positive and negative eigenvalues) and non-singular, x* is a saddle point. Small eigenvalues indicate large uncertainties in the parameter set, suggesting that some of the model parameters may be poorly determined by the data.

The condition number of the Hessian provides valuable information about the rate of convergence of the minimisation technique as well as about the singularity of the matrix. It is given by the ratio of its largest eigenvalue to its smallest (all of them being greater than or equal to zero, as **H**(x) is a symmetric and positive semi-definite matrix at the minimum):

$$cond(H(x)) = \frac{\lambda_p}{\lambda_1} \qquad [4.4]$$

If the condition number is large, the matrix will be ill-conditioned and almost singular, indicating that there are some linear combinations of the model parameters not well determined by the data used to calculate the fit. Therefore the solution may be changed substantially by even small changes in the data. On the other hand, the matrix will be well-conditioned if its condition number is close to unity, indicating that the solution is "stable" to small changes in the data (important for noisy data).

The inverse of the Hessian can be calculated from its eigensystem, as the Hessian can

be represented as the sum of products of its eigenvalues and eigenvectors (Thacker, 1989):

$$H(x) = \sum_i \lambda_i u_i u_i^T \qquad [4.5]$$

Similarly, since $H^{-1}(x)\, u_i = \lambda_i^{-1} u_i$,

$$H^{-1}(x) = \sum_i \frac{1}{\lambda_i}\, u_i u_i^T \qquad [4.6]$$

The smallest eigenvalue (λ_{min}) of the Hessian (or the largest eigenvalue of its inverse) and the linear function $u_{min}^T x$ determined by the corresponding eigenvector is the least well determined linear combination of the model parameters.

For the model, the Hessian matrix was evaluated numerically using a centered finite differencing scheme and inverted using a Singular Value Decomposition (SVD) algorithm.

4.3 Model results

The best estimated set of parameters (*P3*) obtained in section 2.7 yielded an indefinite Hessian with five negative eigenvalues. This means that the optimisation algorithm is being computed not at the minimum but at a saddle point of the cost function, which is unsurprising due to the high dimensionality of the parameter space. According to equation 4.5, the smallest eigenvalues provide the worst estimated **H**(x*)*. If we think of saddle points as "instabilities" in the system, it is easy to see that the magnitude of the eigenvalues indicates how severe they are. The analysis of each eigenvector corresponding to each "instability" reveals its nature, and the contribution of each single parameter to the corresponding eigenvalue (figure 4.1). By not optimising (fixing *a priori*) the parameters that mostly contribute to the negative eigenvalues, a positive definite **H**(x*)* can be obtained.

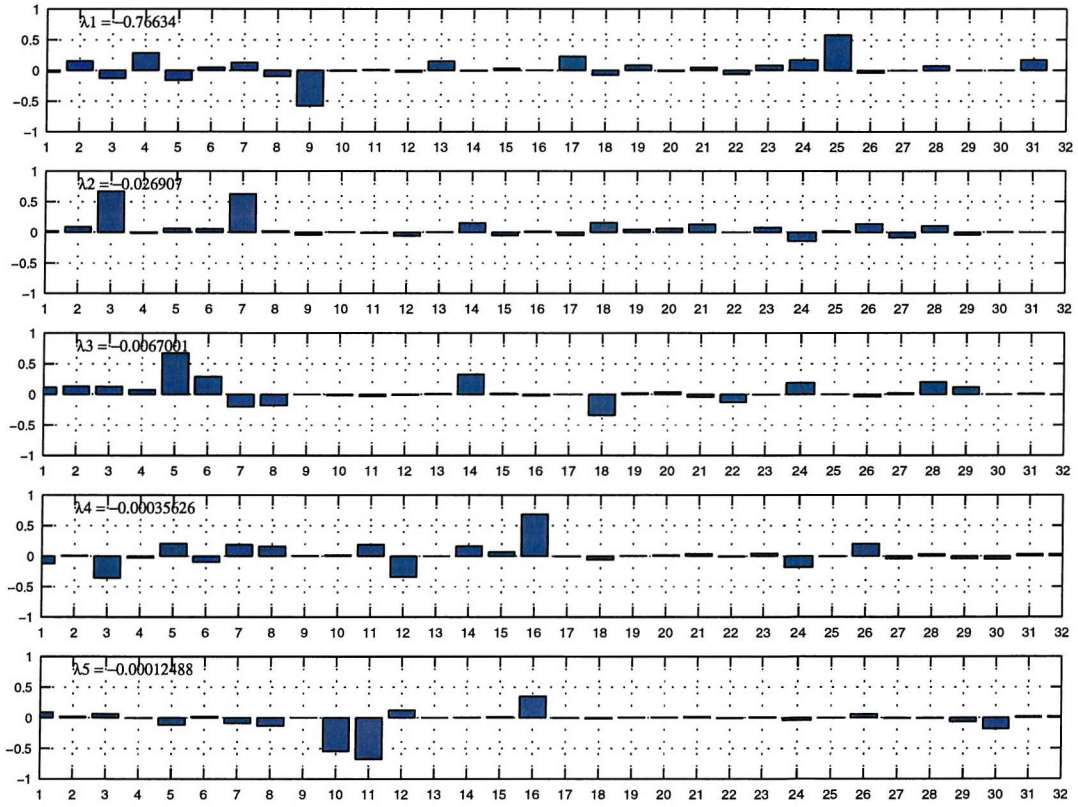

Figure 4.1: Negative eigenvalues and corresponding eigenvectors for the optimal parameter set (*P3*) obtained in section 2. 4 (chapter 2). The x axis shows parameter numbers corresponding to the ecological parameters in table 4.1.

We begin by keeping one parameter at a time fixed, starting with the mesozooplankton mortality rate (parameter 25 or ζ_2) as it is the main contributor to λ_1 (the largest negative eigenvalue) in figure 4.1. The model was rerun (using P3 as the parameter set without optimising ζ_2) and a new **H**(x) was obtained. Then, the changes in magnitude of each negative eigenvalue as well as the different parameter contributions were evaluated, and the same process was repeated until a positive definite **H**(x) was obtained. Figure 4.1 shows that the eigenvectors corresponding to the negative eigenvalues represent a combination of a wide range of parameters, mainly related to microzooplankton grazing and to phytoplankton growth rates (specially non-diatoms). This is not surprising due to the poor quality in the microzooplankton data (high variability within the data set that is very likely to carry significant noise) and the lack of real data to constrain non-diatoms. However, as parameters were kept fixed, the analysis of the corresponding eigenvectors revealed strong parameter correlation also involving mesozooplankton (real data also showed high variability) and larger phytoplankton (diatoms). In the end, a total of 14 parameters had to be fixed to obtain a positive-definite **H**(x), ensuring that it is calculated at either the global or, most likely, at a strong local minimum.

The non-optimised (fixed) parameters were: the microzooplankton ingestion half saturation constant, maximum ingestion rate and assimilation efficiency (K_6, g_1, β_1); mesozooplankton grazing half saturation constant, mortality and assimilation efficiency (K_7, ζ_2, β_2); non-diatom half saturation constant for ammonium uptake, the initial slope of the P-I curve and the nitrate uptake ammonium inhibition parameter (K_2, α_1, ψ_1); diatom half saturation constant for nitrate and silicate uptake, mortality rate and maximum growth (K_3, K_5, μ_2, $Pmax_2$); the subsurface silicate concentration (S_{surf}).

The indefiniteness in the Hessian matrix due to zooplankton parameters is not surprising

as there is great uncertainty associated with zooplankton field observations and they are likely to carry noise as showed by the great variability in the NABE data set. Neither are the parameters corresponding to non-diatoms, as no real data were available for this state variable to be constrained. On the other hand, the need to keep S_{surf} fixed is very likely to be caused by the simple way in which the vertical mixing has been parameterised and the use of a better resolved vertical model should improve this.

4.3.1 Model sensitivity to negative eigenvalues

To check the robustness/sensitiveness of the model to fixing the above parameters, the model was run, and optimised, under the same conditions that led to the *standard run* results, therefore using *P2* as the first parameter guess, but without optimising the set of 14 parameters that yielded the indefinite **H**(x). This model run will be referred to as run P14. The new model results were very similar to the *standard run* as is evident from the similar values of the cost function (ssq_{P14} = 548.6 *versus* $ssq\_{standard\ run}$ = 549.9). The largest differences were observed in the silicate and ammonium compartments (figure 4.2). The winter silicate concentration was around 1 mmol m^{-3} higher than in the *standard run* as there is no constraint by winter NABE data, the diatoms maximum growth rate (P_{max}) was reduced compared to the *standard run* and their silicate assimilating efficiency (K_5) increased (figure 4.3). However, peak diatom biomass was higher than in the *standard run* due to mesozooplankton reduced assimilation efficiency (x=23 in figure 4.3), reduced diatom sinking rate (x=22 in figure 4.3) and higher light efficiency (x=15 in figure 4.3). Non-diatoms also reached higher peak biomass as their maximum growth rate (x=7 in figure 4.3) was higher than in the *standard run*, leading to higher microzooplankton biomass in spring. On the other hand, the nitrate pool was reduced by 0.5 mmol N m^{-3} during autumn and winter, compared to the *standard run*, as the parameter responsible for the nitrate subsurface concentration (N_{nsurf}) was reduced.

Reduced non-diatom efficiency taking up ammonium (x=3 in figure 4.3) and enhanced zooplankton excretion are reflected in the higher ammonium concentration in the mixed layer.

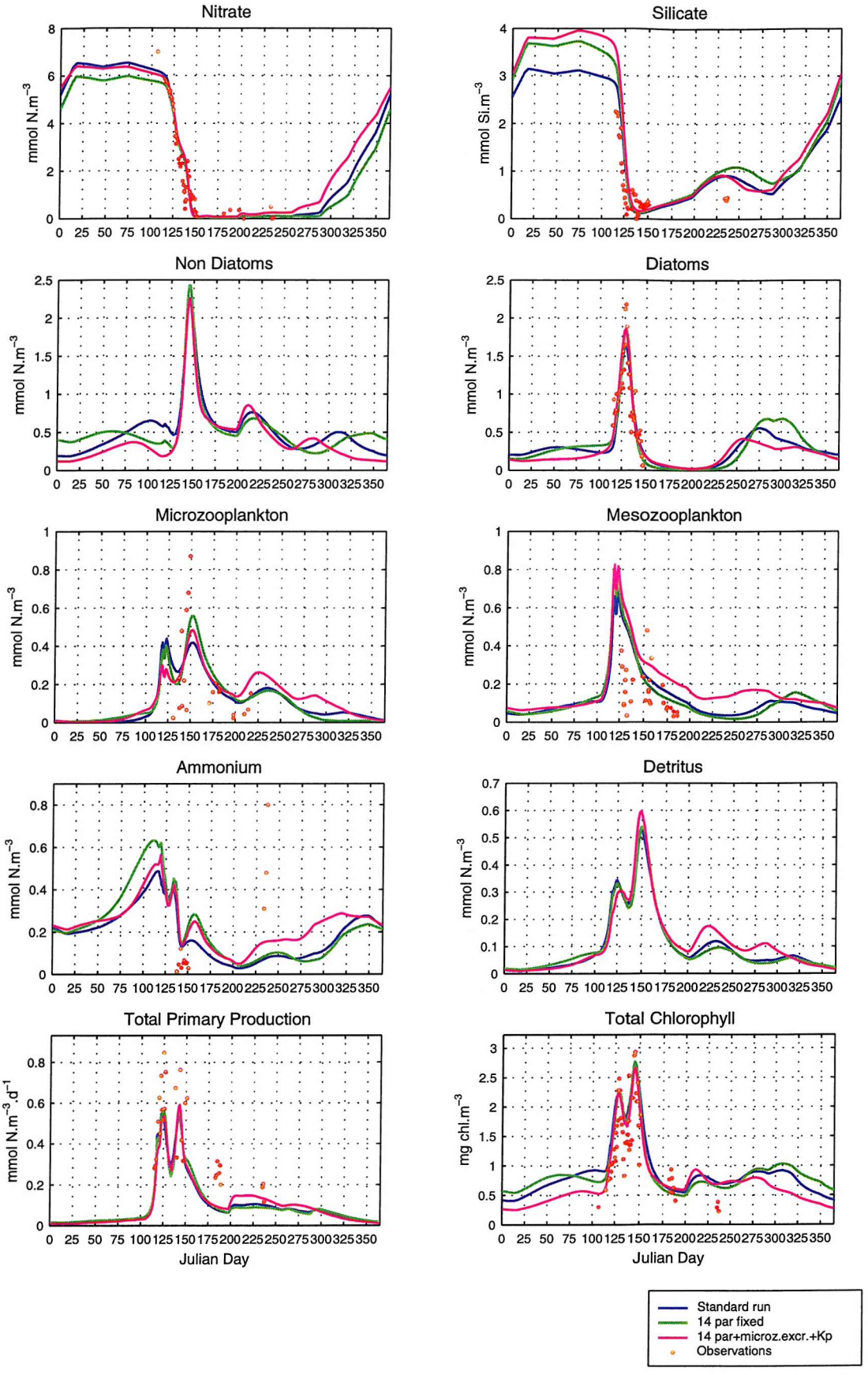

Figure 4.2: Model output corresponding to the *standard run* (blue) and runs P14 (green) and P16 (magenta).

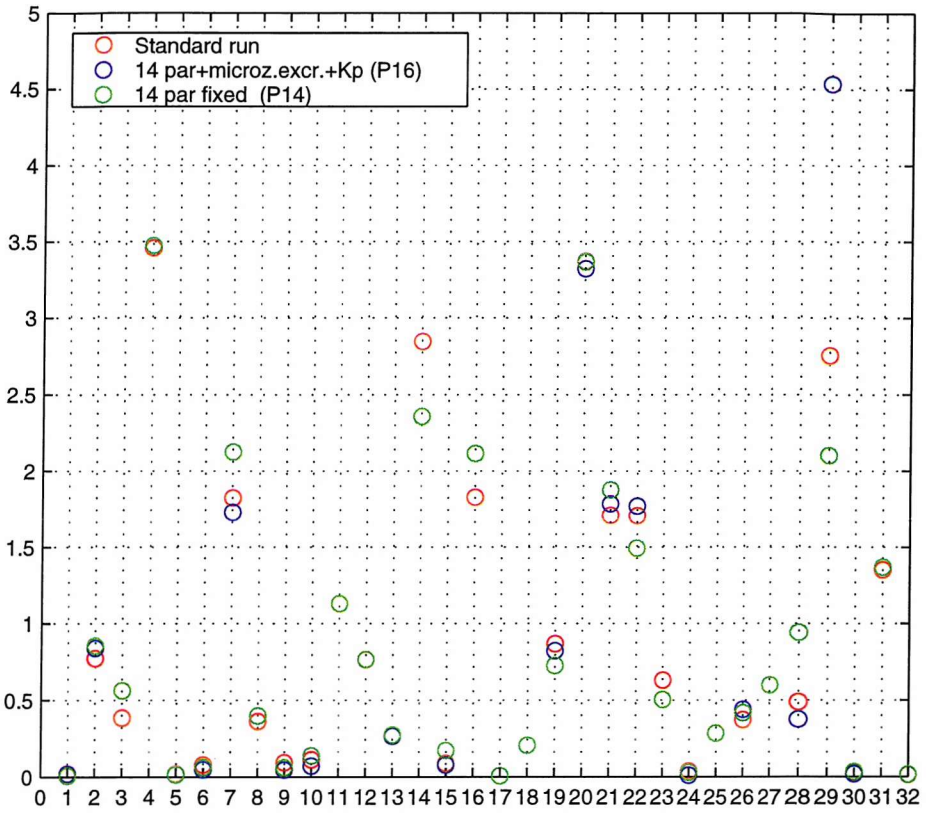

Figure 4.3: Values of the optimal parameter set corresponding to the standard (red), P14 (green) and P16 (blue) runs. Non-optimised parameters in P14 were parameters number 3, 4, 5, 8, 11, 12, 14, 16, 17, 18, 23, 25, 27 and 31. The x axis corresponds to parameters listed in table 4.1.

4.4 Parameter uncertainty, correlation and condition number

After having fixed 14 parameters to obtain a positive definite matrix, the model parameter uncertainties associated with the 18 optimised parameters were estimated. They are given by the diagonal elements of the error-covariance matrix (as a measure of the width of the distribution for the different optimal parameters). Parameter uncertainties were divided by their corresponding optimal value to obtain relative uncertainties. Table 4.2 shows low parameter uncertainties, suggesting that model results are well constrained by the data. The calculated relative uncertainties indicate that the detritus remineralisation rate (δ_1), the silicate to nitrogen ratio for diatoms (Re), the mesozooplankton maximum grazing rate (g_2), the nitrate subsurface concentration (N_{nsurf}) and the gradient of silicate across the thermocline (S_{grad}) are the parameters best determined by the optimisation (as they have the lowest values of the whole set) and hence the model output is more sensitive to those parameters. However, the condition number of the Hessian matrix was $1.03 \times 10^{+6}$, indicating that a number of model parameters are highly correlated and therefore, the problem is ill-conditioned. The correlation matrix provides the degree of correlation between all pairs of the model optimal parameters. Table 4.3 shows the existence of two sets of highly correlated parameters ($|r|>0.8$) and 11 independent parameters. The first set of correlated parameters (set A) are K_4 (diatoms half-saturation constant for ammonium uptake), ν_1 and ν_2 (micro and mesozooplankton excretion rates) and N_{ngrad} (nitrate gradient across the thermocline); the second set (set B) comprised P_{max1} (non diatoms maximum growth rate), K_p (phytoplankton self shading coefficient) and p_2 (mesozooplankton preference for diatoms). As each set of parameters is systematically correlated, the solution they provide is not unique and the applied data set

does not contain enough information to determine those parameters simultaneously. All correlated parameters in set A are related to nitrogen (3 related to ammonium and 1 to nitrate) while parameters in set B are related to phytoplankton growth. Parameter resolution, given by the eigenvalues and eigenvectors of the Hessian (figure 4.4) shows that the major contributions to the smallest eigenvalues are exclusively due to nitrogen related parameters (v_1, $N_{n\,grad}$).

Most of the correlated parameters correspond to state variables that were poorly constrained by the data, such as the zooplankton parameters (v_1, v_2 and p_2) and diatom parameter K_4, directly related to the ammonium pool. As stated earlier, there is high variability associated to the mesozooplankton measurements, which are likely to carry noise as well as the ammonium data, for which cruises Tyro and Atlantis provided very different estimates (< 0.2 mmol NH_4^+ m^{-3} from Atlantis and > 0.8 mmol NH_4^+ m^{-3} from cruise Tyro). The remaining parameters K_p and P_{max1} are used to describe light-based phytoplankton growth and their correlation comes from the model formulation of the light-curve.

As we want to obtain a well-determined set of parameters that result in the best fit to the field observations, any parameter correlation must be avoided. However, it is not clear the best way to do so. One feasible approach, is to analyse the relative parameter uncertainty for both sets of parameters (A and B). According to the distribution of such uncertainty as well as to the diagonal of the Hessian matrix, v_1 is the best estimated parameter, therefore the one chosen to be kept fixed and not optimised as the model output is very sensitive to small changes in its values. An alternative approach, when having few parameter correlations, consists in the computing of the condition number (*cond*) when fixing all different parameters alternatively. In this case, the smallest *cond*

was obtained when not optimising v_1 (3.69 x 10^{+5}) while the largest was provided by not optimising K_4 (8.35 x 10^{+5}). The remaining condition numbers were 6.96 x 10^{+5} when only fixing v_2 and 4.58 x 10^{+5} for $N_{n\,grad}$.

As both approaches led to the same solution, v_1 was fixed at its optimum value. The model output showed the correlation among all the remaining parameters contained in set B was significantly reduced ($|r|<0.8$), the condition number improved and the parameter dependency of the whole model reduced to only two of the parameters in set B (P_{max1}, K_p which were positively correlated).

Using the same procedure, we kept K_p fixed to its optimum value. As expected, the correlation to P_{max1} was also significantly reduced, all the parameter dependencies have been finally overcome and the condition number has also improved (3.51 x 10^{+5}). The formulated optimisation problem was finally able to uniquely determine 16 independent parameters.

Compared to similar studies, the model performance is encouraging. Matear (1995) tested three different ecosystem models studying parameter correlation based on a simulated annealing optimisation technique. The maximum number of independent parameters that he could determine varied between 8 and 9, of a total set of 15 and 20 optimised parameters, respectively. The condition number of his Hessian matrixes varied between 10^{+6} and 10^{+8}. Fennel *et al.* (2001) applied the adjoint method to a 12-parameter NPZD model. Their condition number was 10^{+11} (they did not estimate parameter correlation), which they attributed to their model formulation which was not able to reproduce the main features of their field data.

As in the previous section, the model sensitivity to the non-optimisation of these parameters was tested. Once more, the model was run and optimised, under the same

conditions that led to the *standard run* results, using *P2* as the first parameter guess, but without optimising a set of 16 parameters (the ones specified in run P14 plus v_1 and K_p). This model run will be referred to as run P16. Figures 4.2 and 4.3 show the dynamics followed by the state variables as well as the corresponding optimal parameter set. Again, P16 is very similar to P14 and the *standard run*, as reflected in the final value of the cost function (*ssq* = 547.91).

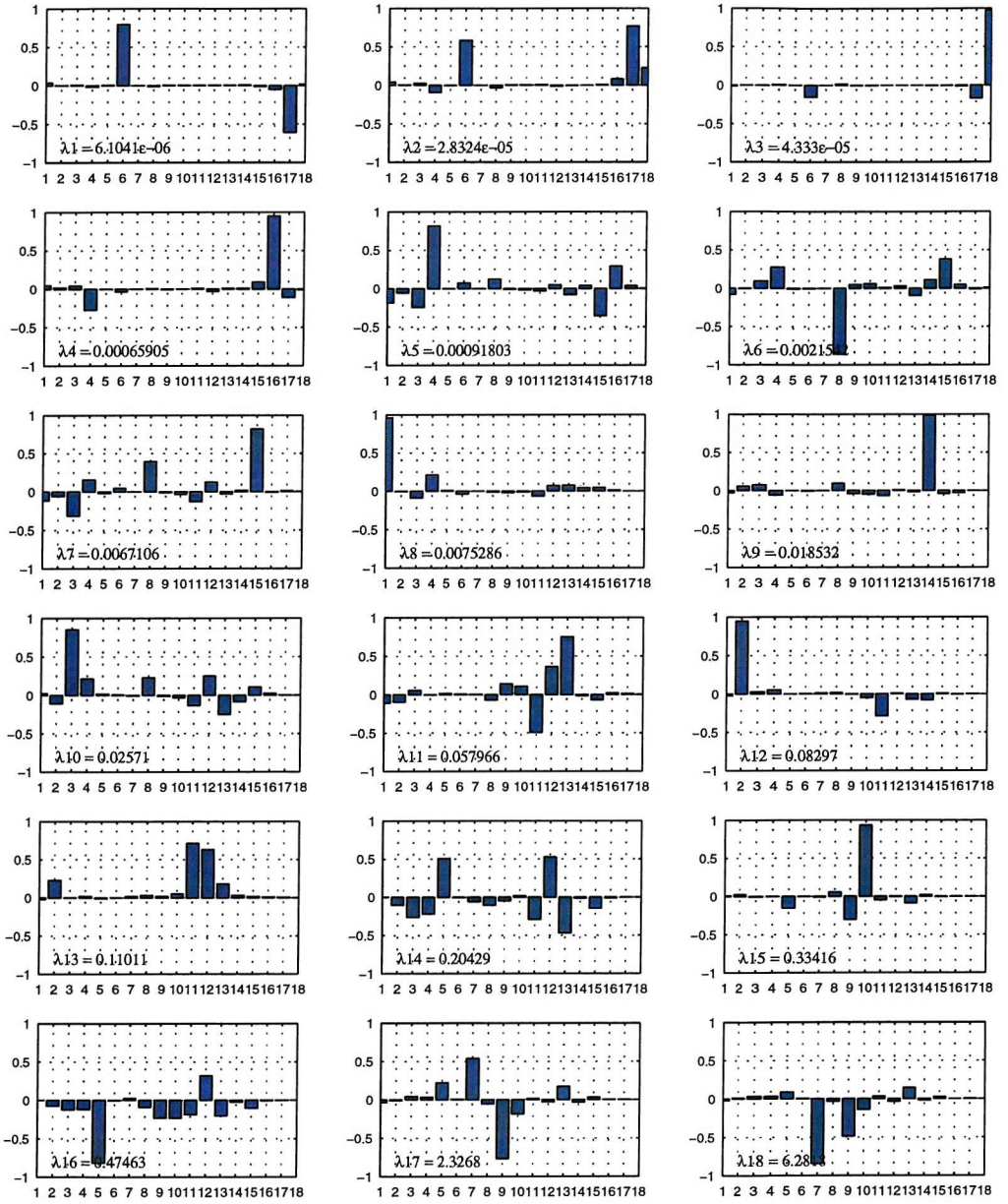

Figure 4.4: Eigenvalues and eigenvectors corresponding to run P14. The x axis corresponds to parameters in table 4.2.

4.5 First guessed parameter values

A final test was carried out aiming to asses the sensitivity of the model to the starting point in the parameter space. We wanted to investigate whether the model optimisation would provide a positive-definite Hessian when the model was run using a different parameter guess (other than P2) and by non-optimizing the same 14 parameters specified in section 4.3. Unfortunately, the optimisation algorithm seems to be highly dependent on the starting point as an indefinite Hessian was obtained (2 negative eigenvalues; ssq=666.91; ssq_o=658.42; ssq_p=8.49 *versus* ssq=549.87; ssq_o=547.11; ssq_p=2.76 from the *standard run*). Why? Inadequate data. The data available are not abundant and carry noise which makes the task of finding the global minimum difficult. Another reason could be non-ideal sampling and model formulation.

The sampling hypothesis could be probed by designing twin experiments, in which bogus data from the *standard run* could be used as observations as in chapter 3. These experiments would also help to determine the most effective temporal sampling to fully constrain model state variables.

Testing model formulation is complex (see for example Fennel *et al.*, 2001). An alternative to fixing (non optimisating) *a priori* values of model parameters could focus on inspecting the model equations, as well as eigenvalues and eigenvectors, to find those parameters that enter the equations as a combination of each other. For instance, figure 4.1 shows that the largest negative eigenvalue is λ_1=-0.766. The corresponding eigenvector ($\vec{v}_1$) has significant contributions mainly from ε and ζ_2. Both parameters are also anti-correlated in $\vec{v}_1$, with opposite signs of the contributions, whereas they do not contribute to the remaining eigenvectors. Inspection of model equations shows that ε and

ζ_2 enter equation 2.26 in multiplicative order and therefore, rather than fixing one of the parameters we could optimise their product ($\hat{\varepsilon} := \varepsilon\xi_2$), reformulate equation 2.26 accordingly and restrict the optimisation to $\hat{\varepsilon}$. A similar appeoach should be taken for the remaining correlated parameters, therefore reducing the complexity of the model.

This is suggested as a future line of research as it goes beyond the scope of this study.

4.6 Time-stepping sensitivity analysis

The ecological model uses a variable time step, which means that continuously monitors the accuracy of the solution during the computation, and adaptively changes the step size to maintain a consistent level of accuracy.

The model sensitivity to the time step was tested by setting up experiments that employed different fixed time steps (0.2 d^{-1}, 0.5 d^{-1} and 0.7 d^{-1}). Results shown that model performance was very similar in all cases (except for ammonium) and also similar to the *standard run* (figure 4.5) However, the choice of a variable step algorithm presents greater advantages as:

- It is much faster than its constant time step version, because they concentrate the computational effort only on those time intervals that need it most (during the bloom time, for instance), taking large strides over intervals that do not need small time steps (i.e. during winter).

- More importantly, varying time step algorithms are more reliable as they can cope with sharp changes in the solution by reducing the time step, where constant time step algorithms will plow right through and could compute erroneous results.

- Also, a varying time step algorithm ensures that numerical instability does not occur.

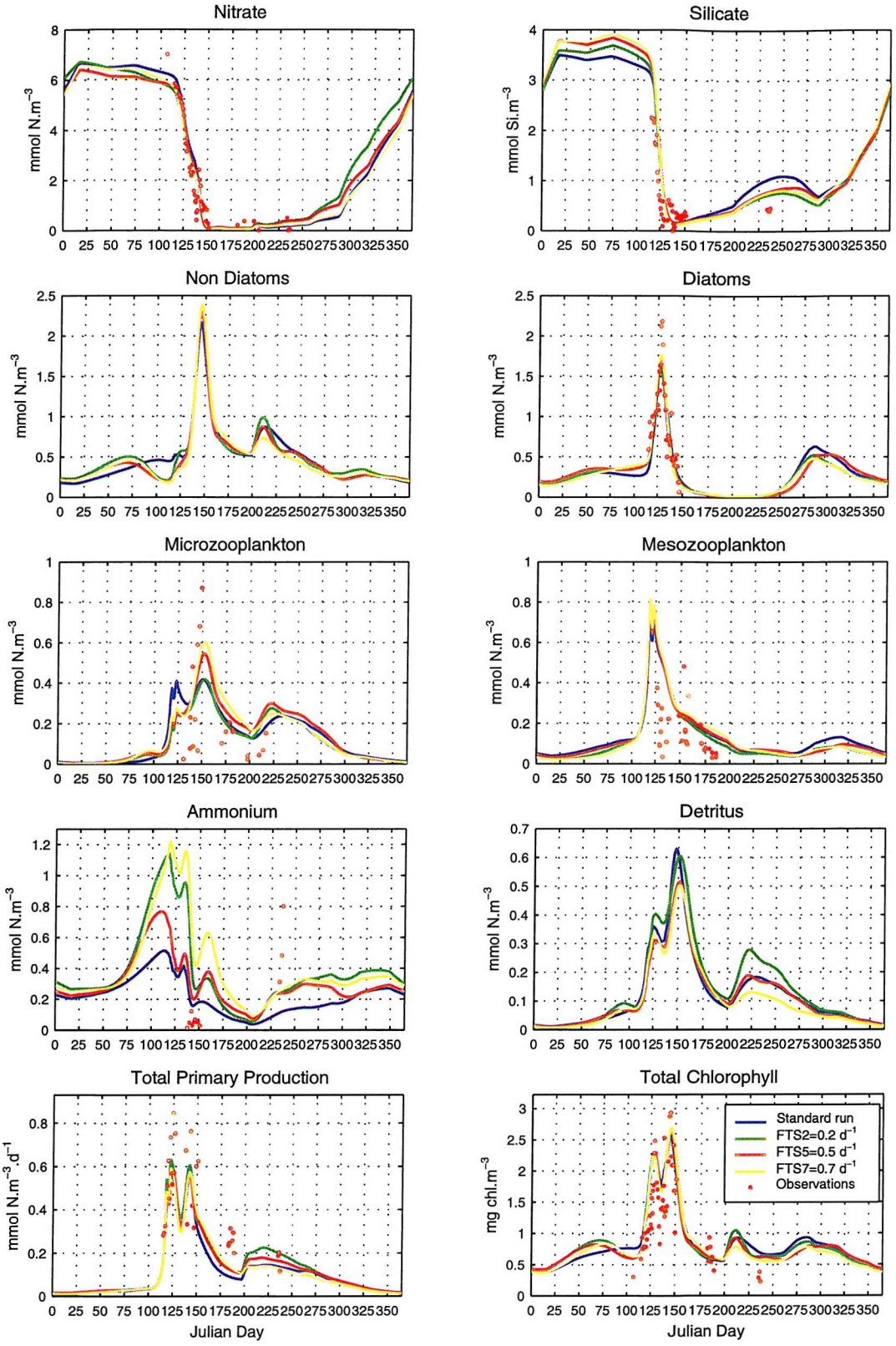

Figure 4.5: Model state variables as well as chlorophyll and primary production using different fixed time steps (FTS2, FTS5, FTS7) and variable time step (*standard run*).

4.8 Summary of key points

- Powell's optimisation technique is effective at determining the optimal parameters for the complex 0-D model. However, the analysis of the Hessian matrix revealed its indefiniteness, suggesting that the cost function had been calculated at a saddle point rather than at the minimum.

- To ensure that the cost function was calculated, at least, at a local minimum, a total of 14 parameters (out of 32) had to be kept fixed during the optimisation. This did not significantly affect the model fit to the NABE data.

- Although the ecological model was able to reproduce the observed data, the correlation matrix showed that 7 out of 18 optimal parameters were highly correlated. As the number of parameters that can be independently determined (16) is less than the number of unknown model parameters (18), the model solution is not unique.

- Parameter correlation involved 2 different groups of parameters: those related to the nitrogen pool and those yielding light-based phytoplankton growth. The former are likely due to the poor data constrain while the latter are due to the model formulation of the P-I curve.

- The definiteness of the Hessian matrix strongly depends on the starting point in the parameter space.

- The 0-D model showed no sensitivity to the time step (fixed or variable) used.

Table 4.1: Model parameters, symbols, ecosystem group and units. Units always refer to nitrogen unless stated otherwise.

Parameter	Number	Symbol	Group	Units
Mortality rate	1	μ_1	P_{nd}	d^{-1}
Half saturation constant for nitrate uptake	2	K_1	P_{nd}	mmol m^{-3}
Half saturation constant for ammonium uptake	3	K_2	P_{nd}	mmol m^{-3}
Nitrate uptake ammonium inhibition parameter	4	ψ_1	P_{nd}	$(mmol\ m^{-3})^{-1}$
Initial slope of P-I curve	5	α_1	P_{nd}	$(ly\ d^{-1})^{-1}\ d^{-1}$
Phytoplankton self-shading coefficient	6	K_p	P_{nd}, P_d	$m^2\ (mmol)^{-1}$
Maximum growth rate	7	P_{max1}	P_{nd}	d^{-1}
Assimilation efficiency on non-diatoms	8	β_1	Z_{mi}	Dimensionless
Fraction of zooplankton mortality recycled to ammonium	9	ε	Z_{mi}, Z_m	d^{-1}
Excretion rate	10	ν_1	Z_{mi}	d^{-1}
Maximum ingestion rate	11	g_1	Z_{mi}	d^{-1}
Ingestion half-saturation constant	12	K_6	Z_{mi}	mmol m^{-3}
Detrital breakdown rate	13	δ_1	D	d^{-1}
Maximum growth rate	14	P_{max2}	P_d	d^{-1}
Initial slope of P-I curve	15	α_2	P_d	$(ly\ d^{-1})^{-1}\ d^{-1}$
Half saturation constant for silicate uptake	16	K_5	P_d	mmol Si m^{-3}
Mortality rate	17	μ_2	P_d	d^{-1}
Half saturation constant for nitrate uptake	18	K_3	P_d	mmol m^{-3}
Half saturation constant for ammonium uptake	19	K_4	P_d	mmol m^{-3}
Nitrate uptake ammonium inhibition parameter	20	ψ_2	P_d	$(mmol\ m^{-3})^{-1}$
Redfield ratio (N:Si)	21	Re	P_d	Dimensionless
Maximum sinking rate	22	S_{max}	P_d	$m\ d^{-1}$
Assimilation efficiency	23	β_2	Z_m	Dimensionless
Excretion rate	24	ν_2	Z_m	d^{-1}
Mortality parameter	25	ζ_2	Z_m	$(mmol\ m^{-3}\ d)^{-1}$
Maximum grazing rate	26	g_2	Z_m	d^{-1}
Ingestion half-saturation constant	27	K_7	Z_m	mmol m^{-3}
Preference for diatoms	28	p_2	Z_m	Dimensionless
Sub-surface nitrate concentration	29	$N_{n\ surf.}$	N_n	mmol m^{-3}
Nitrate gradient across the thermocline	30	$N_{n\ grad.}$	N_n	mmol m^{-4}
Sub-surface silicate concentration	31	$S_{surf.}$	S	mmol Si m^{-3}
Silicate gradient across the thermocline	32	$S_{grad.}$	S	mmol Si m^{-4}

Table 4.2: Optimal model parameters after obtaining a positive-definite Hessian matrix.

Par. number	Symbol	Par. Value	Hess. diagonal	Par. uncertainty	Relative uncertainty
1	μ_1	0.019	472.22	0.0010	0.054
2	K_1	0.772	18.30	0.03095	0.040
3	K_p	0.079	154.73	0.00195	0.025
4	P_{max1}	1.819	1228.245	0.1825	0.100
5	ε	0.095	3.55	0.0199	0.210
6	ν_1	0.112	115460.22	0.0057	0.050
7	δ_1	0.277	0.29	0.0048	0.017
8	α_2	0.088	454.46	0.0129	0.147
9	K_4	0.867	3.44	0.0603	0.070
10	ψ_2	3.368	6.77	0.1148	0.034
11	Re	1.707	21.845	0.0297	0.017
12	S_{max}	1.703	25.43	0.11885	0.070
13	ν_2	0.038	29.84	0.0080	0.211
14	g_2	0.372	64.11	0.0057	0.015
15	P_2	0.517	355.40	0.0432	0.084
16	$N_{n\ surf.}$	2.751	2066.19	0.0532	0.019
17	$N_{n\ grad.}$	0.033	81591.91	0.0019	0.056
18	$S_{\ grad.}$	0.016	23747.63	0.0001	0.005

Table 4.3: Correlation coefficients for the optimal model parameters.

Par. nº	1	2	3	4	5	6	7	8	9	10	11	12	13	14	15	16	17	18
	μ_1	K_1	Kp	P_{max1}	ε	ν_1	δ_1	α_2	K_4	ψ_2	Re	S_{max}	ν_2	g_2	p_2	Nnsurf	Nngrad	Sgrad
μ_1	1	-0.07	-0.32	-0.29	-0.34	-0.76	0.26	0.47	0.61	0.43	-0.09	0.09	-0.59	0.29	-0.34	-0.09	-0.56	-0.02
K_1	-0.07	1	0.17	0.30	0.09	0.14	-0.14	0.13	-0.04	0.03	0.13	-0.09	0.13	-0.08	0.21	0.03	0.19	0.00
Kp	-0.32	0.17	1	0.86	0.37	0.56	-0.25	0.07	-0.43	-0.23	0.37	-0.54	0.65	-0.17	0.68	0.26	0.52	0.04
P_{max1}	-0.29	0.30	0.86	1	0.47	0.68	-0.33	0.03	-0.49	-0.25	0.52	-0.69	0.78	-0.23	0.87	0.27	0.64	0.05
ε	-0.34	0.09	0.37	0.47	1	0.48	-0.12	-0.20	-0.45	-0.24	0.26	-0.34	0.50	-0.18	0.51	0.13	0.51	0.03
ν_1	-0.76	0.14	0.56	0.68	0.48	1	-0.40	-0.46	-0.82	-0.55	0.22	-0.33	0.83	-0.43	0.70	0.17	0.87	0.04
δ_1	0.26	-0.14	-0.25	-0.33	-0.12	-0.40	1	0.28	0.42	0.30	-0.19	0.16	-0.44	0.19	-0.30	-0.02	-0.49	-0.01
α_2	0.47	0.13	0.07	0.03	-0.20	-0.46	0.28	1	0.72	0.68	0.16	-0.19	-0.42	0.45	0.04	-0.01	-0.45	-0.03
K_4	0.61	-0.04	-0.43	-0.49	-0.45	-0.82	0.42	0.72	1	0.56	-0.15	0.18	-0.75	0.46	-0.49	-0.09	-0.77	-0.03
ψ_2	0.43	0.03	-0.23	-0.25	-0.24	-0.55	0.30	0.68	0.56	1	-0.10	0.05	-0.51	0.36	-0.26	-0.09	-0.48	-0.02
Re	-0.09	0.13	0.37	0.52	0.26	0.22	-0.19	0.16	-0.15	-0.10	1	-0.20	0.40	0.03	0.51	0.16	0.30	-0.03
S_{max}	0.09	-0.09	-0.54	-0.69	-0.34	-0.33	0.16	-0.19	0.18	0.05	-0.20	1	-0.43	0.04	-0.63	-0.06	-0.20	0.03
ν_2	-0.59	0.13	0.65	0.78	0.50	0.83	-0.44	-0.42	-0.75	-0.51	0.40	-0.43	1	-0.32	0.70	0.25	0.82	0.07
g_2	0.29	-0.08	-0.17	-0.23	-0.18	-0.43	0.19	0.45	0.46	0.36	0.03	0.04	-0.32	1	-0.21	-0.14	-0.33	-0.02
p_2	-0.34	0.21	0.68	0.87	0.51	0.70	-0.30	0.04	-0.49	-0.26	0.51	-0.63	0.70	-0.21	1	0.19	0.58	0.05
Nnsurf	-0.09	0.03	0.26	0.27	0.13	0.17	-0.02	-0.01	-0.09	-0.09	0.16	-0.06	0.25	-0.14	0.19	1	0.01	0.02
Nngrad	-0.56	0.19	0.52	0.64	0.51	0.87	-0.49	-0.45	-0.77	-0.48	0.30	-0.20	0.82	-0.33	0.58	0.01	1	0.05
Sgrad	-0.02	0.00	0.04	0.05	0.03	0.04	-0.01	-0.03	-0.03	-0.02	-0.03	0.03	0.07	-0.02	0.05	0.02	0.05	1

Chapter 5:

The Physical Model

Chapter 5: The physical model

5.1 Introduction

This chapter describes the physical model chosen to be coupled to the ecosystem model described in chapter 2 as well as the physical aspects affecting the ecosystem, such as mixed layer depth, entrainment/detrainment processes and diapycnal mixing. The model chosen is a one-dimensional version of the Miami Isopycnic Co-ordinate Ocean Model (MICOM) as recent plankton modelling studies focused on the North Atlantic (Spall, 1997; Martin 1999; Spall and Richards, 2000) have obtained encouraging results when biogeochemical models of different complexity were embedded into MICOM.

A brief overview of the physical model has been included in section 5.1. The details of the physical processes relevant to the 1-D model, such as ocean-atmosphere exchanges, the mixed layer scheme and diapycnal mixing are described in section 5.2. Finally, section 5.3 briefly describes the forcing and initial conditions that drive the coupled physical-ecological model.

5.2 The Miami Isopycnal Co-ordinate Ocean Model

The physical model chosen in the present study is version 2.6 of the Miami Isopycnal Co-ordinate Ocean Model (MICOM), developed at the University of Miami by Bleck and co-workers.

MICOM is a primitive equation numerical model, containing four prognostic equations, that uses isopycnal co-ordinates to describe the evolution of momentum, mass, heat and salt in the ocean. This means that the model equations have a coordinate of density (potential density) in the vertical direction rather than the traditional z-coordinate of depth. Therefore, MICOM predicts the depths at which different density values are encountered as opposed to the traditional approach in which water density changes are predicted at fixed depth levels. Amongst others, the advantages of using isopycnal co-ordinate models are:

- the reduction of the vertical truncation error by concentrating coordinate surfaces where there are large density gradients.
- higher vertical resolution in regions of strongest density contrast, therefore reducing the vertical resolution required compared to an Eulerian coordinate system.

There are also shortcomings to this approach, one of the most important ones being the so-called "outcropping" of isopycnals, which refers to the tendency of isopycnals to intersect the sea-surface in regions of near-surface baroclinity. For a more detailed description the reader is referred to Bleck and Boudra (1981).

The dynamic model equations are formulated in terms of an arbitrary vertical coordinate called s (to replace the Cartesian z coordinate) but the x and y Cartesian coordinates remain invariant (Bleck, 1978). After this change of variables over the vertical coordinate,

the general conservation equations, written for the variable *s* are applied in the isopycnic domain and in the surface mixed layer. The thermodynamic variables as well as the variables of motion are treated as layer variables. MICOM does not use a rigid lid. Instead, the model uses a split-explicit numerical scheme, based on Gadd (1978), to calculate the barotropic and baroclinic solutions as it is less expensive than a rigid-lid scheme using iterative methods based on successive overrelaxation (SOR) (Bleck and Smith, 1990). As the solution of the barotropic component is shifted in time (barotropic equations are solved over smaller time steps than the baroclinic equations in order to resolve barotropic gravity waves), a forward-backward scheme, using the mass forward field (in the continuity equation) and the last pressure field (in the equation of motion), is used.

MICOM considers three types of exchanges between the atmosphere and the ocean: radiative exchanges, turbulent heat transfers and mechanical energy transfers. Monthly forcing fields come from the National Centre for Environmental Prediction (NCEP) meteorological re-analysis (Kalnay *et al.*, 1996) and are interpolated to the model's time step. A surface mixed layer of the Gaspar (1988) type provides the linkage between wind, thermohaline forces, freshwater and evaporative fluxes and the isopycnic grid domain.

The MICOM model is documented in Bleck *et al.* (1992). A detailed description of the numerical code can be found in Langlois (1997). The reader is also referred to the MICOM web page for a thorough overview of the MICOM project (http://www.panoramix.rsmas.miami.edu/micom). Here, a 1-D version of the model is used, which means that all horizontal motions are neglected and only vertical ones are considered. This is all that is required for this study. The approach of Martin (1999) is followed.

5.3 The model equations

5.3.1 Ocean-atmosphere exchanges

MICOM considers three types of exchanges between the atmosphere and the ocean:

- Radiative exchanges (*RE*), which account for the balance between incident solar radiation and radiation emitted by the sea surface.
- Turbulent heat transfers of two types:
  - Latent heat transfer (*LH*) due to evaporation of sea water.
  - Sensible heat transfer (*SH*) established by convection when there is a significant difference between sea surface and air temperature.
- Mechanical energy transfers which involve wind speed at a height of 10 meters.

5.3.3.1 Heat balance

Heat is transferred between the surface ocean and the atmosphere by the mechanisms of evaporation (latent heat flux), radiation (both direct short-wave sunlight and net long-wave radiation),and convection (sensible heat flux). In most cases, the incoming short wave radiation and outgoing evaporative heat dominate the fluxes.

The effect of atmospheric-ocean exchanges (apart from wind effects) on the mixed layer is accounted for in the thermal balance (*TB*):

$$TB = RE + LH + SH \qquad [5.1]$$

An upward (positive) flux of sensible heat corresponds to a loss of energy by the sea according to the difference in temperature between air (T_a) and sea surface (T_s):

$$SH = Cp_{air}\, Ex\, (T_s - T_a) \qquad [5.2]$$

where: Ex is an exchange coefficient such that: $Ex = \rho_a\, C_T\, W$ [5.3]

ρ_a is the air density at sea level (1.2×10^{-3} g cm^{-3}), C_T the heat transfer coefficient (1.2×10^{-3}), Cp_{air} the specific heat of the air at constant pressure (1.0057 J g^{-1} ºC^{-1}) and W is wind velocity.

The latent heat flux is responsible for the heat exchanged between air and sea *via* evaporation and it always induces a heat loss by the ocean.

$$LH = Ex\, Lv\, (Hu - Ev) \qquad [5.4]$$

where: Lv is the latent heat of vaporization (2.47×10^{-3} J g^{-1}), Hu the specific humidity and Ev represents evaporation.

5.3.3.2 Mechanical energy transfers

The wind stress on the ocean surface, $\tau_s(t)$, is calculated from the square of the wind speed at 10 meters ($W(t)$), the density of the air (ρ_a) and a drag coefficient ($C_D = 1.3 \times 10^{-3}$) according to the following expression:

$$\tau_s = \rho_a C_D |W|\, W \qquad [5.5]$$

The expression of the drag velocity at the surface u_* is obtained by the relation:

$$u_*^2 = \tau_s / \rho_s \qquad [5.6]$$

where ρ_s represents surface density.

5.3.2 The ocean mixed layer

The evolution of the thermodynamically active mixed layer in MICOM follows the scheme proposed by Gaspar (1988), which treats the parameterisation of the turbulent kinetic energy (TKE) differently than Kraus-Turner. In the latter, the dissipation of TKE is a constant fraction of the creation of TKE, while in the former, it depends on rotation and stability.

The entrainment rate is derived from vertically integrating the TKE equation over the mixed layer and then parameterising the resulting terms using the known variables. The TKE conservation equation in the mixed layer is:

$$(m_2 + m_3)u_*^3 - 0.5h[B(h) - w_e \Delta b] - h\varepsilon_m = 0 \qquad [5.7]$$

where m_2 and m_3 are constants determined from observations, u_* is the surface drag velocity, h is the thickness of the surface layer or mixed layer depth, $B(h)$ represents the sum of surface flux $-\left(\overline{b'w'}\right)_0$ and the increase of buoyancy due to the absorption of solar radiation:

$$B(h) = -\left(\overline{b'w'}\right)_0 + \frac{\alpha_T g}{\rho C_p}\left(R_0 + R_h - \frac{2}{h}\int_{-h}^{0} R(z)\,dz\right) \qquad [5.8]$$

where:

b is the buoyancy $b = g(\rho_o - \rho)/\rho_o$ [5.9]

where ρ_o represents the reference density of seawater.

w is the vertical velocity, α_T is the expansion coefficient given by:

$$\alpha_T = -\frac{1}{\rho}\left(\frac{\partial \rho}{\partial T}\right)_S \qquad [5.10]$$

where T and S are temperature and salinity, respectively.

C_p is the specific heat and R_o and R_z depict solar radiation at the surface and at depth z, w_e is entrainment velocity, Δb represents the discontinuity of the buoyancy at the base of the mixed layer and ε_m is the TKE (E) heat dissipated in the mixed layer.

Gaspar (1988) reintroduced the vertical dissipation scale of Kolmogorov $\ell\varepsilon$ such that:

$$\varepsilon = E^{3/2} / \ell_\varepsilon \qquad [5.11]$$

and over the mixed layer: $\varepsilon_m = u_e^3 / \ell$ [5.12]

where u_e is a characteristic velocity scale of the turbulence in the mixed layer and l a dissipation length that can be expressed as a function of the mixed layer depth, the Monin-Obukov length and the Ekman length scale:

$$\ell = F(h, L, \lambda, L_\Delta, L_N) \qquad [5.13]$$

with:

$L = u_*^3 / B(h)$: Monin-Obukov length

$\lambda = u_* / f$: Ekman length

$L_\Delta = \left(\Delta u^2 + \Delta v^2\right) / \Delta b$: relative scale at the entrainment zone

$L_N = \left(E^{1/2} / N \right)_{-h}$: scale of stratification at the base of the mixed layer

N: Brunt-Vaïsälä frequency

The term L_Δ can be omitted as the dynamic instability at the base of the mixed layer is of a time scale on the order of the inertial period (Gaspar, 1988) as well as L_N which will not have a relevant effect in the ocean. Therefore, equation 5.12 can be expressed as:

$$h\varepsilon_m = u_e^3 G(h/L, h/\lambda) \qquad [5.14]$$

where *G* is a function of the stability of the Monin-Obukov length *h/L* and the rotation parameter h/λ. Gaspar realised that the setting $u_e = u_*$ underestimates the turbulent velocity scale by causing convective deepening and defined:

$$u_e^2 = E_m = \frac{1}{h}\int_0^h E\, dz \qquad [5.15]$$

The stability parameter (*h/l*) can be expressed as:

$$G(h/L, h/\lambda) = \frac{h}{\ell} = a_1 + a_2 \max[1, h/(0.4\lambda)] \exp(h/L) \qquad [5.16]$$

Finally, the prediction of *h* is given by equation 5.7, in which the turbulent dissipation comes from equations 5.14, 5.15 and 5.16:

$$(m_2 + m_3)u_*^3 - 0.5h[B(h) - w_e\Delta b] - (h/\ell)E_m^{2/3} = 0 \qquad [5.17]$$

The entrainment velocity is calculated numerically from the following formula:

$$h\,\Delta b\,w_e = \frac{\left[\left(0.5A_p - C_{p1}S_p\right)^2 + 2C_4\left(h/\ell\right)^2 A_p S_p\right]^{1/2} - \left(0.5A_p + C_{p1}S_p\right)}{C_4\left(h/\ell\right)^2 - C_{p1}} \qquad [5.18]$$

with:

$$A_p = C_{p3}u_*^3 - C_{p1}h\,B(h) \qquad [5.19]$$

$$S_p = \left(m_2 + m_3\right)u_*^3 - 0.5\,h\,B(h) \qquad [5.20]$$

$$C_{p1} = \frac{\left[2\left(1 - m_5\right)\left(\ell_p/\ell\right) + m_4\right]}{6} \qquad [5.21]$$

$$C_{p3} = \frac{\left[m_4\left(m_2 + m_3\right) - \left(\ell_p/\ell\right) + \left(m_2 + m_3 - m_5 m_3\right)\right]}{3} \qquad [5.22]$$

$$C_4 = 2m_4 m_1^{-2} \qquad [5.23]$$

The necessary and sufficient condition for entrainment at the base of the mixed layer ($w_e > 0$) is:

$$A_p = S_p - \frac{h}{\ell}E_{m0}^{3/2} > 0 \qquad [5.24]$$

In the case where this condition is not satisfied, h automatically adjusts itself to maintain $A_p = 0$. When the heat balance $B(h)$ is not zero, this is equivalent to:

$$h = \frac{C_{p3}}{C_{p1}}L \qquad [5.25]$$

Following the theory of Niiler and Kraus (1977), the equilibrium of the mixed layer is attained by:

$$h = \frac{2mu_*^3}{(-B_0)} \qquad [5.26]$$

where B_0 is the surface buoyancy flux, which is assumed to vary linearly inside the mixed layer and is zero at the base.

Values of Gaspar's mixing coefficients are: $m_1 = 0.45$; $m_2 = 2.6$; $m_3 = 1.9$; $m_4 = 2.3$; $m_5 = 0.6$; $a_1 = 0.6$; $a_2 = 0.3$.

5.3.3 Diapycnal mixing

The term diapycnal mixing refers to concept of turbulent diffusion to express the turbulent fluxes associated with the vertical distribution of potential density (ρ) and biological state variables (C).

The temporal evolution of ρ and C at depth z is described as:

$$\left(\frac{\partial \theta}{\partial t}\right)_z = \frac{\partial}{\partial z}\left(K_v \frac{\partial \theta}{\partial z}\right) \qquad [5.27]$$

where θ refers to ρ and C and the term $K_v \, {}^{\partial\theta}/_{\partial z}$ represents the turbulent flux (F) and will be zero at the surface and at the bottom of the ocean ($F_s = F_b = 0$), when neither a source term nor horizontal advection are considered. The integration of equation 5.27 over z conserves θ in the water column.

Following Spall (1997), K_v is maintained constant (1×10^{-4} m^{-2} s^{-1}) in the mixed layer while is parameterised as a function of the buoyancy frequency, as suggested by Gargett (1984), below the mixed layer:

$$K_v = \frac{1x10^{-7}}{N} \qquad [5.28]$$

where N represents the buoyancy frequency. N^2 is defined as:

$$N^2 = \frac{g}{\rho}\frac{\partial \rho}{\partial z} \qquad [5.29]$$

where g is the gravitational constant.

5.4 The coupled physical-biological model

The coupled model consists of 26 unevenly spaced isopycnal layers starting at the surface and reaching 1000 m. This depth layering ensures a vertical resolution that is less than 30 m in the upper 200 m, a resolution of 50 m between 200 and 800 m, and a coarser resolution from 800 to the bottom. In a similar model, Spall (1997) found that the depth integrated vertical biological concentrations (for a 7-compartment model) were insensitive to the depth layering resolution, when he compared 10 m, 15 m and 30 m layering below the mixed layer.

In this study, the vertical resolution is higher at the top of the ocean in order to get a better representation of the biological processes restricted to low depths due to strong light limitation as well as to better model the summer pycnocline. The initial depth layering (isopycnal thickness), starting from the surface, are as follows: 10, 20, 30, 40, 45, 50, 65, 80, 90, 100, 130, 160, 180, 200, 250, 300, 350, 400, 450, 500, 600, 650, 700, 750, 850, 1000 m. The depth layering in MICOM is dynamic. As the model run progresses, the number of vertical layers changes due to the "outcropping" inherent to isopycnal models. This means that vertical layers can converge and reach 0 m thickness and hence, the model losses vertical resolution in unstratified waters. In the same way, as stratification progresses, the thickness of the layer decreases and higher vertical resolution is achieved. In MICOM, the depth of the top layer corresponds to the mixed layer depth. Each layer in the ecosystem is considered homogeneous.

At each time step, the state variables of the biological model are redistributed by vertical diffusion and entrainment/detrainment by the mixed layer according to the equations in the preceding section.

The mixing of biogeochemical compartments across layer interfaces is related to the mixing of a slice of water across the interface and the absorption of the water back into the respective layers as in Spall (1997).

The physical model needs to be run for 22 years before reaching equilibrium or steady state (considered as such when the annual rate of deepening of the mixed layer is less than or equal to 1 m). On the other hand, the biological model needs only 8 years spin up. In order to make the model runs shorter, the physical model was run for 14 years (being the biological model switched off) while for the remaining 8 years, the biological model was turned on and both modules run together.

- **Physical forcing and initial conditions**

The model is physically forced with fields corresponding to 1988 for the first 23 years and is forced with data from 1989 to 1996 thereafter in order to study the interannual variability associated to varying physical regimes. Monthly forcing fields come from the NCEP meteorological re-analysis (Kalnay *et al.*, 1996) and are interpolated to the model's time step using a quasi-hermite scheme. The NCEP variables extracted were: air temperature, precipitation rate, specific humidity at 2 m, solar radiation, long wave radiation, wind stress (u, v) and wind speed. All of them are available from the following URL: http://www.cdc.noaa.gov/cdc/data.ncep.reanalysis.derived.html.

The interannual variability in the atmospheric forcing at the surface is presented in chapter 7 (figure 7.1).

Initial temperature and salinity data used to calculate density come from Levitus data (Levitus, 1982). The mixed layer depth is constrained to be greater than 10 m to ensure computational stability. The model time step is 400 s.

- **Biological initial conditions**

Initial values for all the state variables at the surface are the ones provided by the 0-D model (see chapter 2) whereas below the surface, initial profiles were calculated according to an exponential 1% decrease dependent on depth ($e^{-0.01\,z}$, where z represents depth in meters), for all variables except nitrate and silicate. Initial nitrate and silicate vertical concentrations (N_z and Si_z) increase from the surface to the bottom of the ocean similarly to equation 2.24 (chapter 2):

$$N_z = N_{surf} + N_{grad} * z \qquad [5.31]$$

$$Si_z = Si_{surf} + Si_{grad} * z \qquad [5.32]$$

where N_{surf}, Si_{surf} are the initial nitrate and silicate concentrations at the surface as provided by the 0-D model (5 and 2 mmol m^{-3}, respectively); N_{grad}, Si_{grad} depict the vertical nitrate and silicate gradient (0.03 and 0.015 mmol m^{-3}, respectively) and z represents depth (m). These parameter values were obtained from the optimisation of the 0-D model also described in chapter 2. The nitrate and silicate concentrations at the bottom (N_b and Si_b, respectively) of the modelled ocean (1000 m) were set to 20 and 14 mmol m^{-3}, respectively, as suggested by NABE data. It is evident from the above equations, that nitrate and silicate will be higher than N_b and Si_b at greater depths than 500 m (for nitrate) and 800 m (for silicate). From those depths downwards, nitrate and silicate concentrations were initially set to their values at 1000 m.

The evolution of the state variables in the different layers of the model is due to vertical diffusion, entrainment/detrainment processes and ecology. The ecological equations ruling the temporal evolution of the ecosystem are used to calculate the biological concentrations over the model time step using a leapfrog time scheme. The equations can be expressed as:

$$\frac{\partial C}{\partial t} = \frac{\partial}{\partial z}\left(K_v \frac{\partial C}{\partial z} \right) + \textit{biological sources} - \textit{biological sinks} \qquad [5.33]$$

where C is a generic state variable, K_V is the vertical diffusion coefficient and the last 2 terms represent the source and sink terms of biogeochemical processes previously described in chapter 2. In the case of diatoms, equation 5.33 needs an extra term so as to account for variable sinking:

$$\frac{\partial P_d}{\partial t} = \frac{\partial}{\partial z}\left(K_v \frac{\partial P_d}{\partial z} \right) + \frac{\partial}{\partial z}(w_s P_d) + P_d \ \textit{sources} - P_d \ \textit{sinks} \qquad [5.34]$$

where w_s depicts sinking speed (m d^{-1}). The derivate $\partial w_s / \partial z$ can be calculated from $\frac{dw_s}{dSi} \cdot \frac{\partial Si}{\partial z}$ (as equation 2.15 in chapter 2), where Si represents silicate concentration.

The depths to which solar radiation penetrates follow:

$$I = I_0(t) exp\left[-K_w z - K_p \int_0^z (P_d(z,t) + P_{nd}(z,t)) dz \right]$$

where I_0 is the PAR radiation at the surface (see equation 2.7 in chapter 2) and K_w and K_p are the light attenuation coefficient for water and the self-shading coefficient, respectively as stated in chapter 2. The calculation of I_0 was described in equation 2.7 (chapter 2), where cloudiness enters such equation as a constant fraction.

Chapter 6:

The Coupled Physical-Biological Model

Chapter 6:

The Coupled Physical-Biological Model

6.1 Introduction

In 1953, Sverdrup established that the intensity and extent of mixing within the water column influence the ability of plankton to develop under favorable conditions (Sverdrup, 1953). As described in Chapter 1, the accurate simulation of the physical forcing is vital in ecological modelling as it affects many biological processes such as physiological rates (temperature and light dependent) and also abiotic processes as nutrient availability (influenced by the stratification of the upper mixed layer). In order to improve the ecological model performance, a more realistic description of the physical forcing as well as mixed layer depth dynamics is needed and for this reason, the next step in this research will be the coupling of the ecological model to a 1-D version of the Miami Isopycnic Coordinate Model (referred to as MICOM, hereafter). In this chapter, several aspects of the coupling process are described in detail. Section 6.2 explains the 0-D model changes that proved necessary for the accurate vertical representation of the biochemical processes of interest. Results for the 'standard' run of the coupled physical-ecosystem model are shown in section 6.3. Section 6.4 outlines model tuning to the North Atlantic Bloom Experiment (NABE) observational data set for spring in 1989 and briefly describes physical and biological variability within the data set. Section 6.5 presents the coupled model validation with an independent data set at 48°N, 21°W (BIOTRANS area) in autumn 1996. It also explores problems highlighted by a pre-validation test, the need of model re-tuning to the 1989 data set and the fit to the observations as well as model agreement with other field and model studies. Finally, a summary of the key points found in this study are highlighted.

6.2 The 0-D model adaptations

The eight compartment ecological model described in previous chapters was slightly modified in order to be coupled to the 1-D version of the Miami Isopycnal Co-ordinate Ocean Model (MICOM) (Martin, 1999). In this study two important alterations were thought to be necessary. On the one hand, the need to parameterize nitrification could not be avoided as remineralisation-nitrification processes lead to pronounced gradients in the vertical nitrate profile. Nitrification is mainly carried out by aerobic and chemosynthetic bacteria which oxidize ammonium to produce nitrates and nitrites. Due to the absence of bacteria as a model variable, nitrification was not explicitly modelled but parameterised as a constant transfer rate (nr = 0.03 d^{-1}) from ammonium into the nitrate pool (Martin *et al.*, 2001).

On the other hand, a detailed description of the role of detrital biogenic silica in the water column was also included and an extra compartment, detrital biogenic silica, was added as remineralisation processes involving this variable also have an effect on the vertical gradient of dissolved silicate present in the water column and it is also subjected to sinking.

The role of silica in biogeochemical modelling studies has often been ignored, as nitrogen is regarded as the main limiting nutrient of marine primary production, and also due to the fact that biochemistry of silica is still poorly known (Smetacek, 1999). Until very recently it was believed that dissolution of diatom shells was mainly controlled by physico-chemical factors. Bidle and Azam (1999) have shown that biological factors not only affect the diatom shells dissolution process but that bacteria-mediated silica regeneration may be critical in controlling diatoms productivity and the cycling and fate of silicon and carbon in the ocean. Dudgale and co-workers (1995) showed the important role of silica in driving

new production in their coupled silicon-nitrate model and recent studies have started to include silica as well as nitrogen in their modelling approaches (Pondaven *et al.*, 1998).

The model equation that explicitly describes detrital biogenic silica dynamics was formulated as follows:

$$\frac{dD_s}{dt} = \frac{\mu_2 P_d^2}{\mathrm{Re}} + \frac{G_2}{\mathrm{Re}} - \delta_2 D_s - D_s \frac{[m + h^+(t) + V_s]}{M} \qquad [6.1]$$

where the first term represents diatom mortality, the second term represents mesozooplankton egestion of silica component of ingested diatoms, the third term represents the breakdown of detrital biogenic silica (δ_2) and V_s is the sinking rate of detrital biogenic silica .

Mesozooplankton grazing on diatoms takes up nitrogen and biogenic silica. Because mesozooplankton are non siliceous organisms their nutritional requirements are fulfilled by uptake of carbon and nitrogen alone and the grazed silica will be entirely rejected as faecal pellets (term 2 on the right hand side of equation 6.1).

Therefore, the silicate equation previously described in Chapter 2 (equation 2.26) needs to be reformulated, to include the new remineralisation term, as follows:

$$\frac{dS}{dt} = -\frac{J(t,M)Q_3(S)[Q_{1d}(N_n,N_r) + Q_{2d}(N_n,N_r)]P_d}{Re} + \delta_2 D_s + (S_o - S)\frac{[m + h^+(t)]}{M} \qquad [6.2]$$

Initial values for δ_2 (0.012 d^{-1}) and V_s (5 m d^{-1}) were taken from Pondaven *et al.* (1998).

These are the processes that ultimately control biogeochemical variability of the water column and affect the entire nitrogen and silicate budget of the system. Therefore, the

mentioned adaptations provide a more realistic and also accurate framework for the biogeochemical processes that will occur in a vertically resolved water column.

The new 0-D ecological model (nine compartment) was run, without being optimised, to investigate whether or not the structural changes made provided a different solution from the previously called *standard run*. Initial conditions were those corresponding to such run (table 2.3) apart from the inclusion of the new parameters specified in equation 6.2 (δ_2 and V_s). Model results show that there is no significative differences between variables in the *standard run* and the extended 0-D model (figure 6.1). Detrital biogenic silica dynamics (data only available from the new 0-D model) respond to diatoms and mesozooplankton development as expected. Its concentration increases steadily from Julian day 25 until day 119 due to the slow diatom growth accompanied by mesozooplankton grazing, reaching less than 0.08 mmol Si m^{-3}. After Julian day 119, detrital silica concentration drops due to the switching feeding behaviour of mesozooplankton which turns to graze mainly on microzooplankton (as it has slightly lower preference for diatoms) and therefore, takes up more nitrogen than silica at this stage. Due to the relaxation in grazing and also to the improvement in physical conditions (reduced vertical mixing and increased irradiance), diatoms grow fast and so does mesozooplankton, generating a maximum in the detrital biogenic silica concentration (0.16 mmol Si m^{-3}) on Julian day 129 that is due to an increasing excretion of faecal pellets as well as to increased diatom natural mortality. Thereafter, detrital biogenic silica concentration declines rapidly as diatoms growth recedes and mesozooplankton biomass is mainly maintained by microzooplankton once more. Later in the year, from Julian day 250, a second increase in detrital silica concentration takes place for the same reasons explained above. Hereafter when the 0-D model is mentioned it will be understood to be the new 0-D model (nine compartment).

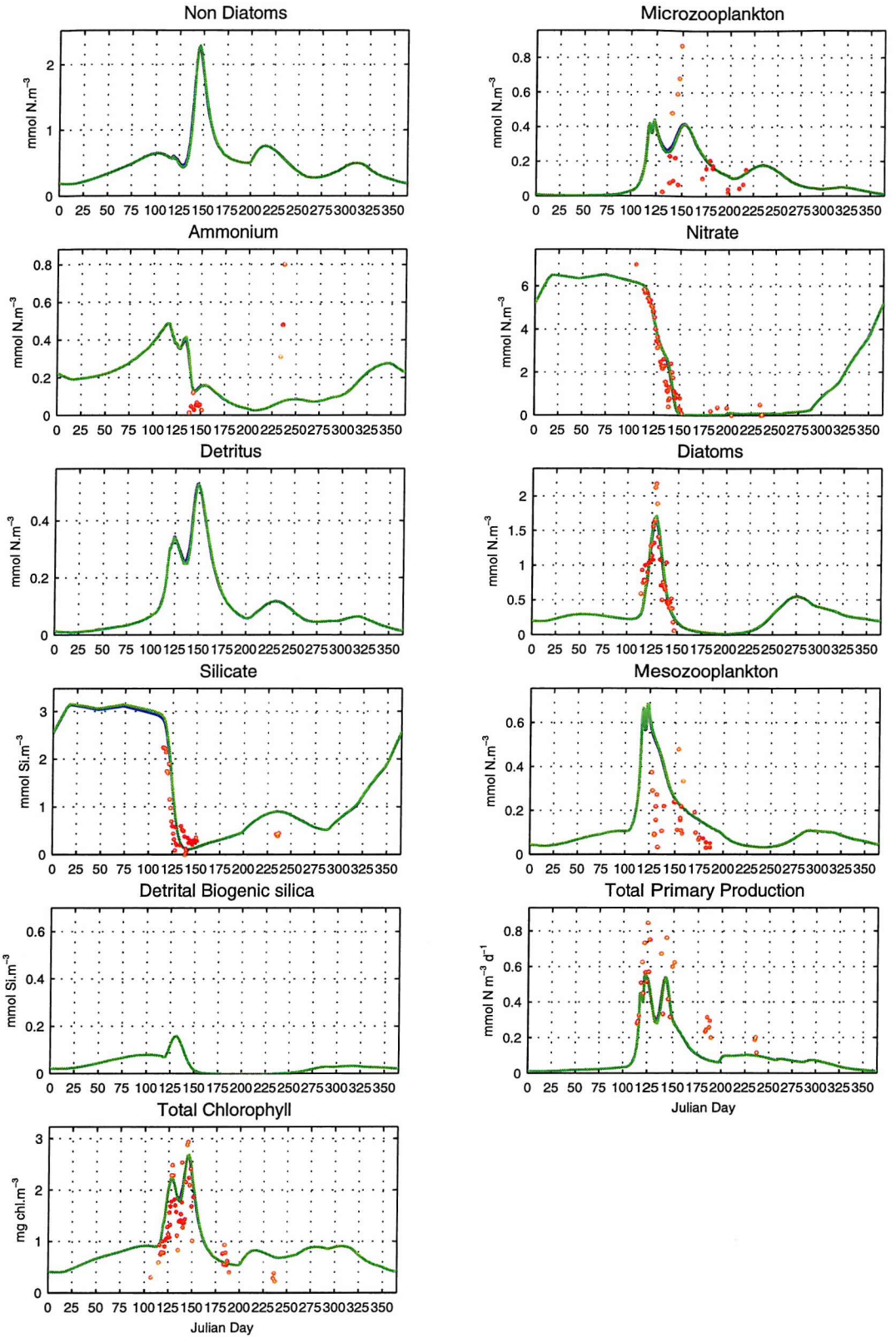

Figure 6.1: Seasonal variability of all the state variables corresponding to the *standard run* (blue) and the new 0-D model (green) and real NABE observations (red dots) in the mixed layer. Notice that there is no detrital biogenic silicate data for the *standard run*. Blue line is hidden by green line as both of them are identical.

6.3 The 1-D "*standard run*"

The first run of the coupled model is carried out using the set of ecological parameters previously discussed in the extended 0-D model as initial parameters (in tables 2.3 and 6.1). Initial conditions for all the state variables at the surface are the same used in the 0-D model (biogenic silica set to 0.1 mmol Si m^{-3}). As the coupled model is divided into 26 vertical levels (see chapter 5), initial values for all the state variables below the surface were calculated according to an exponential decrease dependent on depth. Silicate and nitrate concentrations at the bottom of the modelled ocean (1000 m) were set to 14 and 20 mmol m^{-3} as suggested by NABE data.

Simulated results, averaged within the mixed layer, for all the state variables, total chlorophyll, primary production as well as mixed layer depths are shown in figure 6.2.

Differences between the 0-D *standard run* and the 1-D model were observed in the seasonal cycles of many state variables and also in the mixed layer depth. The latter was particularly important as mixed layer depth will determine the light regime and nutrient availability and therefore, favorable or adverse trophodynamic development conditions. The maximum deep winter mixed layer specified in the 0-D model (derived from CTD NABE data for spring and summer and from Levitus' climatology (1982) for the rest of the year) reached 314 m on Julian day 73, slightly shallower than the mixed layer depth predicted by MICOM (ca. 333 m) on Julian day 78. Fasham *et al.* (1990) discussed the physical forcing of their model and suggested that Levitus' mixed layer depths underestimated the mixed layer in winter which underpins our choice of Gaspar's formulation of the mixed layer depth (figure 6.2l) (see chapter 5). Other studies (Garside and Garside, 1993) state that Levitus' Atlas winter mixed layer depths are around 350 m, about 50 m less that winter depths shown in Robinson's Atlas (Robinson *et al.*, 1979).

Even more relevant than mixed layer depth is the difference in the onset of stratification in both models. The coupled model re-stratifies faster and 30 days earlier than its 0-D counterpart with striking consequences for phytoplankton and nutrient seasonal cycles, especially regarding the timing of the spring bloom, with effects that will extend beyond the bloom period. Moreover, the shallowest depth of the mixed layer in the coupled model is nearly twice as deep as the 0-D model one (29 *versus* 15 m, respectively) reducing light availability, therefore, the 0-D model prediction of more intense spring blooms and higher phytoplankton biomass than in the 1-D case, is not surprising (figure 6.2).

Seasonal cycle discrepancies between both models can be fully explained by different mixing and stratification regimes to which state variables are subjected in each model. Although in both models the onset of stratification starts approximately at the same time (Julian day 75 in the 0-D model and day 79 in the 1-D case), mixed layer stability occurs faster in the 1-D case. Both models show a mixed layer profile consisting of two phases, defined in terms of speed of the stratification process. In the 0-D case, stratification starts with the slow shoaling of the mixed layer (phase 1), followed by fast stratification over a shorter period of time (phase 2), which is the opposite trend to what is observed in the 1-D case, where phase 1 is fast and phase 2 occurs more gradually for the same time scales (see figure 6.2l).

The first phase, in the 0-D model, shows the slow shoaling of the mixed layer from Julian day 75 up to Julian day 106, when mixed layer depths are 314 m and 257 m, respectively, therefore a depth reduction of 57 m in 31 days. On the other hand, mixed layer depths, in the 1-D model, vary between 333 m and 86 m, on Julian days 79 and 106, respectively, and therefore, a depth reduction of 247 m. This temporal shift in the phase of the mixed layer will have important consequences on phytoplankton development, as favorable light regimes are sooner achieved in the 1-D case,

phytoplankton will be no longer limited by light and with plenty of nutrients in the water column, they will be able to bloom earlier than in the 0-D model.

In phase 2, from Julian day 106 to Julian day 119, stratification in the 0-D model is fast and mixed layer depth shallows 236 m in only 13 days, being the crucial period for triggering phytoplankton growth as favorable light regimes are achieved during this period. Mixed layer stratification is complete by Julian day 119 although it will be broken by a weak mixing event on Julian day 120, lasting less than five days, after which vertical stability of the water column will be restored. In the 1-D model, phase 2 is characterised by a brief period (2 days) of faster stratification of the mixed layer followed by a gradual and slow decrease in mixed layer depth, varying from 86 m, on Julian day 106, to 50 m on Julian day 119 (*versus* a depth of 21 m predicted by the 0-D model). No episodic mixing events were predicted by the 1-D model.

Moving onto model state variables, the most important difference between both runs is in terms of nutrients (figure 6.2d and 6.2g). The coupled model predicts very little amount of nitrate and silicate. Nitrate highest concentration slightly reaches over 3 mmol m^{-3} while silicate concentration stays lower than 1 mmol m^{-3}. These results seem to be pointing at the need of modification in the nutrient remineralisation and sinking rates as they are among the most variable parameters in the data set, as reported in the literature available.

Fasham *et al.* (1990) tried, in their model, three different sinking rates for biogenic nitrogen (detritus) ranging from as little as 1 m d^{-1} up to 10 and also 100 m d^{-1}. They found that model results were very similar when using the last two rates but also pointed at the difficulty in determine a single sinking rate, as detritus accounts for different components of the food web which are variable in size and sinking rates (i.e. faecal

pellets, dead zooplankton, etc.). As to dissolution rates, the same uncertainty applies, as their values can range from as low as 0.004 up to 0.18 d^{-1} (Jones and Henderson, 1986).

In terms of detrital biogenic silica, large specific-species variability exists in the rate of breakdown of diatom cells (Smetacek, 1999), being as variable as for nitrogen, and its rates being almost considered to be free parameters.

The lack of nitrate and silicate in the model are primarily responsible for the low phytoplankton biomass (0.87 and 1.14 mmol N m^{-3} for diatoms and non-diatoms, respectively) compared to the 0-D *standard run* (1.72 and 2.29 mmol N m^{-3} for diatoms and non-diatoms, respectively) therefore, zooplankton are unable to reach as high biomass as in the 0-D case, apart from microzooplankton, which responds to non-diatoms bloom by reaching as high biomass as in the simple model (0.36 *versus* 0.44 mm N m^{-3} for the 1-D and 0-D model, respectively). Mesozooplankton barely exceeds 0.06 mmol N m^{-3} mainly sustained above the level of winter standing stock by grazing on microzooplankton.

In terms of the timing of the spring bloom, the coupled model also shows several differences compared to the 0-D version, mainly due to the early and fast re-stratification of the water column. Both phytoplankton groups bloom nearly at the same time, non-diatoms 23 days earlier than its 0-D counterpart while there is only a 13 days difference for diatoms, which results in one single but wider peak in terms of chlorophyll and primary production (also 20 days earlier), compared to the 0-D case. The same situation is observed for total primary production, being underestimated by the coupled model (maximum of 0.40 *versus* 0.56 mmol N m^{-3} d^{-1} for the 1-D and 0-D model, respectively). These results point to the need of new *prior* values for phytoplankton light efficiency (α) and maximum growth (P_{max}) as the physics of the mixed layer seem to be well

represented by Gaspar's scheme and consistent to values provided by field studies for the same area.

The state variables that best resemble the 0-D model results are microzooplankton (maximum of 0. 36 *versus* 0.44 mmol N m^{-3} d^{-1} for the 1-D and 0-D model, respectively), ammonium (maximum of 0.45 *versus* 0.49 mmol N m^{-3} d^{-1} for the 1-D and 0-D model, respectively) and biogenic nitrogen or detritus (maximum of 0.39 *versus* 0.53 mmol N m^{-3} d^{-1} for the 1-D and 0-D model, respectively).

Generally, the coupled model predictions did not match the 0-D model output well in terms of timing and phytoplankton blooms and significantly underestimated their biomass in many cases.

The common process of parameter transference between models has important implications in terms of parameter portability as it is not unusual to initialise complex models (i.e., general circulation models or GCMs) with parameter sets previously tested in simpler ones. The results obtained here will give some insight into this matter and will be discussed later as part of a sensitivity analysis described in chapter 8.

These results clearly pointed to the need of a tuning exercise including real observations for the NABE site.

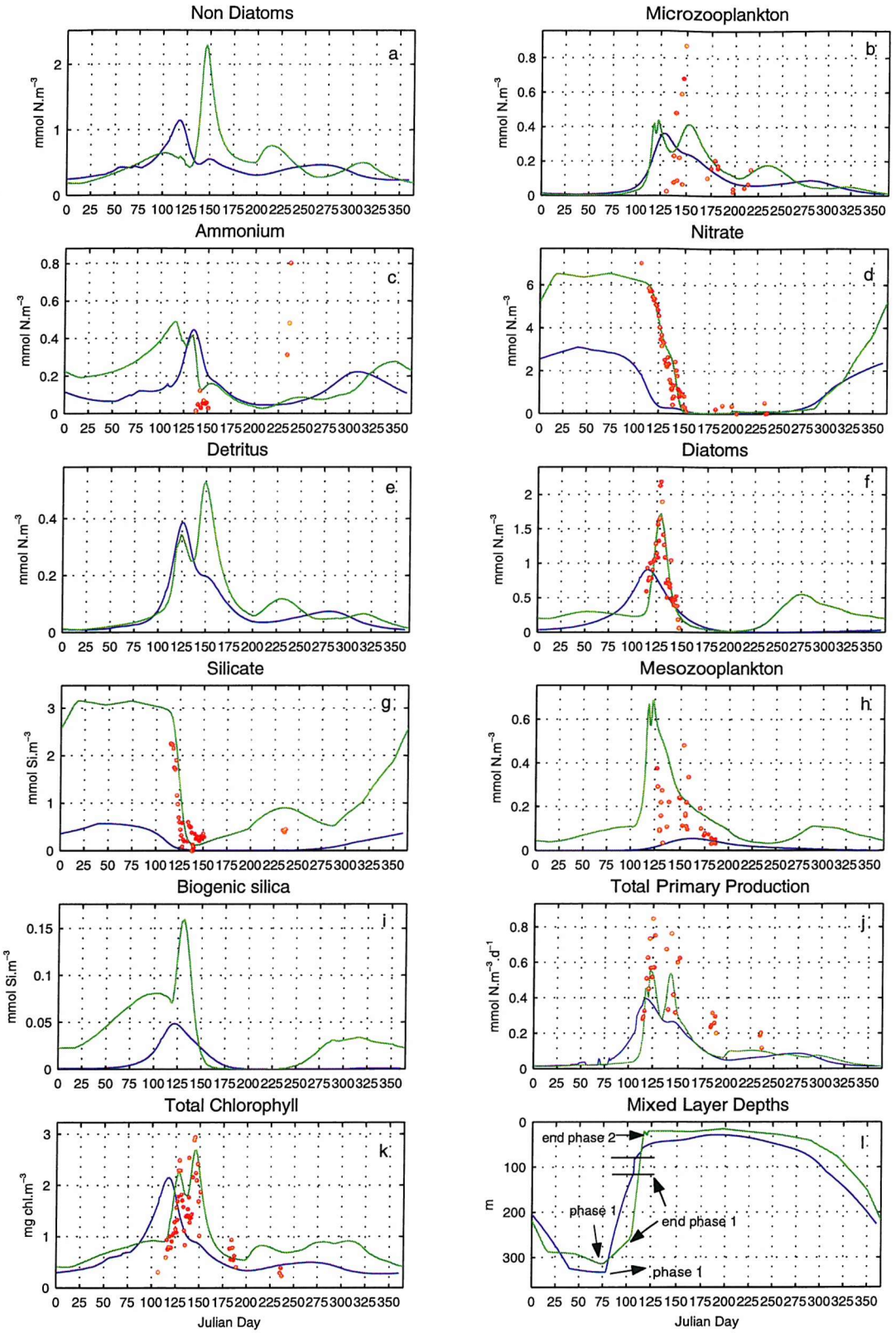

Figure 6.2: Seasonal variability of all the state variables corresponding to the 0-D *standard run* (green) and the 1-D *standard run* (blue) and also the NABE observations (red dots) in the mixed layer.

6.4 Tuning the coupled model: the NABE 1989 data set

It has been previously shown that tuning of the 1-D model is needed in order to get a more realistic description of the ecological processes occurring in the water column. However, this exercise involved a more complex data set than the one used to calibrate the 0-D model (figure 2.2) as vertical profiles of such variables have been considered, when available, for the same cruises specified in chapter 2. We wanted to have as many observations as possible but as the coupled model ignores spatial variability, we also wanted to know whether the observational data showed any structure that could not be resolved by the relative simplicity of the 1-D model.

Observational data: physical variability in 1989

Prior observations in this area have shown the existence of mesoscale eddies with varying characteristics (Le Groupe Tourbillion (1983); Mittelstaedt (1987); Robinson *et al.*, 1993) also showing interesting biological and chemical variability (Lochte and Pfannkuche,1987). In this study, observations came from a varying number of cruise stations that lay between 47.6°N and 46.2°N and 17.5°W and 22°W (figure 6.4a). Temperature and salinity data from the surface down to 1000 m were compared to establish whether samples were taken within the same body of water or whether there was intrusion of different water masses. No major changes in surface water properties were observed, as shown by T-S diagrams (figure 6.3), for the four cruises.

Surface and vertical salinity and temperature were also plotted (figures 6.4b, 6.4c and 6.5) showing a well stratified water column for most of the cruise time although there are eddy-like structures present on days 126 (cruise Atlantis 1) and 133 (cruise Meteor) which always developed below 500 m (figure 6.5). Two eddy features are revealed by

surface data plots (figure 6.4b and c). Both temperature and salinity showed the presence of eddies located at 47.15°N 19.5°W and 46.5°N 19°W. There is also a front located at 46.6°N 18.5°W although this seems to be relying on only one datum. These structures are coincident in time with the so-called small and standard eddies described in Robinson *et al.* (1993) at times when cruises Atlantis and Meteor took place. The rest of the vertically resolved data available (cruises Discovery and Tyro) showed no mesoscale variability.

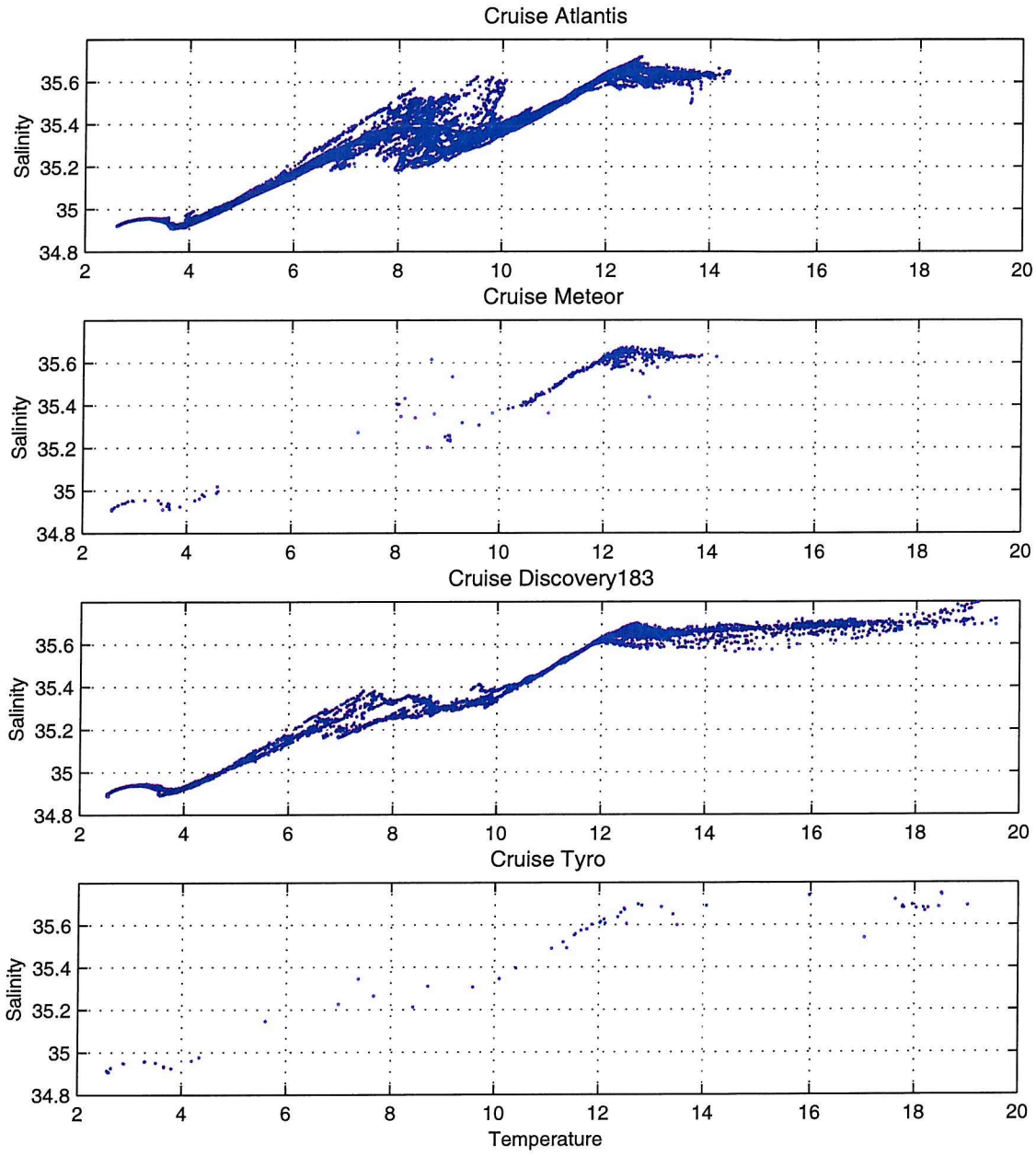

Figure 6.3: T-S diagrams corresponding to cruises Atlantis (I and II), Meteor, Discovery 183 and Tyro.

These results show that the biochemical observations carried out during the spring bloom at 47ºN 20ºW correspond to an area of complex mesoscale hydrographic variability. Nevertheless, there is no easy way to quantify the effect of such variability in the 1-D ecosystem model described in this work unless a 3-D model is used instead. Three dimensional model approaches often show lack of ecological complexity although tend to represent physical processes more accurately. The aim of this work is concentrated on complex ecological behaviour in response to a realistic physical framework and therefore there are obvious limitations in terms of physics and dynamics as there are obvious ecological limitations when 3-D models are used. Hence, the effects of horizontal spatial variability will be neglected in this work (and regarded as noise) which does not invalidate our model results, as it will be a good exercise to quantify how relevant the physical environment is in determining realistic and complex patterns in plankton behaviour, in an area where cyclonic and anticyclonic eddies influence plankton development.

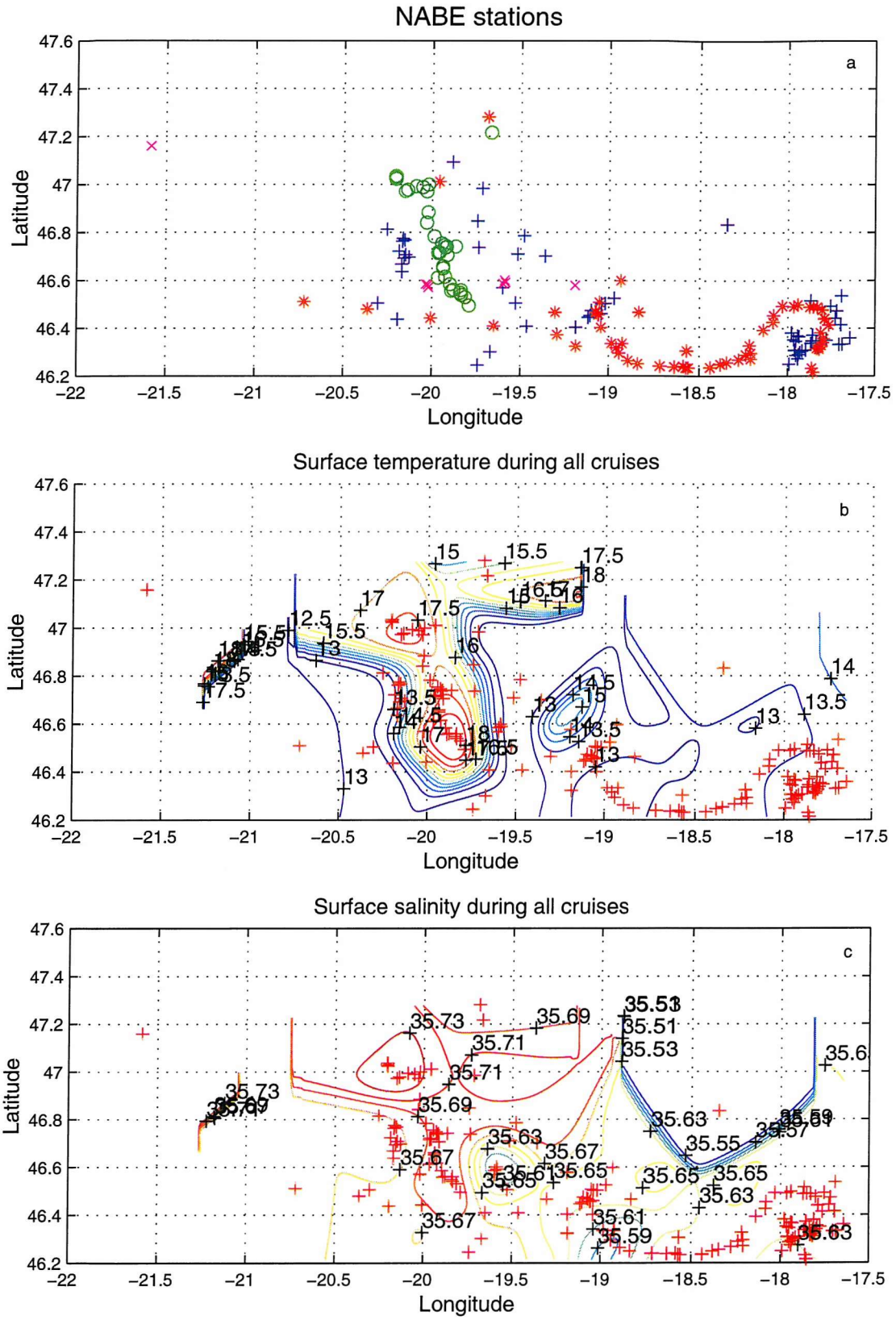

Figure 6.4: Top figure: North Atlantic Bloom Experiment stations used in this study (blue crosses represent Atlantis data; red stars are Meteor data; green circles are Discovery 183 data and red x are Tyro data).
Middle figure: composite of surface temperature from all cruises at the chosen stations.
Bottom figure: composite of surface salinity from all cruises at the chosen stations.

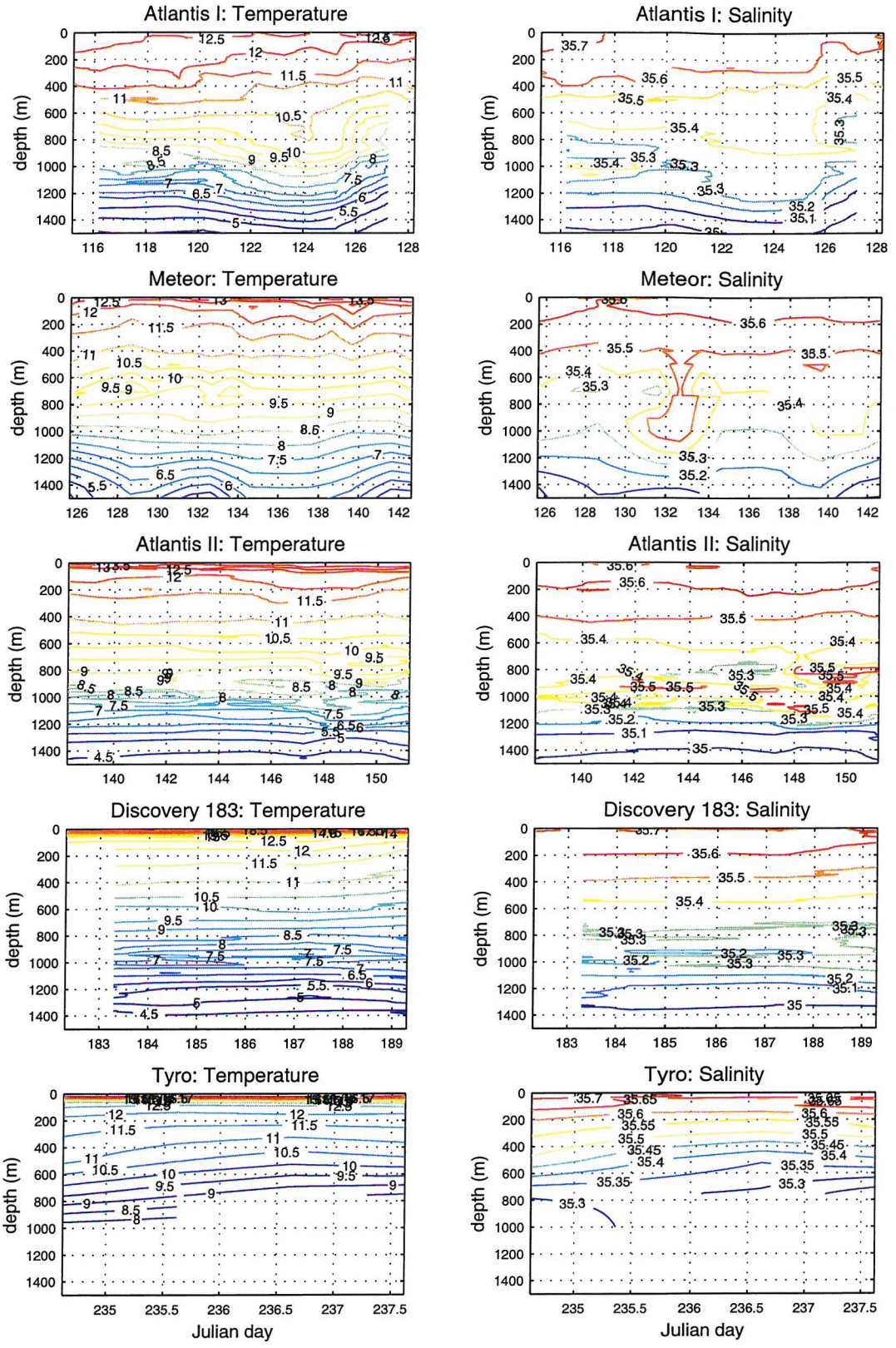

Figure 6.5: Vertical temperature and salinity as measured on cruises Atlantis (I and II), Meteor, Discovery 183 and Tyro.

Observational data: biochemical variability in 1989

Vertical profiles of chlorophyll a, nitrate, ammonium, silicate and particulate organic nitrate (PON) were obtained from all cruises. For all nutrients, data down to 1000 m where available but PON and chlorophyll a were only sampled down to 300 m and 150 m, respectively (figure 6.6).

Chlorophyll data remained low (below 1 mg chl m^{-3}) for the first part of the sampling period on board Atlantis I (Julian days 115 to 122) and nitrate and silicate concentrations were relatively high (above 6 and 2 mmol m^{-3}, respectively). After Julian day 122, the onset of the spring bloom could be seen at the surface and extending in the vertical down to 50 m, reaching a maximum chlorophyll value of 1.99 mg m^{-3}. Silicate started decreasing at the same time, suggesting that this was a diatom bloom. A possible diatom subsurface chlorophyll maximum (1.30 mg chl m^{-3}) was also observed at 72 m depth. The spring bloom was completely developed by Julian day 132 (cruise Meteor), reaching a maximum of 2.78 mg chl m^{-3}, all the silicate being depleted and therefore phytoplankton (diatoms) starting to progressively decay afterwards. Eight days later (cruise Atlantis II), when there was no silicate left but some nitrate available (not clearly shown in figure due to scale), the start of a shallower second bloom, presumably a non-diatom one, took place near the surface, also migrating to deeper layers (down to 25 m) and reaching its maximum (3.32 mg chl m^{-3}) at 13 m on Julian day 145. Cruise Discovery 183 measured the occurrence of a second non-diatom bloom (above 40 m) on Julian day 182 no higher than 1.50 mg chl m^{-3}. From then onwards, chlorophyll would remain below 0.60 mg chl m^{-3}. Regarding ammonium, there is no data available from cruises Atlantis I or Discovery 183 and data from Tyro seemed to have been contaminated in the analysis process (ammonium analysis is a very delicate procedure). Meteor data showed a vertical patchy structure (figure 6.6) dominated by higher concentrations (up to 2.61 mmol N m^{-3}) in the

top 100 m from Julian day 130, immediately after phytoplankton development had started. Atlantis II showed the same trend in the upper 60 m (maximum values around 1.00 mmol N m^{-3}). There were two peaks on Julian days 140 and 149. The first one matched bloom deepening observed during cruise Meteor where nitrate was still available but no silicate was left. The second peak occurred after the phytoplankton bloom had ceased. In between both peaks, ammonium seemed to have been consumed as there was barely any silicate and phytoplankton will preferentially take up ammonium rather than nitrate to support their growth.

PON data, down to 150 m, were available from cruises Atlantis I, Atlantis II and Meteor. Its concentration remained high during all the Meteor cruise, for which the highest values were measured (over 3.49 mmol N m^{-3} in the upper 40 m). Atlantis cruises showed a patchier PON distribution, with peak values at the same times and depths for which phytoplankton blooms were described earlier. Maximum PON values were ca. 2.60 mmol N m^{-3} on Julian day 127 (Atlantis I) and 2.82 mmol N m^{-3} from Julian day 150 to 155 (Atlantis II).

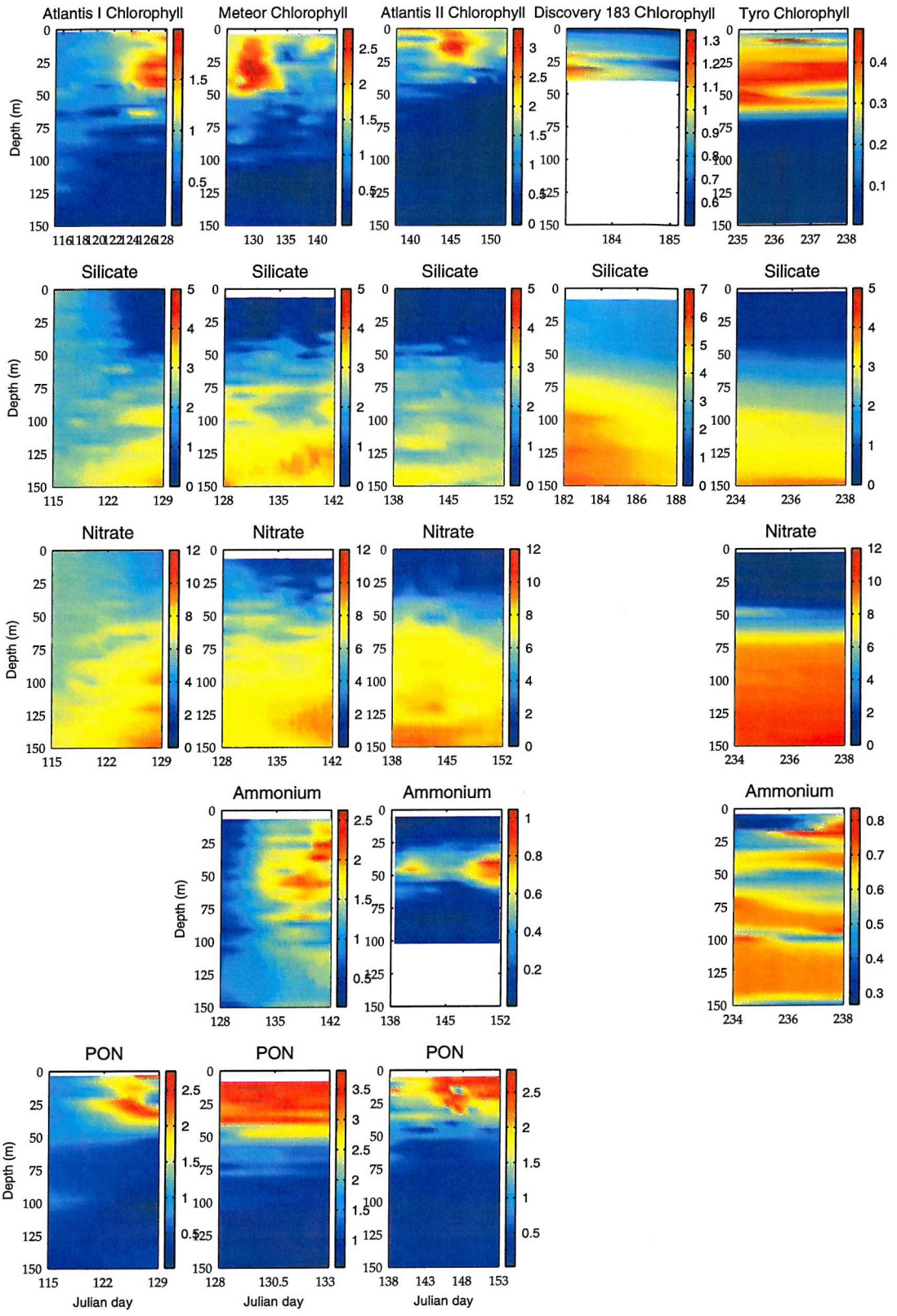

Figure 6.6: Seasonal variability of all the ecological variables corresponding to cruises Atlantis I, Meteor, Atlantis II, Discovery 183 and Tyro.

Tuning the model

Discrepancies found between the 1-D and 0-D *standard runs* led to the need for a tuning exercise so as to get the best fit to the vertically resolved NABE89 data set. Although an inverse approach method had previously been applied in the 0-D case, such technique was computationally too expensive to run and implement in the 1-D case, and therefore, a traditional trial and error adjustment was used instead.

In order to run the model faster, the trial runs were performed by forcing the model using physical fields corresponding to 1989 only; this way, the length of a single run is shortened by 50 minutes, taking only 40 minutes to complete on a Sun station at 600 MHz and 512 MB.

The misfit between model output and observations was quantified as stated in equation 2.29 (chapter 2). After many trial runs, searching for a smaller misfit but also seeking a good fit to the timing of the bloom, a total of five *a priori* parameters were modified (see table 6.2): detrital silica remineralisation rate (δ_2) (increased), detrital nitrogen sinking rate (V) (increased), maximum growth rate (P_{max2}) for diatoms (decreased), initial slope of the P-I curve for both diatoms (α_2) (increased) and non-diatoms (α_1) (decreased).

A five fold increase in δ_2 significantly increases the amount of regenerated dissolved silicate in the water column. In the mixed layer, silicate averaged values varied from 0.57 to 1.80 mmol Si m^{-3} (see figure 6.7). As silicate concentration increases, favorable conditions allow diatoms to develop very quickly. The need to constrain their growth pointed to a lower P_{max2} but also to an increase in α_2 so as to avoid blooms overlapping. Non diatoms are prevented from blooming, due to a less efficient use of nitrate than diatoms, until later in the year when an increased ammonium concentration is observed after the diatom bloom has passed.

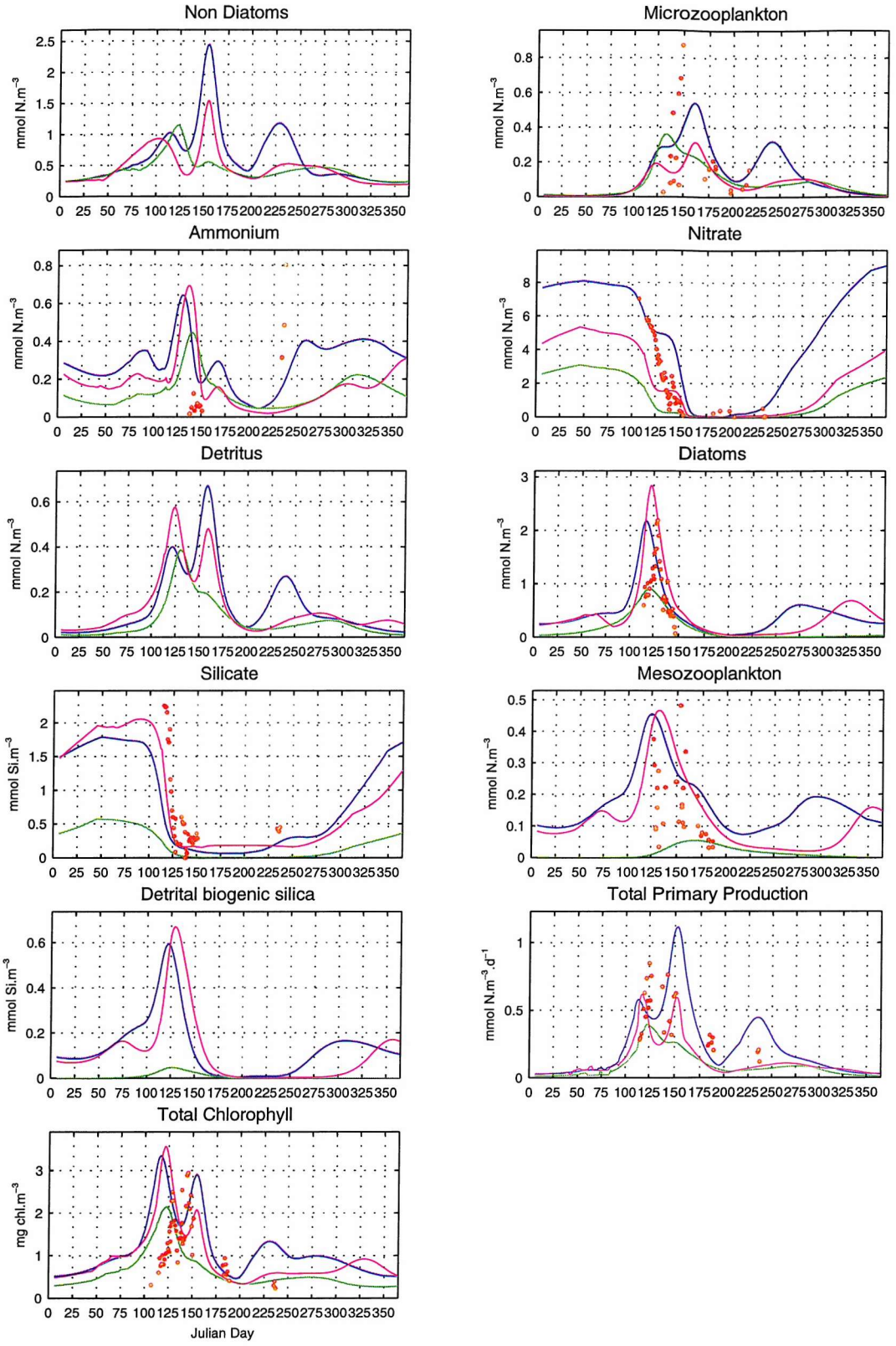

Figure 6.7: Seasonal variability of all the state variables corresponding to the 1-D *standard run* (green), model tuning (blue) and re-tuning (magenta). Values shown are averaged mixed layer values.

The sinking rate of detrital nitrogen was also increased in order to avoid extremely high concentrations of ammonium (due to remineralisation processes) and detrital nitrogen (due to accumulation). All these parameter changes helped to regulate nitrate concentration, generating more realistic winter values (8 *versus* 3.10 mmol N m^{-3} in the 1-D *standard run*). Mesozooplankton dynamics also benefited from the tuning, as diatoms abundance allows them to fulfil their food requirements and reach higher biomass (0.46 *versus* 0.05 mmol N m^{-3} in the 1-D *standard run*). Figure 6.8 shows the 1-D tuned model output, depth-resolved, for all the state variables and also chlorophyll and primary production. The vertically resolved model shows the presence of two subsurface or deep chlorophyll maxima (DCM), right below the mixed layer, due to diatoms. Both maxima occur at the same depth (59 m) and after the main spring bloom takes place, when silicate in the mixed layer has been depleted. The first deep maximum occurs in May, reaching less than 1 mg chl m^{-3}, while the second bloom reaches 1.26 mg chl m^{-3} in June. As the model does not take into account physiological variability of the carbon to chlorophyll Redfield ratio, both maxima are also biomass maxima. A peak in mesozooplankton biomass (0.34 mmol N m^{-3}) and also in biogenic detrital silica (0.38 mmol N m^{-3}), are observed at the same time and depth as the DCM.

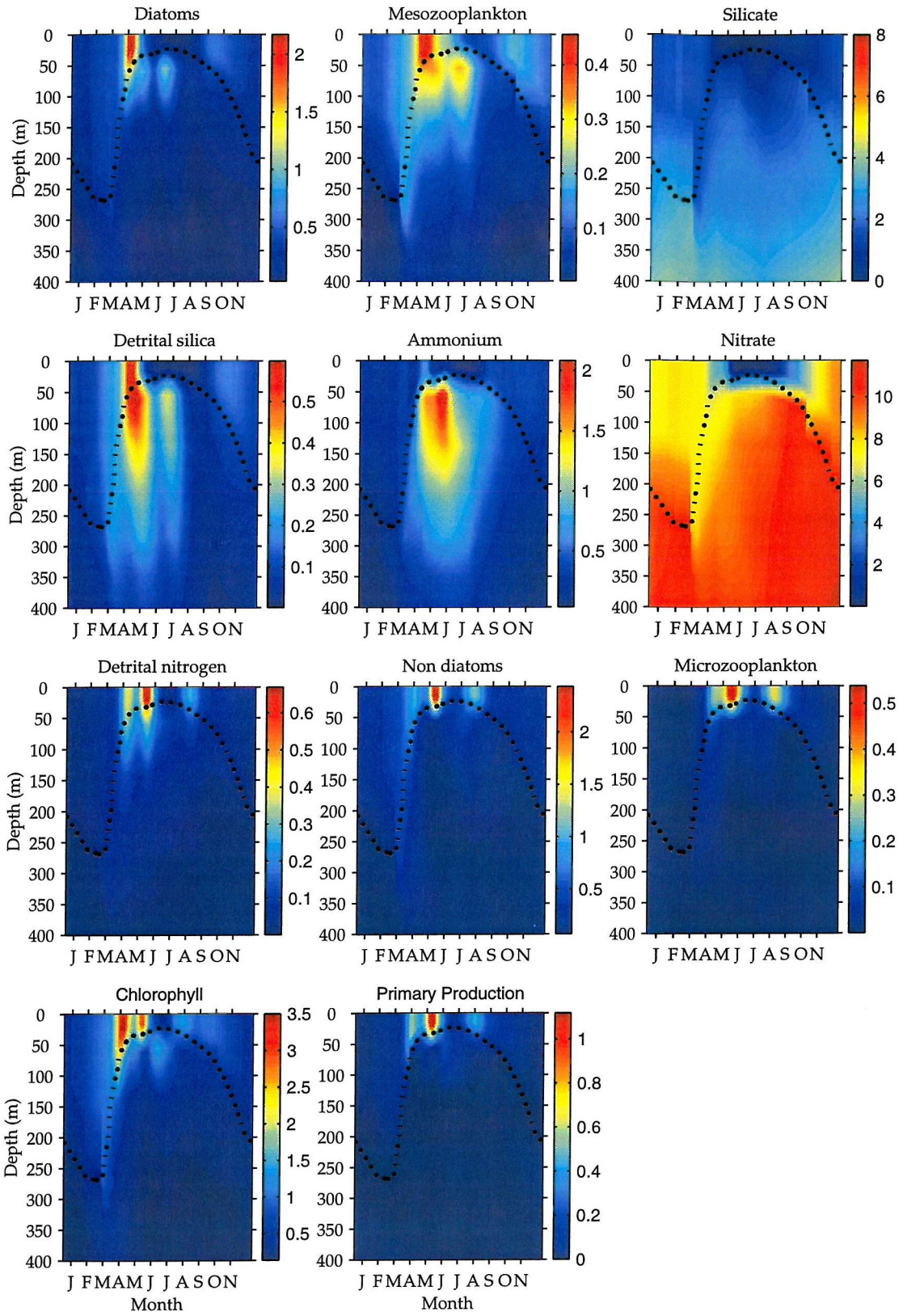

Figure 6.8: 1-D tuned model state variables, chlorophyll and primary production for 1989 in the upper 400m. Dotted line represents mixed layer depth.

Regarding bloom timing and misfit, it can be said that overall, the new parameter set gave a good fit to the NABE89 data set (see table 6.3). It is worth noting that the greater fraction of the misfit could be due, in certain cases, to heterogeneous data availability (i.e. nitrate, silicate and ammonium were measured down to a depth of 1000 m while data for other variables data, such as chlorophyll or PON, were taken in the upper 300 m) and also to different orders of magnitude characterizing different processes (i.e. nitrate values range from 0 to 23 mmol N m^{-3} while chlorophyll varies between 0 and 3.50 mg m^{-3}). In order to avoid contribution by heterogeneous data availability, the misfit was normalised by the number of observations of each type but no attempt to scale the observational data was made. The highest contribution to the misfit was due to nitrate (49.28%) and silicate (24.42%) and the lowest by chlorophyll (5.21%) followed by ammonium (8.39%) and PON (12.77%).

In terms of bloom timing, the 1-D model tends to predict an earlier phytoplankton bloom compared to real data, and also to 0-D model results. The initiation of the spring bloom, as well as bloom intensity and duration, depend on the physical variables that determine the onset of thermal stratification of the mixed layer and therefore, its stability. Such 1-D model results can be explained by the earlier stratification of the mixed layer compared to its 0-D counterpart, as discussed earlier in section 6.3.

Regarding bloom timing and intensity, the 1-D model predicts a chlorophyll bloom (diatom) about eight days earlier (Julian day 120) than observed in cruises Atlantis I (between Julian days 126 and 128) and Meteor (between Julian days 128 and 132), overestimating maximum phytoplankton biomass by 0.55 mg chl m^{-3} (3.34 mg chl m^{-3} modelled *versus* 2.78 mg chl m^{-3} from Meteor data) but describing PON and nutrient variability quite well (figures 6.9 and 6.10), specially during the Atlantis I cruise. The

mismatch observed between modelled PON and Meteor data is due to the earlier occurrence of the bloom in the 1-D model, which leads to the underestimation of PON by 1.21 mmol N m^{-3}. The model reproduces the lack of silicate in the upper 50 m of the water column during both cruises (although modelled silicate concentration below 50 m is nearly half the concentration suggested by Atlantis I and Meteor data), keeping nitrate concentrations in the upper 50 m ca. 4.51 mmol N m^{-3}. Ammonium data from Meteor shows a vertical patchy structure that the model is not able to reproduce due to its physical limitations (figure 6.10). Nevertheless, subsurface ammonium concentrations vary within the limits set by Meteor data. Meteor data show the existence of several subsurface ammonium maxima down to a depth of 125 m, accounting for up to 2.61 mmol N m^{-3} whereas modelled ammonium is less than 0.5 mmol N m^{-3} in the upper 45 m, showing a peak value of 1.80 mmol N m^{-3} between 62 and 75 m. Below 75 m, modelled ammonium concentration decreases down to 1.23 mmol N m^{-3}, similar to the values measured on board Meteor.

The second chlorophyll bloom (Atlantis II), attributed to non diatoms, is better reproduced by the model, both in terms of biomass and also timing, and so are silicate, nitrate and ammonium concentrations in the water column for the times and depths at which such bloom occurred, when compared to Atlantis II data. A subsurface ammonium maximum, between 25 and 75 m, is observed in both, model and observational data, but the 1-D model tends to overestimate such quantity below 75 m (figure 6.10).

Discovery 183 cruise data showed the occurrence of a subsurface chlorophyll bloom in summer (from Julian day 183 to 185), located between 23 and 40 m, which was also reproduced by the model. Modelled silicate during Discovery 183 cruise underestimated measured values, as 1-D model values varied from 0 to 2 mmol m^{-3} *versus* 2 and 5 mmol m^{-3} from Discovery data. No nutrient data, other than silicate, were available from this

cruise. Later in the year, Tyro data show low chlorophyll concentration, up to 0.43 mg chl m^{-3} between the surface and 70 m, from Julian day 234 to 238. Below 70 m, chlorophyll values remain below 0.1 mg chl m^{-3}. Modelled data for this period, showed chlorophyll concentrations up to three times higher (1.2 mg chl m^{-3}) in the upper 25 m. In terms of nutrients, modelled and measured nitrate are in good agreement but the 1-D model tends to underestimate silicate concentration by half the measured values on Tyro.

Figure 6.11 shows that vertical distribution of nitrate and silicate down to 900 m was generally well reproduced by both model results.

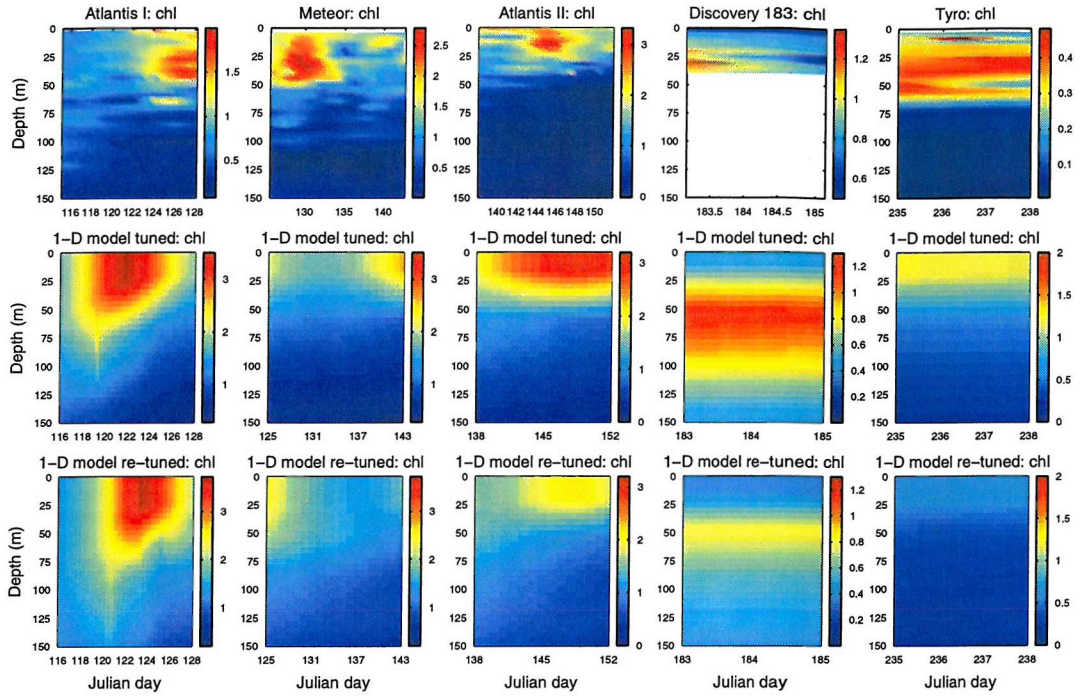

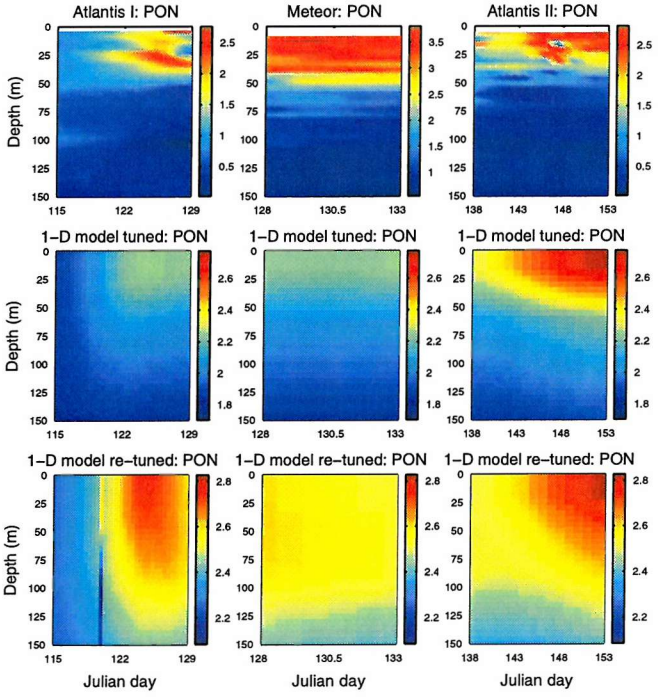

Figure 6.9: 1-D model tuning and re-tuning chlorophyll and PON and also NABE89 observations. Dotted line represents modelled mixed layer depth.

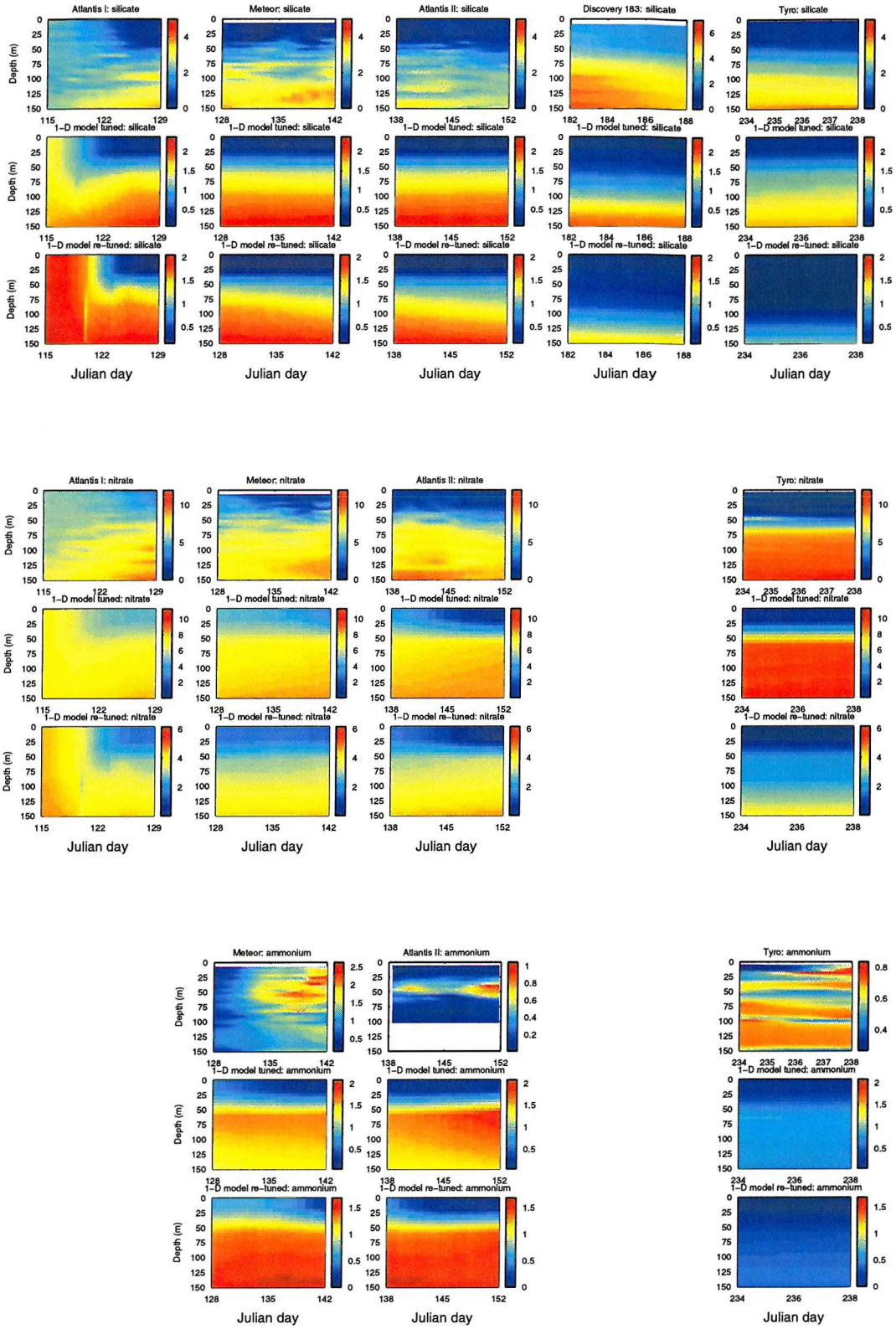

Figure 6.10: 1-D model tuning and re-tuning and also NABE89 nutrients to 150 m. Dotted line represents modelled mixed layer depth.

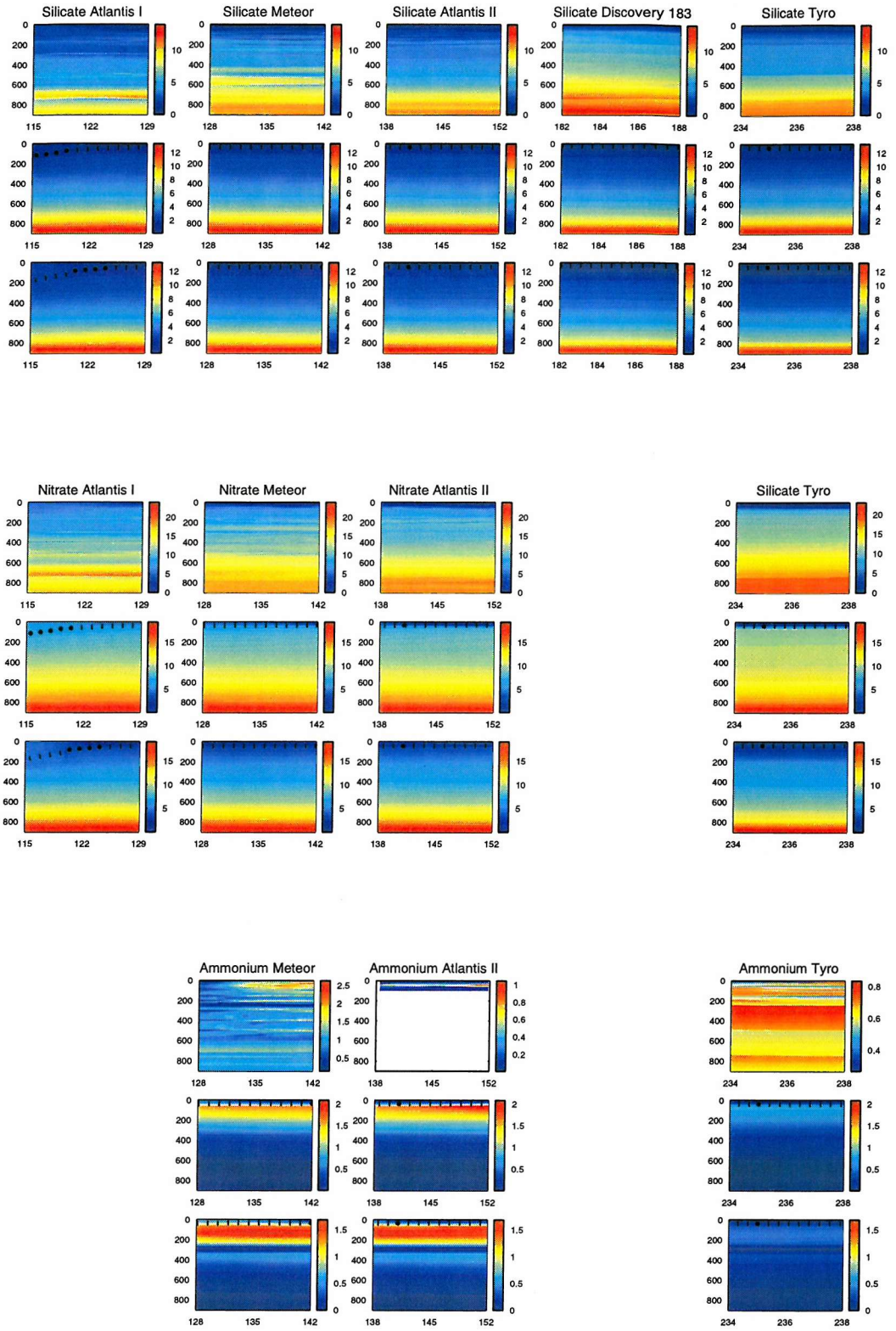

Figure 6.11: 1-D model tuning and re-tuning and also NABE89 nitrate and silicate to 1000 m. Dotted line represents modelled mixed layer depth.

6.5 Validating the coupled model: the NABE 1996 data set

Field data for the NABE site were available from early July until October 1996 from German cruise Meteor 36/2 and were used to perform an independent model validation (referred to as NABE96 data, hereafter). The 1-D model was run using physical forcing corresponding to 1996, having been tuned to NABE89 data, only in order to test that model results were within reasonable limits. Once the suitability of the initial conditions were checked, the model was rerun and physically forced by a nine year series of variables from 1988 to 1996 and model output was compared to the NABE96 data set.

Observational data: biochemical variability in 1996

Vertical profiles of nitrate, silicate, ammonium, chlorophyll *a* and PON were available, ranging from 05/07/96 to 07/07/96, from 10/09/96 to 03/10/96 and from 23/10/96 to 31/10/96 and therefore, setting the prevailing physical and chemical conditions in the transition time from summer to autumn.

As for the NABE96 data set, nitrate, silicate and ammonium were sampled down to a depth of 1000 m while chlorophyll and PON data were only available in the upper 200 and 150 m, respectively (figure 6.12). The first two days of cruise data registered a late summer bloom (Julian days 187 to 189, corresponding to early July), when there was a well established vertical gradient of chlorophyll *a*, ranging from 1.50 mg chl m^{-3} in the upper 35 m to less than 0.30 mg chl m^{-3} at depths of 65 m and below. For the second part of the data (from Julian day 254 to 278, September to early October), the stratified chlorophyll *a* distribution is broken and the occurrence of a less intense deep chlorophyll maximum is evident, accounting for 1.10 mg chl m^{-3}. The fact that there is lack of nitrate at such depths strongly suggests a diatom bloom, supported by an observed silicate

reduction from 2 to less than 1 mmol Si m^{-3}, at times and depths at which the bloom was observed. For the final part of the data (from Julian days 297 to 306), chlorophyll remained below 0.60 mg m^{-3}.

Ammonium and PON showed a remarkable vertical structure. The former showed a deep maximum between 400 and 500m accounting for 0.92 mmol N m^{-3}. PON showed four subsurface peaks (resembling chlorophyll variability), from Julian day 298 to 300, at depths ranging from 20 to 82 m. Maximum PON was found at 82 m, reaching a peak of more than 3 mmol N m^{-3}.

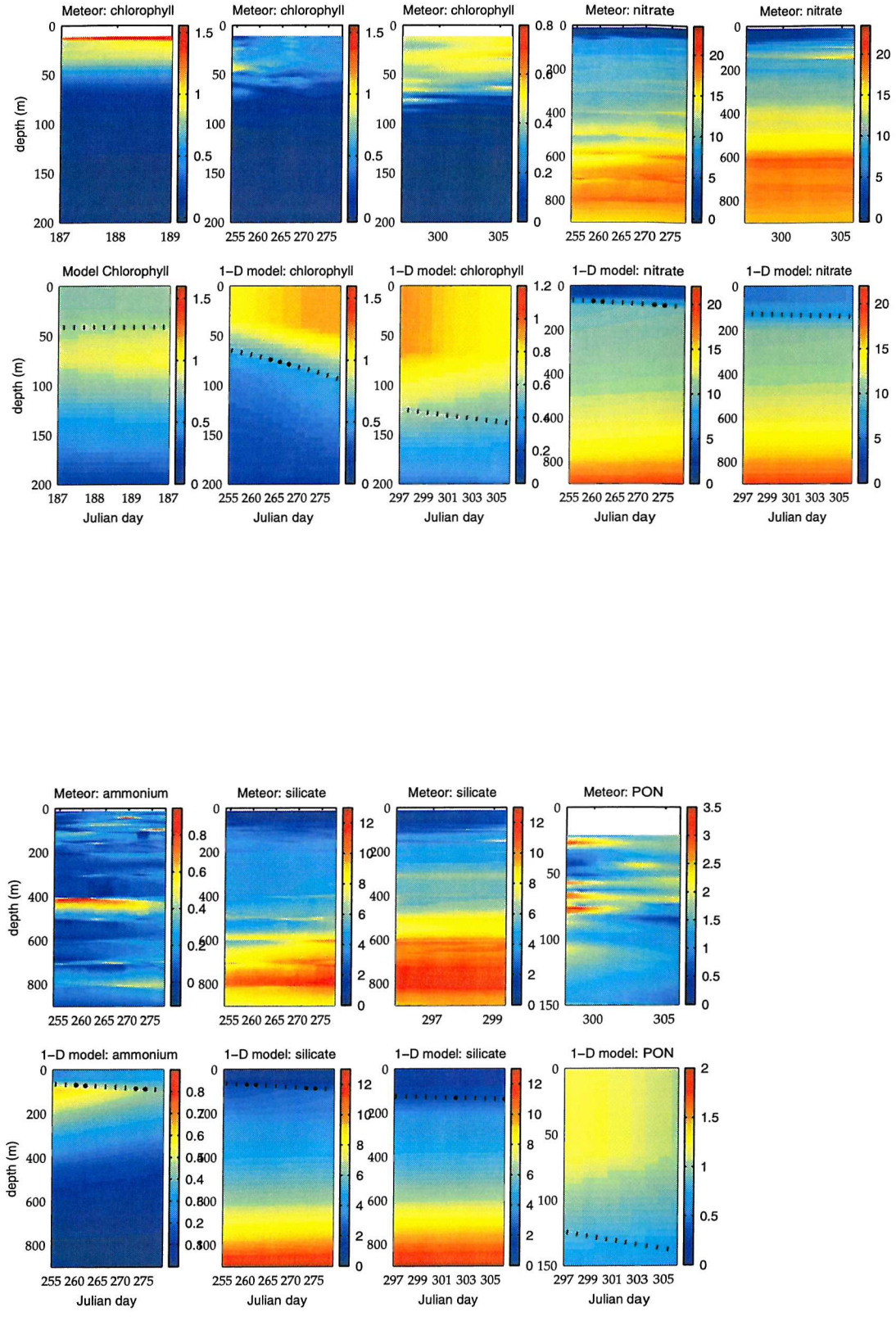

Figure 6.12: 1-D model and also NABE96 data split up into three different batches. Dotted line represents modelled mixed layer depth.

Model validation

1. Problems encountered

When the tuned model was run, using 1996 physical fields, results showed that nitrate reached unreasonably high values in winter (up to 15 mmol N m^{-3}) and remained above 6 mmol N m^{-3} in spring, never being depleted. The rest of the variables showed a more realistic pattern in terms of biomass but in some cases bloom conditions extended for too long due to the nitrogen bonanza; diatoms, for instance, were able to grow uninterruptedly for as long as 2 months, allowing mesozooplankton to do so for almost 90 days.

As there were no data available for either spring or summer, model results could not be checked for this period but previous field studies for this area (Glover and Brewer,1988; Garside and Garside, 1993) gave winter nitrate concentrations ranging between 11 and 13 mmol N m^{-3}, suggesting that the model was showing an unusual pattern. These results probably indicate the use of one or more unsuitable parameters regulating modelled nitrogen (possibly detrital nitrogen remineralisation (δ_1) or nitrification rates (*nr*) or both). In order to understand what was causing this behaviour, a series of tests with varying *nr* and δ_1 were set up (table 6.4).

First, the model was rerun with the nitrification rate being switched off (test1). Model results predicted too much ammonium (12 mmol N m^{-3}) and too little nitrate. In the second test (test2), the model was rerun as in test1 but also using a remineralisation rate reduced by a fourth from its *a priori* value. Model results still predicted a very high ammonium concentration (6 mmol m^{-3}) and low nitrate, pointing to the unavoidable need of modelling nitrification so as to balance both nitrogen nutrients. The third test was carried out by using the reduced remineralisation rate in test2 and nitrification as in the

tuned model, showing good ammonium, detritus and nitrate (slightly low) concentrations. Finally, several tests with varying remineralisation rates were performed as to determine the more suitable rate to achieve a winter nitrate concentration lower than 11 mmol m^{-3} as reported in the literature (Garside and Garside, 1993), given by δ_1=0.10694 d^{-1}. As previously stated, detritus remineralisation rate is a key parameter in ecological dynamics.

Having found what it seemed to be an appropriate remineralisation rate, the model was rerun using this rate and the fit to the NABE89 data set was checked once more. The new model output showed that the fit was not as good as before (mainly in terms of phytoplankton, as both diatoms and non diatoms spring blooms overlapped in time which led to nitrate and silicate underestimation) and it was necessary to re-tune the model (see figure 6.7 for re-tuned model results). The best fit to NABE89 data was found when α_1 and K_1 and K_2 (the half saturation constants for nitrate and ammonium uptake, respectively) were decreased (see table 6.2) and δ_1 increased (δ_1=0.12694). The total misfit (see equation 2.29) was slightly higher than when the model was first tuned (table 6.3); silicate, ammonium and PON were better fitted (table 6.3) but fit to chlorophyll and nitrate was poorer. Although the model seems to get a slightly worse fit to real data during 1989, in the long run it is expected to produce a better fit to both years 1989 and 1996 and this points at the non uniqueness of the *a priori* values to provide a good solution.

This case epitomizes the usually neglected problem of data overfitting (a simple idea with deep implications), in which a very good fit to a single data set might provide a solution that is not suitable for real forecasting (as a model that passes through every real datum is also fitting noise, so will not generalize) while a relative worse fit to the same data set,

makes the new solution more universal and therefore, more applicable when testing using independent data sets. Successful model fitting has to be able to interpolate or extrapolate and needs to find the balance between underfitting, where model mismatch errors exist as the model cannot describe the data, and overfitting, where there are model estimation errors from poor parameter choices in a flexible model (Gershenfeld, 1999). In our case, the choice between a reliable estimate from a biased model and a poorer estimate from a model capable of a better fit was decided in favor of the latter.

2. The re-tuned model

2.1 General dynamics

The 1-D re-tuned ecological model was physically forced with fields from years 1988 to 1996 and model output corresponding to 1989 was studied (figure 6.13). Model results showed the typical spring bloom structure described earlier for the North Atlantic but differed from the previous runs in several aspects. The first striking difference is the occurrence of a subsurface non-diatom maximum, triggered in July, just below the mixed layer, supported by ammonium concentrations. A diatom subsurface bloom also occurs in late spring (not clearly visible in figure 6.13 due to the scale used), slightly less intense than the 1-D tuned model one (see figure 6.8), reaching 1.15 mmol N m^{-3}.

The second most noticeable difference is the higher diatom peak biomass (2.85 mmol N m^{-3}), chlorophyll (3.72 mg chl m^{-3}), winter surface silicate (2.06 mmol N m^{-3}) and biogenic detrital silica concentration (0.78 mmol N m^{-3}) but less non-diatom peak biomass (1.53 mmol N m^{-3}), winter surface nitrate (5.37 mmol N m^{-3}), ammonium (1.44 mmol N m^{-3}), biogenic detrital nitrogen (0.56 mmol N m^{-3}), microzooplankton (0.31 mmol N m^{-3}) and primary production (0.62 mmol N m^{-3} d^{-1}) as it can be clearly seen in figure 6.7 (also figures 6.8 and 6.13).

The new model, the 1-D re-tuned model, predicts six phytoplankton bloom phases: 3 in spring, 2 in summer and 1 in autumn. Diatoms bloom in spring (April and June) and also in autumn (November) while non diatoms bloom in spring (in early April just before diatoms), May and July (subsurface maximum), maintaining a biomass ca. 0.5 mmol N m^{-3} until late September. The non diatom bloom in April started off at the end of winter and extended in the vertical down to the base of the mixed layer (300 m), reaching a maximum biomass of 1.15 mg chl m^{-3}. Both zooplankton groups follow the same pattern as the phytoplankton group they feed on, showing a lag time response of, approximately, 15 days. Detrital nitrogen shows two main peaks, the first one resulting from both phytoplankton and mesozooplankton losses and the second one accounting for the late non-diatom spring bloom and microzooplankton, while detrital biogenic silica peak reflected mesozooplankton inefficient feeding on diatoms. Ammonium tends to accumulate below the mixed layer where there is barely any consumption, reaching a maximum 1.7 mmol m^{-3}.

In terms of vertical resolved observational data (figure 6.9), the model matched timing of the phytoplankton bloom better than previously found for the Atlantis I data set (still overestimating peak biomass). Generally, the fit to chlorophyll was very similar to the previous case (5.21% *versus* 5.51% for 1-D tuned and re-tuned model, respectively; see table 6.3). Model onset of the diatoms spring bloom still occurred three days earlier than suggested by Atlantis I data and maximum diatom biomass is reached about seven days earlier than Meteor observed. Meteor data also showed the occurrence of a third bloom, reaching 1.80 mg chl m^{-3} on Julian day 140 and presumably attributed to non diatoms, due to the removal of nitrogen observed at the same time and depth (not clearly noticeable in figure 6.10 due to scale used), that was not reproduced by the model. The main non diatom bloom on Julian day 145 was also well matched in time, while bloom

intensity was slightly underestimated (model prediction was 2.26 *versus* observations of 3.32 mg chl m^{-3}). Discovery 183 subsurface chlorophyll maximum extends for a 3 day period, as predicted by the model, ranging from 1.31 to 0.90 mg chl m^{-3} while modelled subsurface chlorophyll is ca. 0.92 mg chl m^{-3}. According to Tyro data, late summer chlorophyll remained low (less than 0.6 mg chl m^{-3}) and so did in the model.

Vertically resolved ammonium data show a better fit than before as well as PON and silicate and a worse fit to nitrate. Ammonium contributes to the total misfit by 6.62% *versus* 8.39% (table 6.3). The 1-D re-tuned model still underestimates ammonium at 50 m (1.17 *versus* 2.61 mmol N m^{-3} from model output and Meteor data, respectively) but it is in good agreement with cruise data below this depth (ca. 1.52 mmol N m^{-3}). Fit to Atlantis II data within the upper 60 m is reasonably good but below such depth the model overestimates ammonium concentration. PON model results show good agreement, in magnitude and also time, with both Atlantis cruises (real data suggest peak values of 2.62 and 2.82 mmol N m^{-3} for Atlantis I and II, *versus* model values of 2.68 and 2.81 mmol N m^{-3}). Modelled data underestimate PON during the Meteor cruise (peak value of 3.49 mmol N m^{-3} *versus* 2.62 mmol N m^{-3} suggested by the model), due to the mismatch in chlorophyll for the same period of time. Regarding silicate and nitrate, the model resolves well the vertical structure observed in all cruises (depletion at the surface and increasing nutrients below the mixed layer) although tends to slightly underestimate silicate (by 1 mmol Si m^{-3}) and nitrate concentration (by nearly 3 mmol N m^{-3}) below 60 m.

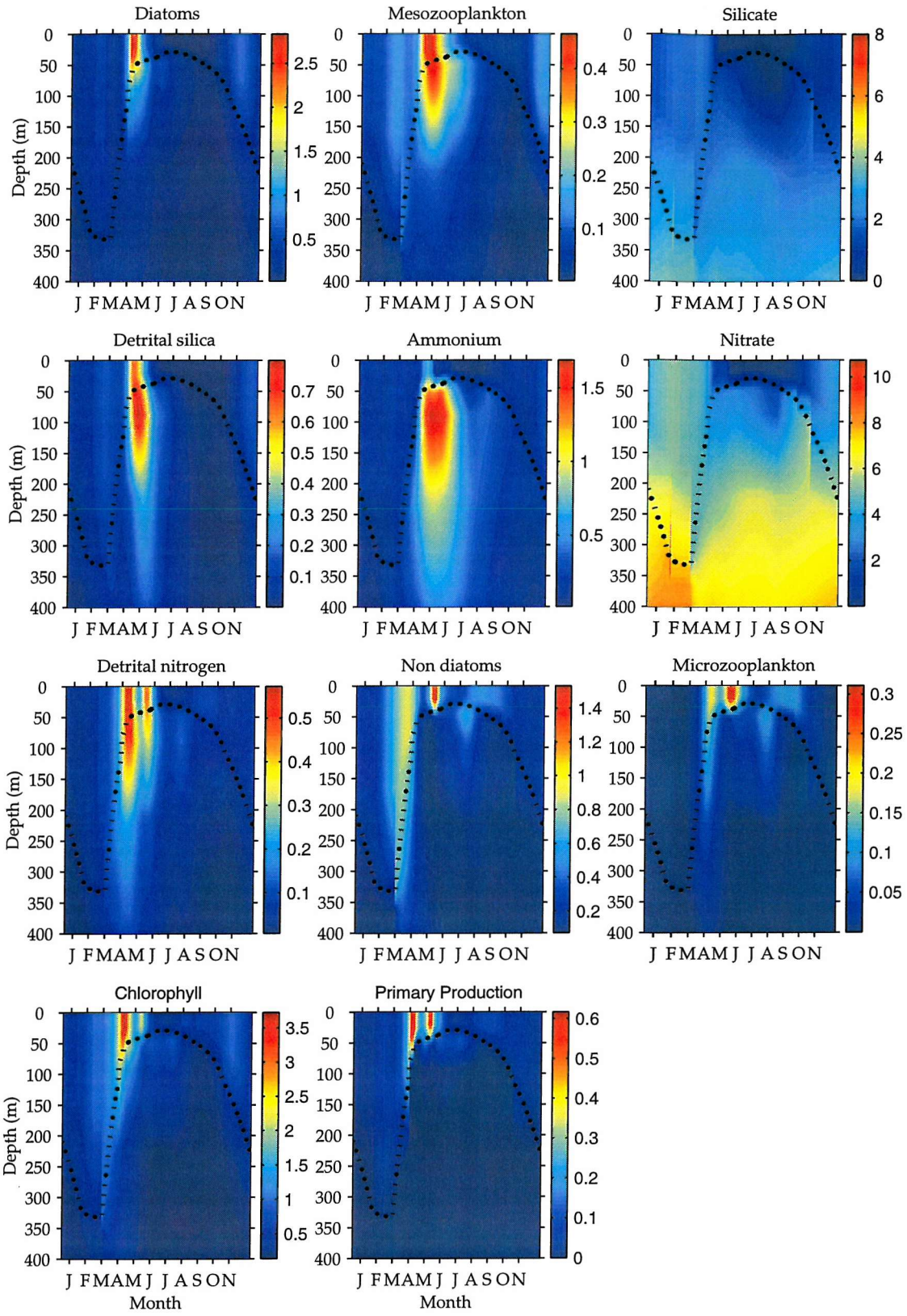

Figure 6.13: 1-D model state variables, chlorophyll and primary production for 1989 down to 400 m. Dotted line represents mixed layer depth.

2.2 Primary production in the mixed layer

As the model distinguishes between ammonium and nitrate, it was possible to calculate how much of the total primary production (TPP) was new production (NP), which is derived from nitrogen supplied by hydrodynamical processes, and how much was regenerated production (RP), fuelled by nitrogen regenerated *in situ* by heterotrophs. NP is of vital importance in the physical equilibrium between anthropogenic atmospheric CO_2 perturbations and the ocean interior by facilitating such equilibrium through the sinking flux of particulate organic matter. This flux couples sea surface/atmosphere CO_2 balance with the carbonate system in the interior of the ocean on varying time scales, from years to decades (Garside and Garside, 1993).

Model-predicted total annual primary production, integrated over the mixed layer, was 1.95 mol N m^{-2} yr^{-1} (or 154.20 g C m^{-2} yr^{-1}) of which 1.06 mol N m^{-2} yr^{-1} (55%) were NP and 0.88 mol N m^{-2} d^{-1} (45%) were RP. Small organisms seem to play an important role as the non-diatom contribution to TPP is 12% higher than diatom's (56% *versus* 44%). They also accounted for 43% of the total NP and 71% of the total RP, while diatoms dominate NP by accounting for 57% and only for 29% of the total RP (tables 6.5 and 6.6).

According to Eppley and Peterson (1979), the annual *f* ratio represents a measure of exportable production from the euphotic zone. As expected, winter phytoplankton standing stocks relied on nitrate (high *f* ratio) to maintain their biomass. When improved environmental conditions in the water column triggered phytoplankton development, the onset of all the surface blooms are sustained by nitrate for, approximately, 10 days while bloom progression and subsurface ones are mainly supported by ammonium as a result of biological activity (mortality, excretion and remineralisation processes). In 1989, the *f* ratio was 0.55 indicating that the ecosystem is mainly supported by nitrate and, therefore,

there is relative high matter export (≅ 55%). Model estimates of the annual export (*e* ratio) were only 35.54% of the total PP, a total of 54.81 g C m^{-2} yr^{-1}, at a daily rate of 0.15 g C m^{-2} d^{-1} on average.

Model fluxes show the relevance of grazing in the system. Microzooplankton grazing pressure on non diatoms tend to be higher than mesozooplankton's pressure on diatoms (75.93% *versus* 69.57%). Total primary production is mainly grazed by mesozooplankton (38.84%) closely followed by microzooplankton (33.55%), the remaining phytoplankton losses being due to natural mortality (17.37%) and sinking (10.23%). Egestion processes (production of faecal pellets) represent the least of the zooplankton losses (only 3.10% for mesozooplankton and 0.60% for microzooplankton) and while excretion accounts for most of the reduction in mesozooplankton biomass (56.98%), microzooplankton declining is mainly due to natural mortality (65.74%). Overall, secondary production declines mainly due to natural mortality (52.03%), followed by excretion (44.56%), egestion (1.92%) and mesozooplankton grazing on microzooplankton (1.49%). Mesozooplankton is also the main contributor to the detrital biogenic silica compartment (85.23%) *versus* diatom natural mortality (14.77%).

But how do model results compare to previous studies?.

2.3 Fit to observations

In order to make results directly comparable to other studies, phytoplankton chlorophyll values were converted into nitrogen units using a constant N:chlorophyll ratio of 14 (Ducklow *et al.*, 1993), carbon was converted into nitrogen by assuming a constant phytoplankton C:N Redfield ratio of 6.7 (Ducklow *et al.*, 1993) and a C:N zooplankton ratio of 4.5.

Primary Production

The 1-D model estimates an annual PP of 154.20 g C m^{-2} yr^{-1}, that is 98 g C m^{-2} yr^{-1} higher than the annual PP obtained by the 0-D model (table 6.7). Fasham and Evans (1995) estimated an annual PP of 122 g C m^{-2} yr^{-1} in the mixed layer, 32 g C m^{-2} yr^{-1} less than the 1-D coupled model for the same period of time and the same set of NABE observations for the upper mixed layer. Their NP reaches 65 g C m^{-2} yr^{-1}, 20 g lower than our 1-D model and about 41 g higher than the 0-D model. Three dimensional model studies, such as Oschlies *et al.* (2000) based on a NPZD model, estimate an annual PP of 108 g C m^{-2} yr^{-1} for the NABE area, slightly lower than 1-D model estimates.

A number of global annual PP maps based on ^{14}C data have been produced from as early as 1957 (Steeman Nielsen and Jensen, 1957). The most recent one has been published by Berger (1989) based on 8000 data points, who estimated an annual PP of 35-60 g C m^{-2} yr^{-1} at 47°N 20°W, which is two and a half times lower than suggested by the 1-D model. However, there has been some criticism about the uncertainty associated to such maps as it has been suggested that ^{14}C based production rates have been underestimated (Martin *et al.*, 1987; Knauer, 1993) and it seems that new clean ^{14}C techniques provide values about twice those historical production rates (in Fasham and Evans, 1995). New ways of inferring primary production from observations came with the development of satellite technology. In 1995, Longhurst *et al.* estimated an annual PP of 240 g C m^{-2} yr^{-1} (at 47º N 20º W) based on seven years of monthly mean near-surface chlorophyll fields obtained by the Coastal Zone Color Scanner (CZCS) radiometer. In the same year, Sathyendranath *et al.* (1995) divided the Atlantic Ocean into different biogeochemical provinces, estimating an annual PP of 230-243 g C m^{-2} yr^{-1} at 47°N 20°W, based on the compilation of field (cruise and satellite data) and laboratory measurements of chlorophyll and P-I parameters. Behrenfeld and Falkowski (1997) also

assembled ^{14}C-based productivity measurements and satellite-based chlorophyll concentration to asses PP. Their annual estimates at 47°N 20°W, vary between 200-270 and 150-225 g C m^{-2} yr^{-1} depending on the type of temperature dependent model used to calculate photosynthesis. The latter was inferred using the same algorithm than Antoine *et al.* (1996), whose annual production estimates range between 120-160 g C m^{-2} yr^{-1} based on CZCS data. A combination of CZCS and AVHRR (Advanced Very high Resolution Radiometer) data was used by Field *et al.* (1998), who obtained annual surface PP values of 200-250 g C m^{-2} yr^{-1} at 47°N 20°W. Therefore, PP annual estimates vary widely depending on the data set and the algorithms used to calculate phytoplankton productivity. Estimates based on satellite data shown above are about four times greater than production estimates from historical maps. The former provide annual PP values ranging from 120 to 270 g C m^{-2} yr^{-1}, which agree with our 1-D model estimates.

In general, the model shows a good agreement to observational studies carried out in the same area (table 6.7). Minimum and maximum daily PP estimates from Joint *et al.* (1993) and also peak values from Weeks *et al.* (1993), during cruise Discovery 183, are well matched by the 1-D model. Martin *et al.* (1993) estimated an averaged PP of 0.37 mmol N m^{-3} in the top 35 m over a period of 38 days (from Julian day 114 to 152). For the same period of time, we estimated an averaged 0.39 mmol N m^{-3} (*versus* 0.41 mmol N m^{-3} obtained by the 0-D model). Lochte *et al.* (1993) studied the succession of plankton communities at 47°N 20°W from 24 April to 31 May in 1989 based on data gathered from several cruises, which included the same data set used in our 1-D model calibration. Their integrated (down to 80 m) PP estimates for such period ranged from 0.6 to 1.8 g C m^{-2} d^{-1}, while 1-D and 0-D model estimates are between 0.64-1.48 g C m^{-2} d^{-1} and 0.44-0.92 g C m^{-2} d^{-1}, respectively. On the other hand, Chipman *et al.* (1993) also measured integrated PP in the mixed layer -based on data gathered on cruise Atlantis I -from 25

April to 10 May- being between 10-33% lower than Lochte *et al.* (1993) values (see table 6.7). Difference between chlorophyll measurements had also been observed between Atlantis and Meteor cruises data and differences in water masses sampled has been suggested as a possible explanation (Lochte *et al.*, 1993).

Size-fractionated PP measurements, integrated to 35 m, showed that, between 12-18 May, microplankton (fraction > 5μm, therefore diatom growth) were responsible of 51.2% of the TPP while between 2-8 July, smaller phytoplankton fractions contributed to the phytoplankton standing stock by 57.1% (Joint *et al.*, 1993). One dimensional and 0-D model results show a similar pattern. During the same period in May, the 1-D model diatom fraction accounted for 65% of the total phytoplankton standing stock (the 0-D model estimated 63%) while non diatoms dominated in July (85.6% and 95%, 1-D and 0-D model results, respectively).

Chlorophyll

The coupled model predicted a maximum chlorophyll peak of 3.55 mg m^{-3} in 1989 (0-D model maximum was 2.69 mg chl m^{-3}) matching observational values given by Joint *et al.* (1993) for the 1989 spring bloom (4.2 mg chl m^{-3}), but 0-D model chlorophyll peak estimates are closer to values found by Lochte *et al.* (1993) based on Meteor data (>2.5 mg m^{-3}). Both authors found subsurface chlorophyll maxima in the top 50 m of the water column and so did the coupled model. Joint *et al.* (1993) described a chlorophyll maximum higher than 2 mg m^{-3}, between 25 and 50 m, composed mainly of diatoms, on Julian day 134. Exactly at the same depth, although a few days earlier, Lochte *et al.* (1993) also described a maximum above 2.5 mg chl m^{-3} that coincides in time with an increase in diatom biomass, shown by the coupled model on Julian day 132 (middle May in figure 6.13), accounting for up to 1.15 mg chl m^{-3}.

Modelled integrated chlorophyll in the mixed layer was slightly higher than observational spring values and lower than observed in summer. Joint *et al.* (1993) reported integrated chlorophyll ranging from 25.0 to 52.0 mg m^{-2} over the top 35 m between 12 and 18 May (1-D and 0-D model estimated 62.42-72.18 mg m^{-2} and 35.6-41.22 mg m^{-2}, respectively). The same authors provided values ranging from 22.8 to 34.6 mg m^{-2} during the first week in July (1-D and 0-D model are 9.97-10.36 mg m^{-2} and 10.38, respectively). Integrated chlorophyll (over the top 80 m), between 24 April and 31 May lay between 30-175 mg m^{-2} (Lochte *et al.*, 1993), which is about 25% lower than the 1-D model estimated and 66% higher than 0-D model results. Peak integrated chlorophyll simulated by the 1-D model (32.59 mg m^{-2}) was similar to values described in Weeks *et al.* (1993), from 12 June to 13 July, based on Discovery 183 data (0-D peak chlorophyll was only 20.83 mg m^{-2}).

Zooplankton

Due to the lack of zooplankton observational data, model integrated zooplankton was also compared to other model studies carried out for the same area. Our 1-D model compared well to Oschlies *et al.* (2000) which predicted similar figures (between 60 and 80 mmol N m^{-2}) to the 1-D and 0-D model estimates (50 and 39.35 mmol N m^{-2}, respectively).

Observational zooplankton data were available from the Atlantis I cruise (in Marra and Ho, 1993) although it has been reported that zooplankton samples became so contaminated with phytoplankton, that biomass determination was not reliable (Dam *et al.*, 1993). Therefore, comparisons between our model output and real data should be taken with care. Observational zooplankton limits vary from 5 to 12 mmol N m^{-2} sampled over 100 m between Julian days 115 and 121 (in Marra and Ho, 1993) while model results from both models (0-D and 1-D) are nearly three times higher (table 6.7).

Regarding maximum microzooplankton biomass, the 1-D model predicted values (10.90 μg C l^{-1}) that match observational values (13 μg C l^{-1}) obtained by Burkill *et al.* (1993) during cruise Discovery 183 (Julian days 168 to 189). They also provided estimates of microzooplankton standing stock, integrated over the mixed layer, reaching up to 303 mg C m^{-2} at 47°N 20°W and stated that microzooplankton standing stocks ranged between one-quarter to one-third of those of phytoplankton. Model results reached up to 349.67 mg C m^{-2} (1-D model) and 307.39 mg C m^{-2} (0-D model), representing one-quarter of the total phytoplankton stock in both cases.

Modelled microzooplankton biomass ranged between 2.20-16.79 mg C m^{-3} (1-D model) and between 5.60-22.46 mg C m^{-3} (0-D model) *versus* 6-14 mg C m^{-3} provided by observational studies (In Taylor *et al.*, 1993).

In terms of PP channeled via zooplankton, there are some discrepancies in the literature. Boyd and Newton (1995) and Verity *et al.* (1993) both agreed that less than 64% of PP was grazed by microzooplankton during late April and May, while Burkill *et al.* (1993) estimated between 39-100% of PP grazed from middle June to early July (see table 6.7). Regarding mesozooplankton grazing, the majority of literature consulted (Morales *et al.*, 1991; Dam *et al.*, 1993; Verity *et al.*,1993; Burkill *et al.*, 1993; Weeks *et al.*, 1993) give values between 1% and 6% but other estimates (Lentz *et al.*,1993), point at much higher values, up to 45% (they also suggest that only 6% of PP was grazed by microzooplankton), which shows the high degree of uncertainty (up to 50%) inherent to secondary production measurements.

Model results are half way through between both trends: the 1-D model predicts less than 50% of PP grazed by microzooplankton during May and up to 94% during the June-July period while the 0-D model predicts more grazing pressure in May (27.91%) than during

the summer months (10.33%). Mesozooplankton grazing pressure is high (65.44%), agreeing with figures given by Lentz *et al.* (1993), from late April to early May. From then on, such pressure is reduced down to 20% during late May and to less than 6% from late May to July, agreeing with the general trend found in the literature. Regarding the 0-D model, mesozooplankton grazes between 0.10%-9% of the total PP in all cases (see table 6.7).

Modelled mesozooplankton biomass varied between 12.64-25.14 mg C m^{-3} (1-D model) and 13.12-37.10 mg C m^{-3} (0-D model) from 25 April to 7 May. Similar results were described by Dam *et al.* (1993), based on Atlantis I data for the same period of time (see table 6.7).

Particle export

Particle export was estimated at the NABE site by using sediment traps and ^{234}Th models. Martin *et al.* (1993), deployed free-floating shallow drifting traps to estimate export fluxes at 47°N 20°W during the 24 April to 1 June period. Their organic flux estimates for the upper 35 m and 150 m represented 45% and 11% of PP, respectively, and a total of 45 and 1.5 mmol N m^{-2} d^{-1}. On the other hand, Buesseler *et al.* (1992), also calculated export fluxes for the NABE area based on a non-steady state ^{234}Th scavenging model. Maximum carbon exports of 20-42% of PP (from the upper 35 m) were produced by this model between 24 April and 1 June.

Although sediment traps and ^{234}Th model produced similar results at shallow depths, significant higher fluxes are predicted by Buesseler's model at higher depths. Buesseler and co-authors pointed out that export fluxes calculated by Martin *et al.* (1993) greatly underestimate particle flux at 150 and 300 m depth (by factors of 4 to 7 times), as there

are remarkable differences between model (up to 11.67 mmol N m^{-2} d^{-1} at 150 m) and sediment trap (1.5 mmol N m^{-2} d^{-1} at 150 m) estimates (see figure 6.14).

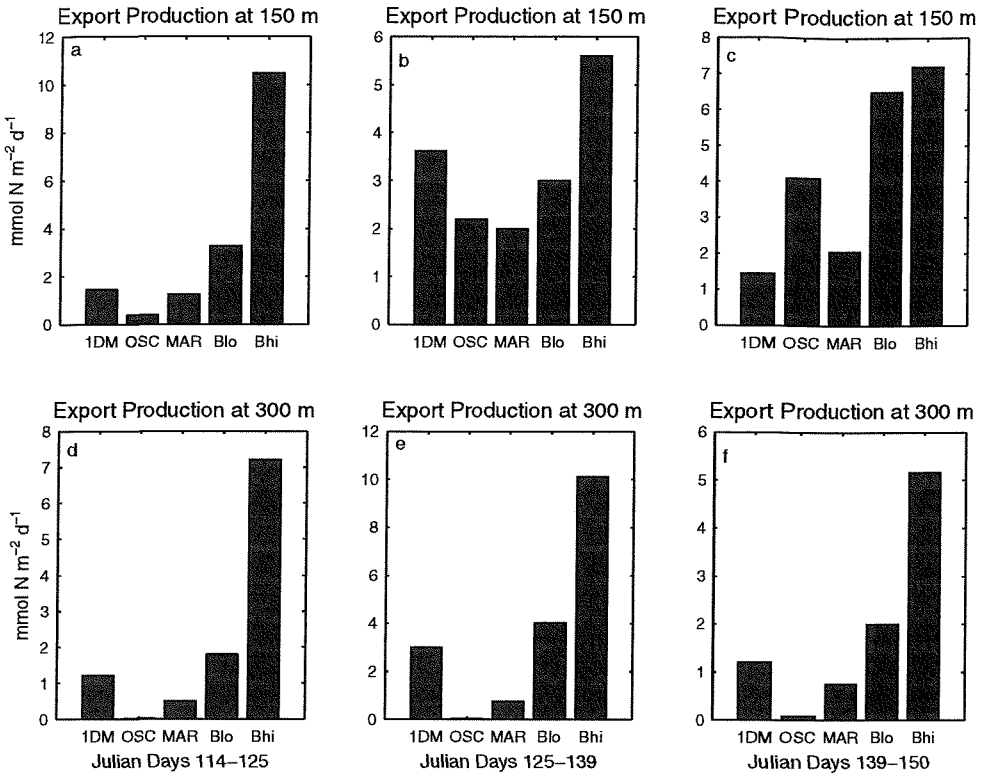

Figure 6.14: Particle nitrogen export at 150 m (a-c) and 300m (d-f). Results from the 1-D model (1DM) are shown *versus* other estimates. OSC stands for Oschlies *et al.* (2000), MAR are sediment trap data by Martin *et al.* (1993) and Bhi, Blo are high and low flux estimates from Buesseler *et al.* (1992).

Our 1-D model nitrogen export, agree well with rates given by both authors in the upper 35 m (42.78% of PP), resulting in an *f* ratio of 0.43 *versus* a ratio of 0.45 given by Martin *et al.* (1993) (data not shown). In terms of deeper estimates, as shown in figure 6.14, 1-D model results also show a good agreement with Martin's observations at 150 m, although they are slightly higher (between 1.5 to 3 times) than suggested by sediment traps at 300 m. One dimensional model results are 3 to 6 times lower than Buesseler's high flux estimates at 300 m and agree well with their low flux estimates at such depth. Other model estimates (Oschlies *et al.*, 2000), provide similar export rates to sediment traps between days 125-139 at 150 m but strongly underestimate fluxes at 300 m.

3. The re-tuned validated model

3.1 General dynamics

Model results corresponding to 1996 can be seen in figure 6.15. They resemble the typical spring bloom structure described earlier for the North Atlantic although bloom timing and duration are very different. Mixed layer depths also differ from those in 1989. Maximum depths go down only to 300 m (332 m in 1989) and stratification of the water column shows two clear phases. Shoaling of the mixed layer stars in early March (around Julian day 75) but gets interrupted 20 days later at a depth of 100 m ("phase 1") due to increasing wind speed and decreasing solar heating, causing the mixed layer to deepen again reaching 110 m in April (around Julian day 130). After that day, "phase 2" starts, physical conditions improve and stratification continues from early May (Julian day 140), reaching a minimum depth of 41 m a month later (on Julian day 180, as in 1989). Thereafter, mixed layer dynamics are similar to the ones observed in 1989. Consequently, there is a boost in the amount of nutrients (silicate and nitrate) available in the mixed layer in early April. This is especially important for nitrate, whose concentration had nearly been halved by then (from 8 mmol N m^{-3} at the beginning of the year to 4.5 mmol N m^{-3} in April). As usual, increasing light and a shallower mixed layer triggered the initiation of the spring bloom, conditions than are achieved earlier (March) than in 1989. Both phytoplankton groups start developing at the same time in March, but although diatoms reach their maximum biomass (2.72 mmol N m^{-3}) in early April (Julian day 93), non diatoms bloom only account for 1.16 mmol N m^{-3}. By middle April, both blooms start declining as grazing pressure increases and nitrate and silicate are consumed, but due to the boost in nutrients (mixed layer phase1), diatom decline is much slower and the bloom extends for 30 more days until silicate has been depleted in the mixed layer. They bloom

ephemerally again in autumn (mid October) when silicate and nitrate concentrations increased in the mixed layer and light conditions were still favorable. A subsurface diatom maximum was also predicted in July, reaching 0.7 mmol N m^{-3} where there was plenty of ammonium and also silicate. Mesozooplankton dynamics followed closely those of diatoms, showing a time lag response of less than 10 days and reaching maximum biomass after each diatom bloom (0.5 mmol N m^{-3} in April, 0.26 mmol N m^{-3} in October in the mixed layer and 0.28 mmol N m^{-3}, in early August, below the mixed layer) and so does detrital silica, whose concentration rises and falls according to natural diatom mortality and mesozooplankton faecal pellets. Regarding non diatoms, the most intense bloom occurred in June after diatoms have completely declined, reaching 2.87 mmol N m^{-3}, considerably more biomass than in 1989, completely depleting nitrate in the mixed layer. Microzooplankton response to this bloom is observed four days later, reaching 0.5 mmol N m^{-3}. Both phytoplankton and zooplankton groups are responsible for ammonium and detrital nitrogen behaviour. The former was depleted in the mixed layer from late May to November but accumulated below, where it would support the subsurface diatom bloom. Detrital nitrogen showed two maxima, the first one (0.73 mmol N m^{-3}) mainly due to diatom mortality and mesozooplankton excretion, and the second one, also the most intense of the two (over 1 mmol N m^{-3}) accounting for non diatom mortality, microzooplankton and mesozooplankton excretion processes.

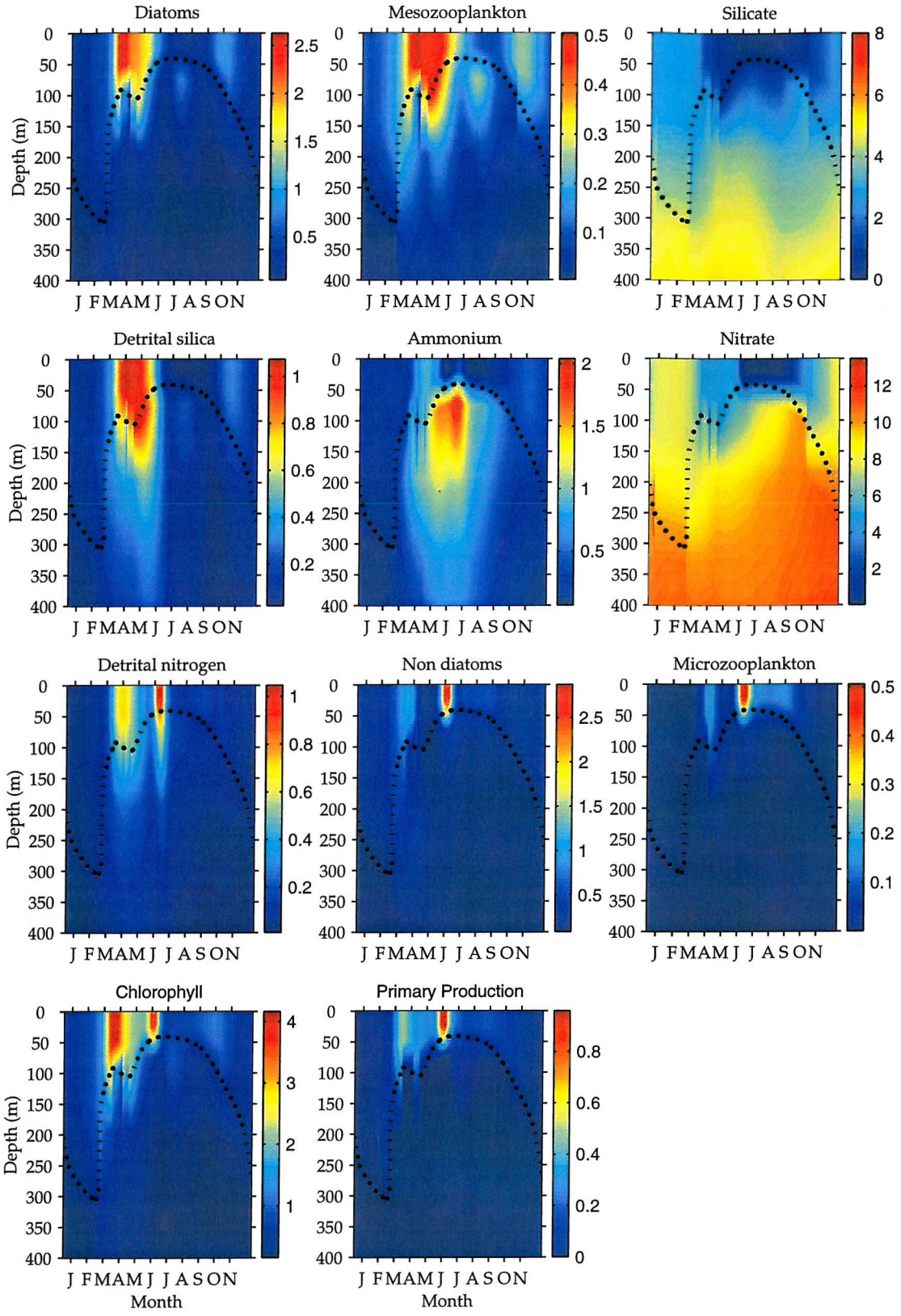

Figure 6.15: 1-D model state variables, chlorophyll and primary production for 1996 down to 400 m.

3.2 Primary production

As for 1989, primary production was also calculated (table 6.5). TPP was higher than in 1989 (3.19 mol N m^{-2} yr^{-1}), 42% of which was NP and 58% was RP. It seems that the larger food chain is dominating as diatoms account for 59% of TPP while only 41% is due to non diatoms (table 6.6). Diatoms also accounted for more of the total NP and RP (64% and 55%, respectively). The annual f *ratio* was 0.42 which indicates that the ecosystem is mainly supported by ammonium as figures on RP suggested, but surprisingly, the larger food chain prevailed in the ecosystem, therefore an exported production higher than 42% should be expected. Model estimates of the *e* ratio predicted an export production of 31.16% of the total PP (78.65 g C m^{-2} yr^{-1}) at a daily rate of 0.22 g C m^{-2} d^{-1}.

Mesozooplankton plays a more important grazing role in 1996 than it did in 1989, as one would expect, due to an increase in the diatom population compared to 1989. They consumed 50.87% of the total PP (*versus* 38.84% in 1989) and microzooplankton only grazed 25.38% of the phytoplankton population. The rest of the fluxes were very similar to those observed in 1989.

3.3 Fit to observations

Unfortunately, there were less observational data available for 1996 than there were for 1989 but agreement between model and real data and misfit can be seen in figure 6.9 and table 6.3, respectively. As in the 1989 case, most of the disagreement came from nitrate and silicate (55.81 and 24.28%, respectively) while the best fitted variables were ammonium, chlorophyll and PON in this order (1.11%, 2.34% and 16.43%, respectively). Qualitatively, the model successfully reproduced the trends observed in the field. Chlorophyll concentration during the three cruise batches were very similar for Julian days between 187 to 189 (maximum of 1.09 mg m^{-3} from the model *versus* 1.49 mg m^{-3}

from data), days 255 to 276 (maximum of 1.32 mg m^{-3} from the model *versus* 0.99 mg m^{-3} from data) and days 297 to 306 (maximum of 0.90 mg m^{-3} from the model *versus* 0.67 mg m^{-3} from data) although the model predicts an autumn bloom about 6 days earlier than observed. Nitrate and silicate model results agreed well for the upper 400 m and 600 m, nitrate being slightly underestimated between 400 and 800 m. In terms of ammonium, the real data showed a maximum of 0.8 mmol N m^{-3} at 400 m that the model reproduces at 200 m. For PON, the coupled model predicts concentrations of less than 1.5 mmol N m^{-3} which are in accordance with background PON measured, but fails to reproduce four maxima (up to 3 mmol N m^{-3}) observed in the real data set.

However, care must be taken when interpreting these model results for reasons than will become clear in chapter 7.

6.6 Summary of key points

- The 0-D ecological model was modified in order to include biogenic silica as well as nitrification processes due to their importance in the vertical gradients of nitrate and silicate.

- Differences between 0-D and 1-D model *standard runs* were observed in terms of mixed layer depth and seasonal cycles of the state variables. Gaspar's mixed layer scheme was consistent with observations available for the NABE area.

- The 1-D coupled model was tuned to the NABE89 data set and validated to the NABE96 data set.

- Model tuning needed a total of 5 parameters to be modified: detrital silica remineralisation rate, detrital nitrogen sinking rate, diatom maximum growth rate and slope of the P-I curve and also non-diatom slope of the P-I curve.

- Validation revealed the need of model re-tuning as nitrate concentration was unreasonably high for 1996. Detrital nitrogen remineralisation rate needed to be decreased.

- The coupled model showed a good agreement with the observational data and also matched well the bloom timing and intensity for 1989. It predicted a subsurface diatom maximum (reported in the literature) and also a non diatom subsurface maximum. The ecosystem primary production was dominated by small organisms.

- Model validation reproduced the trends observed in the NABE96 data set well. This time, the larger food chain dominated the ecosystem and therefore, the export production was higher in 1996 than in 1989.

Table 6.1: Model parameters used in the 1-D coupled model.

Parameter	Symbol	Group	Value	Units	Source
Nitrification	nr	N_r	0.03	d^{-1}	Martin *et al.*, 2001
Biogenic silica breakdown rate	δ_2	D_s	0.012	d^{-1}	Pondaven *et al.*, 1998
Biogenic silica sinking rate	V_s	D_s	5	m d^{-1}	Pondaven *et al.*, 1998

Table 6.2: Parameter changes amongst runs.

Parameter	1-D *standard run*	1-D tuned	1-D retuned
α_2	0.088	0.098	-
α_1	0.021	0.015	0.010
$Pmax_2$	2.841	2.541	-
V	6	10	-
δ_2	0.012	0.052	-
K_1	-	-	0.37175
K_2	-	-	0.18516

Table 6.3: Misfit between 1-D model state variables and NABE89 and NABE96 observations.
Data have been normalised by number of observations of each type.
Figures given in brackets represent percentages of the corresponding total misfit.

Model run	MISFIT					
1989	Chl	Nitrate	Silicate	Ammonium	PON	Total
1-D tuned	0.28 (5.21%)	2.64 (49.28%)	1.31 (24.42%)	0.45 (8.39%)	0.685 (12.77%)	5.365
1-D retuned	0.40 (5.51%)	3.90 (53.79%)	1.63 (22.48%)	0.48 (6.62%)	0.84 (11.59%)	7.25
1996	Chl	Nitrate	Silicate	Ammonium	PON	Total
1-D validation	0.16 (2.34%)	3.77 (55.81%)	1.64 (24.28%)	0.075 (1.11%)	1.11 (16.43%)	6.755

Table 6.4: Tests carried out for model re-tuning.

Test run	Parameters	
	nr	δ_1
Test1	0	*A priori*
Test2	0	0.07694
Test3	*A priori*	0.07694
Final	*A priori*	0.10694

Table 6.5: Annual total and size-fractionated primary, new and regenerated production in the mixed layer (units are mol N m^{-2} yr^{-1}).

TPP, TNP and TRP stand for total primary, new and regenerated production. Subindexes d and nd refer to diatoms and non diatoms, respectively. Figures in brackets refer to percentage of TPP.

Year	TPP	TNP	TRP	NP_d	NP_{nd}	RP_d	RP_{nd}	*f* ratio
1988	2.16	1.00 (46)	1.16 (54)	0.63	0.37	0.43	0.73	0.46
1989	1.95	1.06 (55)	0.88 (45)	0.60	0.46	0.26	0.63	0.55
1990	1.53	0.85 (56)	0.67 (44)	0.59	0.27	0.24	0.43	0.56
1991	1.72	0.90 (52)	0.82 (48)	0.59	0.31	0.28	0.54	0.52
1992	1.91	0.86 (45)	1.05 (55)	0.52	0.34	0.35	0.71	0.45
1993	2.16	0.96 (44)	1.20 (56)	0.62	0.33	0.51	0.69	0.44
1994	3.24	1.30 (40)	1.94 (60)	0.74	0.56	1.00	0.94	0.40
1995	2.58	1.24 (48)	1.34 (52)	0.83	0.41	0.62	0.72	0.48
1996	3.19	1.33 (42)	1.86 (58)	0.85	0.47	1.02	0.84	0.42
mean	2.27	1.06	1.21	0.66	0.39	0.52	0.69	0.48

Table 6.6: Annual total and size-fractionated primary, new and regenerated production in the mixed layer.

TPP, TNP and TRP stand for total primary, new and regenerated production. . Subindexes d and nd refer to diatoms and non diatoms, respectively.

Year	$\%TPP_d$	$\%TPP_{nd}$	$\% NP_d$	$\%NP_{nd}$	$\%RP_d$	$\%RP_{nd}$	$f\,ratio_d$	$f\,ratio_{nd}$
1988	0.49	0.51	0.63	0.37	0.37	0.63	0.60	0.34
1989	0.44	0.56	0.57	0.43	0.29	0.71	0.70	0.42
1990	0.54	0.46	0.69	0.31	0.36	0.64	0.71	0.38
1991	0.50	0.50	0.65	0.35	0.34	0.66	0.67	0.37
1992	0.46	0.54	0.61	0.39	0.33	0.67	0.60	0.32
1993	0.52	0.48	0.65	0.35	0.42	0.58	0.55	0.33
1994	0.54	0.46	0.57	0.43	0.51	0.49	0.43	0.37
1995	0.56	0.44	0.67	0.33	0.47	0.53	0.57	0.36
1996	0.59	0.41	0.64	0.36	0.55	0.45	0.46	0.36
mean	0.52	0.48	0.63	0.37	0.41	0.59	0.59	0.36

Table 6.7: Model output for 1989 *versus* field data.

* integrated over the euphotic zone
+ integrated over top 35 m
# depending on which algorithm is used to calculate photosynthesis (see text for details)
§ at 35 m
@ at 150 m

Property	0-D model	1-D model	Observational	Other models	Source
Annual PP ($g\ C\ m^{-2}\ yr^{-1}$)	56.20	154.20	35-60 120-160 150-225# and 200-270# 230-243 240 200-250	 122 108#	Berger (89) Antoine *et al.* (96) Behrenfeld and Falkowski (97) Sathyendranath *et al.* (95) Longhurst *et al.* (95) Field *et al.* (98) Fasham and Evans (95) Oschlies *et al.* (2000)
Annual NP* ($g\ C\ m^{-2}\ yr^{-1}$)	23.76	83.90		65	Fasham and Evans (95)
Average PP+ ($mmol\ N\ m^{-3}\ d^{-1}$)	0.41	0.39	0.37 (Julian days 114 - 152)		Martin *et al.* (93)
Daily PP* ($g\ C\ m^{-2}\ d^{-1}$)	0.10-0.86	0.08-0.62	0.24-0.64 (12 May-8 July)		Joint *et al.* (93)
	0.30	0.62	0.43 (12 June-13July; peak)		Weeks *et al.* (93)
	0.44-0.92	0.64-1.48	0.60-1.80 (24 April-31 May)		Lochte *et al.* (93)
	0.72-0.92	0.43-1.48	0.54-1.20 (24 April-10 May)		Chipman *et al.* (93)
f ratio	0.44 (annual)	0.55 (annual)		0.53	Fasham and Evans (95)
Integrated chl* ($mg\ m^{-2}$)	35.60-41.22	62.42-72.15	25.4-52.0 (12 May-18 May)		Joint *et al.* (93)
	10.38	10.36-9.97	22.8-34.6 (2 July-6 July)		Joint *et al.* (93)
	20.83	32.59	30 (12 June-13July; peak)		Weeks *et al.* (93)
	22.8-60.11	62.42-229	30-175 (24 April-31 May)		Lochte *et al.* (93)
Maximum chl* ($mg\ m^{-3}$)	2.69	3.55	>2.5 (spring bloom; surface)		Lochte *et al.* (93)
	1.8	3.55	4.2 (14th May; subsurface)		Joint *et al.* (93)
Integrated zooplankton* ($mmol\ N\ m^{-2}$)	21.03-33.35	31.32-33.32	5-12 (Julian days 115-121)		Marra and Ho (93)
	39.35	50		60-80	Oschlies *et al.* (2000)
Microzoop. standing stock ($mg\ C\ m^{-2}$)	307.39	349.67	303 (17 June-8 July)		Burkill *et al.* (93)
Maximum microzoop.* ($\mu g\ C\ l^{-1}$)	14.85	10.9	13 (17 June-8 July)		Burkill *et al.* (93)
Microzoop. Biomass ($mg\ C\ m^{-3}$)	5.6-22.46	2.2-16.79	6-14 (Julian days 130-210)	4-10	Taylor *et al.* (93)
Microzoop. Grazing* (% daily PP)	16.9	38.77	<64 (24 April-9 May)		Boyd and Newton (95)
	17.4	8.74	6.1 (7 May-21 May)		Lentz *et al.* (93)
	27.9	47.92	<64 (18 May-29 May)		Verity *et al.* (93)
	10.3	94.4	39-100 (17 June-8 July)		Burkill *et al.* (93)
Mesozoop. Grazing* (% daily PP)	8.4	65.44	0.6-5.2 (25 April- 7 May)		Dam *et al.* (93)
	8.5	63.68	45.43 (7 May-21 May)		Lentz *et al.* (93)
	2	18.92	<6 (18 May- 31 May)		Dam *et al.* (93)
	2.4	19.90	<5 (18 May-29 May)		Verity *et al.* (93)
	0	5.6	1-2 (17 June-8 July)		Burkill *et al.* (93)
	0	4.3	<2 (1 July-5 July)		Morales *et al.* (91)
	0.1	5.9	<2 (12 June-13 July; peak)		Weeks *et al.* (93)
Mesozoop. Biomass ($mg\ C\ m^{-3}$)	13.12-37.10	12.64-25.14	5.5-25.3 (25 April-31 May)		Dam *et al.* (93)
Export flux (% PP)	N/A	42.78	45§ (25 April-31 May)	20-42	Martin *et al.* (93) Buesseler *et al.* (92)
		27	11.4@ (25 April-31 May)		Martin *et al.* (93)

Chapter 7:

Interannual Variability

Chapter 7: Interannual variability

7.1 Introduction

This chapter describes the intra and interannual variability of the one dimensional ecological model associated to the changing environmental conditions, especially mixed layer depth, derived from the physical forcing. Originally, the aim of this chapter was to investigate the interannual variability of a nine-year period, starting in 1988 and ending in 1996. This period was chosen based exclusively on data availability as a wide range of biogeochemical data were available for 1989 (provided by NABE cruises), and used for model tuning, whereas model validation was tested again BIOTRANS data (German JGOFS) during 1996. As model results strongly depend on previous winter conditions, the model was run starting in 1988 and run forward until 1996, being physically forced by NCEP model data (described in section 7.2).

Model results showed the build-up of nutrients in the ecosystem (mainly nitrate but also silicate) at the end of the time-series modelled (1995 and 1996). Further investigation of such feature led to the conclusion of a numerical problem as result of strong non-linearity of the biological model and limitations of the isopycnal formulation in the 1-D version of MICOM used in this work. A detailed description is presented in section 7.3.

Section 7.4 describes the biological variability predicted by the model in the upper mixed layer from 1988 to 1993, the period chosen to avoid the effects of the numerical problem. Finally, section 7.5 describes the ecological variability observed below the mixed layer, especially regarding the much debated subsurface chlorophyll maximum, and looks at the mechanisms that trigger such maxima in the 1-D model.

At the end of the chapter, a summary of the key points found is also presented.

7.2 Physical variability

Interannual variability of all forcing physical fields for the period of interest (1988-1996) is shown in figure 7.1 as well as surface water temperature, air temperature, salinity flux and mixed layer depth (figure 7.2). All the fields come from the NCEP meteorological re-analysis for the period 1989-1996 (Kalnay *et al.*, 1996). Monthly NCEP data for the nine year period of interest were used to force the 1-D model where they are interpolated to the simulation's timestep. For the whole nine-year period, model fluxes annual means (corresponding to thermal energy, buoyancy, evaporation minus precipitation and salinity) are zero. The strong interannual variability in all fields is evident and this fact will determine annual differences in the onset of the stratification of the water column, and also in the mixed layer depth, therefore setting the hydrographic conditions for the initiation of the spring bloom. The general behaviour observed consisted in high winds and strong negative thermal fluxes during the winter months, which set up a typical scenario of deep winter convective mixing ending up in winter mixed layer depths reaching up to 400 m during March at 47°N and 27°W (Robinson *et al.*, 1979), and between 235 and 367 m according to our model (for the 1988-1996 period). In spring, increasing solar heating and low winds allow for an increase in the vertical stability of the water column (buoyancy) that raised the modelled mixed layer to its shallowest (between 29 m and 57 m), allowing phytoplankton to grow rapidly until nutrient depletion and/or grazing prevent further accumulation. Thermal energy fluxes in the model varied between a minimum of –178 W m^{-2} in 1996 and a maximum of 156 W m^{-2} in 1993, wind speeds varied between 5.62 m s^{-1} in 1989 to 17.39 m s^{-1} in 1990 and modelled minimum and maximum sea surface temperatures between 11.48°C in 1991 and 20.88°C in 1989. Deepest winter and summer mixed layers (367 m and 57 m, respectively) occurred in 1994 coinciding with the highest summer wind speeds and temperatures (figure 7.2).

Shallowest winter and summer mixed layer depths were observed in 1992 (235 m) and 1989 (29 m); the former coincided with the lowest winter wind speeds (12.84 m s^{-1}) while the latter was associated to the lowest wind speeds for the nine-year period (5.62 m s^{-1}), the highest surface temperatures (20.88 °C) and also strong heating (154 W m^{-2}). Wind speed during the period of study showed great variability.

The physics may not be optimal but the aim of this project was the biological part of the coupled system so we did not attempt any optimisation of the physical system.

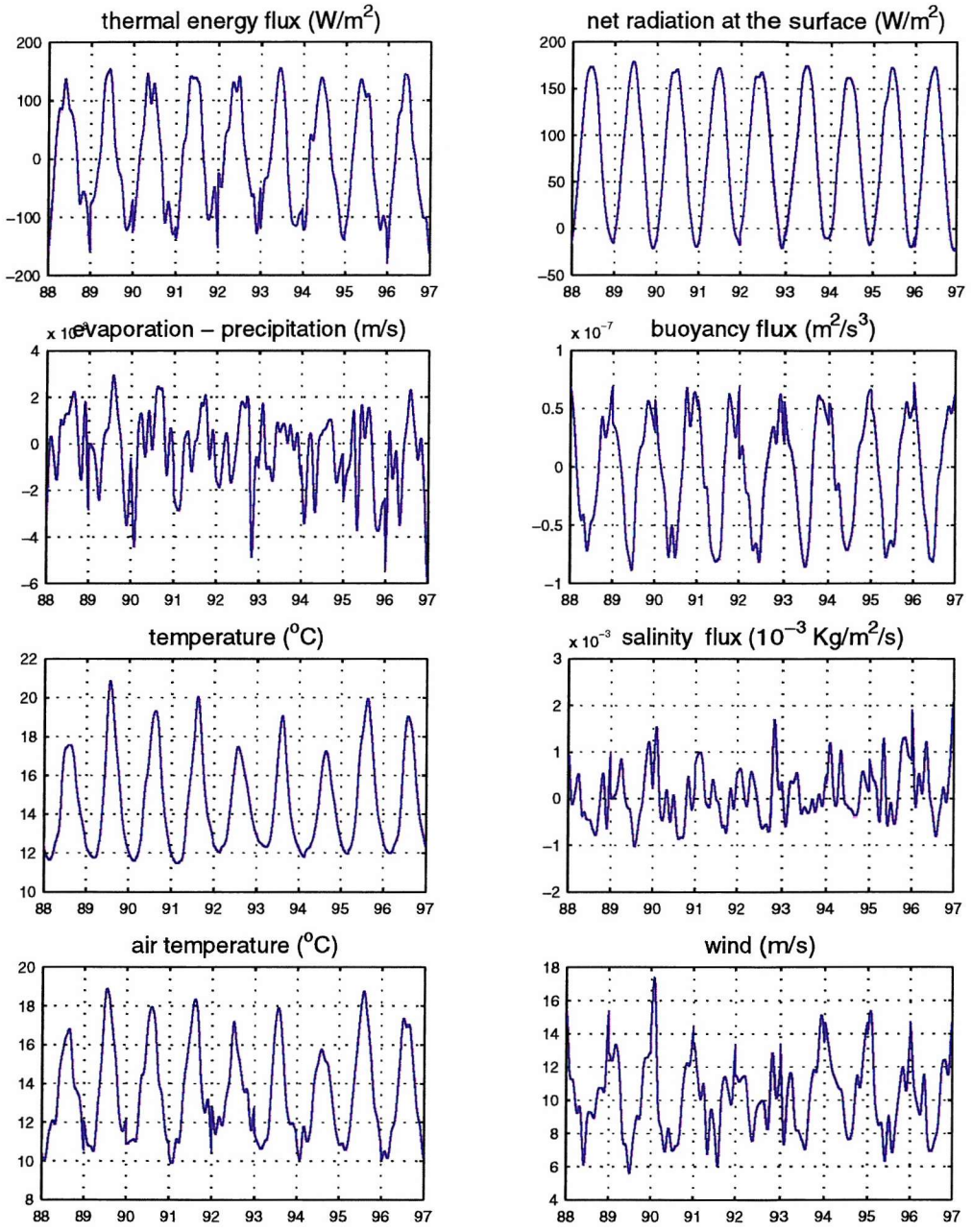

Figure 7.1: Annual physical fluxes forcing the 1-D model.

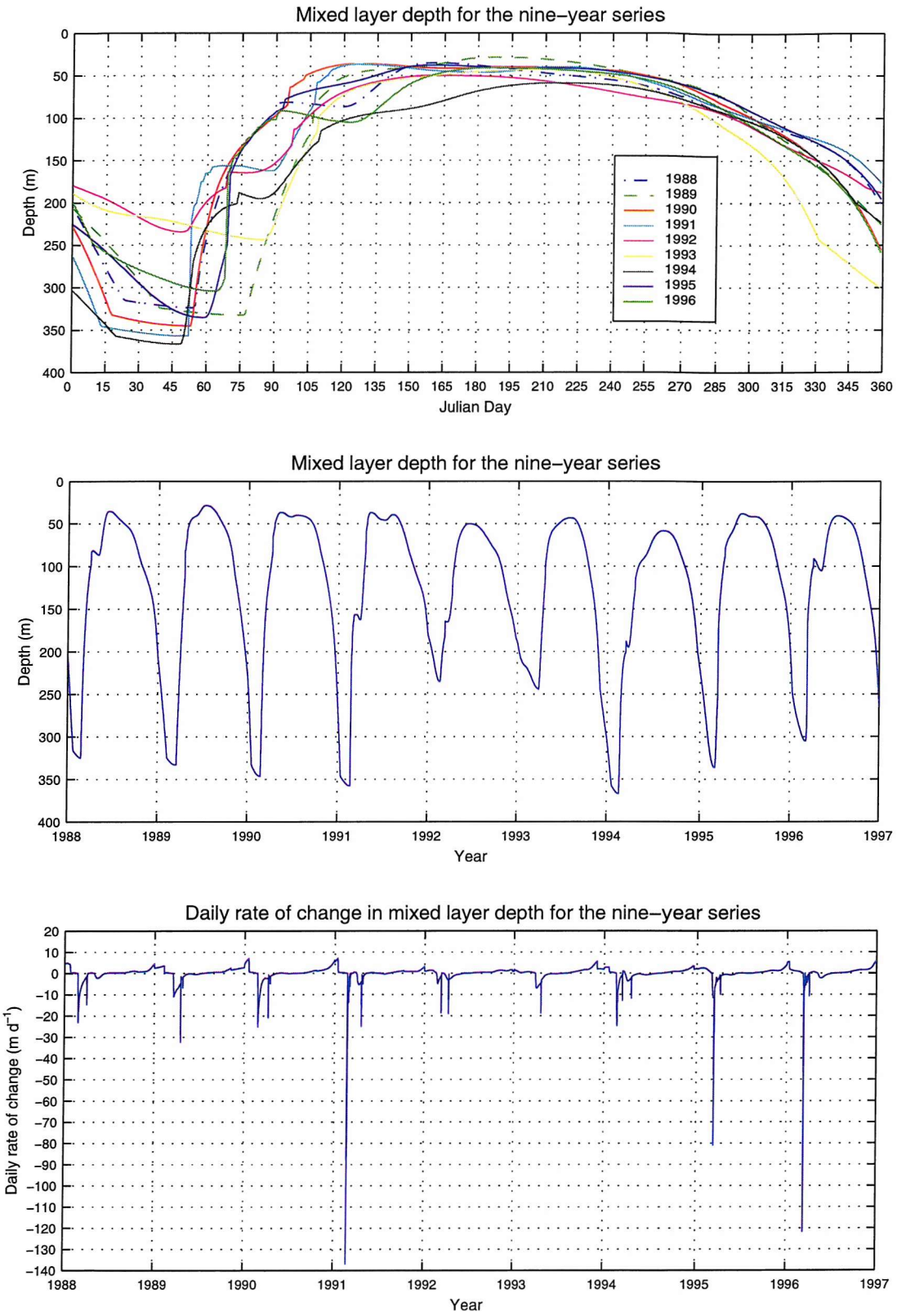

Figure 7.2: Top: Superimposed mixed layer depths corresponding to the nine-year period of study (1988 to 1996);
Middle: mixed layer variability from 1988 to 1996;
Bottom: daily rate of change in mixed layer depth as an indication of mixing. Negative values indicate shallowing while positive values reflect deepening of the mixed layer.

7.3 The coupled model assumptions

Several points need to be considered before entering into the discussion of the model results regarding interannual variability. First, the quadratic mortality term in equations 2.16 and 2.18 (chapter 2) is a closure term representing mortality due to higher predators. In the 0-D model it was considered as an "immediate export" term, therefore instantaneously leaving the mixed layer without being subjected to remineralisation. In the 1-D model, it is assumed that its sinking velocity is such that is instantaneously exported at depths greater than 1000 m (the bottom of our modelled ocean) as in previous studies (Martin, 1999; Waniek, 2002).

Second, and more important, no vertical relaxation of dissolved nitrate or silicate was used. Relaxation is a numerical technique widely used in general circulation models (see Killworth, 1999; Killworth *et al.*, 2000). It consists in the adjustment of the model results (for instance nitrate and silicate) by a term proportional to the difference between the model output and field observations, such as:

$$\frac{dN}{dt} = \lambda(N_o - N_M) + biological\,processes \qquad [7.1]$$

where N is the any model state variable (for instance, nitrate), λ is the relaxation coefficient, N_o is the observed nitrate to which we are relaxing and N_M is the model predicted nitrate concentration. The choice of λ will depend on how fast or slow we want the model solution to converge towards the observations. The choice of N_o could vary from climatology (Levitus) to observations corresponding to a particular year or even mean profiles obtained by a combination of observations from several years.

Relaxation is a key point that must be taken into account when interpreting the ecological processes occurring in the vertical domain of the model, which is often omitted in the

literature. Recent 1-D model studies have applied relaxation techniques in different modelling scenarios. Martin (1999) coupled a complex biological model (phytoplankton, zooplankton, bacteria, nitrate, ammonium, dissolved organic matter and detritus) to the same 1-D MICOM model used in this study, also applied to the North Atlantic. He prescribed the annual mixed layer depth and relaxed the vertical profile of nitrate to Levitus data but did not attempt to investigate interannual variability. Waniek (2002) investigated interannual variability in the North Atlantic by using a simple NPZD model, physically forced by ECMWF model data with mixed layer depths obtained *via* a Kraus-Turner scheme. In this case, it is not clear how to perform the vertical relaxation of nitrate, as observational data were only available for 2 years (1989 and 1996) out of the nine-year series modelled (from 1989 to 1997). Waniek (personal communication) chose to calculate a mean vertical nitrate profile (based on 1989 and 1996 nitrate observations) to which the vertical modelled nitrate was relaxed (although this fact was not mentioned in the paper). The reason for such a relaxation scheme was the consistent build up of nitrate from early years, which constrained any possibility of achieving a repeatable cycle (Waniek, personal communication).

However, the use of relaxation techniques imposes huge limitations worth considering and questioning. On the one hand, it could hide inconsistencies (numerical or otherwise) within the model formulation, creating what could be a false sense of confidence in model results, especially when repeatability of the biological cycle is unachievable otherwise. On the other hand, calculation of any kind of fluxes among and within biological compartments is impossible to perform in a realistic way, as model results would be biased towards the relaxation scheme, preventing the model from showing any "unusual" behaviour and making model interpretation a difficult task.

Third, the coupled model in this study was spun up for 22 years with repeated annual forcing (see chapter 5) as this is needed for the physical model to reach equilibrium. As a biological repeatable cycle is achieved in only eight years (without the need of vertical nutrient relaxation being obvious), all the biology was switched off for the first 14 years of spin up, and the physical model was independently run. The biological model was turned back on for the last eight years of spin up. For the whole 22-year model spin up, the coupled model was physically forced by NCEP data corresponding to 1988.

7.4 Problems highlighted by the interannual variability studies

Vertical interannual variability of all the state variables, chlorophyll and primary production and their variability in the top 400 m of the water column is shown in figure 7.3. This plot reveals a clear increase in nitrate and silicate subsurface concentrations from 1994 onwards.

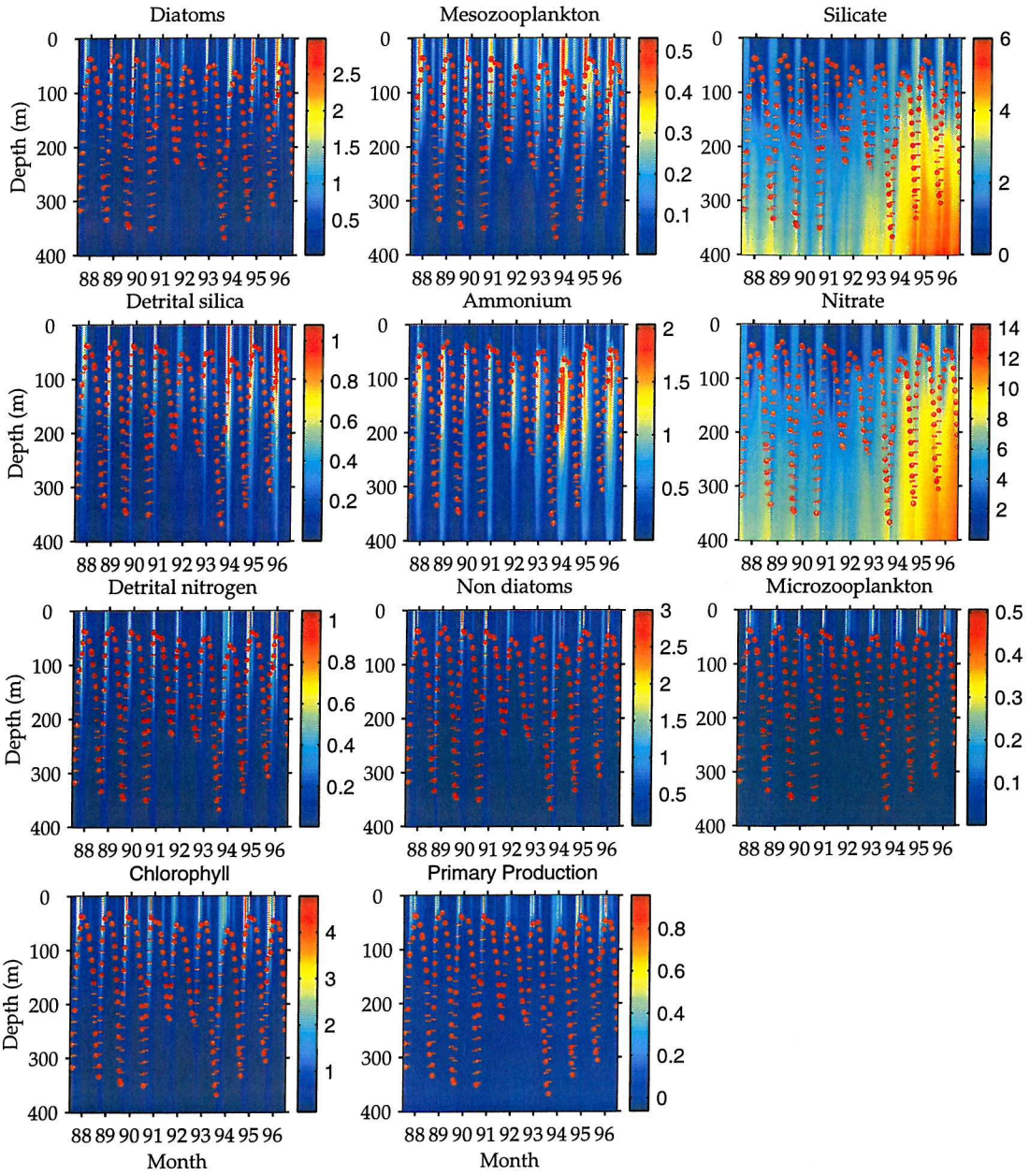

Figure 7.3: Interannual vertical variability of the model state variables (mmol N m^{-3}) as well as total chlorophyll (mg chl m^{-3}) and primary production (mmol N m^{-3} d^{-1}) in the upper 400 m from 1988 to 1996. The dotted red line represents mixed layer depth.

Initially, it was thought that biological processes could have been responsible as nitrification and detrital silica remineralisation below the mixed layer also increased significantly from 1994 to 1996 due to higher primary production. However, such regeneration processes could only account for the small increase observed in nitrate and silicate during 1994 and not for the concentrations observed in subsequent years.

In order to pin down what was causing such a significant increase in the nitrate and silicate pools, total (dissolved and particulate) nitrogen and silicate were calculated for the full nine-year period (figure 7.4). This figure supports our previous argument against nitrification processes, as the build up starts at 750 m, where no significant biological activity takes place.

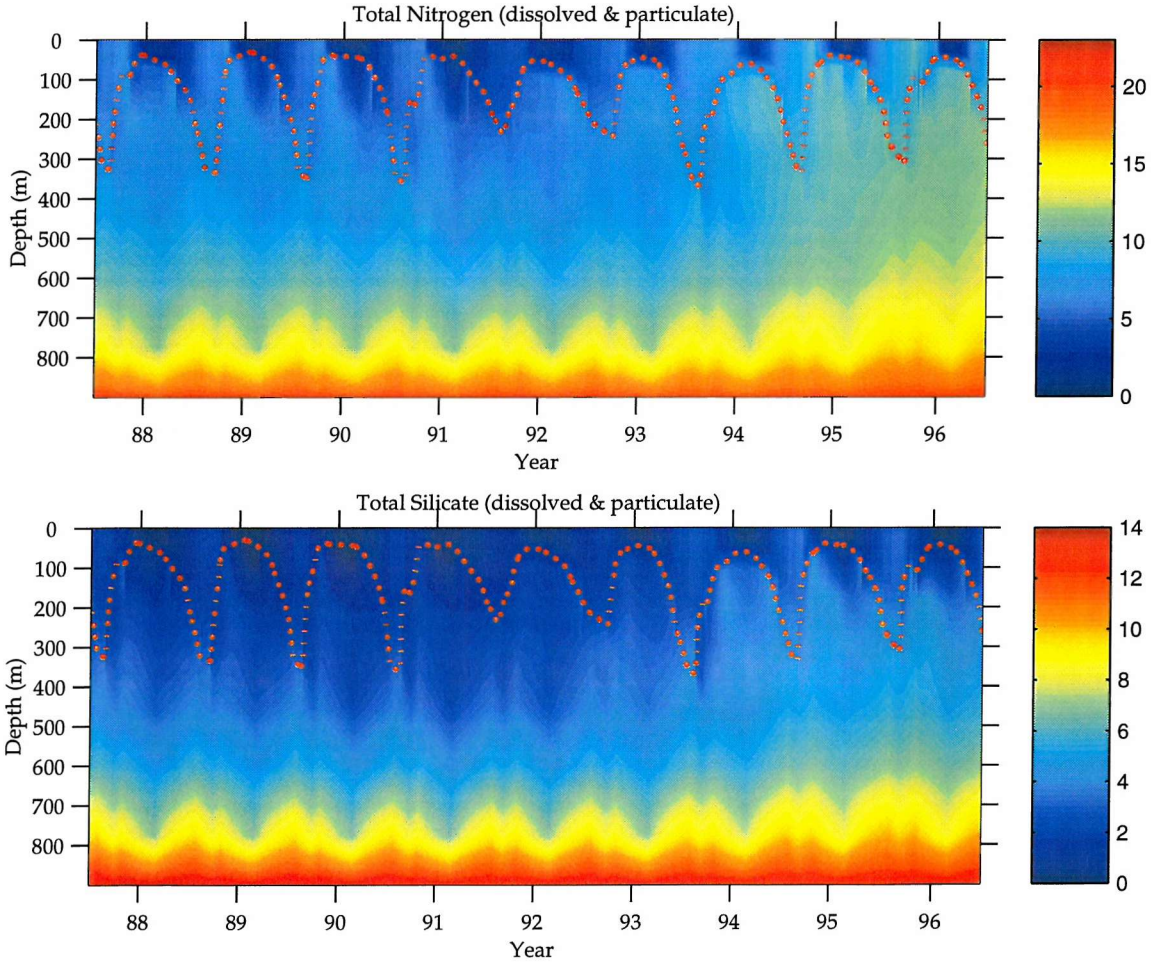

Figure 7.4: Total (dissolved and particulate) nitrogen and silicate down to 900 m from 1988 to 1996. The dotted red line represents mixed layer depth.

Other alternatives led us to consider physical processes such as an increase in the cross-isopycnal diffusion, and/or a faulty redistribution of tracers (state variables) associated to model layer-thickness variability or a numerical problem due to the interaction and high complexity of the ecosystem and physical models. To test these hypothesis different experiments were performed. Firstly, the sinking speed of both detrital compartments was set to twice as much as in the 1-D standard run, as this is regarded as an uncertain ecological parameter. This high sinking rate would remove nitrogen and silicate at a faster rate, therefore increasing the difference between nutrients in the upper layers and at the bottom of the modelled ocean, leading to higher diffusion rates (as diffusion is calculated as a second derivative, the curvature of the total nitrogen function would tend to increase). However, results showed that cross-isopycnal diffusion was not significant.

The next step was to run the coupled model for an extra 9 years (a total of 40 years) using "loop" forcing and the same detrital sinking rates as in the 1-D standard run in order to investigate whether or not the coupled model was able to return to its previous state, before any nutrient build up started. In other words, the model was spun up for 22 years using NCEP data corresponding to 1988. Thereafter, the coupled model was run for a further 18 years with cyclic physical forcing (the 23rd model year forced by 1988 NCEP data, the 24th model year forced by 1989 NCEP data and so on, until model year 31st which was forced by 1996 data. After this point, model year 32nd was forced by 1988 NCEP data, model year 33rd by 1989 NCEP data and so on until reaching model year 40th, which was forced by 1996 NCEP data). Model results shown that the coupled model switches into a different state, in which a positive feedback mechanism is activated causing the blow up of the coupled model (see figure 7.5), which strongly suggests the existence of a numerical problem. However, as this discovery was made at the very last stage of this work and due to high complexity of the coupled model, no time was available

to solve this problem and further research in the field of the coupled model numerics is suggested for the future. Relaxation may be a way to solve this problem, however for the reasons stated earlier we decided not to use it in this work. For this reason, interpretation of model results will only be given for the six-year period between 1988 and 1993, prior to the impact of the numerical problem on the results.

These results also illustrate the point made earlier regarding vertical relaxation. If such technique had been used in the present model, numerical instabilities would have never been found. It is also interesting to stress that those instabilities would not have been detected either if no interannual variability studies had been attempted, as when the model was forced with the same NCEP data (regarding the chosen year) a repeatable cycle was always obtained.

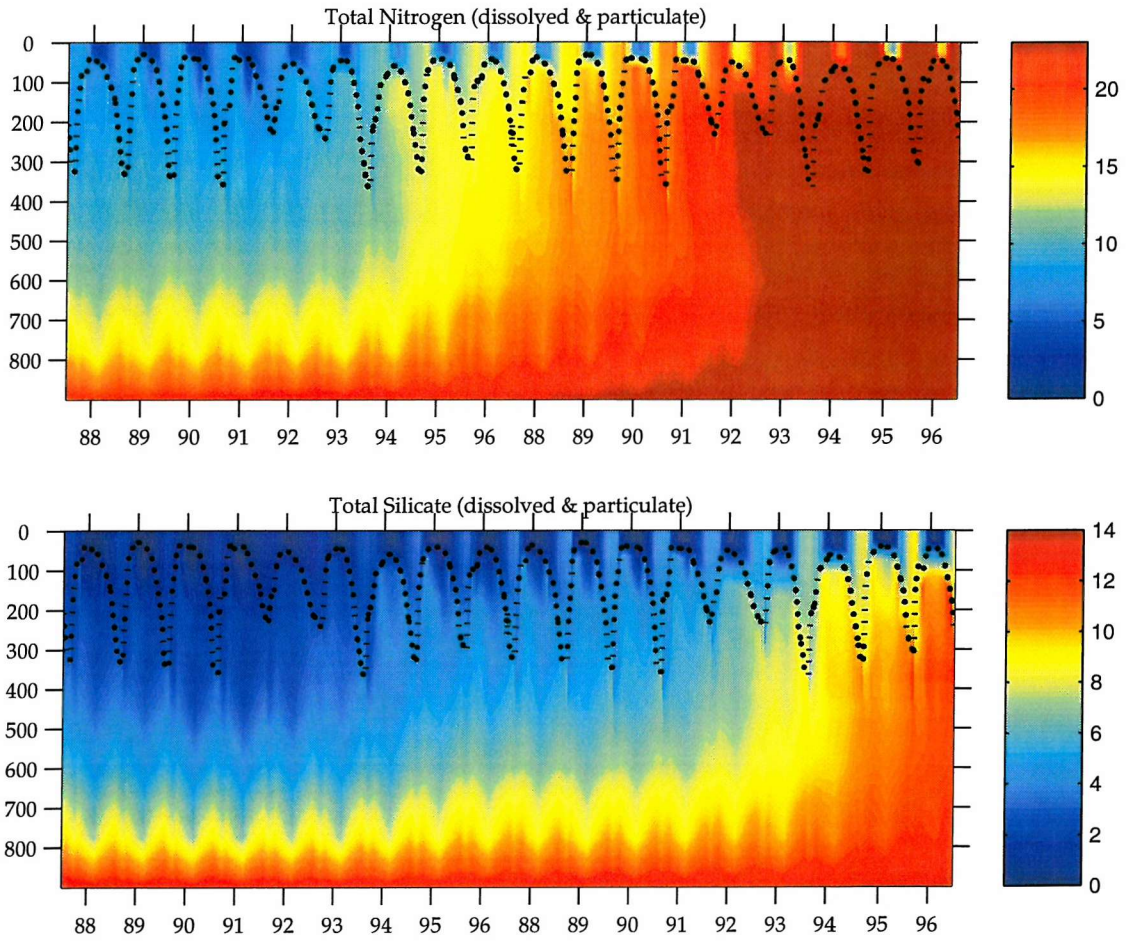

Figure 7.5: Total (dissolved and particulate) nitrogen and silicate down to 900 m. The model was run for 40 years using cyclic forcing for the last 18 years (see text for details). The x axis represents the physical forcing used. The dotted black line represents mixed layer depth.

7.5 Biogeochemical variability in the mixed layer (1988 - 1993)

Initiation of the spring and autumn blooms

The initiation of the phytoplankton spring bloom, and also bloom intensity and duration, widely varied from one year to the next, depending on the physical variables that determine the onset of stratification and therefore, stabilisation of the mixed layer depth. Figure 7.6 shows the evolution of diatoms and non-diatoms according to changing mixed layer depth. Years with similar stratification regimes have been plotted together. By stratification regime we mean "fast" and "slow" stratification. The former was defined in this work as the one with a rate of change in the mixed layer greater than 20 m d^{-1}, while a smaller change was considered as slow stratification (figure 7.2 bottom). When stratification is fast (years 1988, 1990 and 1991) phytoplankton start to develop in late winter (February), blooming earlier in the year. On the other hand, when stratification occurs at a slower pace (in 1989, 1992 and 1993), phytoplankton start their development in spring (March/April), typically blooming in May (diatoms) or June (non-diatoms).

Mixing events (interruptions in the development of the mixed layer) were simulated in 1988, 1991 and 1992. This occurrence, due to enhanced mixing, is associated with the early development of a diatom bloom in all cases. The earlier in the year the mixing event took place, the less intense the diatom bloom, clearly related to light limitation (figure 7.6).

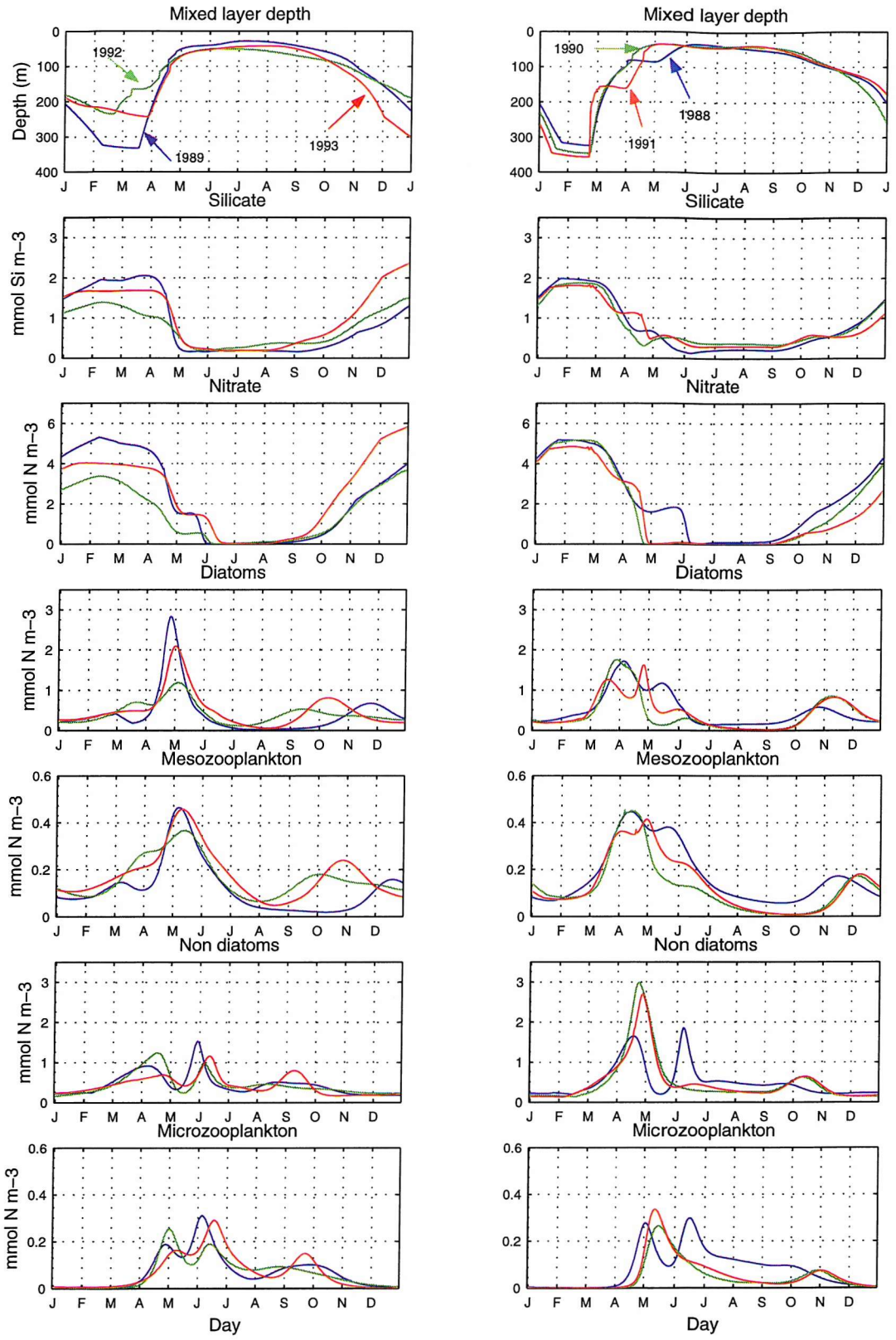

Figure 7.6: Year to year variability of modelled phytoplankton, zooplankton and nutrients in the mixed layer, from 1988 to 1993, in mmol N m^{-3}.

The deepest winter mixed layer depths were simulated in 1990 and 1991, preventing diatoms from developing early in the year due to light limitation. However, non-diatom peak biomass was the highest (> 2.5 mmol N m^{-3}) of the six-year period, coinciding with their highest nitrogen uptake rates whereas diatoms had the lowest silicate uptake rates and were also intensely grazed by mesozooplankton.

The build up of these series of phytoplankton biomass maxima is particularly important for mesozooplankton, as when late phytoplankton blooms occur (in summer or late autumn), zooplankton can continue growing and bloom, therefore being better prepared for overwintering (Radach *et al.*, 1998) as can be seen in figure 7.7

Non-diatom autumn blooms take place earlier than in the diatom case for light limitation reasons, as due to parameter choice the former are less efficient than the latter in poor light conditions. The diatom autumn bloom was triggered either in July (in 1992), August (in 1989) or early September (in 1988, 1990, 1991, 1993), due to the deepening of the mixed layer and entrainment of nutrients. The deeper the summer mixed layer, the earlier the autumn bloom was observed. Non-diatoms followed the same trend although bloom earlier than diatoms due to light limitations.

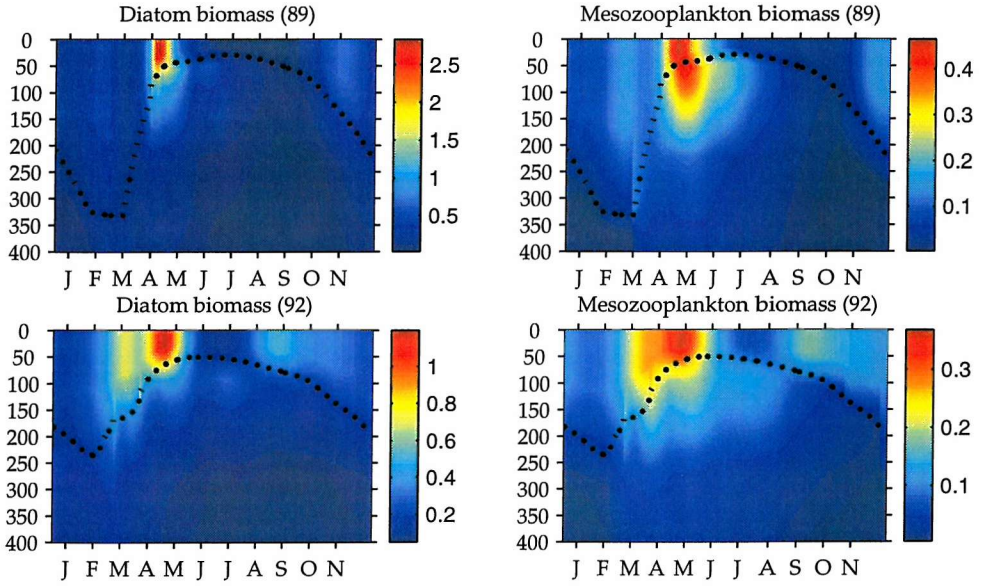

Figure 7.7: Diatoms and mesozooplankton biomass in 1989 and 1992.

State variables

Maximum peak diatom biomass, in the mixed layer, varied from 1.19 mmol N m^{-3} in 1992 to 2.83 mmol N m^{-3} in 1989 while non-diatoms ranged from 1.16 mmol N m^{-3} in 1993 to 3.00 mmol N m^{-3} in 1990 (figure 7.8). Surprisingly, diatoms accounted for a small majority of the annual primary production in 1990 (54%; see table 7.1) even when their peak biomass for that year was only 1.76 mmol N m^{-3}. This is related to their nutrient uptake and mortality rates as well as zooplankton grazing pressure (figure 7.9). Although non-diatom peak nitrogen uptake is about twice as much as diatoms, the latter uptake nitrate and ammonium for longer time. The annual nitrogen uptake rate was 0.83 for diatoms *versus* 0.70 mol N m^{-2} yr^{-1} for non diatoms in the mixed layer, leading to slightly higher PP (54% versus 46%). On the other hand, microzooplankton grazing pressure on non-diatoms is slightly higher than that of mesozooplankton on diatoms, but non-diatom natural mortality is 5 times higher than its phytoplankton counterpart.

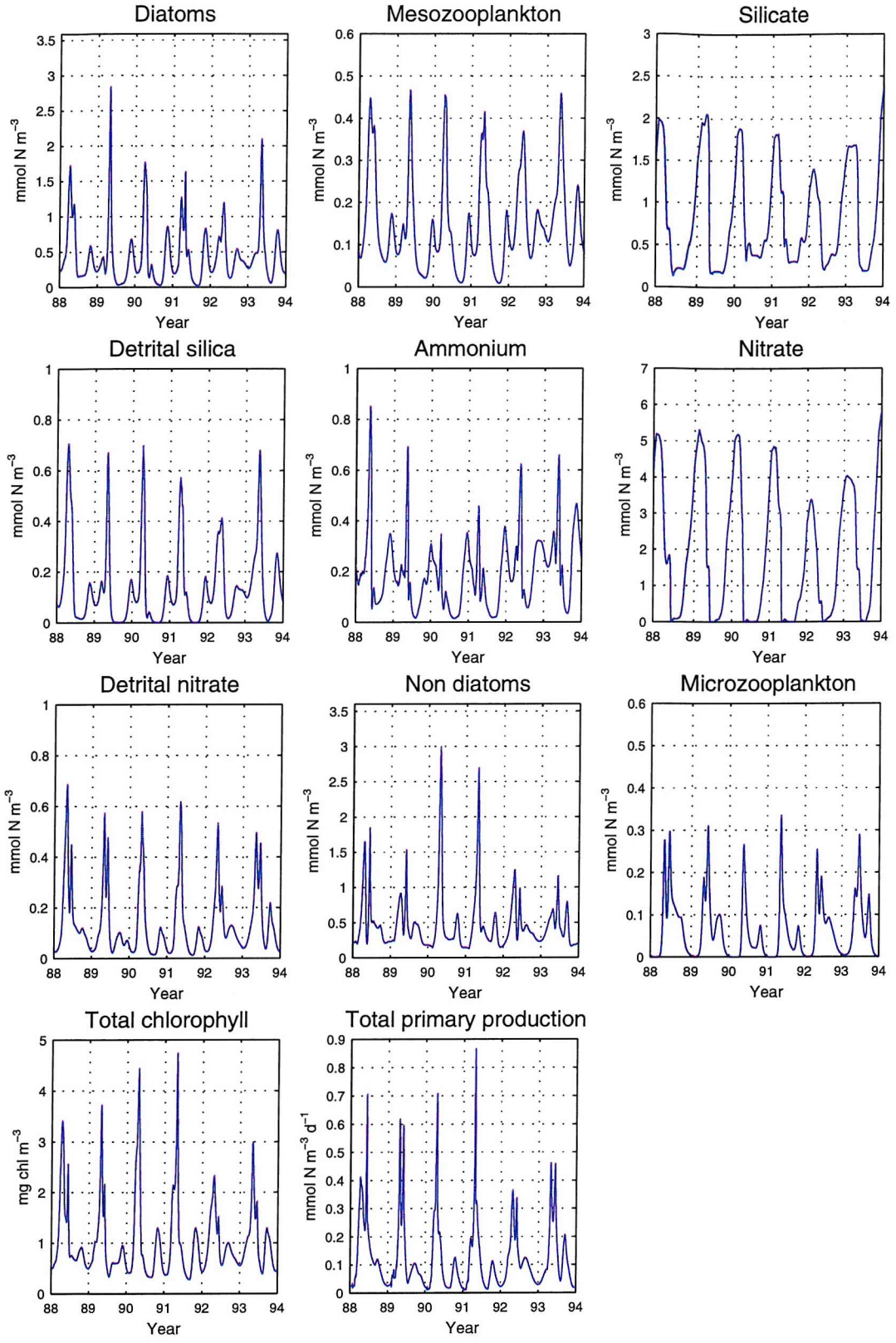

Figure 7.8: Interannual variability of the model state variables (mmol N m^{-3}) as well as total chlorophyll (mg m^{-3}) and primary production (mmol N m^{-3} d^{-1}) in the mixed layer from 1988 to 1993.

In terms of zooplankton, both groups followed the same trend shown by the phytoplankton group they feed on, microzooplankton showing a longer time lag between their maximum and the non-diatom peak (up to a maximum of 25 days) than mesozooplankton (maximum 17 days lag) with respect to the diatom maximum (figure 7.6). A minimum time lag (between phytoplankton and zooplankton peaks) of four days was exhibited by mesozooplankton (in 1991) and microzooplankton (in 1993), usually after an earlier increase in their biomass has been triggered by moderate phytoplankton blooms, therefore allowing for a quicker response to further phytoplankton growth. Maximum and minimum mesozooplankton biomass were predicted in 1989 and 1992, ranging from 0.48 mmol N m^{-3} to 0.36 mmol N m^{-3}, respectively, while microzooplankton minimum was also observed in 1992 (0.25 mmol N m^{-3}) and their maximum in 1991 (0.34 mmol N m^{-3}), coinciding with maxima and minima of the phytoplankton groups they feed on.

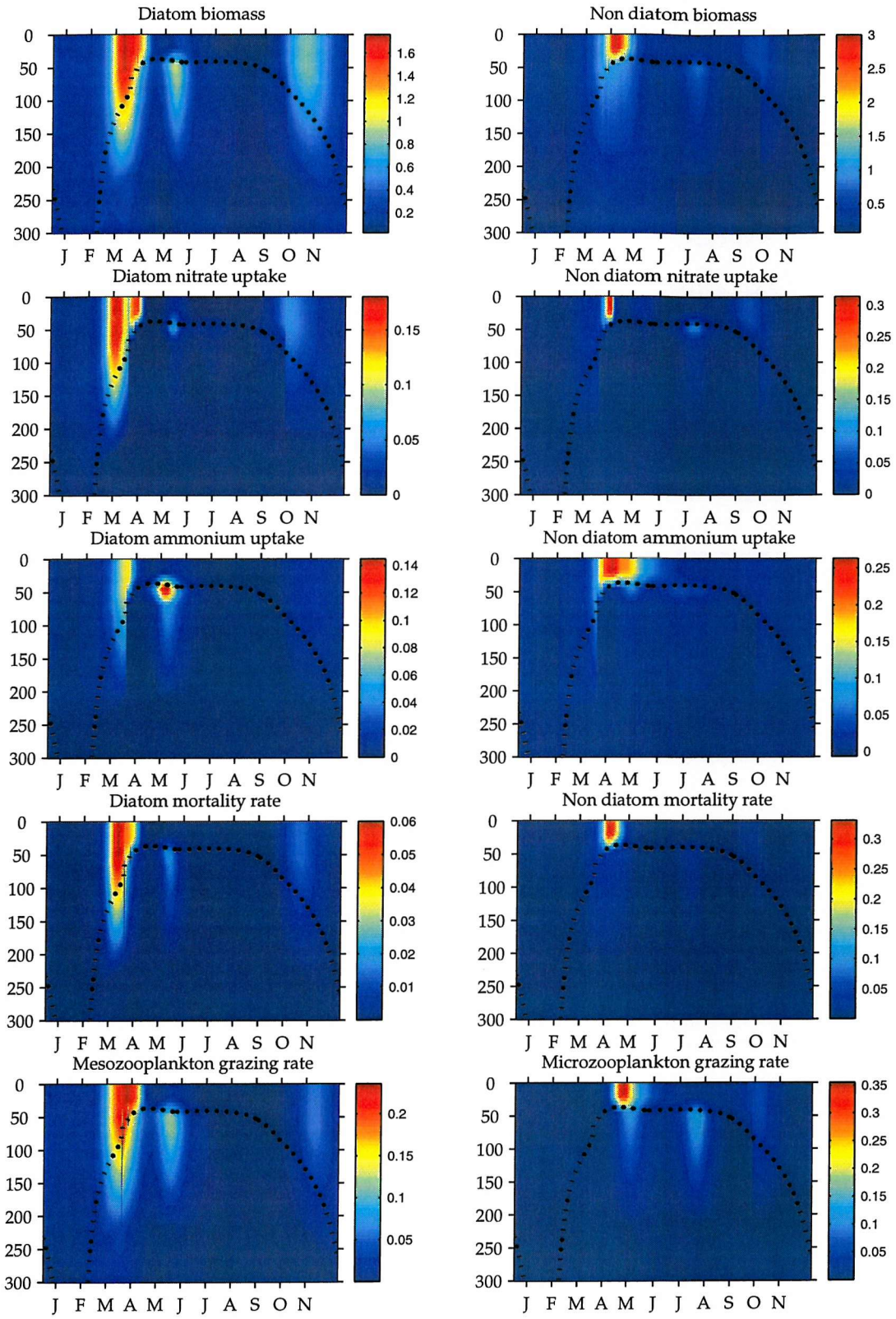

Figure 7.9: Phytoplankton biomass, nitrogen uptake and mortality rates as well as zooplankton grazing rates during 1990. Biomass units are mmol N m^{-3} while rates are mmol N m^{-3} d^{-1}. The dotted line represents mixed layer depth.

Annual variability in both biogenic detrital compartments (silica and nitrogen) and ammonium follows the seasonality observed in the phytoplankton and zooplankton pools. A common feature for the six-year period studied is ammonium exhaustion in the mixed layer but accumulation below it, being exclusively of biogenic origin (figure 7.10). By contrast, nitrate and silicate concentrations are renewed due to diffusion processes as well as ecological processes such as detrital silica and nitrogen remineralisation and nitrification. Remineralisation and mesozooplankton excretion always accounted for at least 83% of the total ammonium fluxes, therefore excretion due to microzooplankton is only responsible for the smallest fraction ($\leq$17%). Mixed layer maximum and minimum ammonium concentrations varied from 0.85 mmol N m^{-3} in 1988 to 0.35 mmol N m^{-3} in 1990. In contrast, detrital nitrogen and silica maxima are observed in the surface layers ranging from 0.69 mmol N m^{-3} in 1988 to 0.50 mmol N m^{-3} in 1993, and from 0.70 to 0.41 mmol Si m^{-3} in 1988 and 1992, respectively. Both detrital compartments sink to the bottom of the ocean and generate a significant signature that can be followed down to 600 m, therefore affecting the seasonal cycle of deep nitrate and silicate via remineralisation processes. Zooplankton senescence (natural mortality) was the major contributor to detrital nitrogen (between 60% and 76%), while phytoplankton mortality only accounted for a maximum of 39.5% of the total budget. In terms of detrital silica, the same tendency was observed as mesozooplankton egestion accounted for more than 85% of the pool of biogenic silica *versus* a maximum of 15% due to diatom mortality.

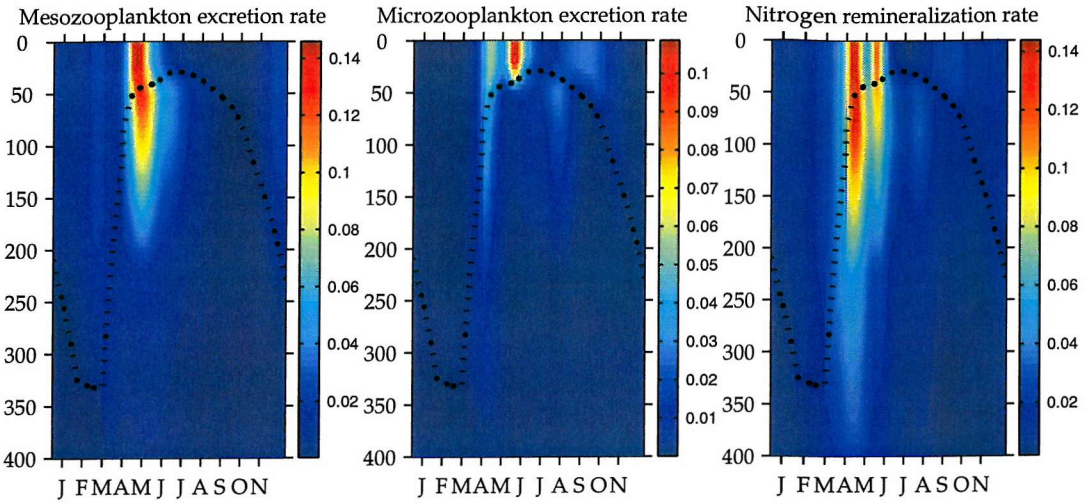

Figure 7.10: Sources of ammonium in the water column. Units are mmol N m^{-3} d^{-1}. The year shown is 1989.

Primary production and *f* ratio

The interannual variability in total primary production (TPP) is shown in figures 7.3 and 7.8. The minimum peak value was obtained in 1992, when the lowest nitrate and silicate winter concentrations were generated as winter mixed layer depths were the shallowest simulated for the six-year period (figure 7.2b). The maximum peak TPP was obtained in 1991 although nutrient concentrations were similar to other years (apart from 1992; see figure 7.6). However, the mixed layer depth was very distinctive as stratification slowed in early spring and summer (figure 7.2b). The first time occurred in early March establishing a mixed layer depth of 156 m by Julian day 83, which allows diatoms to bloom (reaching 1.25 mmol N m^{-3}) as nutrients are abundant and diatoms are better suited to low light levels than non-diatoms. As stratification re-starts in early April and light levels are less restrictive, a second diatom bloom occurs (reaching 1.62 mmol N m^{-3}) as well a non-diatom one (2.70 mmol N m^{-3}), which overlap in time, producing the highest TPP peak (figure 7.6).

Maximum annual TPP (2.16 mol N m^{-2} yr^{-1}) was achieved in 1988 and 1993 whereas minimum production (1.53 mol N m^{-2} yr^{-1}) was observed in 1990. TPP follows a pattern that is inverse to that of the annual *f* ratio as can be seen in figure 7.11. In fact, an inverse linear regression between annual TPP and *f* ratio was found (TPP = -8.55 *f* ratio + 6.335; r= 0.79; n=6).

In terms of size, both phytoplankton groups equally contributed to TPP in 1991 while non-diatoms were the main contributors in 1988, 1989 (both years registered the shallowest summer mixed layer depths) and 1992 (when the shallowest winter mixed layer depth was observed) and diatoms in 1990 and 1993 (figure 7.12 and table 6.6), when the highest nitrogen uptake rates by diatoms were observed.

Annual total new production (TNP) varied between 52% and 56% of TPP from 1989 to 1991 (coinciding with the highest *f* ratios modelled) and for the rest of the six-year series, total regenerated production (TRP) was dominant (between 54% and 56%) as can be seen in table 6.5. For the six-year series of this study, diatom NP accounted for at least 57% of TNP (in 1989) and the maximum TNP due to non-diatoms was 43% (also in 1989) as shown in table 6.6.

Regarding TRP, non-diatoms clearly dominated for all the years studied (see table 6.6). The size-fractionated *f* ratio reflects the relevance of non-diatoms as contributors to regenerated production (*f* ratio <0.5 in all cases) and diatoms as contributors to new production (*f* ratio >0.5 in all cases; table 6.6). Both phytoplankton groups registered the highest *f* ratios in 1989, 1990 and 1991 (the only years in which slower stratification in spring was observed) when the lowest ammonium concentrations were simulated.

The *f* ratio seem to be physically controlled as the greatest annual *f* ratios were observed when the deepest winter mixed layer depths occurred (figure 7.11), as deeper winter mixed layer depths would make higher nitrate concentrations available for phytoplankton.

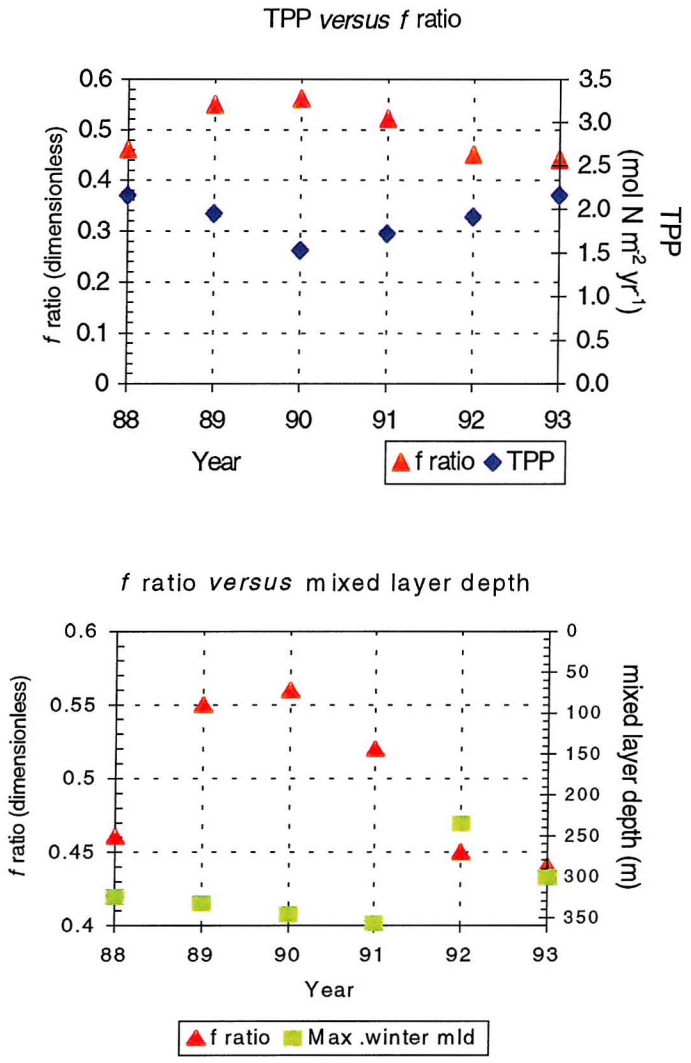

Figure 7.11: Top: Total PP and *f* ratio in the mixed layer.
Bottom: *f* ratio annual variation related to depth of the winter mixed layer.

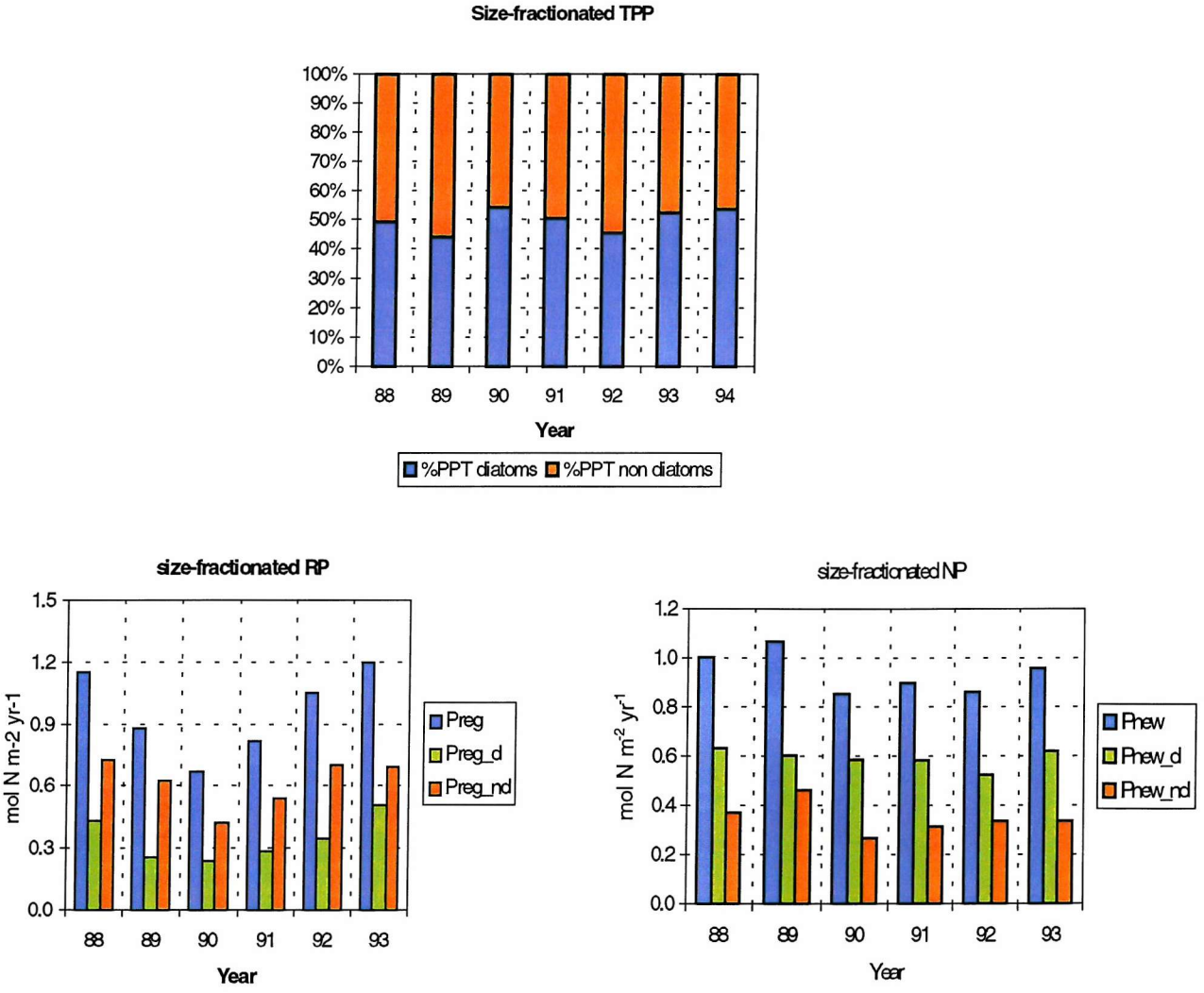

Figure 7.12: Annual size-fractionated TPP, TNP, TRP in the mixed layer.

Model comparison to other studies

Model and observational studies

Although many modelling efforts have focussed in the North Atlantic (Fasham *et al.*, 1993, Marra and Ho, 1993; Oschlies and Garcon, 1998 amongst many others), the NABE site has not been the object of many modelling studies looking at interannual variability. Waniek (2002) is the only modelling study, that we are aware of, that has taken the same approach as this work, in terms of investigating the intra and interannual variability of the food web in the North Atlantic region. Waniek used a simple ecological model (nitrate-phytoplankton-zooplankton-fast and slow sinking detritus) driven by physical forcing (ECMWF) and with dynamic mixed layer depth provided by a Kraus-Turner scheme. Her work also studied a nine-year period starting in 1989 and ending in 1997.

Although our estimates of the annual PP fall within the limits set by other model studies (table 7.3), they are twice as large as those predicted by Waniek as are the maximum estimates of daily PP. Our daily PP estimates were confronted with observational data from Bury *et al.* (2001) for 1990, who gave values between 0.5 to 1 g C m^{-2} d^{-1} for the first fortnight in May, very similar to the values predicted by this model (0.61-0.71 g C m^{-2} d^{-1} for the same period). They also estimated NP, giving figures between 45% to 76% of the TPP *versus* 56% predicted by our model. The reader is referred to chapter 6 for discussion of 1-D model fit to 1989 data.

In terms of chlorophyll, our model estimates are slightly lower than Waniek's but once more, our model was in good agreement with observational data coming from four different sources. Integrated chlorophyll data from Savidge *et al.* (1995) give estimates between 20-120 mg m^{-2} for the period lying between 1 May and 19 June in 1990, for which the model predicted values ranging from 25.7 to 116.08 mg chl m^{-2}. For a shorter

period of time (1-19 May in 1990), Bury *et al.* (2001) measured between 20-114 mg chl m^{-2}, which agree with our model estimates. Observational peak chlorophyll for the spring bloom in 1990 was above 3.5 mg chl m^{-3} (Boyd and Newton, 1995; Bury *et al.*, 2001) while model estimated between 4.0 and 4.4 mg chl m^{-3}.

Regarding zooplankton, Waniek's model estimation of integrated biomass within the mixed layer ranged from 10 to 33 mmol N m^{-2} *versus* 19 and 38 mmol N m^{-2} predicted by our model. As mentioned in previous chapters, zooplankton observations are usually scarce, therefore only model data were available for comparison.

These results show that the 1-D model is in good agreement with real data available for the North Atlantic and also with most other model estimates for the period studied.

7.6 Biological variability below the mixed layer

The subsurface or deep chlorophyll maximum

Subsurface chlorophyll maxima (SCM), also called deep chlorophyll maxima (DCM), have been observed in almost all areas of the world ocean during periods when the water column is stratified, i.e., in the North Atlantic (Lochte and Pfannkuche, 1987), at Ocean Station P (McAllister, 1962), in the Sargasso Sea (Cox *et al.*, 1982) or in the Azores (Fasham *et al.*, 1985). SCM are generally associated with the nitrate gradient and are predominant features of vertical profiles in stratified waters in late spring and summer. However, the origin of the DCM and their coincidence with the nitracline may be explained by several mechanisms, each of which has different ecological implications (Cox *et al.*, 1982). The mechanisms creating SCM probably vary from place to place, depending on environmental conditions, and several mechanisms may act at once. Surface waters above the SCM are usually exhausted of nutrients, especially nitrogen, and chlorophyll levels are low. The SCM can be found between 10 to 150 m, depending on the location, and is usually near or below the 1% light level depth (Dortch, 1987) during late spring and early summer (Kiefer and Kremer, 1981).

There has been much controversy over the physical and biological mechanisms responsible for the SCM and it has been suggested that, in some cases, vertical variation of the chlorophyll concentration within the euphotic zone does not necessarily correspond to a variation of phytoplankton biomass (Djurfeldt, 1994; Taylor *et al.*, 1997) but shows a physiological response to irradiance, nutrient availability and temperature (Cloern *et al.*, 1995; Geider *et al.*, 1997). Other hypotheses also include accumulation of cells due to changes in cell sinking (Menzel and Ryther, 1960; Steele and Yentsch, 1960), increased chlorophyll/cell due to shade adaptation (Steele, 1964), presence of non-growing relicts

of an earlier spring bloom (Kiefer and Kremer, 1981) and differences in grazing rates (Jamart *et al.*, 1977; Ortner *et al.*, 1980; Longhurst and Herman, 1982).

Studies carried out in Southern California Bight showed that the DCM often was a biomass maximum (Cullen and Eppley, 1981), as has been observed too in the Northeast Atlantic (Lochte and Pfannkuche, 1987; Joint *et al.*, 1993). Dortch (1987) suggests that in eutrophic coastal areas, the DCM is a biomass maximum whereas in oligotrophic areas phytoplankton biomass at the DCM is a much smaller fraction of the total.

The environmental conditions under which the DCM develops indicate adequate light but lack of nitrogen above the DCM while below the DCM, nitrogen is abundant, but there is not enough light, and phytoplankton growth may be light-limited (Taylor *et al.*, 1986; Taylor, 1988). At the depth of the DCM, there is usually observed a subsurface maximum of nitrite and/or ammonium (Cox *et al.*, 1982; Dortch, 1987). In some cases, the relative greater spatial separation between the DCM and the nutricline suggests that other factors, such as light availability and regenerated nutrients, may exert a more important influence upon DCM depth and chlorophyll concentrations at the DCM than cross-isopycnal supply of nitrate (Cox *et al.*, 1982). It is worth mentioning that all the literature consulted focused on phytoplankton growth exclusively limited by nitrogen, ignoring any other nutrients, such as silicate, probably due to the fact that no size-fractionated studies were attempted.

Modelling studies (Jamart *et al.*, 1977) suggest that grazing pressure is a major factor that affects the value of the chlorophyll concentrations at the DCM while data studies (Ortner *et al.*, 1980) have shown that zooplankton aggregations at the DCM are a common feature.

There is also debate about the phytoplankton group that dominates the DCM as Fasham *et al.* (1985) observed that about 60% of the PP was due to small phytoplankton in the region of the Azores front, while Lochte and Pfannkuche (1987) and Yallop (2001) found that, in the Northeast Atlantic, it was mainly composed of diatoms.

The 1-D model subsurface chlorophyll maximum

Different times and intensity of the spring and autumn blooms are clearly shown in figure 7.14. As mentioned earlier, a subsurface phytoplankton maximum, less intense than its spring predecessor in the mixed layer, was distinctively predicted every year. Even more, the model predicted two maxima (a diatom and a non-diatom subsurface bloom), at different times of the year, in 1988, 1989, 1990, 1991. The subsurface maxima in the model are always found between 28 m and 120 m. The maxima are mainly dominated by large phytoplankton (diatoms), which peaked every year. Diatom maxima tend to develop in May or in late June/early July, depending on the stability of the water column, at the depth of the ammonium maximum, after phytoplankton have peaked in the surface and nutrients have been depleted in the upper layers. Those DCM are always terminated by mesozooplankton grazing pressure, showing the importance of enhanced grazing as suggested by other studies (Harris, 1988). The non-diatom subsurface maxima, in 1988, 1989, 1990 and 1991, developed under the same circumstances, although later in the year (July), and after the diatom subsurface bloom has ceased (May), leaving plenty of nitrate and ammonium to be taken up by non-diatoms. All non-diatom subsurface blooms developed immediately after stratification of the mixed layer was completed, reaching 0.34 mmol N m^{-3} in 1988, 0.64 mmol N m^{-3} in 1989, 0.815 mmol N m^{-3} in 1990 and 0.45 mmol N m^{-3} in 1991 (subsurface maxima for 1991 not clearly visible in figure 7.14). Those four years also registered the shallowest mixed layer depth for the six-year series studied. The non-diatom subsurface bloom ends due to a combination of grazing

pressure and worsening light conditions (figure 7.13). Microzooplankton also peak in the deep layers, showing a time lag response of less than 15 days.

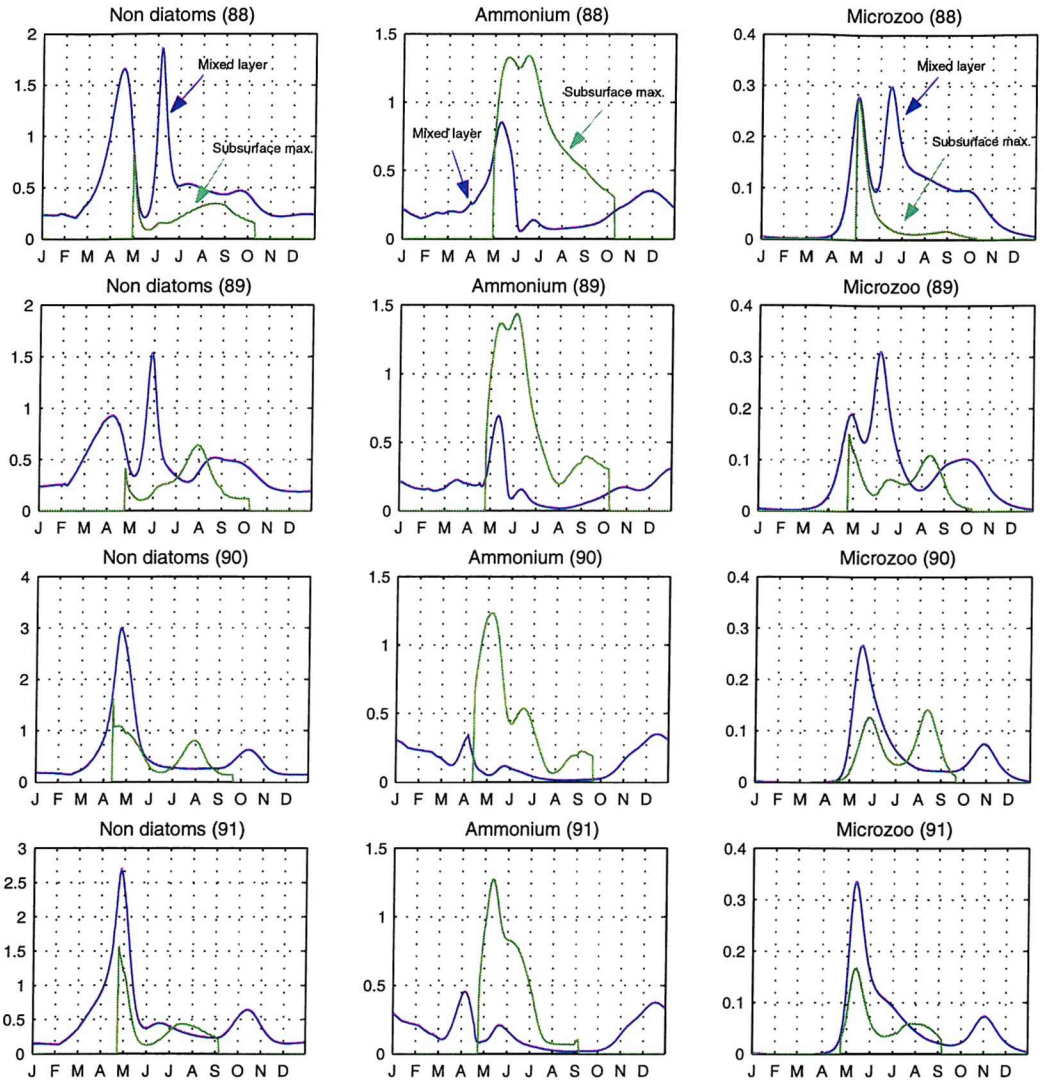

Figure 7.13: Non-diatoms, ammonium and microzooplankton variability at the isopycnal corresponding to the depth of the subsurface maximum in 1988, 1989, 1990 and 1991. Units are mmol N m^{-3}.

All subsurface phytoplankton maxima are also chlorophyll maxima and therefore, biomass blooms, as the model does not take into consideration physiological variability of the carbon to chlorophyll ratio. Bloom intensity is related to the existence of summer mixing events that break the vertical stability of the water column. When those events happened, the diatom spring bloom in the mixed layer occurred earlier and as a

consequence, the subsurface bloom occurred in May, being particularly intense, reaching over 1 mmol N m^{-3}, in 1990 and 1991 (see figures 7.2 and 7.14). Parallel to the diatom subsurface bloom, mesozooplankton subsurface biomass also developed showing very little or no lag response (by contrast to what was observed within the mixed layer). The grazing pressure exerted was responsible for the termination of the bloom, in contrast to the termination of the surface blooms caused by lack of nutrients. For the rest of the six-year period, the diatom subsurface bloom was observed in summer (late June/early July), reaching less than 1 mmol N m^{-3} and also being terminated by mesozooplankton grazing.

Minimum and maximum diatom biomass at the subsurface maximum was 0.32 mmol N m^{-3} in 1992 and 1.15 mmol N m^{-3} in 1989. Regarding non-diatoms, maximum and minimum peak values below the mixed layer were 0.815 mmol N m^{-3} and 0.34 mmol N m^{-3}, in 1990 and 1988, respectively.

The DCM ranged from 1.99 mg chl m^{-3} in 1988 to 0.62 mg chl m^{-3} in 1992. In our case, the DCM was always triggered by physical events (mixed layer depth and irradiance) but relied on subsurface nutrient abundance (especially ammonium) to fully develop at depths at which light is not the main limiting factor.

Therefore, the 1-D model suggests that the formation of the DCM is driven by the nutrient regime *via* a combination of the physical and biological mechanisms proposed by earlier authors. As the DCM is always associated with lack of nutrients in the mixed layer, subsurface growth will be restricted by light limitation. Physically, the DCM formation always occurred when the mixed layer depth was at its shallowest, showing a response to light availability. Biologically, the DCM developed at the depth of the ammonium maximum (mainly due to detrital remineralisation and zooplankton excretion), where silicate was also available for diatoms.

Primary production below the mixed layer

Primary production is mainly limited by light below the mixed layer. Maximum depth at which primary production takes place in the model is 400 m, reaching between 8% (in 1992) and 40% (in 1990) of the total primary production observed in the upper layers above (table 7.2), showing that the importance of the DCM for the total annual production is far from negligible. The model of Jamart *et al.* (1977) also addressed the question of the importance of the DCM in terms of TPP. Their model showed that the summer DCM accounts for more than 50% of the daily production, which is higher than the maximum estimate (50%) for the Pacific Ocean.

By contrast to what was observed in the mixed layer, our model shows that most of the TPP below the mixed layer is regenerated production (between 65% and 97%), new production playing a minor role and only accounting from 3% to 35% of the TPP (figure 7.15). Jawed (1973) measured zooplankton excretion rates, ammonium and PP, between 20 and 100 m, in the oceanic waters off the coasts of Washington and Oregon. His work showed that the ammonia excreted by zooplankton provided about 90% of the nitrogen requirements of observed primary productivity, which agrees with our model results. Correlation between chlorophyll and ammonium maxima is supported by observations (Jawed, 1973) and model studies (Jamart *et al.*, 1977) but no modelling attempt has been made before to quantify the amount of new and regenerated production ascribed to the DCM.

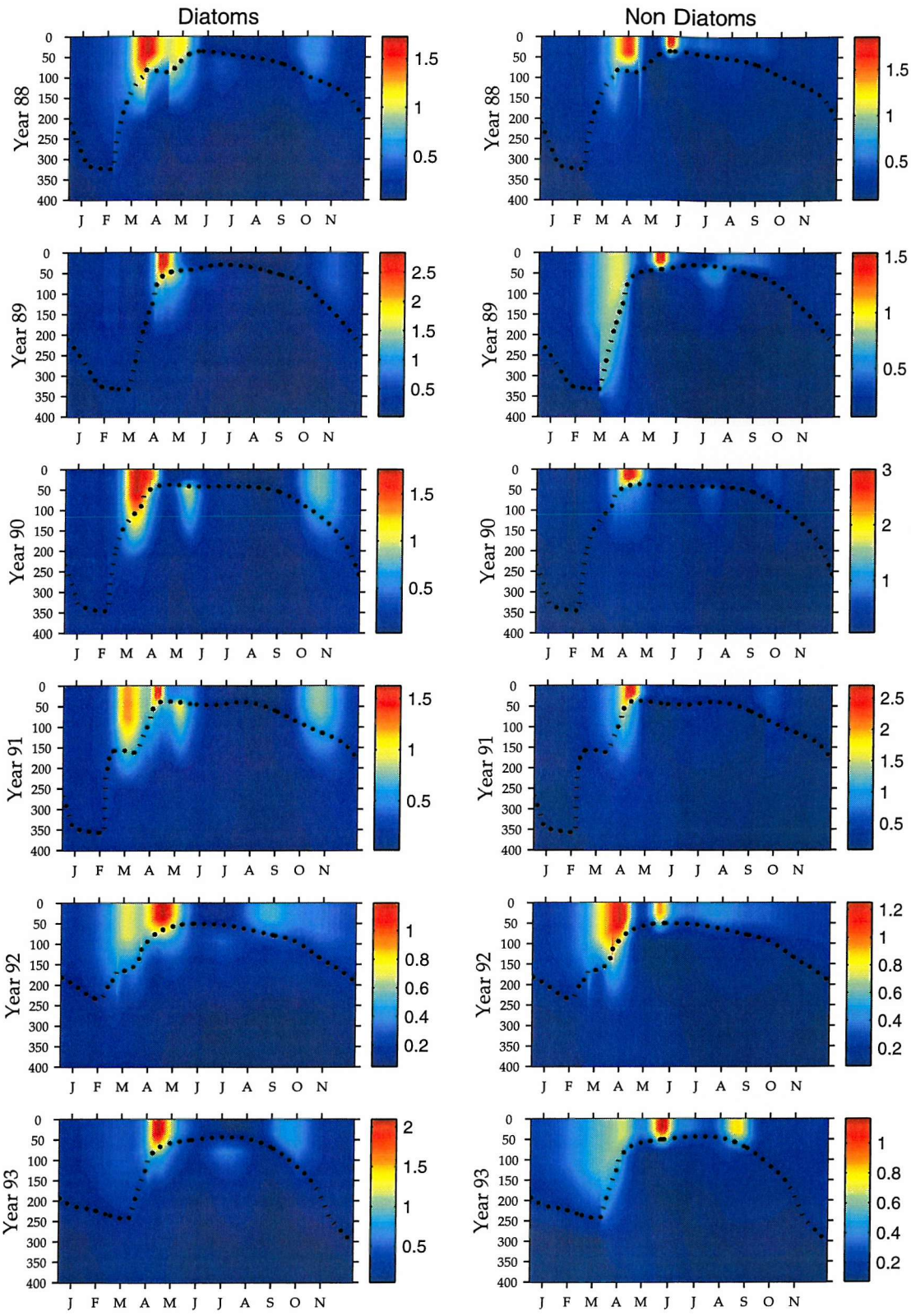

Figure 7.14: Year to year vertical variability of the 1-D model phytoplankton from 1988 to 1993 in mmol N m^{-3} (x axis represents months and the y axis shows depth, in meters).

In terms of PP, diatoms are still the dominant phytoplankton group in most cases despite the large amount of RP, only being relegated to a secondary role in 1990. They contributed to TPP by at least 57%, as they are better suited to low nitrate and light conditions than smaller phytoplankton. *F* ratios were always less than 0.5. Non-diatoms contributed to PP by more than 40% in 1989, 1990 and 1991, when the highest temperatures and shallowest mixed layers of the six-year period of study were recorded. They were therefore less handicapped in terms of light and able to compete with diatoms, as non-diatoms are more efficient using ammonium than their competitors. Those years also recorded the most intense diatom sinking, between 21% and 24%, about a third of the amount of production lost *via* mesozooplankton grazing. Diatom sinking was negligible for the rest of the period studied and up to 90% of their losses were due to grazing, showing the key role played by mesozooplankton in terms of detrital silica and, ultimately, in the silicate cycle.

Regarding non-diatoms, microzooplankton grazing also led to declining of the population, being less intense than mesozooplankton, but still consuming, between 63% to 89% of the non-diatom biomass, *versus* 11% to 37% of non-diatom population lost due to natural mortality.

Detrital remineralisation is the main process replenishing the ammonium pool (between 52% and 60%). Zooplankton excretion processes are also important, with mesozooplankton accounting for 75% to 93% of the total zooplankton contribution.

Regarding detrital nitrogen, zooplankton play a major part once more. Mesozooplankton are always the major contributor (between 35% and 72%) during all the six-year period of study. Microzooplankton contributed by 12% to 38%.

Thus, recapitulating the sequence of events set forth earlier, the 1-D model shows that during spring a substantial increase in irradiance and a coincident reduction in mixing are responsible for a remarkable increase in phytoplankton biomass in the mixed layer and therefore, PP. Although phytoplankton biomass is reduced by grazing, nutrient depletion is the main cause for their growth to decline in the mixed layer. Moreover, regeneration and vertical transport of nutrients by turbulent diffusion occurred too slowly to compensate the uptake rate. However, as the mixed layer shallows and light energy increases, phytoplankton developed at greater depths, below the mixed layer, where the presence of increased amounts of nutrients sustain growth for longer. Mesozooplankton grazing is of great importance in terminating the diatom subsurface bloom, whereas ammonium exhaustion and worsening light are the key factors in the non-diatom case, as microzooplankton restrict the non-diatom bloom but are not able to fully consume it.

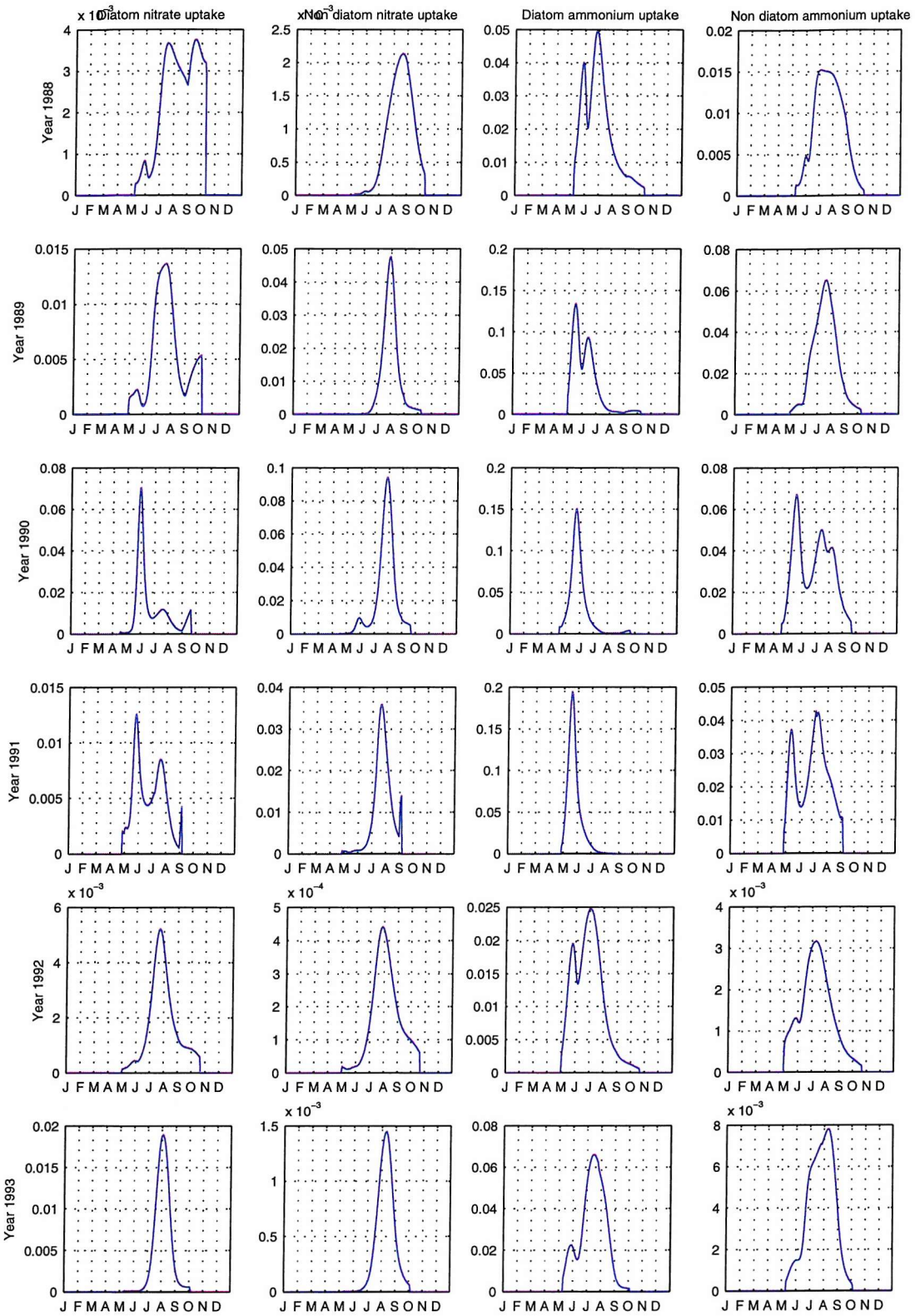

Figure 7.15: Vertical ammonium and nitrate uptake by phytoplankton below the mixed layer. Units are mmol N m^{-3} d^{-1}.

7.7 Summary of key points

- Interannual variability was studied from 1988 to 1993. Although initially, a longer time series was chosen (up to 1996), it was reduced to only six years due to numerical problems highlighted by the build up of the dissolved nitrate and silicate pools.

- Model results show that competition between different phytoplankton groups will be different according to external conditions (physical forcing). Diatoms will become dominant in turbulent water rich in nutrients (due to their higher light and nitrate assimilation efficiency) and non-diatoms will constitute the bulk of population in stratified water, poorer in nutrients.

- Regular succession runs parallel to consumption of nutrients and decay of mixing. Mixed-layer blooms are terminated due to a combination of grazing and lack of new nutrients.

- A common feature, for the six-year period studied, is ammonium exhaustion in the mixed layer but accumulation in deeper layers, where supply is greater than demand.

- The *f* ratio is dependent on mixed layer depth (shallowest summer mixed layer produced higher *f* ratios), therefore being physically controlled.

- The initiation of the spring bloom also depends on the type of mixed layer stratification. Fast re-stratification regimes led to earlier phytoplankton blooms than slow ones. Summer mixing events encouraged mesozooplankton growth, which prepares them better for overwintering. Autumn phytoplankton blooms are triggered by the deepening of the mixed layer, as new nutrients are entrained from deeper layers.

- The 1-D model predicted the annual occurrence of a deep chlorophyll maximum (DCM), of varying intensity, during the period of study, at the depth of the ammonium maximum (mainly due to detrital remineralisation and mesozooplankton excretion, followed by microzooplankton's). Diatoms peaked every year, while non-diatoms only developed in four occasions, when the shallowest summer mixed layer were modelled. The diatom deep maximum is ended by mesozooplankton grazing, while non-diatoms ended due to a combination of grazing and light limitation.

- Primary production below the mixed layer only accounts for 2-40% of the TPP predicted within the mixed layer. Most of the deep production is regenerated (65-79%). Generally, diatoms are responsible of most of it (except in 1990).

Table 7.1: Annual TPP in the mixed layer, phytoplankton group responsible for most of the mixed-layer TPP (percentage in brackets), mixed layer stratification regime, and minimum and maximum mixed layer depths in meters.

TPP stands for total primary production.

Year	Annual total primary production (mol N m^{-2} yr^{-1})	Phytoplankton PP	Mixed layer		
			Stratification	Min. (m)	Max. (m)
1988	2.16	Non-diatoms (51%)	Fast	36.56	324.40
1989	1.95	Non-diatoms (56%)	Slow	28.72	332.77
1990	1.53	Diatoms (54%)	Fast	36.78	346.02
1991	1.72	Both (50% each)	Fast	37.08	357.26
1992	1.91	Non-diatoms (54%)	Slow	50.44	235.13
1993	2.16	Diatoms (52%)	Slow	43.36	300.63

Table 7.2: Total and size-fractionated primary, new and regenerated production down to 400 m below the mixed layer in mol N m^{-2} y^{-1}.

TPP, TNP and TRP stand for total primary, new and regenerated production. Figures in brackets refer to percentage of TPP.

Year	TPP	TNP	TRP	NP_d	NP_{nd}	RP_d	RP_{nd}	*f* ratio
1988	0.26 (12%)	0.03	0.23	0.02	0.01	0.16	0.07	0.12
1989	0.49 (25%)	0.09	0.39	0.04	0.06	0.24	0.15	0.19
1990	0.61 (40%)	0.21	0.40	0.08	0.13	0.19	0.21	0.35
1991	0.44 (26%)	0.10	0.34	0.04	0.06	0.21	0.13	0.23
1992	0.15 (8%)	0.02	0.13	0.02	0.00	0.12	0.02	0.13
1993	0.31 (14%)	0.04	0.26	0.04	0.00	0.23	0.03	0.14

Table 7.3: Model output interannual variability from 1988 to 1994

Minimum and maximum range values are given.
depending on which algorithm is used to calculate photosynthesis (see chapter 6 for details)
* integrated over the euphotic zone
+ integrated over top 35 m

Property	1-D model	Observational	Other models	Source
Annual PP ($g\ C\ m^{-2}\ y^{-1}$)	120.78-170.91		51-78*	Waniek (2002)
		35-60	108	Oschlies *et al.* (2000)
		120-160	122	Fasham and Evans (95)
		150-225# and 200-270#		Berger *et al.* (93)
		230-243		Antoine *et al.* (96)
		240		Behrenfeld and Falkowski (97)
		200-250		Sathyendranath *et al.* (95)
				Longhurst *et al.* (95)
				Field *et al.* (98)
Daily PP* ($g\ C\ m^{-2}\ d^{-1}$)	1.20-1.79		0.9-1.2*	Waniek (2002)
	0.61-0.71	0.5-1 (1-19 May;1990)		Bury *et al.* (2001)
New production (% PP)	56%	45%-76% (1-20 May;1990)		Bury *et al.* (2001)
Integrated chl* ($mg\ m^{-2}$)	138.27-172.49		161-233*	Waniek (2002)
			150-180	Oschlies and Garçon (99)
	25.7-116.08	20-120 (1 May-15 June; 1990)		Savidge *et al.* (95)
	34.41-116	20-114 (1-19 May;1990)		Bury *et al.* (2001)
Maximum chl* ($mg\ m^{-3}$)	4.44	>3.5 (spring bloom; surface; 1990)		Boyd and Newton (95)
	4.00	3.5 (1-19 May;1990)		Bury *et al.* (2001)
	1.21	1.5 (10 Sep.-30 Oct.; 50 m; 1996)		Schiebel *et al.* (2001)
Integrated zoop.* ($mmol\ N\ m^{-2}$)	19.09-28.99		10-33*	Waniek (2002)
			60-80	Oschlies and Garçon (99)

Chapter 8:

Sensitivity Analysis

Chapter 8: Sensitivity analysis

8.1 Introduction

The tuning of the 1-D model (chapter 6) highlighted the inadequacy of several ecological parameters if a good fit between model and NABE data was to be achieved. Unrealistic winter nitrate concentrations in the mixed layer (up to 15 mmol N m^{-3}) were predicted for 1996, when using the detrital breakdown rate for nitrogen (δ_1) obtained *via* optimisation of the 0-D model. Even more, when the model was re-tuned to comply with well documented winter concentrations for the area (Glover and Brewer,1988; Garside and Garside, 1993), a distinctive non-diatom subsurface maximum, not predicted in earlier runs, was observed. Although interannual variability studies (chapter 7) revealed the existence of a numerical problem that caused the building up of nutrients, the sensitivity shown by the ecological model to certain parameters (δ_1 amongst others) requires the evaluation of the model response by assessing the uncertainties associated with the modelling process. Therefore, further investigation on what seems to be a critical parameter (δ_1 determines the vertical distribution of nitrate and ammonium) was carried out by performing a sensitivity analysis (SA) exercise involving a subset of five parameters related to nutrient regeneration processes (δ_1 and δ_2 -detrital breakdown rate for silicate) and to phytoplankton physiology: α_1 (non-diatom slope of the P-I curve), K_1 and K_2 (non-diatom half-saturation constants for nitrate and ammonium uptake, respectively).

Section 8.2 introduces the concept of SA as well as looking at how previous model studies dealt with it. Section 8.3 explains the SA technique used in this work, from selection of ranges and distribution of parameters to uncertainty and sensitivity analysis. Finally, a summary of the key points found in this work are included.

8.2 Sensitivity analysis

Sensitivity analysis (SA) studies how the variation in a model output can be apportioned, either qualitatively or quantitatively, depending on the sources of variation, and of how such model depends on the information fed into it (Saltelli, 2000). Numerical models are often used to represent systems and processes of different nature and complexity. Many times, those systems and processes are so complicated that experimentation is not feasible and investigators turn to the use of models to explore such systems, otherwise constrained by physical limitations. However, model results are also limited by our knowledge of the system in question and, therefore, biased by our own uncertainty. The model initial conditions and parameters might also be subjected to uncertainty, due to errors of measurement and/or lack of information and even the impossibility of a precise representation of the system due its intrinsic variability (i.e., stochastic events). Therefore, SA techniques help to increase the confidence in the model and its results, as well as to understand how the model responds to variations in its initial conditions, parameters, data used for calibration and even model structure.

The use of SA is a common practice in biogeochemical models. The most used approach being the modification of each parameter by a certain amount of its *prior* value (Jamart *et al.*, 1979; Taylor and Joint, 1990; Marra and Ho, 1993; McGuillicuddy *et al.*, 1995; Fasham, 1995; Pondaven *et al.*, 1998 amongst others). Model complexity (dimensional and structural) usually restricts the number of tests to be performed, as models often are computationally expensive to run and interpretation of the results can be a difficult task. Although ecological modelling has seen much progress in the last decade, the attention paid to formal SA has not evolved at the same rate, and the same methods used 20 years ago are still in vogue amongst modellers. On the other hand, sophisticated SA

techniques such as Monte Carlo analysis, Fourier amplitude sensitivity tests (FAST) or Sobol's sensitivity indices (see Saltelli 2000) are often unaffordable when the analysis focuses on a large parameter set.

The boundary between sensitivity and uncertainty analysis is sometimes blurred as the techniques are closely related. The latter (uncertainty analysis) quantifies the changes in the model response to a series of factors (i.e., initial conditions, parameters) while the former (SA) looks at the proportion of uncertainty according to the source. In this work, we have used both techniques to have an insight into the reliability of the 1-D model results and they will be discussed in detail later (section 8.3).

Due to the problems encountered when the 1-D model was tuned (previously discussed in chapter 6), it was necessary to perform a formal SA. After the tuning exercise for 1989 was carried out, discrepancies between model output and winter nitrate concentration during 1996 were found. This result led to the need of further modification of the *prior* value for the nitrogen detritus breakdown/remineralisation rate (δ_1), to which the ecosystem showed particular sensitivity. Although nitrate built up (from 1994) is due to numerical problems (as discussed in chapter 7), the model sensitivity to nitrogen remineralisation rates was still investigated as there is great uncertainty associated with this parameter.

In the model, nitrate enters the mixed layer *via* 3 different processes: vertical diffusion, vertical mixing (entrainment) and regeneration processes (nitrification). The latter is highly variable, closely related to ammonium, and directly dependent on ecosystem changes (remineralisation and zooplankton excretion inject ammonium in the ecosystem; see equations in chapter 2). This fact, as well as previous evidence of phytoplankton subsurface development linked to deep ammonium maxima, led to the need to monitor

the sensitivity shown by the ammonium pool. Other variables of interest were phytoplankton biomass, total chlorophyll as well as annual total primary production (TPP), regenerated and new production (TRP, TNP), nitrate and silicate-based export production (NBEP, SBEP) and *f* ratio.

The SA carried out in this work was focused on a subset of five parameters on which the balance among the variables seem to be dependent: δ_1, α_1, K_1, K_2 and δ_2. Previously discussed in chapter 6 was the need of modification of α_1, K_1, K_2 in order to avoid the diatom/non-diatom bloom overlapping in spring time. The detrital silicate breakdown rate (δ_2) was also included due to its importance to the vertical gradient of silicate in the water column and also to the great uncertainty associated to its determination (see chapter 6). The analysis tested the model response not only to individual parameter variations but also to interaction among them. Results from the analysis would be quantitatively assessed in terms of maximum values of certain model state variables as well as primary and export production, and *f* ratio. Special attention will be paid to the factors that trigger the presence/absence of a non-diatom subsurface maximum.

Only a few model studies have investigated the formation of the DCM -Jamart *et al.*, (1977 and 1979) in the Pacific Ocean and Taylor *et al.* (1986), Taylor (1988) and Marra and Ho (1993) in the North Atlantic- and no attempt has been made before to characterise such maximum in relation to phytoplankton size. Jamart *et al.* (1979) used a simple chlorophyll-ammonium-nitrate model (with varying carbon-to chlorophyll and carbon-to-nitrogen ratios) and found that nutrient limitation in the surface layers led to the formation of the deep maximum. Taylor *et al.* (1986) used a time-dependent advection-diffusion model to study the vertical distribution of phytoplankton in stratified waters in the open ocean and also in the shelf. The biological model had only 2 compartments

(phytoplankton and a single nitrogen nutrient). Model results showed the development of a DCM (at 40 m in the ocean case and 30 m in the shelf case) as a result of nutrient depletion in the upper water column whereas there are plenty of nutrients at the depth of the DCM. The authors also tested the model sensitivity to changing environmental conditions (such as diurnal variation of light and turbulence) and obtained no change in model results.

On the other hand, Marra and Ho (1993) applied a mixed layer and a NPZ model (nitrate) to investigate the spring bloom at the NABE site. Although their results regarding the surface spring bloom were satisfactory, the model failed to reproduce the DCM shown by empirical data, unless photoinhibition in the phytoplankton growth (for which, they admitted, there is no evidence) was assumed.

We expect that the SA would clarify the critical parameter/s that trigger such maximum in the model and illuminate which aspects of the ecosystem are in most need of further study.

A complete SA of the model involving all the parameters is too complex, and computationally expensive, to pursue here (see section 8.3.1 below).

8.3 The Analysis Methodology

Our starting point:

$$Y = f(X_1, X_2, ..., X_i)$$

where Y is a descriptor of the model output (e. g. maximum chlorophyll concentration) and X_i are a set of input factors (parameters) whose value can either be fixed or sampled from a distribution. In our case, i=5.

Here, the objective of SA is to identify the most important factor or factors that would lead to the development of deep chlorophyll maxima and also to the greatest changes of the above statement Y. It is also possible to group the factors in subsets, so the solution will be influenced by the interactions among factors.

There are many different strategies to choose from when performing SA (see Saltelli *et al.*, 2000 for a thorough description). The one used in this work resembles a Monte Carlo analysis as it is based on the multiple evaluation of the 1-D model performance using randomly selected model parameters from a given distribution. The model results will be used to study the uncertainty in the model predictions and quantifying the contribution of the input factors to such uncertainty. There are five steps involved: selection of ranges and distribution of X_i; generation of a sample based on ranges and distributions obtained by the first step; evaluation of the model for each element of the sample; uncertainty analysis and finally, SA.

8.3.1 Selection of ranges and distribution of parameters

As explained earlier, a subset of five parameters out of the complete ecological parameter set (32 in total) were thought to play a key role in determining the ecological dynamics observed at 47°N 20°W and in obtaining a good fit to the field data available. Those parameters (also referred to as factors throughout the text) were: δ_1, δ_2, α_1, K_1 and K_2. As the length of time that one model simulation takes was a limiting factor, only five different values, for each key parameter, were investigated. They were randomly generated (within the upper and lower limits used by the 0-D model optimisation) according to a normal distribution with mean the parameter *prior* value and standard deviation of 1/3 of its *prior* (table 8.1).

8.3.2 Sampling

The new parameter space was sampled based on the Latin Hypercube Method (McKay *et al.*, 1979), hereafter referred to as LHM, although our approach is much simpler than McKay *et al*'s, and therefore requires a reduced number of model runs. The Latin Hypercube Method is a stratified sampling technique where the random parameter distributions (X_j, $j = 1, ..., k$) are divided into equal probability intervals (N). A probability ($1/N$) is randomly selected from within each parameter interval, ensuring that the entire range is sampled. This means that there are N non-overlapping values for each of the k input parameters (five in our case) and that each instance is equally likely to be chosen. One of the instances on X_1 is randomly selected, matched with a randomly selected instance of X_2, and so on, until X_k.

In our case:

$$X = \{X_1, X_2, X_3, X_4, X_5\}$$

$$X_1 = \delta_1 = \{\delta_{11}, \delta_{12}, \delta_{13}, \delta_{14}, \delta_{15}\};$$

$X_2 = \alpha_1 = \{\alpha_{11}, \alpha_{12}, \alpha_{13}, \alpha_{14}, \alpha_{15}\}$;

$X_3 = K_1 = \{K_{11}, K_{12}, K_{13}, K_{14}, K_{15}\}$

$X_4 = K_2 = \{K_{21}, K_{22}, K_{23}, K_{24}, K_{25}\}$

$X_5 = \delta_2 = \{\delta_{21}, \delta_{22}, \delta_{23}, \delta_{24}, \delta_{25}\}$

Table 8.1 shows the range of values for each parameter.

8.3.3 Model evaluation

A total of 45 tests or experiments were performed in order to asses the model performance not only to single instances of each parameter (tests 1-5; 26-45; see table 8.2) but also to interaction among parameters (tests 6-25) using the combinations generated by the LHM (table 8.2).

The output variables of interest were maximum diatom and non-diatom biomass, maximum chlorophyll and maximum ammonium during 1989. As the changes in the model state variables will crucially affect primary production, export production and *f* ratio, the annual total and size-fractionated primary production (TPP), new and regenerated production (TNP and TRP, respectively), and the *f* ratio in the mixed layer were also calculated as well as the total nitrogen and silicate-based export productions (NBEP and SBEP, respectively) at the base of the mixed layer.

The presence/absence of subsurface phytoplankton maxima was also considered. Due to the high complexity of the model, the uncertainty and SA were studied in 1989 only, as this was the year used for the model tuning and also for which a larger amount of field data were available.

The reader must take into account that parameters were varied across the central or *prior* values used in preceding chapters. Each of the experiments described below consisted of 5 simulations in which parameter variation was not symmetrical but randomly generated.

The difference in the qualitative and quantitative behaviour amongst those simulations and the control run will elucidate the dependence of the model solution on the parameter(s). Interpretation of model results related to individual and simultaneous parameter changes will be discussed. The control run chosen was the one obtained when the 1-D model was first tuned (chapter 6) and $\delta_1 = 0.107$ d^{-1} (figure 8.1), which produced a diatom and a non-diatom subsurface maximum. The former reached 1.21 mmol N m^{-3} at 65 m of depth in May while the latter only reached 0.80 mmol N m^{-3} at 53 m in July (less light efficient than diatoms). Both blooms are mainly supported by deep ammonium concentrations (figure 8.2).

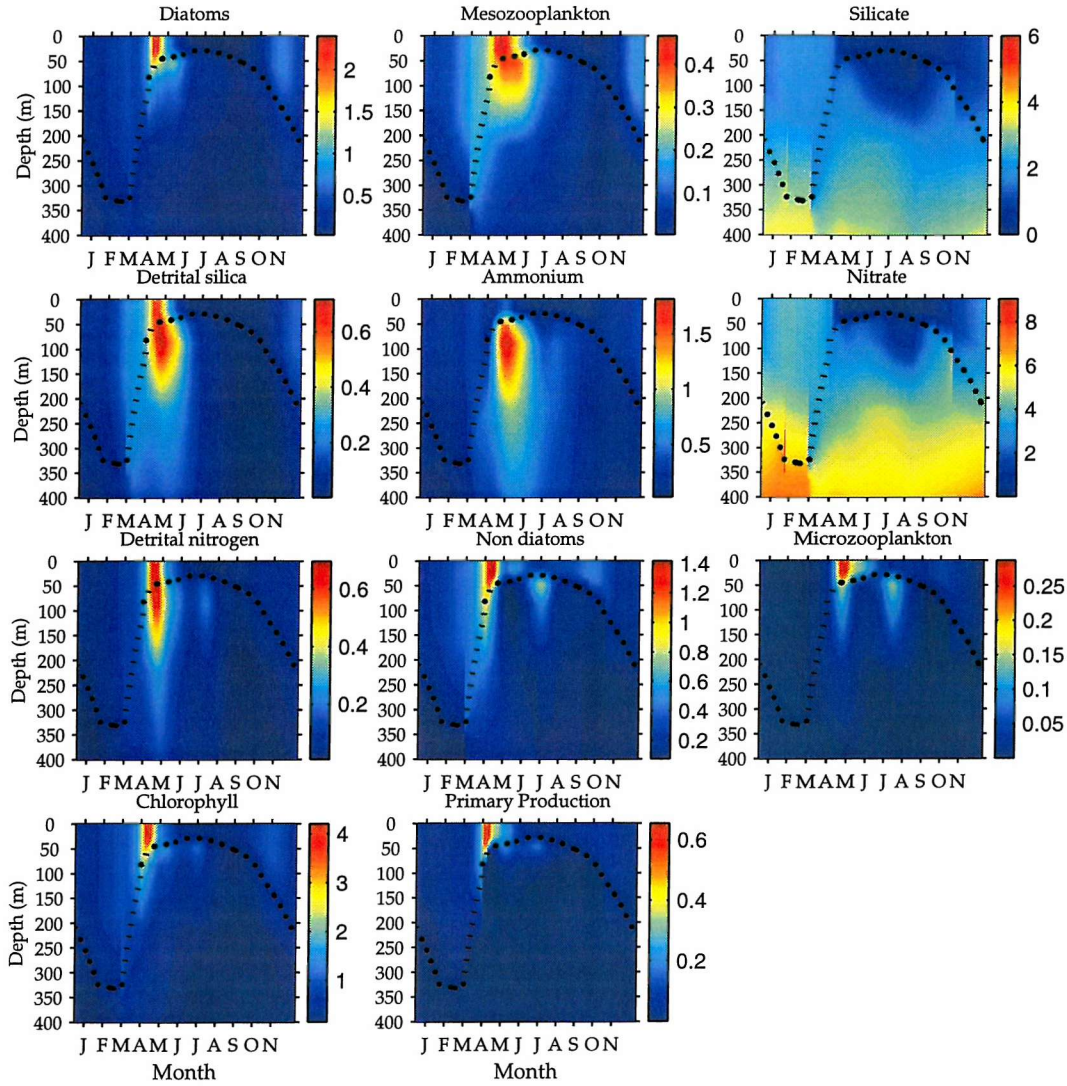

Figure 8.1: 1-D model state variables, chlorophyll and primary production for 1989 down to 400 m from the control run. Dotted line represents mixed layer depth. All units are in mmol N m^{-3} except chlorophyll (mg chl m^{-3}) and PP (mmol N m^{-3} d^{-1}).

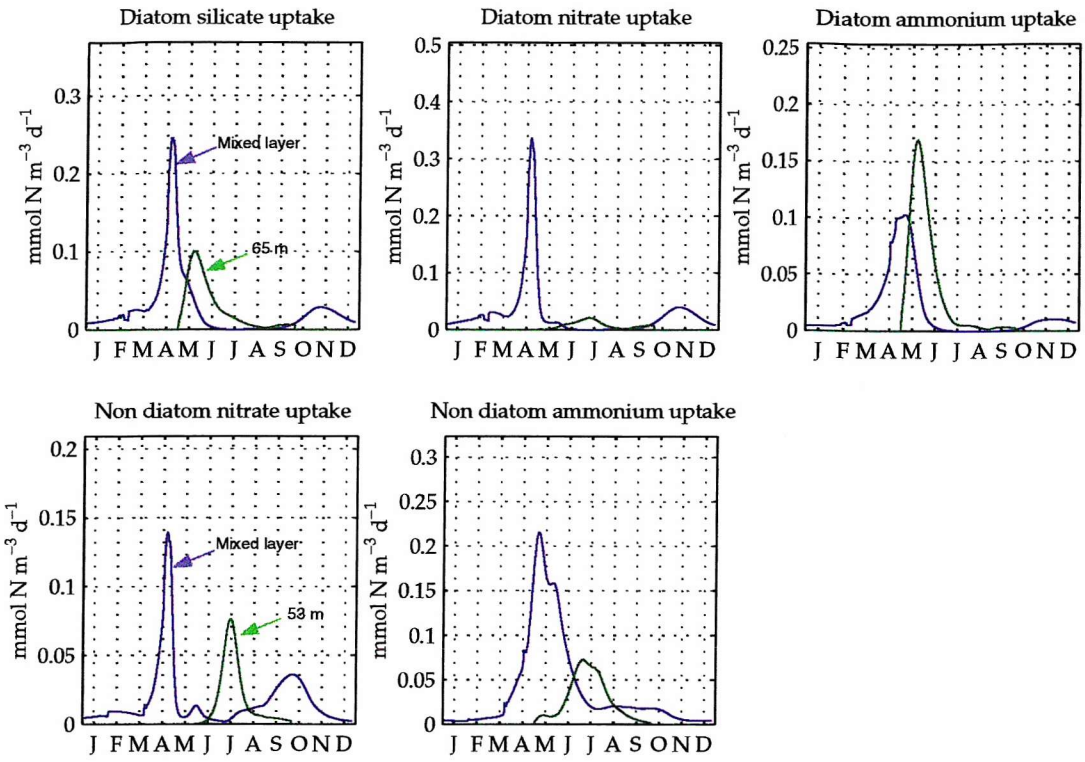

Figure 8.2: Silicate, nitrate and ammonium phytoplankton uptake in the mixed layer (in blue) and at the depth of the deep maximum (green) according to the control run.

8.3.4 Uncertainty analysis and sensitivity analysis

First of all, we want to investigate which are the parameters that, individually, have a greatest effect on the model output. Secondly, we also want to quantify how different values of the same parameter affect the model output. Finally, we will be looking at the combination of several parameters and the joint effect on the model output.

Figure 8.3 represents the changes in maximum phytoplankton biomass (diatom and non-diatom), total chlorophyll and ammonium concentration according to the modification of the parameter subset as shown in table 8.2. The changes in annual TPP, TNP, TRP, NBEP, SBEP and *f* ratio in the mixed layer are shown in figure 8.7. Figure 8.8 shows size-dependent phytoplankton contribution to primary production, export production and *f* ratio.

❑ Detrital nitrogen remineralisation rate (δ_1)

The detrital nitrogen remineralisation rate was varied between 0.123 and 0.299 d^{-1}, which is up to 3 times higher than the control value (0.107 d^{-1}), corresponding to tests 1 to 5 (table 8.2). In general, one would expect higher ammonium and also nitrate concentration (due to nitrification processes) as δ_1 increases, which would lead to higher phytoplankton biomass, specially non-diatom biomass, as they are only limited by nitrogen and are more efficient assimilating ammonium than diatoms (also limited by silicate). Model results agreed with what was expected. The most significant changes (compared to the control run) occurred in the non-diatom case (figure 8.3 and table 8.3).

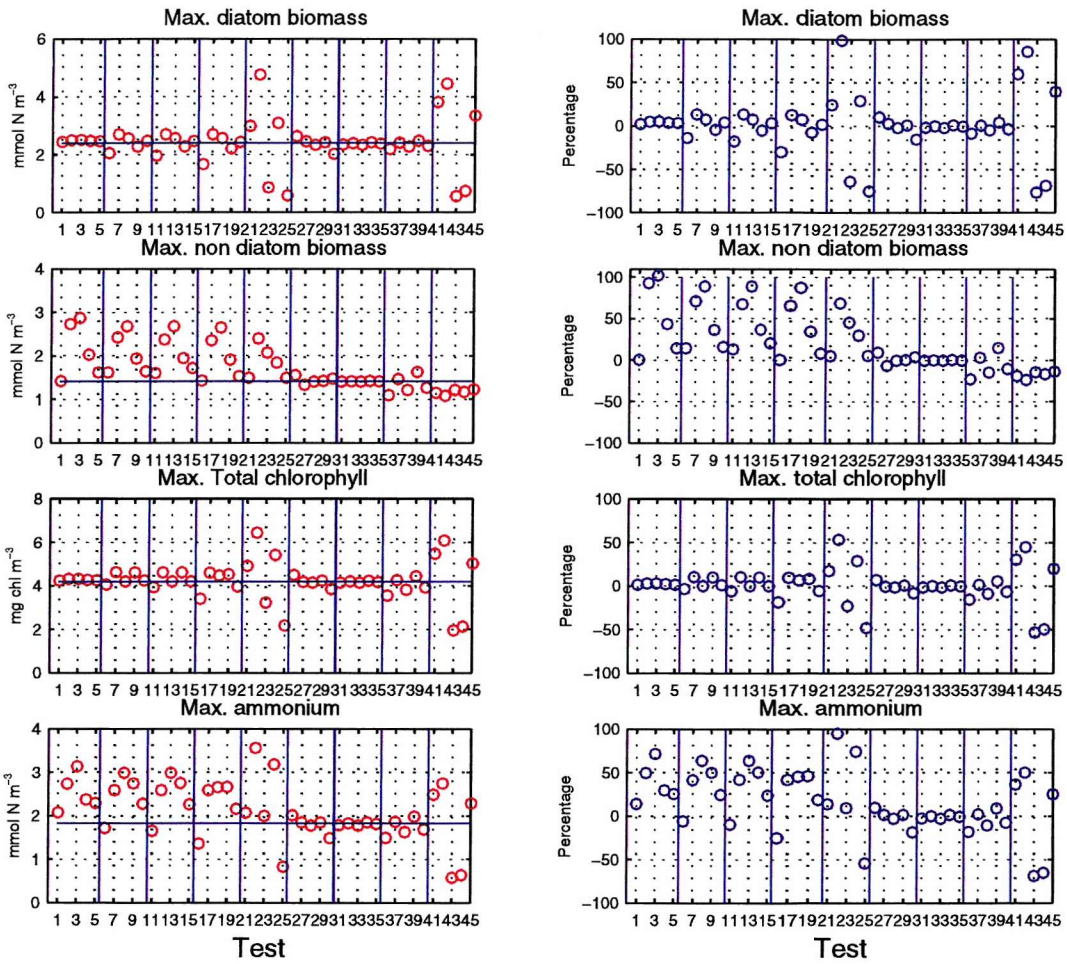

Figure 8.3: Variation in the maximum phytoplankton biomass, total chlorophyll and ammonium concentration after the uncertainty analysis was performed. The left column represents magnitude changes while the right column shows percentage of change relative to the control run. Test 1 to 5 and 26 to 45 show the effects when one single parameter was changed at a time (vertical solid lines). The rest of the tests represent different parameter combinations as stated in table 8.2. The solid horizontal blue line shows the control value. Results correspond to 1989.

Model results also shown the occurrence of a non-diatom subsurface bloom in 2 out of 5 cases (tests 1 and 5) in mid July (figure 8.4).

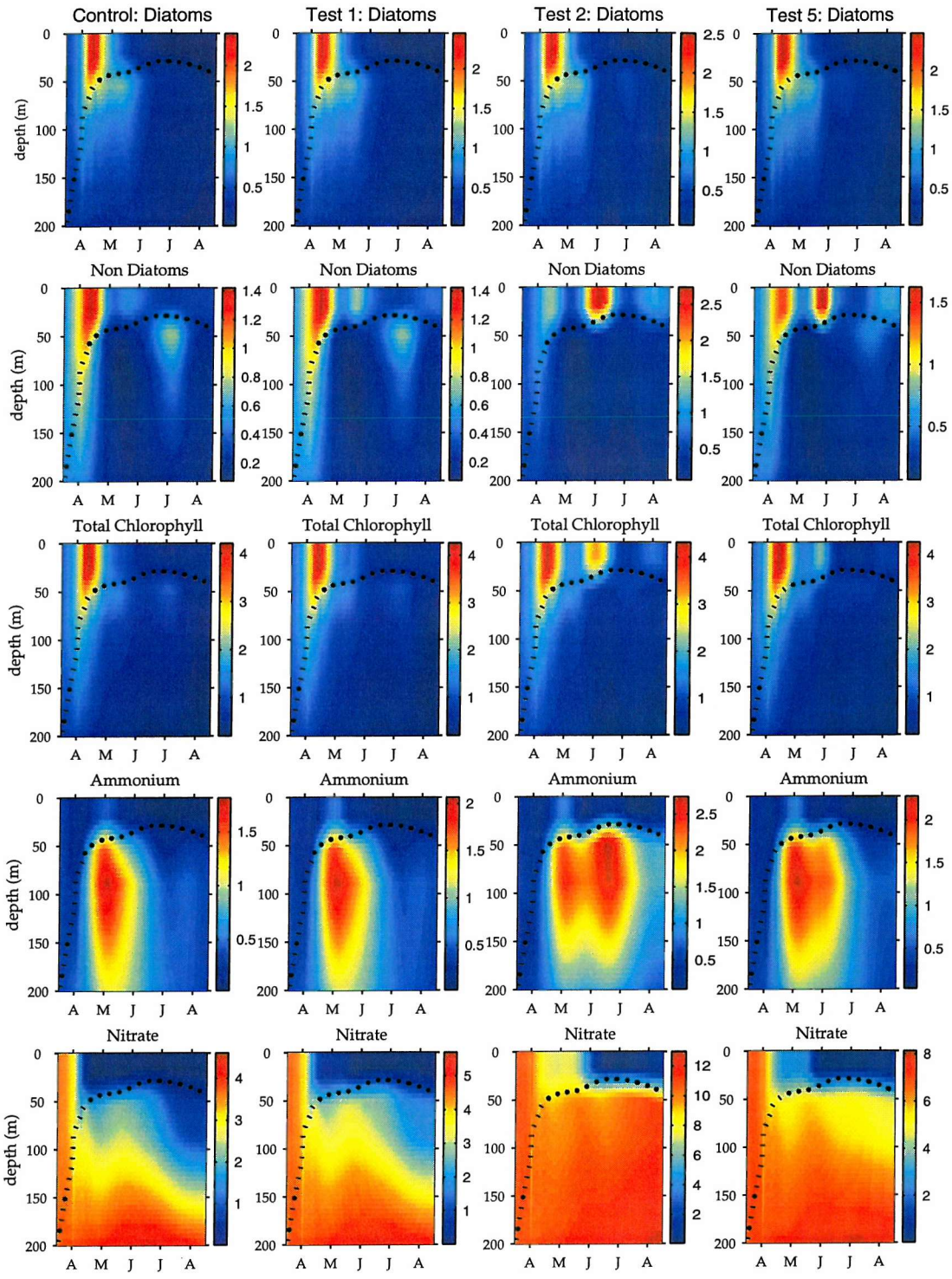

Figure 8.4: Vertical distribution (down to 200 m) of diatom and non-diatom biomass, total chlorophyll, ammonium and nitrate from the control run and tests 1, 2 and 5. Results shown correspond to 1989. Dotted line shows mixed layer depth. Units are mmol N m^{-3} apart from chlorophyll (mg chl m^{-3}).

This subsurface bloom is related to nitrate availability in the upper mixed layer. When winter nitrate concentration is higher than a threshold (8 mmol N m^{-3} according to our experiments), there is no subsurface bloom but the bloom is observed when nitrate concentration falls below that threshold. This behaviour is closely related to the diatom dynamics as they are mainly limited by silicate, when nitrate is abundant. In this situation, diatoms will decline when nitrate still remains high (up to 6 mmol N m^{-3}) due to the lack of silicate (<0.5 mmol Si m^{-3}), allowing non-diatoms to thrive in the mixed layer until nitrate is depleted and therefore no subsurface bloom was observed as in tests 2 to 4 (figure 8.5).

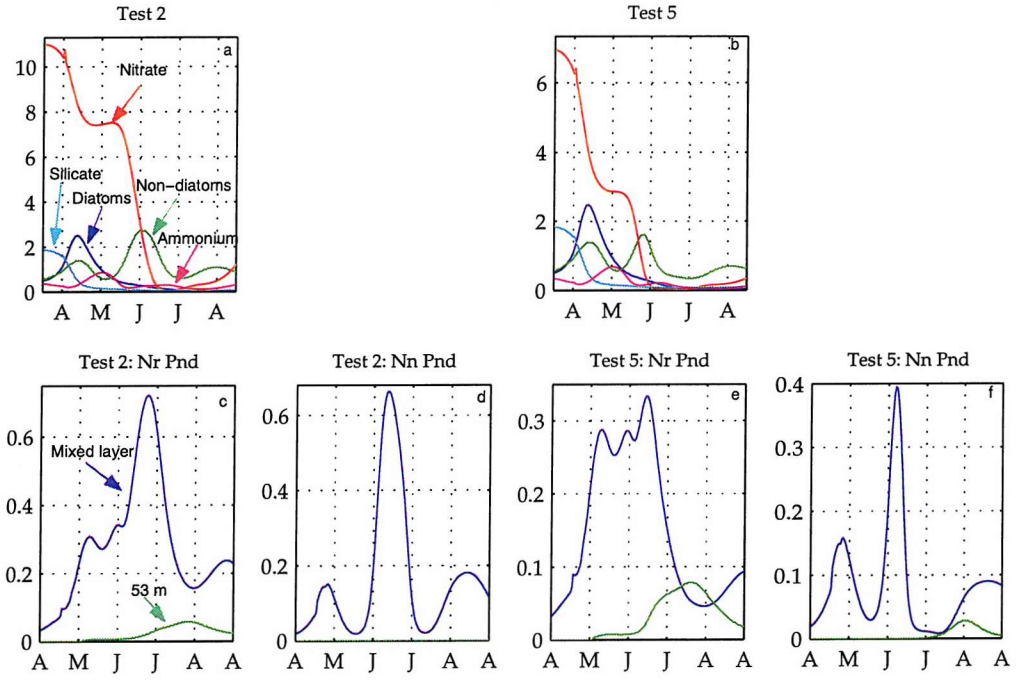

Figure 8.5: Nutrients *versus* phytoplankton variability in the mixed layer shown by test 2 (a) and test 5 (b) during 1989. Nitrate (d, f) and ammonium (c, e) uptake rates by non-diatoms in the mixed layer (blue) and at the depth of the subsurface maximum (green) are also shown. Nn, Nr and Pnd represent nitrate, ammonium and non-diatoms.

On the other hand, when winter nitrate is below the threshold, diatoms take up most of nitrate and ammonium, and very little nitrogen is available for non-diatom development, after diatoms have decayed. However, light below the mixed layer is sufficient for non-diatoms to develop, where there is plenty of ammonium (due to regeneration and excretion processes) and nitrate (figure 8.5).

A diatom subsurface maximum (DSM) was observed in May in all cases, as silicate is their main limiting nutrient in the mixed layer but higher concentrations can be found below it. A second diatom subsurface bloom was observed in late June (tests 4 and 5) and in mid July (tests 2 and 3). In all cases, this maximum only accounted for 0.7 mg chl m^{-3}. Why does it happen? The second diatom subsurface bloom is related to the generation of two ammonium deep maxima (ADM) and to their intensity. Only one ammonium maximum was predicted when the lowest δ_1 was used (test 1), caused by the overlapping of the main phytoplankton surface blooms and leading to simultaneous zooplankton development, being reflected in the detritus and ammonium temporal and vertical profiles (figure 8.4). On the other hand, higher δ_1 (tests 2 to 4) led to a later development of the main non-diatom bloom (preceded by a lower intense bloom, closely followed by microzooplankton and also mesozooplankton), generating a second ammonium maximum (of varying intensity) due to mortality, excretion and remineralisation processes.

In general, non-diatom phytoplankton reached higher biomass when the amount of nitrate in the mixed layer was high (test 3 resulted in a 103% increase compared to the control case; figure 8.3; table 8.3) as their growth is only dependent on nitrogen.

The main surface diatom bloom was invariably observed in late April/early May, independently of δ_1. However, the timing of the main surface non-diatom bloom was inversely correlated to nitrate concentration in the mixed layer. The higher the nitrate concentration, the later in the year the main bloom occurred (June), due to a combination of favourable light and nitrogen abundance (figure 8.4), suggesting that nitrate limitation plays a more important role than light. Even more, non-diatoms reached higher biomass

than diatoms in 2 out of 5 cases, when the highest δ_1 were used to force the model (tests 2 and 3), also indicating strong silicate limitation for diatoms.

Maximum total chlorophyll in the mixed layer was very similar in all tests (maximum 3% change compared to the control; table 8.3), varying from 4.26 to 4.32 mg m^{-3}. This is not surprising, as the surface chlorophyll maximum occurred in April/May, resembling the profile shown by diatom biomass, as they are the main contributors to such maximum (figure 8.4).

As expected, ammonium maximum concentration was subjected to greater variations, from 2.08 to 3.14 mmol N m^{-3} (between 14% and 72% higher than the control), corresponding to the lowest and the highest δ_1 (figures 8.3 and 8.4), remarkably following the variability shown by non-diatoms. Those variations are mainly due to the balance between microzooplankton excretion (increased due to higher non-diatom biomass) and detrital nitrogen remineralisation (increased due to higher microzooplankton egestion and non-diatom natural mortality), whereas larger zooplankton and phytoplankton respiration remained as in the control run (figure 8.6).

In terms of annual TPP, δ_1 is the parameter that produces the greatest variation, from 1.90 to 3.06 mol N m^{-2} yr^{-1}(between 9% and 76% higher than the control; see figure 8.7). As expected, higher TPP was achieved when the highest δ_1 were used to run the model. The same pattern was invariably associated with TNP, TRP and NBEP whereas in terms of *f* ratio the inverse trend was shown (lowest values achieved when δ_1 is high) but it had no effect on SBEP. As higher δ_1 increase the ammonium concentration in the water column, one would expect to have a greater effect on regenerated production rather than on new production, which is exactly what it is observed, leading to lower *f* ratios.

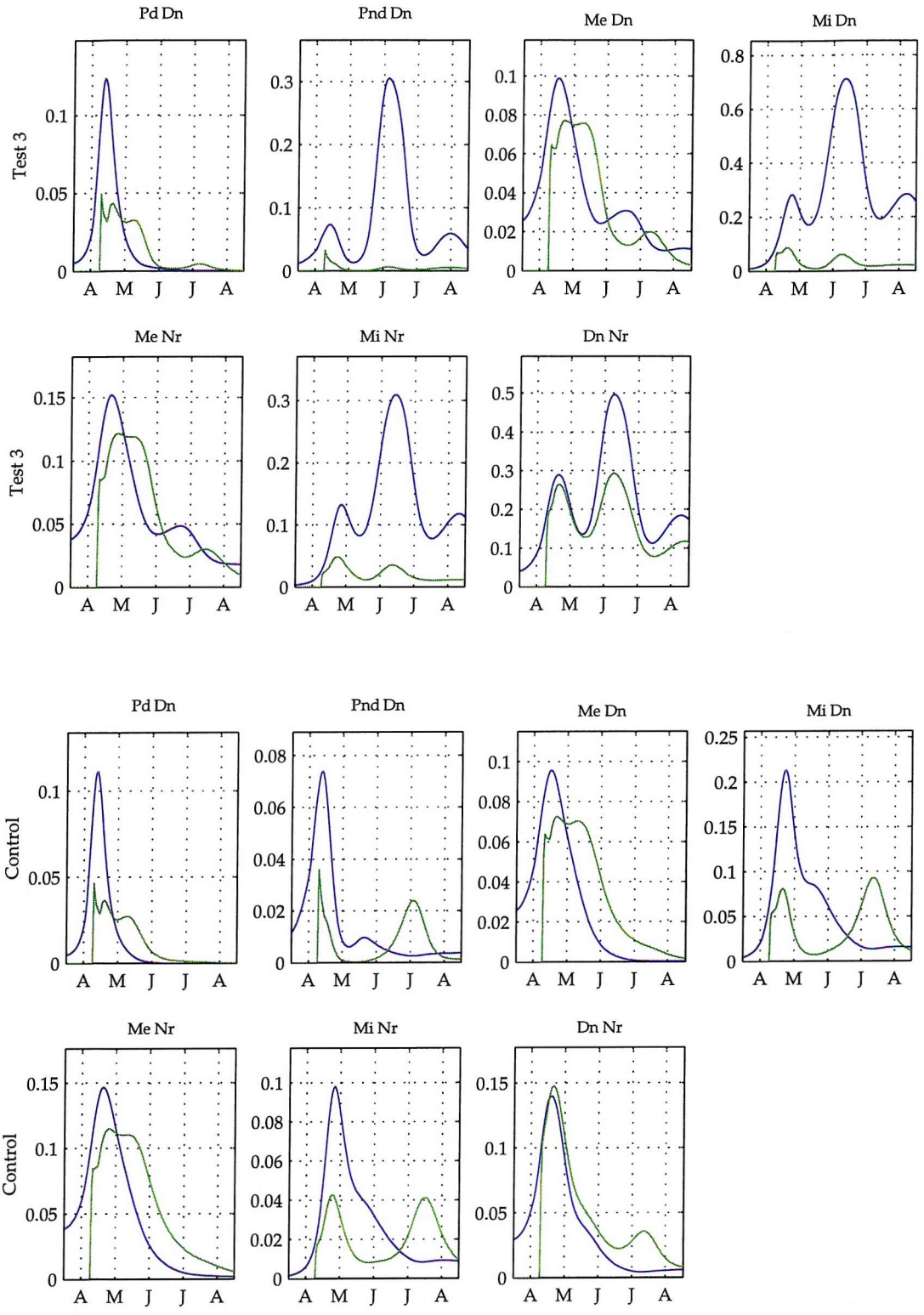

Figure 8.6: Phytoplankton and zooplankton contribution to detrital nitrogen as well as zooplankton contribution to ammonium and detrital nitrogen remineralisation rate corresponding to the control run and test 3. Values in the mixed layer (blue) and at the isopycnal corresponding to the depth of the subsurface maximum (green). Pd and Pnd represent diatoms and non-diatoms, Me and Mi are meso and microzoo, Dn is detrital nitrogen and Nr is ammonium. All units are mmol N m^{-3} d^{-1}.

In terms of size (figure 8.8), the fraction of non-diatom TPP increased in all cases (higher efficiency assimilating ammonium than diatoms) whereas, the fraction due to diatoms decreased compared to the control (due to the favourable light and nitrogen levels, non-diatom exerted higher pressure when diatoms were still present in the water column). An increase was also observed in both, new and regenerated PP, in the non-diatom case opposed to diatoms (figure 8.8) .

Both phytoplankton *f* ratios reflect the changes seen in the patterns of PP. Diatoms *f* ratio always decreased compared to the control (following a reduction in TRP and TNP), whereas non-diatom *f* ratio was lower than the control only in 2 out of 5 cases (when the highest δ_1 were used). From these results can be concluded that, as expected, the ecosystem is most sensitive to high δ_1 values. Maximum total chlorophyll and diatoms were insensitive to δ_1 variations whereas non-diatoms and ammonium showed the highest sensitivity (table 8.3).

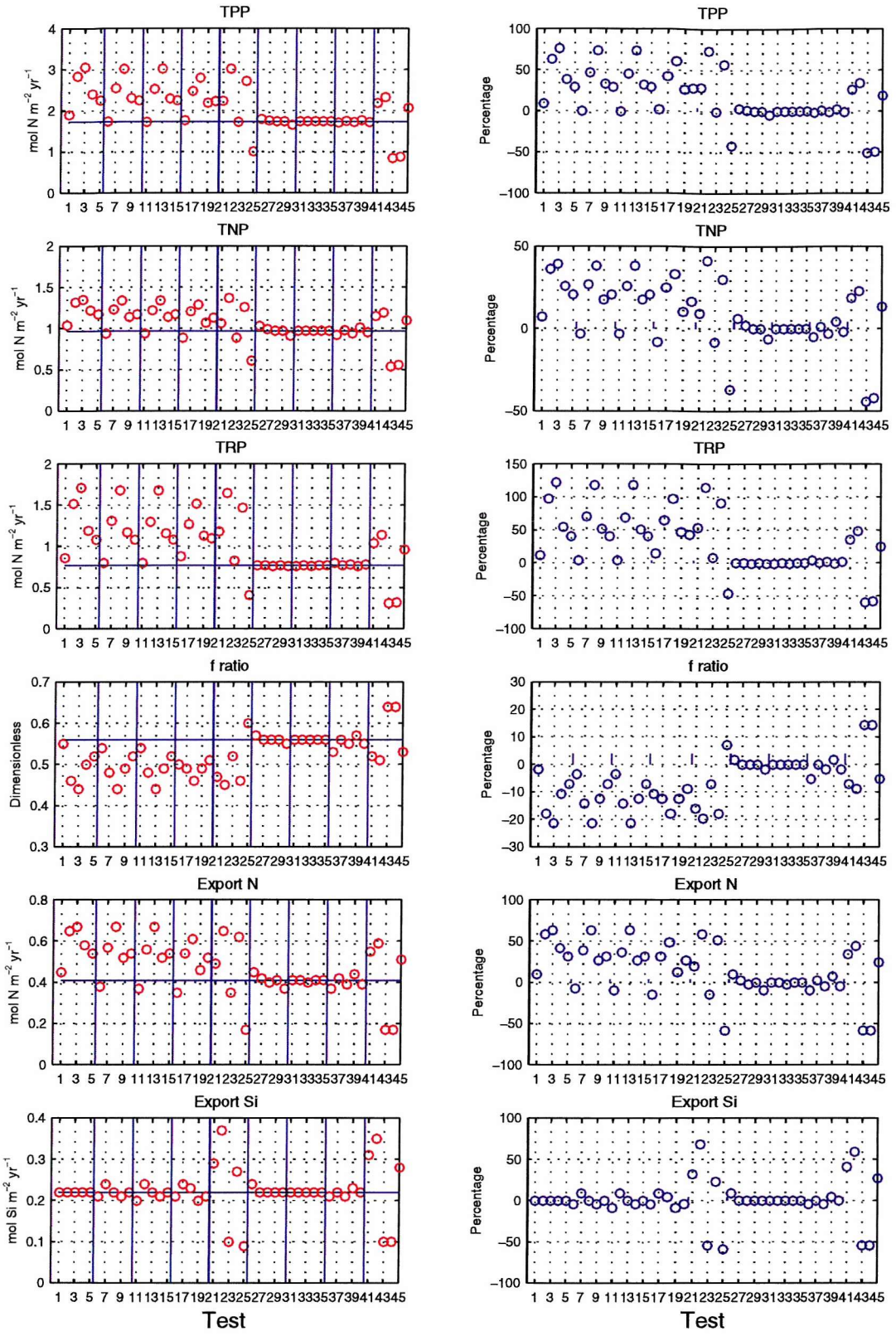

Figure 8.7: Variation in the total primary (TPP), new (TNP) and regenerated (TRP) production as well as *f* ratio in the mixed layer. The last four plots show nitrate and silicate-based export production at the base of the mixed layer. The left and right columns represent magnitude changes and percentage of change relative to the control. Test 1 to 5 and 26 to 45 show the effects when one single parameter was changed at a time. The rest of the tests represent different parameter combinations as stated in table 8.2. The horizontal blue line shows the control value. Results correspond to 1989.

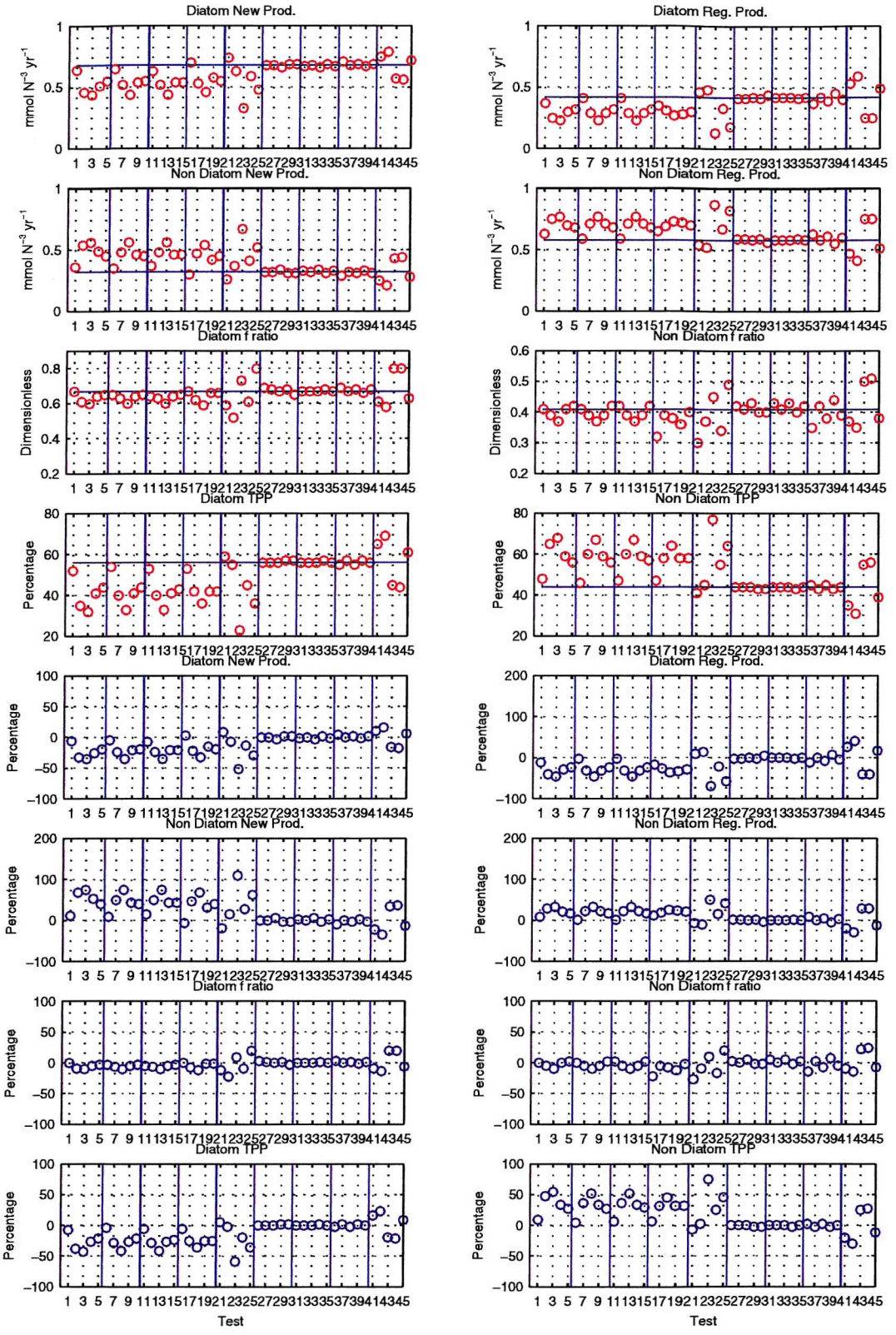

Figure 8.8: Variation in the annual size-fractionated total primary (TPP), new (TNP) and regenerated (TRP) production as well as *f* ratio in the mixed layer. Test 1 to 5 and 26 to 45 show the effects when one single parameter was changed at a time. The rest of the tests represent different parameter combinations as stated in table 8.2. Top 8 plots represent magnitude changes and the last 8 plots are percentage of change relative to the control run. The horizontal blue line shows the control value. Results correspond to 1989.

- **Non-diatom initial slope of the P-I curve (α_1)**

The initial slope of the P-I curve was varied between 0.010 and 0.023 ly^{-1}, around 43% lower and 51% higher than the control value (0.015 ly^{-1}), corresponding to tests 26 to 30 (table 8.2). Higher non-diatom biomass would be expected when α_1 is increased (tests 28 and 30) and lower biomass otherwise (tests 26, 27 and 29). Although model results showed little change in the biomass of both phytoplankton groups, diatoms suffered the greater changes (a reduction of 15% compared to the control). Diatom biomass showed a variation that is inverse proportional to α_1 changes, as expected, but the effects on non-diatoms were not as clear. In fact, the highest non-diatom biomass was achieved when the maximum reduction in α_1 (43%) was used. Generally, higher α_1 led to higher non-diatoms biomass (up to 4% as they become better light competitors) and diatoms biomass decreased (15%). On the other hand, when the lowest α_1 was used (test 26), diatoms biomass was higher (10%) and so was non-diatoms (9%) due to the greater role of remineralisation and regeneration processes, as the large food chain operates in the system.

Diatoms accounted for the highest biomass in the mixed layer (between 2.03 and 2.64 mmol N m^{-3}) in all cases (figure 8.3). Maximum surface non-diatom biomass varied between 1.33 and 1.55 mmol N m^{-3}. As in the previous case, very little changes in terms of total chlorophyll were observed (up to 8% compared to the control). Maximum chlorophyll (4.51 mg chl m^{-3}) coincided with the highest ammonium concentration in the water column (2.01 mmol N m^{-3}) and the lowest non-diatom light efficiency (test 26).

Once more, no significant changes were observed in terms of annual primary production (4%), NP (7%), RP (2%) export production (7% and 10% for silicate and nitrogen-based,

respectively) or *f* ratio (2%), either when looking at total or size-fractionated changes (figures 8.7 and 8.8; table 8.3).

In all cases, a diatom and a non-diatom subsurface maximum were observed at times and depths seen in the control case. The former always occurred in mid May and reached between 1.01-1.21 mmol N m^{-3} while the latter was observed in mid July and varied between 0.77-0.84 mmol N m^{-3}.

- **Non-diatom half-saturation constant for nitrate uptake (K_1)**

K_1 was modified between 0.570 and 0.923 mmol N m^{-3}, between 26% lower and 20% higher than the control value (0.772 mmol N m^{-3}), corresponding to tests 31 to 35 (tables 8.2 and 8.3). Model results showed no significant effect on the maximum biomass reached by either phytoplankton group (2%) or on the total chlorophyll (1%) and ammonium pools (3%). In terms of annual primary and export production, either total (<2%) or size-fractionated (<4%), showed no sensitivity. Slight increases in the non-diatom *f* ratio were observed (up to 4%) when lower K_1 were used (figure 8.8).

Once more, a diatom and a non-diatom subsurface maximum were observed at the same times and depths, and for the same reasons, described earlier. Maximum subsurface values ranged from 0.79 to 0.84 mmol N m^{-3} in the non-diatom case, while diatoms subsurface maximum was 1.19 mmol N m^{-3} in all cases.

- **Non-diatom half-saturation constant for ammonium uptake (K_2)**

K_2 values were modified between 0.179 and 0.567 mmol N m^{-3}, that is 53% lower and 47% higher than the control value (0.385 mmol N m^{-3}), corresponding to tests 36 to 40 (tables 8.2 and 8.3). Higher K_2 (tests 37 and 39) would be expected to produce lower non-diatom maxima (as they are mainly supported by ammonium; figure 8.2). Lower K_2

(tests 36, 38 and 40), therefore more efficient ammonium uptake by non-diatoms, are expected to simulate higher non-diatom maxima. However, model results showed the opposite trend. Higher non-diatom biomass was observed when K_2 was high and up to 23% reduction in non-diatom biomass was observed when K_2 was low. Why? The reason lies in the diatom behaviour. When non-diatom ammonium uptake is low (K_2 is high), diatoms are able to take more nitrogen up and therefore, they are able to reach higher biomass and so are mesozooplankton. As the large food chain operates in the ecosystem, regeneration processes take place and ammonium accumulates in the mixed layer and below it, where supply is greater than demand. Even more, due to nitrification processes, nitrate will also reach higher concentrations, and once the diatom bloom has decayed, non-diatoms grow in an environment richer in nitrogen, therefore reaching higher biomass than when their efficiency regarding ammonium was higher.

On the other hand, when non-diatom ammonium uptake is high (K_2 is low), diatoms nitrogen uptake is reduced (compared to the previous case) and so is the magnitude of regenerated nutrients in the water column, therefore non-diatom biomass is lower as less regenerated ammonium and also nitrate (due to nitrification) are available.

Once more, diatoms accounted for the highest biomass in the mixed layer and most of the total chlorophyll. High K_2 led to the highest total chlorophyll (4.44 mg m^{-3}), ammonium (1.99 mmol N m^{-3}) and phytoplankton biomass (2.49 and 1.63 mmol N m^{-3} for diatoms and non-diatoms, respectively). Although the 1-D model showed greater sensitivity than in the previous case, changes in the state variables biomass or concentration was less than 30% in all cases (see table 8.3 and figure 8.3).

TPP, NP, RP, NBEP and SBEP shown little sensitivity to changes in K_2 (<10%). Slightly stronger effects were observed when size-fractionated production was considered. As

expected, lower K_2, gave rise to the non-diatom RP (9%) but produced less (9%) NP (diatoms showed the opposite trend), whereas higher K_2 caused the opposite effect (figures 8.7 and 8.8). Non-diatoms *f* ratio decreased by 16% (table 8.3 and figures 8.7 and 8.8).

Subsurface diatom and non-diatom maxima were observed in all cases at the same times and depths described earlier. Higher K_2 (less efficient ammonium uptake by non-diatoms) led to slightly less intense maxima (from 0.82 to 0.74 mmol N m^{-3}).

- **Detrital silicate remineralisation rate (δ_2)**

Minimum and maximum δ_2 values were 0.024 and 0.074 d^{-1}, which corresponds to 53% lower and 42% higher than the control value (0.052 d^{-1}); see tests 41 to 45 and tables 8.1 and 8.2. As expected, model results showed that higher δ_2 (tests 41, 42 and 45) led to higher silicate concentrations and therefore, higher diatom maxima (up to 85%), chlorophyll (45%) and ammonium (50%) but lower non-diatom maxima (24%). The opposite response was observed when δ_2 was reduced (tests 43 and 44).

Diatoms accounted for the maximum biomass in 3 out of 5 cases (figure 8.3). When δ_2 was higher than the control value, the highest diatom biomass was observed (4.45 mmol N m^{-3} in test 42), as well as the highest chlorophyll (6.08 mmol N m^{-3}) and ammonium concentration (2.75 mmol N m^{-3}). The lowest diatom biomass was below 1 mmol N m^{-3} (tests 43 and 44). Less dramatic effects were observed for non-diatoms, and their maximum biomass was always below the control value (highest value was 1.23 mmol N m^{-3} in test 45). For the same reasons explained earlier, an increase in the non-diatom biomass could be expected due to the higher relevance of excretion, remineralisation and nitrification processes that accompanied diatoms growth. However, diatoms consume

more nitrate and ammonium than previously as they are less limited by silicate, leaving less nutrients available for small phytoplankton. Overall, the impact on non-diatoms is small.

As usual, a DSM was observed in all cases. A non-diatom subsurface maximum (NDSM) occurred in 3 out of 5 cases, when the highest δ_2 were used (tests 41, 42 and 45). Why? Because as diatoms remove more nitrogen from the mixed layer, ammonium and nitrate are increased below it. As the mixed layer reached its shallowest point, better light regimes allowed non-diatoms to develop below the mixed layer, where nitrate and ammonium had not been exhausted.

Modification of δ_2 had an important effect on primary and export production. As expected, lower δ_2 led to less TPP (51%), TNP (44%), TRP (60%), NBEP (56%) and SBEP (60%) and to a higher annual *f* ratio (14%).

Remarks

In general, δ_2 generated the most significant changes in the dynamics of the biological ecosystem, followed by δ_1 and K_2. Caution is needed when interpreting these results as parameter variation was not symmetrical about the prior.

In similar circumstances -increases in δ_1 and δ_2 by less than 20% (test 1 and 45) and 50% (tests 5 and 42)-, δ_2 caused significantly higher changes in phytoplankton biomass, chlorophyll, ammonium, PP and export production (table 8.3). Similar changes in K_1 (20% increase; test 34) had the same effect that δ_1 (except for ammonium, which was more heavily affected by δ_1). When α_1 and K_2 were modified by 50% (tests 28 and 39), the former had very little effect on state variables or production while the latter showed model sensitivity equivalent to changes in δ_1 regarding phytoplankton biomass; modelled

ammonium was more sensitive to δ_1 than to K_2 as well as primary production, *f* ratio and NBEP. However, SBEP was more sensitive to K_2 than to δ_1. A similar decrease in K_1 and K_2 (27%; tests 33 and 36), showed a moderate, although slightly higher, model sensitivity to the latter (table 8.3).

Overall, when the limit effect of low nitrogen concentrations is eased by increasing δ_1, the total primary production of the model rises above that of the control run. However, the increase in total chlorophyll and diatom biomass is very small (3% and 5%, respectively for a 180% increase of δ_1), which highlights the significant role played by silicate limitation in the ecosystem. A higher impact was observed in terms of non-diatom biomass, as it increases by 122% under the same circumstances.

The presence/absence of a subsurface non-diatom maximum is also affected by those remineralisation rates, as they will determine the vertical distribution of nutrients, controlling the degree of oligotrophy in the mixed layer. Oligotrophy (silicate for diatoms and nitrogen for non-diatoms) is the main driving force leading to the development of deep phytoplankton maxima. In all cases, a diatom subsurface bloom was observed but the occurrence of a second one was exclusively related to the highest nitrogen remineralisation rates. An interesting result is the influence of δ_2 on the ammonium and nitrate vertical concentrations. When the limiting effect of low silicate is reinforced by decreasing δ_2, the PP and export production of the model dramatically fall below the control run (by up to 59%) as so do the rest of the variables considered apart from non-diatoms (table 8.3). In this case, diatom highest biomass barely reached above 0.80 mmol N m^{-3}, having important consequences in terms of detritus and ammonium, whose concentrations also reached a low point.

Generally, the model showed, for all variables:

- no significant sensitivity (<12%) to small δ_1 changes (+15% of the prior; test 1)
- no significant sensitivity (<15%) to any changes in α_1 (tests 26-30), K_1 (tests 31-35).
- no significant sensitivity (<15%) to relatively high changes in K_2 (±50% of the prior; tests 37-40) although high K_2 led to slightly less intense maxima.
- significant sensitivity (up to 40%) to small δ_2 changes (+19% of the prior; test 45).

The SA shows the relevance of diatoms in the ecosystem. Small phytoplankton benefited from their presence as the larger food chain injects ammonium and detritus in the system, *via* excretion and regeneration processes, which exerted a positive feedback on non-diatoms. Due to this feedback, an antagonist effect was observed when α_1 and K_2 were modified, as what look like physiologically disadvantages (reduced light and ammonium efficiency) led to higher population growth and ecosystem production.

Parameter combination

- δ_1 and α_1

Tests 6 to 10 were performed in order to asses the effect of combinations of both parameters in the model output (tables 8.2 and 8.3). Such effects were classified as "nonergic", synergic, and antagonist. The term "nonergic" refers to the interaction between two or more parameters producing a lower effect compared to their separate effects. Synergic refers to an interaction that produces an enhanced effect compared to the individual effect of each parameter, while an antagonistic effect refers to an effect in the opposite direction (increase *versus* decrease).

This parameter combination did not have much effect on diatoms and total chlorophyll. Non-diatoms and ammonium showed significant sensitivity (changes ≥30%) in 3 out of 5 cases, as when only δ_1 was modified. In all cases, a nonergic effect was observed, apart

from test 9 (high δ_1 and α_1), which had a synergic effect on ammonium (table 8.3). In terms of primary and export production, most cases showed similar effects to those obtained when only δ_1 was modified (table 8.3), although there were exceptions regarding TNP (test 7) and NBEP (test 9). TNP and NBEP sensitivity to δ_1 was reduced compared to its counterpart when only δ_1 was modified, and showed moderate sensitivity (27%) to the parameters interaction. In general, the experiments showed nonergic effects that were not significant compared to when only δ_1 was modified, apart from ammonium (synergic).

Model results showed the occurrence of a non-diatom subsurface maximum (NDSM) in 3 out of 5 cases (tests 6, 9 and 10), which is one more than observed when δ_1 was the only parameter modified. This subsurface maximum is triggered by low nitrate in the surface layers (when non-diatom efficiency to light has been increased) as model tests 6, 9 and 10 correspond to the lowest δ_1 and the highest α_1. The non-diatom subsurface maxima always occurred in mid July and their magnitude seem to vary proportionally to light efficiency and inversely proportional to the nitrogen remineralisation rate. The usual DSM is observed in May as when only δ_1 was modified.

Higher surface phytoplankton maxima occurred when the model was forced by the highest δ_1, therefore generating higher nitrogen concentrations in the water column (tests 7 and 8). Diatoms accounted for the highest biomass (between 2.07 and 2.72 mmol N m^{-3}) in all cases but in test 8 (highest δ_1 of this set), when non-diatoms reached 2.69 mmol N m^{-3}. Highest ammonium is also observed in test 8 but maximum chlorophyll (4.6 mg chl m^{-3}) was obtained in tests 7 and 9 (medium to high δ_1).

- δ_1, α_1 and K_1

Compared to the previous case, K_1 (experiments 11 to 15) does not have a significant effect on the diatom (4%) and non-diatoms maximum biomass (5%), total chlorophyll (3%) or ammonium concentration (3%) or on the primary and export production (3%) or *f* ratio (1%). Subsurface maxima were observed as in the previous case.

- δ_1, α_1, K_1 and K_2

As in the previous section, K_2 shows no significant effect on phytoplankton, chlorophyll or ammonium dynamics in any case but when the lowest K_2 was used (test 16). A synergic effect was observed regarding diatom biomass (increasing by 21%) as a result of high non-diatom ammonium uptake efficiency. Same subsurface maxima as observed in previous cases. TPP and NBEP were less sensitive to changes in δ_1 when K_2 was decreased below the control values (tests 19 and 20; table 8.3).

- δ_1, α_1, K_1, K_2 and δ_2

The detritus silica remineralisation rate accounted for the greatest variation in diatom biomass and total chlorophyll and interestingly, had a significant effect on non-diatoms and ammonium. When these five parameters interacted (experiments 21 to 25), the greatest increase in diatom biomass and chlorophyll were observed (98% and 53% higher than the control and 85% and 43% higher than in the previous section) associated to the highest δ_2 (similarly, lowest biomass occurred when low δ_2 were used). The opposite effect was observed in the non-diatom case, as their biomass decreased between 8% and 57% when compared to individual changes in δ_1.

The lowest δ_2 produced 40% less TPP,TNP and TRP and around 60% less NBEP and SBEP but increased the *f* ratio by 7%. The highest δ_2 produced the opposite effect increasing TPP and TRP by up to 74% and 115%, respectively.

The model showed the occurrence of a NDSM in 3 out of 5 cases (test 21, 24 and 25) in mid July, as observed when the tandem δ_1 and α_1 was simultaneously tested. Earlier experiments performed by only changing δ_2, showed the occurrence of NDSM when the highest remineralisation rates were used (as in tests 21 and 24) but opposed to the new results obtained in test 25 (no NDSM observed in its counterpart test, 43). This result can be easily explained when looking at the ammonium concentration below the mixed layer. Tests 43 and 25 showed similar silicate and nitrate concentration above and below the mixed layer but they differed in the amount of ammonium in the water column. Test 25 used a similar α_1 but a higher δ_1 than test 43, which allows for higher ammonium in the system (0.82 versus 0.58 mmol N m^{-3}). Due to high nitrate limitation, non-diatoms were unable to thrive in the mixed layer but they could develop right below it, supported by the relatively high modelled ammonium concentration in test 25 compared to test 43. Same subsurface maxima as observed in previous cases.

Remarks

Parameter combination confirmed that the 1-D model is most sensitive to individual variations in δ_2, followed by δ_1 and also to the interaction between them both. This is hardly surprising and can be attributed to the influence of both parameters on regeneration processes affecting the vertical profile of nutrients. Therefore, these results might be construed as an indication that silicate and nitrogen play a more crucial role than light not only in terms of peak biomass but also onset of the bloom and presence/absence of subsurface chlorophyll maxima.

The formation of the deep chlorophyll maximum (DCM) was simulated in all the experiments. The DCM develops as a consequence of nitrogen (non-diatoms) or silicate (diatoms) limitation in the mixed layer. In all cases, a diatom deep maximum was developed as a consequence of silicate limitation in the mixed layer. In several cases, a non-diatom deep maximum was also observed when nitrogen limitation in the mixed layer was severe as the lowest δ_1 were used. The hypothesis of nutrient limitation explains all the results obtained in the SA and also coincides with previous modelling studies (Jamart *et al.*, 1979).

Model results also highlighted the need of further investigation of detrital remineralisation rates, specially the poorly known silicate detrital breakdown rate. Due to the highly variable results obtained when they were modified, this work can only suggest model tuning and validation (using independent sets of field data, when possible, or subsets of the same data set) as the only tool to give confidence in simulated results (as done in chapter 6).

The remaining parameter subset (α_1 , K_1 and K_2) had a negligible effect on either state variables, primary and export production or *f* ratio. As a general trend, interaction amongst parameters produced a model output that accounted for less variation than obtained by adding independent parameter effects together (nonergy) with the exception of δ_1 and δ_2 (synergy).

Table 8.1: Model parameters object of the SA corresponding to the control run.

Parameter	Lower	Upper	*Prior*	Random parameter values
Detrital nitrogen breakdown rate (δ_1)	0.000	0.300	0.107	$\{\delta_{11},\ldots, \delta_{15}\}$ = {0.253, 0.123, 0.182, 0.299, 0.161}
Slope of the P-I curve (α_1)	0.000	0.200	0.015	$\{\alpha_{11},\ldots, \alpha_{15}\}$ = {0.010, 0.014, 0.023, 0.016, 0.021}
Nitrate uptake ½ sat. constant (K_1)	0.050	1.000	0.772	$\{K_{11},\ldots, K_{15}\}$ = {0.598, 0.774, 0.570, 0.923, 0.707}
Ammonium uptake ½ sat. constant (K_2)	0.010	1.000	0.385	$\{K_{21}, \ldots, K_{25}\}$ = {0.179, 0.418, 0.250, 0.567, 0.282}
Detrital silicate breakdown rate (δ_2)	0.000	0.300	0.052	$\{\delta_{21},\ldots, \delta_{25}\}$ = {0.067, 0.074, 0.024, 0.027, 0.062}

Table 8.2: Sampling combinations obtained using the Latin Hypercube Method (LHM)

Test	Nitrogen break. rate	Slope P-I curve	Nitrate uptake ½ sat. constant	Ammonium uptake ½ sat. constant	Silicate break. rate
1	δ_{12}				
2	δ_{11}				
3	δ_{14}				
4	δ_{13}				
5	δ_{15}				
6	δ_{12}	α_{13}			
7	δ_{11}	α_{11}			
8	δ_{14}	α_{12}			
9	δ_{13}	α_{15}			
10	δ_{15}	α_{14}			
11	δ_{12}	α_{13}	K_{11}		
12	δ_{11}	α_{11}	K_{14}		
13	δ_{14}	α_{12}	K_{12}		
14	δ_{13}	α_{15}	K_{15}		
15	δ_{15}	α_{14}	K_{13}		
16	δ_{12}	α_{13}	K_{11}	K_{21}	
17	δ_{11}	α_{11}	K_{14}	K_{22}	
18	δ_{14}	α_{12}	K_{12}	K_{24}	
19	δ_{13}	α_{15}	K_{15}	K_{23}	
20	δ_{15}	α_{14}	K_{13}	K_{25}	
21	δ_{12}	α_{13}	K_{11}	K_{21}	δ_{21}
22	δ_{11}	α_{11}	K_{14}	K_{22}	δ_{22}
23	δ_{14}	α_{12}	K_{12}	K_{24}	δ_{24}
24	δ_{13}	α_{15}	K_{15}	K_{23}	δ_{25}
25	δ_{15}	α_{14}	K_{13}	K_{25}	δ_{23}
26		α_{11}			
27		α_{12}			
28		α_{13}			
29		α_{14}			
30		α_{15}			
31			K_{11}		
32			K_{14}		
33			K_{12}		
34			K_{15}		
35			K_{13}		
36				K_{21}	
37				K_{22}	
38				K_{23}	
39				K_{24}	
40				K_{25}	
41					δ_{21}
42					δ_{22}
43					δ_{23}
44					δ_{24}
45					δ_{25}

Table 8.3: Percentage of change in the values of maximum diatom and non-diatom biomass, total chlorophyll and ammonium in the water column as well as total primary production (TPP), new (TNP) and regenerated (TRP) production and *f* ratio in the mixed layer and silicate and nitrogen-based production at the base of the mixed layer. Bold numbers reflect changes higher or equal to ±30%.

Test	Max. Diatoms	Max. non-diatoms	Max. Tot. Chl	Max. amm	TPP	TNP	TRP	*f* ratio	Export Silicate	Export Nitrogen
1	2	0	1	14	9	7	12	-2	0	10
2	5	**93**	3	**50**	**63**	**36**	**98**	-17	-1	**59**
3	5	**103**	3	**72**	**76**	**39**	**122**	-21	0	**65**
4	4	**44**	2	**30**	**38**	25	**55**	-10	-1	**41**
5	3	14	1	26	29	20	**41**	-7	0	**32**
6	-14	15	-3	-6	0	-4	5	-4	-7	-8
7	13	**71**	10	**42**	**46**	27	**71**	-13	6	**38**
8	7	**89**	0	**64**	**73**	**37**	**119**	-21	1	**62**
9	-5	**37**	10	**50**	**33**	17	**52**	-12	-5	26
10	4	15	1	25	29	20	**41**	-7	0	**32**
11	-18	13	-6	-9	0	-4	4	-3	-9	-9
12	13	**68**	10	**42**	**45**	26	**70**	-13	6	**36**
13	7	**89**	0	**64**	**73**	**37**	**119**	-21	1	**62**
14	-5	**37**	10	**50**	**32**	17	**51**	-11	-6	26
15	3	20	0	23	29	20	**41**	-7	-1	**32**
16	**-30**	1	-19	-25	2	-8	14	-10	-7	-14
17	13	**66**	10	**42**	**42**	24	**66**	-13	7	**33**
18	8	**87**	7	**45**	**61**	**32**	**98**	-18	4	**49**
19	-7	**35**	8	**46**	26	10	**47**	-13	-10	12
20	2	8	-5	19	28	16	**43**	-9	-4	27
21	25	5	17	14	29	9	**53**	-15	**31**	19
22	**98**	**69**	**53**	**95**	**74**	**41**	**115**	-19	**66**	**58**
23	**-64**	**46**	**-23**	9	-1	-8	9	-8	**-53**	-16
24	29	**30**	29	**74**	**57**	29	**91**	-17	20	**50**
25	**-75**	6	**-48**	**-54**	**-42**	**-37**	**-47**	7	**-60**	**-58**
26	10	9	7	10	4	6	1	2	7	9
27	3	-6	0	2	1	1	1	0	1	2
28	-2	0	-1	-3	0	0	-1	0	-2	-1
29	1	0	1	2	0	0	0	0	1	1
30	-15	4	-8	-19	-4	-7	-2	-2	-2	-10
31	-2	0	-1	-2	0	0	-1	0	-2	-1
32	0	0	0	0	0	0	0	0	0	0
33	-2	0	-1	-3	0	0	-1	0	-2	-1
34	1	0	1	2	0	0	0	0	1	1
35	0	0	0	-1	0	0	0	0	-1	0
36	-9	-23	-15	-18	-2	-6	4	-4	-5	-9
37	1	3	2	2	0	1	0	0	1	1
38	-5	-15	-9	-11	-1	-4	2	-2	-3	-6
39	4	15	6	9	2	4	-1	2	4	7
40	-3	-11	-6	-8	-1	-3	1	-2	-3	-4
41	**60**	-19	**30**	**37**	26	18	**36**	-6	42	34
42	**85**	-24	**45**	**50**	**34**	22	**48**	-9	**60**	43
43	**-76**	-15	**-53**	**-68**	**-51**	**-44**	**-60**	14	**-56**	**-59**
44	**-69**	-17	**-50**	**-65**	**-50**	**-43**	**-59**	14	**-55**	**-58**
45	**40**	-13	20	25	19	13	25	-4	29	25

Chapter 9:

Conclusions

Chapter 9: Conclusions

9.1 Introduction

A thorough discussion and a list of the key points found in this study has already been presented in each of the previous chapters. However, a summary of the main conclusions will be presented here.

9.2 Main conclusions

This study demonstrates that:

- a 0-D, size-dependent ecosystem model is able to successfully reproduce the seasonal cycle of different phytoplankton and zooplankton groups as well as nutrients and primary production patterns in the North Atlantic at 47°N 20°W, as described in field data. The complexity of the model is a key element in reproducing the double chlorophyll and primary production peaks found in NABE data in both, 0-D and 1-D models.

- non-linear optimisation techniques can successfully be applied to fit model results to observations, even when the ecological model is highly complex (the parameter space studied comprised 32 dimensions).

  However, it was not possible to find a unique parameter set that would give a good fit to all observations probably due to poor data constraints (as, for instance, ammonium and zooplankton NABE data shown high variability) and to model formulation (e.g. high correlation existed between parameters describing light-based phytoplankton growth).

- twin experiments can be successfully employed to determine the best sampling strategy needed to fully capture the seasonal variability of the ecosystem as well as the type and frequency of measurements needed, and therefore could be applied to help design more effective data collection exercises (i.e. ship-based observations). Model results show, for example, that by intensively sampling the spring bloom, the data acquired are adequate to constrain the seasonal cycle.

- the ecosystem model was able to determine the response of plankton to changes in the physical forcing, when the model was embedded into a 1-D physical model.

  The 1-D model successfully reproduced the bloom timing and intensity found in the vertical set of NABE observations. Model estimates of nitrogen export (and *f* ratios) agreed well with particle export at the NABE site obtained by sediment traps.

- it is necessary to vertically resolve water column so as to be able to fully investigate the patterns in ecological behaviour, especially the onset of the spring phytoplankton bloom and the factors governing the development of the deep ammonium and chlorophyll maxima, related to realistic physical forcing and mixed layer development.

- the coupled model becomes unstable after running for 30 years. Model instabilities had never been noticed in either the physical or the biological model before (when independently run) and shorter model runs would not have revealed them either. Those instabilities could have been avoided by relaxing vertical profiles of nitrogen to known reference values (e. g. climatology). However, such techniques (whose use seem to be somehow extensive although not always mentioned in the literature) would not have solved the problem but hide it, also preventing the calculation of fluxes and the realistic interpretation of model results.

- the 1-D coupled-model showed the occurrence of, at least, one annual deep

chlorophyll maximum in spring/summer during the five-year period studied. The deep maximum is triggered by the lack of nutrients above the mixed layer when light is less limiting for phytoplankton. Primary production at the deep maximum mainly relied on ammonium, therefore being regenerated production (up to 79%).

A deep diatom maximum was observed every year, whereas deep non-diatom maxima were strongly restricted by the light field, only occurring when the shallowest mixed layer depths were observed. When a diatom and a non-diatom deep maximum were observed in the same year, the former always developed earlier than the latter as non-diatoms are less efficient than diatoms in terms of light.

The deep biomass maxima also end for different reasons in both cases. Mesozooplankton grazing is responsible for diatom deep maximum decay, whereas a combination of microzooplankton grazing and worsening light conditions caused the end of the non-diatom one.

- interannual variability studies shown that the initiation of the spring bloom depends on how the mixed layer stratifies, as fast stratification led to earlier bloom development than when stratification occurred at a slow pace.

  Summer mixing events influenced the patterns of mesozooplankton overwintering, as those events encourage mesozooplankton growth.

- it is also necessary to better determine critical parameters such as detrital breakdown rates, which determine the vertical distribution of nutrients such as nitrate and silicate, and the rate of organic matter exported to the deep ocean.

9.3 Future research

The need to develop ecosystem models that provide reliable ecological predictions is a key issue, if such models are expected to be employed in investigating feedback mechanisms between the ocean and the atmosphere at global scale. For this reason, testing the biogeochemical model structure as well as the parameters that rule physiological response is basic. For this reason, this study suggests the following lines of future work:

- The use of stochastic optimisation algorithms, such as simulated annealing (SAN) techniques, which might be potentially able to uniquely determine a parameter set which fits available observations, independently of the initial parameter guess.

- The application of artificial neural network (ANN) techniques combined with numerical models, when the dynamics of some of the modelled state variables are poorly known. ANN have shown a great capacity of fitting observations as well as producing reliable hindcasts (Barciela *et al.*, 1999) when applied to pelagic coastal ecosystems.

  The development of "hybrid models", in which variables such as micro and mesozooplankton would be treated as "black boxes", and therefore implemented using ANN techniques, would reduce the number of model parameters as well as undesirable parameter correlation. In those "hybrid models" better known variables (such as phytoplankton or nutrients) would be parameterised in the usual ODE fashion.

- Results obtained via Powell's optimisation technique, (see chapter 2) demonstrated that the best determined state variables (nitrate and silicate) were those for which a greater number of observations were available. For this reason, the assimilation of

ocean colour (derived chlorophyll) should help to improve model results. This study also highlighted the need of improvement in the number and quality of zooplankton measurements.

- It would be also desirable to test the model portability to other regions of the globe, such as, for instance, the Southern Ocean. However, the effect of iron limitation on phytoplankton growth would need to be included.

  A more ambitious project could embed the biogeochemical model into a GCM.

- The coupled model revealed the existence of numerical instabilities which might have developed for different reasons, amongst others, the combination of propagating round-off errors when using a leapfrog time stepping scheme and/or the inherent outcropping of the isopycnals in the mixed layer. The former problem could be investigated by implementing different time-stepping techniques and comparing the robustness of the model.

  Recent efforts have been made to develop HYCOM (Hybrid Co-ordinate Model; Megan, pers. comm.) based on the original work of Bleck and Boudra (1981). This is an isopycnal model which uses a layer model approach in the mixed layer (therefore improving vertical resolution) and could also help to solve numerical instabilities associated with isopycnal outcropping.

Bibliography

Bibliography

Anderson, T. R. (1993). A spectrally averaged model of light penetration and photosynthesis. Limnology and Oceanography, 38 (7), 1403-1419.

Antoine, D., J. M. André and A. Morel (1996). Oceanic primary production. 2. Estimation at global scale from satellite (coastal zone color scanner) chlorophyll. Global Biogeochemical Cycles, 10 (1), 57-69.

Archer, D. (1995). Upper ocean physics as relevant to ecosystem dynamics: a tutorial. Ecosystem Applications, 5(3), 724-739.

Archer, D. and E. Maier-Reimer (1994). Effect of deep-sea sedimentary calcite preservation on atmospheric CO_2 concentration. Nature, 367, 260-264.

Azam, F., T. Fenchel, J. G. Field, J. S. Gray, L. A. Meyer-Reil and F. Thingstad (1983). The ecological role of water-column microbes in the sea. Marine Ecology Progress Series, 10, 257-263.

Barciela R.M., E. Garcia and E. Fernandez (1999). Modelling primary production in a coastal embayment affected by upwelling using dynamic ecosystem models and artificial neural networks, Ecological Modelling, 120, 199-211.

Behrenfeld, M. J. and P. G. Falkowski (1997). Photosynthetic rates derived from satellite-based chlorophyll concentration. Limnology and Oceanography, 42(1), 1-20.

Berger, W. H. (1989). Global maps of ocean productivity. In: Productivity of the ocean: present and past. Berger, W. H., V. C. Smetacek and G. Wefer (Eds.). Chichester: Wiley-Interscience.

Bidle, K. D. and F. Azam (1999). Accelerated dissolution of diatom silica by marine bacterial assemblages. Nature, 397, 508-512.

Bienfang, P. and P. J. Harrison (1984). Sinking rate response of natural assemblages of temperate and subtropical phytoplankton to nutrient depletion. Marine Biology, 83, 293-300.

Bjørnsen, P. K. and Nielsen, T. G. (1991). Decimeter scale hetero-genity in the plankton during pycnocline bloom of *Gyyrodinium aureolum*. Marine Ecology Progress Series, 73: 263-267.

Bleck, R. (1978). Finite difference equations in general vertical coordinates. Contributions to Atmospheric Physics, 51, 360-372.

Bleck, R. and D. B. Boudra (1981). Initial testing of a numerical ocean circulation model using a hybrid (quasi-isopycnic) vertical coordinate. Journal of Physical Oceanography, 11, 755-770.

Bleck, R. and L. T. Smith. (1990). A wind-driven isopycnic coordinate model of the North and Equatorial Atlantic Ocean. 1.Model development and supporting experiments. Journal of Geophysical Research, 95, 3273-3285.

Bleck, R., C. Rooth, D. Hu and L. T. Smith (1992). Salinity-driven thermocline transients in a wind- and thermohaline- forced isopycnic coordinate model of the North Atlantic. Journal of Physical Oceanography, 22, 1486-1505.

Boyd, P. and P. Newton (1995). Evidence of the potential influence of planktonic community structure on the interannual variability of particulate organic carbon flux. Deep-Sea Research I, 42 (5), 619-639.

Boyd, P. W. and C. S. Law (2001). The Southern Ocean Iron RElease Experiment (SOIREE) - introduction and summary. Deep-Sea Research II, 48 (11-12), 2425-2438.

Brock, T. D. (1981). Calculating solar radiation for ecological studies. Ecological Modelling, 14, 1-19.

Buesseler, K. O., M. P. Bacon, J. K. Cochran and H. D. Livingston (1992). Carbon and nitrogen export during the JGOFS North Atlantic Bloom Experiment estimated from $^{234}Th:^{238}U$ disequilibria. Deep-Sea Research, 39, 1115-1137.

Burkill, P. H., E. S. Edwards, A. W. G. John and M. A. Sleigh (1993). Microzooplankton and their herbivorous activity in the northeastern Atlantic Ocean. Deep-Sea Research II, 40 (1/2), 479-493.

Bury, S. J., P. W. Boyd, T. Preston, G. Savidge and N. J. P. Owens (2001). Size-fractionated primary production and nitrogen uptake during a North Atlantic Phytoplankton Bloom: implications for carbon export estimates. Deep-Sea Research I, 48, 689-720.

Chipman, D. W., J. Marra, T. Takahashi (1993). Primary production at 47ºN and 20ºW in the North Atlantic Ocean: a comparison between the 14C incubation method and the mixed layer carbon budget. Deep-Sea Research II, 40(1/2), 151-169.

Cloern, J. E., C. Grenz and L. Videgar-Lucas (1995). An empirical model of the phytoplankton chlorophyll:carbon ratio - the conversion between productivity and growth. Limnology and Oceanography, 7, 1310-1313.

Cox, J. L.., P. H. Wiebe, P. Ortner and S. Boyd. (1982). Seasonal development of subsurface chlorophyll maxima in slope water and northern Sargasso Sea of the northwestern Atlantic Ocean. Biological Oceanography, 1(3), 271-285.

Cullen, J. J. and R. W. Eppley (1981). Chlorophyll maximum layers of the Southern California Bight and possible mechanisms of their formation and maintenance. Oceanologica Acta, 4, 23-62.

Daly, K. L. and W. O. Smith, Jr. (1993). Physical-biological interactions influencing marine plankton production. Annu. Rev. Ecol. Syst., 24, 555-585.

Dam H. G., C. A. Miller and S. H. Jonasdottir (1993). The trophic role of mesozooplankton at 47°N, 20°W during the North Atlantic Bloom Experiment. Deep-Sea Research II, 40 (1/2), 197-212.

Denman, K. L. and A. E. Gargett (1995). Biological-physical interactions in the upper ocean: the role of vertical and small scale transport processes. Annual Review of Fluid Mechanics, 27, 225-255.

Djurfeldt, L. (1994). The influence of physical factors on a subsurface chlorophyll maximum in an upwelling area. Estuarine, Coastal and Shelf Science, 39, 389-400.

Doney, S.C., D.M. Glover, and R.G. Najjar, 1996. A new coupled, one-dimensional biological-physical model for the upper ocean: applications to the JGOFS Bermuda Atlantic Time Series (BATS) site. Deep-Sea Research II, 43, 591-624.

Dortch, Q. (1987). The biochemical composition of plankton in a subsurface chlorophyll maximum. Deep-Sea Research, 34, 705-712.

Dortch, Q. (1990). The interaction between ammonium and nitrate uptake in phytoplankton. Marine Ecology Progress Series, 61, 183-201.

Drange, H. (1994). An isopycnic coordinate carbon cycle model for the North Atlantic and the posibility of disposing of fossil fuel CO_2 in the ocean. Ph.D. thesis, Nansen Environmental and Remote Sensing Center.

Droop, M. R. (1973). Some thoughts on nutrient limitation on algae. Journal of Phycology, 9, 264-272.

Ducklow, H., D. A. Purdie, P. J. Le B. Williams and J. M. Davies (1986). Bacterioplankton: a sink for carbon in a coastal marine plankton community. Science, 232, 865-867.

Ducklow, H. W., R. P. Harris (1993). Introduction to the JGOFS North Atlantic Bloom Experiment. Deep-Sea Research II, 40(1/2), 1-8.

Ducklow, H. W., D. L. Kirchman, H. L. Quinby, C. A. Carlson and H. G. Dam (1993). Stocks and dynamics of bacterioplankton carbon during the spring bloom in the eastern North Atlantic Ocean. . Deep-Sea Research II, 40 (1/2), 245-263.

Dudgale, R. C. and J. J. Goering. (1967). Uptake of new and regenerated forms of nitrogen in primary production. Limnology and Oceanography, 12, 196-206.

Dudgale, R. C., F. P. Wilkerson and H. J. Minas (1995). The role of a silicate pump in driving new production. Deep-Sea Research I, 42 (5), 697-719.

Eppley, R. W. and B. J. Peterson (1979). Particulate organic matter flux and planktonic new production in the deep ocean. Nature 282, 677-680.

Evans, G. T. (1999). The role of local models and data sets in the Joint Global Ocean Flux Study. Deep Sea Research I, 46, 1369-1389.

Evans, G. T. and J. S. Parslow. (1985). A model of annual plankton cycles. Biological Oceanography, 3, 327-347.

Falkowski, P., R. J. Scholes, E. Boyle, J. Canadell, D. Canfield, J. Elser, N. Gruber, K. Hibbard, P. Högber, S. Linder, F. T. Mackenzie, B. Moore III, T. Pedersen, Y. Rosenthal, S. Seitzinger, V. Smetacek and W. Steffen (2000). The global carbon cycle: a test of our knowledge of earth as a system. Science 290, 291-296.

Fasham, M. J. R., T. Platt, B. Irwin and K. Jones (1985). Factors affecting the spatial pattern of the deep chlorophyll maximum in the region of the Azores front. Progress in Oceanography, 14, 129-165.

Fasham, M. J. R., H. W. Ducklow and S. M. McKelvie. (1990). A nitrogen-based model of plankton dynamics in the oceanic mixed layer. Journal of Marine Research, 48, 591-639.

Fasham, M. J. R., J. R. Sarmiento, R. D. Slater, H. W. Ducklow and R. Williams. (1993). Ecosystem behavior at Bermuda Station S and Ocean Weather Station India: a general circulation model and observational analysis. Global Biochemical Cycles, 7, 379-415.

Fasham, M. J. R. (1995). Variations in the seasonal cycle of biological production in subartic oceans: a model sensitivity analysis. Deep-Sea Research I, 42(7), 1111-1149.

Fasham, M. J. R. and G. T. Evans. (1995). The use of optimization techniques to model marine ecosystem dynamics at the JGOFS station at 47° N 20° W. Philosophical Transactions of the Royal Society of London B, 348, 203-209.

Fasham, M. J. R. and G. T. Evans. (2000). Advances in ecosystem modelling within JGOFS. In: The changing ocean carbon cycle. A mid term synthesis of the Joint Global Ocean Flux Study. Hanson, R. B., H. W. Ducklow and J. G. Field (Eds.). Cambridge University Press, International Geosphere-Biosphere Programme. Book series 5.

Fennel, K., M. Losch, J. Schröter and M. Wenzel (2001). Testing a marine ecosystem model: sensitivity analysis and parameter optimization. Journal of Marine Systems, 28/1,45-63.

Field, C.B., M. J. Behrenfeld, J. T. Randerson and P. Falkowski. (1998). Primary production of the biosphere: integrating terrestrial and oceanic components. Science 281 (5374): 237-240.

Fleming, R. H. (1939). The control of diatom populations by grazing. J. Cons. perm. explor. Mer 14, 210-227.

Frost, B. W. (1984). Utilization of phytoplankton production in the surface layer. In: Global Ocean Flux Study Workshop. National Academy of Sciences, Washington, D. C.

Gadd, A. J. (1978). A split-explicit integration scheme for numerical weather prediction. Q. J. R. Meteorol. Soc., 104, 569-582.

Gargett, A. E. (1984). Vertical eddy diffusivity in the ocean interior. Journal of Marine Research, 42, 359-393.

Garside C. and J. C. Garside (1993). The "*f*-ratio" on 20ºW during the North Atlantic Bloom Experiment. Deep-Sea Research II, 40 (1/2), 75-90.

Gaspar, P. (1988). Modeling the seasonal cycle of the upper ocean. Journal of Physical Oceanography, 18, 161-180.

Gaspar, P., Y. Grégoris, J Lefevre (1990). A simple eddy kinetic energy model for simulations of the oceanic vertical mixing: Tests at station Papa and long-term upper ocean study. Journal of Geophysical Research, 95(c9), 16179-16193.

Geider, R. J., H. L. McIntyre and T. M. Kana (1997). A dynamic model of phytoplankton growth and acclimation: responses of the balanced growth rate and the chlorophyll *a*:carbon ratio to light, nutrient-limitation and temperature. Marine Ecology Progress Series, 148, 187-200.

Gershenfeld, N. (1999). The nature of mathematical modelling. Cambridge University Press, pp. 344.

Glover, D. M. and P. G. Brewer (1988). Estimates of winter time mixed layer nutrient concentrations in the North Atlantic. Deep-Sea Research, 35 (9), 1525-546.

Goldman, J. C. and D. A. Caron (1985). Experimental studies on an omnivorous microflagellate: implications for grazing and nutrient regeneration in the marine microbial food chain. Deep Sea Research, 32, 899-915.

Hannon, E., P. W. Boyd, M. Silvoso and C. Lancelot (2001). Modeling the bloom evolution and carbon flows during SOIREE: implications for future in situ iron-enrichments in the Southern Ocean. Deep-Sea Research II, 48, 2745-2773.

Harris, R. P. (1988). Interactions between diel vertical migratory behavior of marine zooplankton and the subsurface chlorophyll maximum. Bulletin of marine science, 43(3), 663-674.

Hooker, S. B. and W. E. Esaias (1993). An overview of the SeaWiFS project, EOS, Trans. AGU, 74, 241 and 245-246.

Hurtt, G. C. and R. A. Armstrong (1996). A pelagic ecosystem model calibrated with BATS data. Deep-Sea Research II, 43, 2/3, 653-683.

Jackson, G. A. (1995). TEP and coagulation during a mesocosm experiment. Deep-Sea Research II, 42, 215-222.

Jamart, B. M., D. F. Winter, K. Banse, G. C. Anderson and R. K. Lam (1977). A theoretical study of the phytoplankton growth and nutrient distribution in the Pacific Ocean off the northwestern U.S. coast. Deep-Sea Research, 24, 753-773.

Jamart, B. M., D. F. Winter and K. Banse (1979). Sensitivity analysis of a mathematical model of phytoplankton growth and nutrient distribution in the Pacific Ocean off the northwestern U.S. coast. Journal of Plankton Research, 1(3), 267-290.

Jawed, M. (1973). Ammonia excretion by zooplankton and its significance to primary productivity during summer. Marine Biology, 23, 115-120.

Joint, I., A. Pomroy, G. Savidge and P. Boyd (1993). Size-fractionated primary productivity in the northeast Atlantic in May-July 1989. Deep Sea Research II, 40 (1/2), 423-440.

Jones, R. and E. W. Henderson (1986). The dynamics of nutrient regeneration and simulation studies of the nutrient cycle. J. Conseil, 43, 216-236.

Kalnay, E., M. Kanamitsu, R. Kistler, W. Collins, D. Deaven, L. Gandin, M, Iredell, S. Saha, G. White, J. Woollen, Y. Zhu, M. Chelliah, W. Ebisuzaki, W. Higgins, J. Janowiak, K. C. Mao, C. Ropolewski, J. Wang, A. Leetmaa, R. Reynolds, R. Jenne

and D. Joseph (1996). The NCEP/NCAR 40-year reanalysis project. Bulletin of the American Meteorological Society, 77(3), 437-471.

Kamamiya, M., M. Kishi, Y. Yamanaka and N. Suginohara (1995). An ecological-physical coupled model applied to station Papa. Journal of Ocenaography, 51, 635-664.

Karl, D. M. and R. Lukas (1996). The Hawaii Ocean Time-series (HOT) program: Background, rationale and field implementation. Deep-Sea Research II, 43, 129-156.

Keller, M. D., W. K. Bellows and R. R. L. Guillard (1989). A survey of DMS production in twelve classes of marine phytoplankton, pages 167-182. In Saltzman and Cooper, editors. Biogenic sulfur in the environment. American Chemical Society, Washington, D.C.

Kiefer, D. A. and J. N. Kremer (1981). Origins of the vertical pattern of phytoplankton and nutrients in the temperate, open ocean: a stratigraphic hypothesis. Deep-Sea Research, 28, 1087-1105.

Killworth, P. D. (1999). Relaxation toward observations in level and isopycnic models. Journal of Atmospheric and Oceanic Technology, 16 (7), 983-986.

Killworth, P. D., D. A. Smeed and A. J. G. Nurser (2000). The effects on ocean models of relaxation toward observations at the surface. Journal of Physical Oceanography, 30 (1), 160-174.

Kiørboe, T. (1993). Turbulence, phytoplankton cell size, and the structure of pelagic food webs. Advances in Marine Biology, 29, 1-72.

Knauer, G. A. (1993). Productivity and new production of the oceanic system. In: Wollast, R. (ed.), Interactions of C, N, P and S Biogeochemical Cycles and Global Change. Springer-Verlag, Berlin, pp. 211-231.

Knox, F. and M. McElroy (1984). Change in atmospheric CO_2: influence of the marine biota at high latitude. Journal of Geophysical Research, 89, 4629-4637.

Kraus, E. B. and J. S. Turner (1967). A one-dimensional model of the seasonal thermocline. II. The general theory and its consequences. Tellus, 19, 98-105.

Kühn, W. and G. Radach (1997). A one-dimensional physical-biological model study of the pelagic nitrogen cycling during the spring bloom in the northern North Sea (FLEX'76). Journal of Marine Research, 55, 687-734.

Lampit, R. S., W. R. Hillier and P. G. Challenor (1993). Seasonal and diel variation in the open ocean concentration of marine snow aggregates (1993). Nature 362, 737-739.

Langlois, G. (1997). Miami Isopycnic Co-ordinate Model. User's manual: details of the numerical code. htpp://www.acl.lanl.gov/CHAMMP/micom.html.

Laws, E. A., P. G. Falkowski, W. O. Smith Jr., H. Ducklow, J. J. McCarthy (2000). Temperature effects on export production in the open ocean. Global Biogeochemical cycles, 14(4), 1231-1246.

Lawson, L. M., Y.H. Spitz, E. E. Hofmann, and R. B. Long (1995). A data assimilation technique applied to a predator-prey model. Bulletin of Mathematical Biology, 57(4), 593-617.

Lawson, L. M., E. E. Hofmann, and Y.H. Spitz (1996). Time series sampling and data assimilation in a simple marine ecosystem model. Deep-Sea Research II, 43(2-3), 625-651.

LeGroupe Tourbillion (1983). The Tourbillion experiment: a study of a mesoscale eddy in the eastern North Atlantic. Deep-Sea Research, 30, 475-511.

Lentz, J., A. Morales and J. Gunkel (1993). Mesozooplankton standing stock during the North Atlantic spring bloom study in 1989 with evaluation of its potential grazing pressure: a comparison between low, medium and high latitudes. Deep-Sea Research II, 40, 559-572.

Levitus, S. (1982). Climatological atlas of the world ocean. NOAA Professional paper 13, U. S. Govt. Printing Office.

Lisitzin, A. P. (1967). Basic relationships in distribution of modern siliceous sediments and their connection with climatic zonation. International Geology Review 9, 631-652; 842-863; 1114-1130.

Lochte, K. and O. Pfannkuche (1987). Cyclonic cold-core eddy in the eastern North Atlantic-II. Nutrients, phytoplankton and bacterioplankton. Marine Ecology Progress Series, 39, 153-164.

Lochte, K., H. W. Ducklow, M. J. R. Fasham and C. Stienen (1993). Plankton succesion and carbon cycling at 47ºN 20ºW during the JGOFS North Atlantic Bloom Experiment. Deep Sea Research II, 40 (1/2), 91-114.

Longhurst, A. R. and A. W. Herman (1982). Do oceanic zooplankton aggregate at, or near, the deep chlorophyll maximum?. Journal of Marine Research, 39, 353-356.

Longhurst, A., S. Sathyendranath, T. Platt and C. Cavehill (1995). An estimate of global primary production in the ocean from satellite radiometer data. Journal of Plankton Research, 17, 1245-1271.

Mann, K. H. and J. R. N. Lazier. (1991). Dynamics of marine ecosystems, biological-physical interactions in the oceans. Blackwell Scientific Publications, Boston, MA, 466 pp.

Margalef, R. (1978). Life-forms of phytoplankton as survival alternatives in an unstable environment. Oceanologica Acta, 1(4), 493-509.

Marra, J. and C. Ho (1993). Initiation of the spring bloom in the northeast Atlantic (47°N, 20° W): a numerical simulation. Deep-Sea Research II, 40(1/2), 55-73.

Martin, J. H., G. A. Knauer, D. M. Karl and W. W. Broenkow (1987). VERTEX: carbon cycling in the northeast Pacific. Deep-Sea Research, 34, 323.

Martin, J. H., S. E. Fitzwater, R. M. Gordon, C. N. Hunter and S. J. Tanner (1993). Iron, primary production and carbon-nitrogen flux studies during the North Atlantic Bloom Experiment. Deep-Sea Research, 40, 115-134.

Martin, A. P. (1999). One-dimensional plankton ecology model. SOC internal report.

Martin, A., K. J. Richards and M. J. R. Fasham (2001). Phytoplankton production and community structure in an unstable frontal region. Journal of marine systems 28, 65-89.

Matear, R. J. (1995). Parameter optimization and analysis of ecosystem models using simulated annealing: A case study at Station P. Journal of Marine Research, 53, 571-607.

McAllister, C. D. (1962). Data record, photosynthesis and chlorophyll a measurements at Ocean Weather Station P. July 1959 to November 1961. Manuscript Report Series, 126. Fisheries Research Board of Canada, 14 pp.

McClain, C. R., W. E. Esaias, G. C. Feldman, J. Elrod, D. Endres, J. Firestone, M. Darzi, R. Evans, and J. Brown (1990). Physical and biological processes in the North Atlantic during the first GARP global experiment. Journal of Geophysical Research, 95, 18027-18048.

McGuillicuddy Jr., D. J., J. J. McCarthy and A. R. Robinson (1995). Coupled physical and biological modeling of the spring bloom in the North Atlantic (I): model formulation and one dimensional bloom processes. Deep-Sea Research, 42(8), 1313-1357.

McKay, M. D., W. D. Conover and R. J. Beckham (1979). A comparison of the methods for selecting values of input variables in the analysis of output computer code. Technometrics, 21, 239-245.

Mellor, G. L. and T. Yamada (1982). Development of a turbulence closure model for geophysical fluid problems. Rev. Geophys. Space Phys., 20, 851-875.

Menzel, D. W. and J. H. Ryther (1960). The annual cycle of primary production in the Sargasso Sea off Bermuda. Deep-Sea Research, 6, 351-367.

Michaels, A. F., A. H. Knap, R. L. Dow, K. Gundersen , R. J. Johnson, J. Sorensen, A. Close, G. A. Knauer, S. E. Lohrenz, V. A. Asper, M. Tuel and R. Bidigare (1994). Seasonal pattern of ocean biogeochemistry at the U.S. JGOFS Bermuda Atlantic Time-series Study site. Deep-Sea Research I, 41, 1013-1038.

Mitchell, B. G., E. A. Brody, O. Holm-Hansen, C. McClain and J. Bishop. (1991). Light limitation of phytoplankton biomass and macronutrient utilization in the Southern Ocean. Limnology and Oceanography, 36, 1662-1677.

Mittelstaedt E. (1987). Cyclonic cold-core eddy in the eastern North Atlantic- I. Physical description. Marine Ecology Progress Series, 39, 145-152.

Moloney, C. L. and J. G. Field. (1991). The size-based dynamics of plankton food webs. I. A simulation model of carbon and nitrogen flows. Journal of Plankton Research, 13, 1003-1038.

Morales, C. E., A. Bedo, R. P. Harris and P. R. G. Tranter (1991). Grazing of copepod assemblages in the north-east Atlantic: the importance of the small size fraction. Journal of Plankton Research, 13, 455-472.

Niiler, P. P. and E. B. Kraus (1977). A one-dimensional model of the upper ocean. In: Modelling and prediction of the upper layers of the ocean. Pergamon Press.

Olesen, M. (1995). Comparison of the sedimentation of a diatom spring bloom and of a subsurface chlorophyll maximum. Marine Biology, 121, 541-547.

Ortner, P. B., P. H. Wieve and J. L. Cox (1980). Relationships between oceanic epizooplankton distributions of the seasonal deep chlorophyll maximum in the Northwestern Atlantic Ocean. Journal of Marine Research, 38, 507-531.

Oschlies, A. and V. Garçon (1998). Eddy-induced enhancement of primary production in a model of the North Atlantic Ocean. Nature, 266-269.

Oschlies, A. and V. Garçon (1999). And eddy-permitting coupled physical-biological model of the North Atlantic. Part I: Sensitivity to advection numerics and mixed layer physics. Global Biogeochemical Cycles, 13(1), 135-160.

Oschlies, A., W. Koeve and V. Garçon (2000). An eddy-permitting coupled physical-biological model of the North Atlantic. 2. Ecosystem dynamics and comparison with satellite and JGOFS local studies data. Global Biogeochemical Cycles, 14 (1), 499-523.

Parker, R. L. (1977). Understanding inverse theory. Ann. Rev. Earth Planet. Sci., 5, 35-64.

Peixoto, J.P. and A. H. .Ooit (1992). Physics of climate. New York: American Institute of Physics.

Pingree, R. D., P. R. Pugh, P. M. Holligan and G. R. Foster (1975). Summer phytoplankton blooms and red tides along tidal fronts in the approaches to the English Channel. Nature, 258, 672-677.

Pingree, R. D. (1978). Mixing and stabilization of phytoplankton distribution on the Northwest European continental shelf. In: Spatial patterns in plankton communities, edited by J. H. Steele, Plenum Press, New York, 181-220.

Platt, T., K. H. Mann, R. E. Ullanowich. (1981). Mathematical models in biological oceanography. Unesco Press. Monographs on oceanographic methodology. Paris. United Nations Educational, Scientific and Cultural Organization.

Pondaven, P., C. Fravalo, D. Ruiz-Pino, P. Treguer, B. Queguiner, C. Jeandel (1998). Modelling the silica pump in the permanently open ocean zone of the Southern Ocean. Journal of Marine Systems, 17, 587-619.

Pomeroy, L. R. and D. Deibel (1986). Temperature regulation of bacterial activity during the spring bloom in Newfound-land coastal waters. Science, 233, 359-361.

Press, W. H., S. A. Teukolsky, W. T. Vetterling and B. P. Flannery. (1992). Numerical Recipes in C. Cambridge University Press.

Price, J. R., A. Weller and J. Pinkel (1986). Diurnal cycling: observations and models of the upper ocean response to diurnal heating, cooling, and wind-mixing. Journal of Geophysical Research, 91, 8411-8427.

Prunet, P., J.-F. Minster, V. Echevin and I. Dadou (1996). Assimilation of surface data in a one-dimensional physical-biogeochemical model of the surface ocean. 2. Adjusting a simple trophic model to chlorophyll, temperature, nitrate, and pCO_2 data. Global Biogeochemical Cycles, 10(1), 139-158.

Radach, G., F. Carlotti and A. Spangenberg (1998). Annual weather variability and its influence on the population dynamics of *Calanus finmarchicus*. Fish. Oceanogr., 7 (3/4), 272-281.

Riley, G. A., H. Stommel and D. F. Bumpus. (1949). Quantitative ecology of the plankton of the Western North Atlantic. Bull. Bingham Oceanogr. Coll., 12, 1-169.

Robinson, M. K., R. A. Bauer and E. H. Schroeder (1979). Atlas of North Atlantic-Indian Ocean monthly mean temperatures and mean salinities at the surface layer. Naval Oceanographic Office NOO RP-18.

Robinson, A. R., D. J. McGillicuddy, J. Calman, H. W. Ducklow, M. J. R. Fasham, F. E. Hoge, W. G. Leslie, J. J. McCarthy, S. Podewski, D. L. Porter, G. Saure and J. A. Yoder. (1993). Mesoscale and upper ocean vaiability during the 1989 JGOFS bloom study. Deep Sea Research II, 40 (1/2), 9-35.

Ryther, J. H. (1969). Photosynthesis and fish production in the sea. Science, 166, 72-76.

Saltelli, A. (2000). What is sensitivity analysis. In: Sensitivity analysis, edited by A. Saltelli, A., K. Chan and E. M. Scott (2000). Wiley Series in probability and statistics, John Wiley & Sons, Ltd., England, 3-13.

Sarmiento, J. L. and J. R. Toggweiler, (1984). A new model for the role of the oceans in determining atmospheric pCO_2. Nature, 308, 621-624.

Sarmiento, J. L., R. D. Slater, M. J. R. Fasham, H. W. Ducklow, J. R. Toggweiler and G. T. Evans (1993). A seasonal three-dimensional ecosystem model of nitrogen cycling in the North Atlantic euphotic zone. Global Biogeochemical Cycles, 7(2), 417-450.

Sathyendranath, S., A. Longhurst, C. Caverhill and T. Platt (1995). Regionally and seasonally differentiated primary production in the North Atlantic. Deep-Sea Research I, 42 (10), 1773-1802.

Savidge, G., P. Boyd, A. Pomroy, D. Harbour and I. Joint (1995). Phytoplankton production and biomass estimates in the northeast Atlantic Ocean, May-June 1990. Deep-Sea Research I, 42(5), 599-617.

Schartau, M., A. Oschlies, and J. Willebrand (2001). Parameter estimates of a zero-dimensional ecosystem model applying the adjoint method. Deep-Sea Research II, 48, 1769-1800.

Schiebel, R., J. Waniek, M. Bork, and C. Hemleben (2001). Planktic foraminiferal production stimulated by chlorophyll redistribution and entrainment of nutrients. Deep-Sea Research I, 48, 721-740.

Siegenthaler U. and T. Wenk (1984). Rapid atmospheric CO_2 variations and ocean circulation. Nature, 308, 624-626.

Siegenthaler, U. and J. L. Sarmiento (1993). Atmospheric carbon dioxide in the ocean. Nature, 365, 119-125.

Sieracki, M. E., P. G. Verity and D. Stoecker. (1993). Plankton community response to sequential silicate and nitrate depletion during the 1989 North Atlantic Spring Bloom. Deep Sea Research II, 40 (1/2), 213-225.

Smetacek, V. (1999). Bacteria and silica cycling. Nature, 397, 475-476.

Spall, S. A. (1997). The impact of mesoscale jet activity on plankton heterogeneity and primary production; a numerical modelling study. Ph.D. thesis, University of Southampton.

Spall, S. A. and K. J. Richards (2000). A numerical model of mesoscale frontal instabilities and plankton dynamics- I. Model formulation and initial experiments. Deep-Sea Research I, 47, 1261-1301.

Spitz, Y.H., J. R. Moisan, M. R. Abbott and J. G. Richman (1998). Data assimilation and a pelagic ecosystem model: parameterization using time series observations. Journal of Marine Systems, 16, 51-68.

Steele, J. H. and C. S. Yentsch (1960). The vertical distribution of chlorophyll. J. Mar. Biol. Assoc. U.K., 39, 217-226.

Steele, J. H. (1964). A study of production in the Gulf of Mexico. Journal of Marine Research, 22, 211-221.

Steele, J. H. (1974). The structure of marine ecosystem. Harvard University Press, Cambridge.

Steele, J. H. and E. W. Henderson (1993). The significance of interannual variability. In: Towards a model of ocean biogeochemical processes. Evans, G. T. and M. J. R. Fasham (Eds.).: Towards a Model of Ocean Biogeochemical Processes, pages 237-260.Springer, Berlin.

Steeman Nielsen, E. and E. A. Jensen (1957). The autotrophic production of organic matter in the oceans. Galathea Rep., 1, 49-124.

Sverdrup, H. U. (1953). On conditions for the vernal blooming of phytoplankton. Journal du Conseil International d'Exploration de la Mer, 18, 287-295.

Tabata, S. and W. E. Weichselbaumer (1992). An update of the statistics of hydrographic/CTD data taken at Ocean Station P (May 1956-September 1990). Canadian Data Report of Hydrography and Ocean Sciences, Number 107, Institute of Ocean Sciences, Sydney BC, Canada, 75 pp.

Taylor, A.H., J.R.W. Harris and J. Aiken (1986). The interaction of physical and biological processes in a model of the vertical distribution of phytoplankton under stratification. Marine Interfaces Ecohydrodynamics, ed. by J.C.J. Nihoul, Elsevier Publs., p. 313-330.

Taylor, A.H. (1988). Characteristic properties of models for vertical distribution of phytoplankton under stratification. Ecological Modelling, 40, 175-199.

Taylor, A. H. and I. Joint (1990). A steady-state analysis of the 'microbial loop' in stratified systems. Marine Ecology Series Progress, 59, 1-17.

Taylor, A. H., D. S. Harbour, R. P. Harris, P. H. Burkill and E. S. Edwards. (1993). Seasonal succession in the pelagic ecosystem in the North Atlantic and the utilization of nitrogen. Journal of Plankton Research, 15, 875-891.

Taylor, A. H., Geider R. J. and F. J. H. Gilbert (1997). Seasonal and latitudinal dependencies of phytoplankton carbon-to-chlorophyll *a* ratios: results of a modelling study. Marine Ecology Progress Series, 152, 51-66.

Thacker, W. C. (1987). Three lectures on fitting numerical models to observations. No External report GKSS-Forschungszentrum Geesthacht, GmbHGeesthacht, Federal Republic of Germany.

Thacker, W. C. (1989). The role of the Hessian matrix in fitting models to measurements. Journal of Geophysical Research, 94, C5, 6177-6196.

Tziperman, E. and W. C. Thacker (1989). An optimal-control/adjoint-equations approach to studying the oceanic general circulation. Journal of Physical Oceanography, 19, 1471-1485.

Tukey, J. W. (1962). Ann. Math. Stat., Vol. 13, page 13.

Vallino, J. J. (2000). Improving marine ecosystem models: use of data assimilation and mesocosm experiments. Journal of Marine Research, 58, 117-164.

Varela, R. A., A. Cruzado, J. Tintore and E. C. Ladona (1992). Modelling the deep-chlorophyll maximum: a coupled physical-biological approach. Journal of Marine Research, 50, 441-463.

Verity, P. G., D. K. Stoecker, M. E. Sierachi and J. R. Nelson (1993). Grazing, growth and mortality of microzooplankton during the 1989 North Atlantic spring bloom at 47°N, 18° W. Deep-Sea Research I, 40(9), 1793-1814.

Vézina, A. F. and T. Platt. (1987). Small-scale variability of new production and particulate fluxes in the ocean. Canadian Journal of Fisheries and Aquatic Sciences, 44, 198-205.

Vézina, A. F. and T. Platt. (1988). Food web dynamics in the ocean. I. Best-estimates of flow networks using inverse methods. Marine Ecology Progress Series, 42(3), 269-287.

Waniek, J. (2002). The role of physical forcing in initiation of spring blooms in the Northeast Atlantic. *Submitted.*

Weeks, A., M.H. Conte, R. P. Harris, A. Bedo, I. Bellan, P. H. Burkill, E. S. Edwards, D. S. Harbour, H. Kennedy, C. Llewellyn, R. F. C. Mantoura, C. E. Morales, A. J. Pomroy and C. M. Turley (1993). The physical and chemical environment and changes in community structure associated with bloom evolution: the Joint Global Flux Study North Atlantic Bloom Experiment. Deep-Sea Research II, 40(1/2), 347-368.

Weeks, A. R., M. J. R. Fasham, J. Aiken, D. S. Harbour, J. F. Read and I. Bellan (1993a). The spatial and temporal development of the spring bloom during the JGOFS North Atlantic Bloom Experiment. J. mar. biol. Ass. U. K., 73, 253-282.

Wroblewski, J. (1977). A model of phytoplankton plume formation during variable Oregon upwelling. Journal of Marine Research, 35, 357-394.

Wrobleski, J. S. (1989). A model of the spring bloom in the North Atlantic and its impact on ocean optics. Limnology and Oceanography, 34(8), 1563-1571.

Wunsch, C. (1978). The north Atlantic general circulation west of 50° W determined by inverse methods. Rev. Geophys. Space Phys., 16, 583-620.

Yallop, M. (2001). Distribution patterns and blomass estimates of diatoms and autotrophic dinoflagellates in the NE Atlantic during June and July 1996. Deep-Sea Research II, 48, 825-844.

Yakushev, E. V. (1998). Modeling of the carbonate system balance changes connected with phytoplankton bloom. In: http://fadr.msu.ru/mmc/bloom/carbloom.html.